An Inelastic Electron Tunneling Spectroscopic Study of the Interactions of Cyclic Hydrocarbons with a Zirconium Polymerization Catalyst Supported on Aluminum Oxide

Thesis by

Lynn Forester

In Partial Fulfillment

of the Requirements for the Degree of

Doctor of Philosophy

California Institute of Technology

Pasadena, California

1986

(submitted May 23)

Acknowledgments

I am really happy I decided to spend my graduate career at Caltech. For the most part, I think Caltech is a remarkable place to do science. I've learned a lot and had some fun doing it.

I would like to thank my research advisor, Henry Weinberg, for his assistance and support of this research. I would also like to express my appreciation to John Bercaw and Bob Grubbs for many insightful chemistry discussions. John Lambe has been a great friend since he came to Caltech as a Fairchild Scholar in 1981. I have learned a great deal about science and life from our weekly dinner meetings. His wisdom and insight are greatly appreciated.

The past and present members of the Weinberg research group, as well as the Chemical Engineering staff, deserve thanks for their friendship and help. Both Kathy Lewis and Maria Buyco are to be commended for their excellent typing.

I also want to thank Rory Rice of Advanced Micro Devices for encouraging me to finish this thesis and for providing the time-off to do it.

Lastly, I want to thank Miles and my family for their love and encouragement. They never lost faith even when mine wavered. In lasting appreciation, I dedicate this thesis to them.

Abstract

Inelastic electron tunneling spectroscopy (IETS) has been used to investigate the temperature and exposure-dependent reactions of two cyclic hydrocarbons, cyclohexene and 1,3-cyclohexadiene, with $Zr(BH_4)_4$ supported on Al_2O_3, a known olefin polymerization catalyst.

The interactions of cyclohexene with the adsorbed catalyst have been studied at exposures of 150, 1200 and 6000 Torr s at temperatures ranging from 298 to 623 K. At 150 Torr s and 298 K, the adsorbed cyclohexene is clearly an unsaturated hydrocarbon and cyclohexene coordination to the Zr catalyst does not require an appreciable displacement of BH_4 ligands. There is evidence of both tridentate and bidentate BH_4 stretching vibrations. The initial complex formed by the adsorbed cyclohexene is probably a π-complex. The IET spectra support this conclusion as well as the possibility of conversion to a η^3-allyl ligand. The unsaturated surface species are converted to a saturated hydrocarbon at intermediate and high exposures of cyclohexene. The saturated specie accumulates on the surface as a function of both exposure and substrate temperature and the spectra show no olefinic increases in intensity. The saturated specie has been identified as polycyclohexene, a saturated polymer consisting of cyclohexane rings formed by homopolymerization.

The interactions of 1,3-cyclohexadiene with $Zr(BH_4)_4$ supported on Al_2O_3 have been studied at exposures of 150 and 6000 Torr s. Adsorbed 1,3-cyclohexadiene has been shown to form an unsaturated hydrocarbon similar to cyclohexene at moderate exposures which continues to accumu-

late on the surface as a function of temperature. At high exposures, evidence has been presented that the catalyst may initiate the polymerization of 1,3-cyclohexadiene to form poly-1,3-cyclohexadiene. As with cyclohexene, there is no apparent saturation limit as based on increases in the intensity of key hydrocarbon spectral features and on junction resistance. Adsorbed 1,3-cyclohexadiene continues to accumulate on the surface as a function of temperature at 6000 Torr s. The spectral intensity of the ring breathing modes increases dramatically and their variability in position provide evidence of different types of substituted rings. Adsorption of 1,3-cyclohexadiene perturbs the catalyst much more than cyclohexene, promoting the disassociation of the BH_4 ligands.

Design changes and improvements to a high vacuum system used for the fabrication of tunnel junctions, as well as a detailed account of the experimental procedures, are described. Programs for computer spectral analysis are presented.

Table of Contents

Chapter 1

Introduction

1. Supported Homogeneous Catalysts

1.1 Advantages of the New Catalysts

The immobilization of catalytically-active transition metal complexes on oxide supports is an exciting and challenging subject of great scientific and technological importance (1-4). This new generation of catalysts combines the best aspects of traditional heterogeneous and homogeneous systems: selectivity, activity, and re-use or recovery of the costly transition-metal catalyst. The goals of this research are to obtain the desired composition of active centers, develop methods for the synthesis of active centers in high yield, achieve complete use of the supported transition metal for propagation centers, and control the steric accessibility of the propagation centers by the proper choice of ligand. This research has centered largely on polymerization catalysis. The possibility of improving and refining Ziegler-Natta catalysts and polymerization products is important both scientifically and economically.

One industrial advantage of the new catalysts is that the process involves only one component as compared to the traditional two-component Ziegler-Natta polymerization systems which utilize an organo-aluminum co-catalyst. The new catalysts can thus be used in gas phase processes as opposed to the traditional fluidized bed or batch processes for Ziegler-Natta catalysis (5). This is particularly suitable for the production of ethylene and polypropylene. The main advantage of the gas phase method is that the polymer is easily separated from the monomer and requires no

further processing either to remove catalyst residues or undesirable polymeric product (i.e., atactic material in polypropylene). Further impetus has also been provided by the practical problems associated with the use of homogeneous catalysts on an industrial scale, which include corrosion and deposition of the catalyst on the reactor walls.

1.2 Attempts to Preserve the Molecular Nature of the Catalyst

Recent work on supported homogeneous catalysts may be roughly divided into two areas (1); one in which the molecular nature of the catalyst is kept and the other in which it is lost or unknown. The first area has been primarily concerned with grafting known homogeneous catalysts onto polymers or inorganic supports, using the principles of ligand exchange to preserve the molecular nature of the catalyst. The desired characteristics of the catalyst support include chemical durability, insolubility in the reaction medium, and catalytic centers which are easily accessible to the reagents. Most polymers cannot meet these criteria. Of the polymers investigated (6), two of the more suitable are high surface area cross-linked polystyrene and cross-linked poly(styrene-divinylbenzene) co-polymer. However, these organic polymers do not have a rigid structure and their conformation, and thus the size and shape of particles, can be strongly influenced by temperature, pressure, and solvents. In contrast, inorganic oxides such as silica and alumina are mechanically very rigid and are affected by only the most severe conditions. They are preferred for large-scale industrial operations where long catalyst beds or large pressure drops may occur. In the studies attempting to preserve the molecular nature of the catalyst, the surface

is first reacted with a molecule containing the desired ligand to which the metal center is subsequently attached (7-9). However, there is often a lack of information on the real coordination sphere of the supported complexes, except for those containing carbonyls. In some instances, the complex is able to migrate easily onto the surface of the support. This depends on many factors, including the hydrophilic nature of the support and the rigidity of the ligand (1). With some complexes, highly dispersed metal particles may form on the surface. Another potential difficulty is the reversibility of ligand dissociation. Theoretically, supported complexes should be coordinatively unsaturated if the support is rigid enough to prevent coordination to nearby ligands but the situation is often more complicated (10-12).

1.3 The Solid Support as Ligand

The alternative major research effort on supported homogeneous catalysts differs from that discussed above in that the molecular nature of the catalyst may be lost or unknown. In this case, the surface of the support itself acts like a ligand and the organometallic complexes are grafted onto the support so that the transition metal is directly bonded to the support. In these systems the support is not inert and plays an intimate role in controlling the activity of the catalyst. The early research in this field has been done primarily by D.G.H. Ballard (2) at I.C.I. and by V. A. Zacharov and Yu. I. Yermakov (3) of the Institute of Catalysis in Novosibirsk, U.S.S.R.

The majority of the complexes investigated comprise the same polymerization-active transition metals commonly used in traditional Ziegler-Natta catalysts: Ti, Zr, Hf, V and Cr. Ligands have included allyl ($-C_3H_5$), neopentyl ($-CH_2C(CH_3)_3$), cyclopentadienyl (Cp) ($-C_5H_5$), arene ($-C_6H_6$), benzyl ($-CH_2C_6H_5$), methyl ($-CH_3$), trimethyl silylmethyl ($-CH_2SiC(CH_3)_3$), and borohydride ($-BH_4$). Solid supports were SiO_2, Al_2O_3, or aluminosilicate and the supported catalysts were formed by reacting the organometallic complexes directly with the support surfaces.

The most outstanding general characteristic of these catalysts is their greatly enhanced activity over their homogeneous counterparts. The rate of olefin polymerization by solutions of individual organometallic compounds is quite low generally, ranging from 0.1 to 10 g C_2H_4/mmole M/hr/atm, where M is a transition metal. Ziegler-Natta catalysts range from 10 to 10^3 g C_2H_4/mmole M/hr/atm. The activity of the supported systems is usually two to three orders of magnitude greater than in solution. The increased activity may be due in part to the inability of the supported transition metal to form dimers. Species such as $(C_6H_5CH_2)_3ZrH$ are inactive in solution as a result of dimerization but the hydrides of transition metal compounds are active centers for polymerization which can be readily realkylated (13).

1.4 Formation of the Surface Complexes

The transition metal complexes form supported species by interacting with the hydroxyl groups on the surface of the support. The resultant product depends in part on the preliminary dehydration temperature (Td)

of the support which determines the concentration and predominant type of surface hydroxyl. This may also determine the nature of the resulting catalyst. For instance, when $Cr(C_3H_5)_3$ is supported on SiO_2 with Td > 600°C, oligomerization centers are formed in addition to the high-polymer chain propagation centers (14). The optimum Td varies with the system, ranging from 25°C for $Zr(C_3H_5)_4 + SiO_2$, to 750°C for $Zr(C_3H_5)_3X + SiO_2$ where X = Cl, Br, I. The maximum amount of organometallic complex which adsorbs on the support surface also decreases as the dehydration temperature is increased (15).

The formation of the surface complex is represented by reaction 1. The resulting structure can be confirmed by reaction with n-butanol (2, 16) as shown in reaction 2, as well as followed in the infrared (17).

(1) 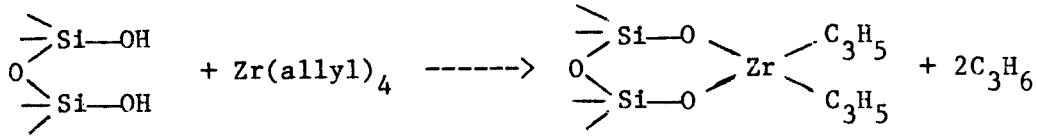

(2) 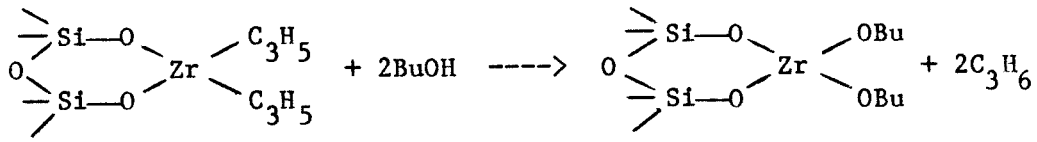

Similar structures have been deduced for other organo-zirconium and titanium complexes. Alumina may replace silica as the support in these equations. If some of the hydrocarbon ligands of Ti, Zr, or Hf complexes are replaced by halogens, structures 2 and 3 may be obtained (2, 16) as shown on the following page. $Zr(allyl)_3Cl$ gives primarily structure 2, whereas $Cr(allyl)_3$ results in a transition metal center with structure 4.

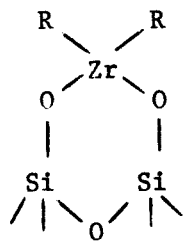

(1)

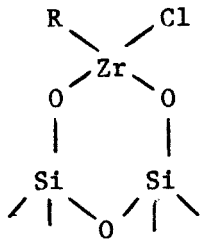

(2)

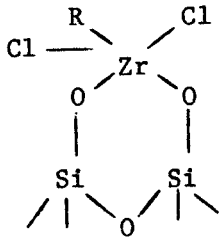

(3)

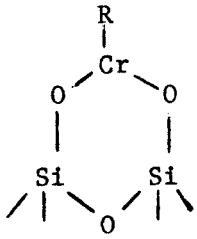

(4)

From the structures of the surface complexes, it appears that a significant number of hydroxyl groups occur in pairs on the surface. On 200°C dehydrated silica this implies that the transition metal centers are approximately 10 Å apart (16). The surface hydroxyl concentration can be measured by several methods, including TGA, neutralization, D_2O exchange, and reactions with thionylchloride, CH_3MgI, and metal chlorides (18). The fraction of paired hydroxyl groups can be estimated from the stoichiometries of reactions with $SiCl_4$ and $AlCl_3$ (19) and infrared spectroscopy may be used to differentiate between hydrogen-bonded and free hydroxyl groups (20). Chien (21, 22) developed a method which involves titration of the surface hydroxyls with gaseous VCl_4 followed by recording the electron paramagnetic resonance spectrum. From those studies it was found that γ-Al_2O_3 also has close-packed hydroxyls which react according to reaction 3. Based on its unit cell structure, γ-Al_2O_3 has

(3) VCl_4 + 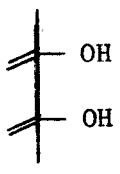 ----->

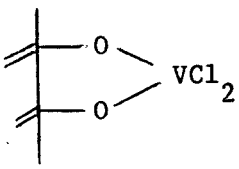

VCl_2 + 2HCl

17 OH/100 $Å^2$ of surface and the average separation is particularly favorable for reaction 3.

After formation of the "initial" supported catalyst, its activity may be altered greatly by further treatment with hydrogen, γ- or UV-irradiation, or by heating (3). Metal hydrides, formed when the alkyl groups are removed by hydrogenolysis, as in reaction 4, are also active polymerization catalysts. Transition metal borohydrides, shown in reaction 5, may be used as well (16). In these compounds, the bonding to the metal is through the hydrogen atom and not the boron. During polymerization, B_2H_6 is evolved initially and they behave like transition metal hydrides (23).

(4) 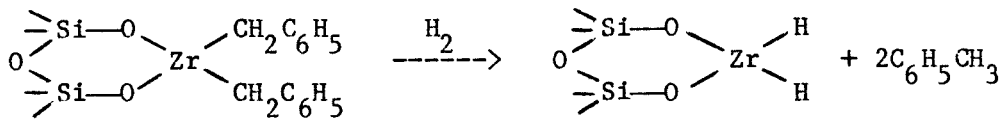

(5) 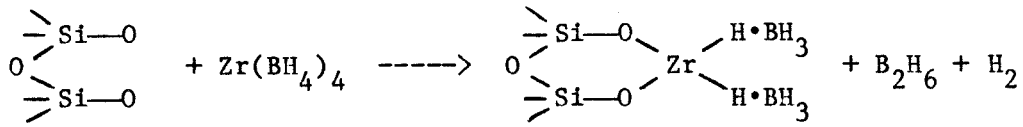

1.5 The Development of Polymerization Catalysts

Historically, α-$TiCl_3$ with an organo-aluminum co-catalyst was the preferred catalyst for the production of polycrystalline polypropylene (21). The efficiency of Ti utilization, expressed as grams of polymer produced per mmole Ti, is very low since only the coordinatively unsaturated Ti atoms along the lateral edges of the crystals form active centers. The active center concentration is only 0.05 to 20% of the available surface sites (24). In addition, there may be several kinds of active sites with differing polymerization activity and stereospecificity

(25). The polymers obtained may have broad molecular weight distributions and be difficult to process. Such considerations spurred the development of a more active catalyst system based primarily on increased activity through increased surface area. After an undistinguished series of new catalysts, $TiCl_4$ with magnesium compounds (MgO, Mg(OH), $Mg(OR)_2$, $MgCl_2$, Mg alkyls, etc.), together with an aluminum co-catalyst, was found to have a polymerization activity which was more than a thousand times greater than the original Ziegler systems. With solid magnesium chloride supports, highly isotactic polypropylene is obtained (24). In the late 1960's it became clear that if organotitanium species were the true catalysts formed by reaction of titanium compounds and aluminum alkyls, and if the compounds could be reacted with supports, then very active polymerization catalysts could be obtained. This led to the series of catalysts based on tetrabenzyls, tetraallyls, and tetraalkyls, or di-arene metal(0) complexes of the Group IV metals in combination with high surface area alumina. In the past 15 years, new solid catalysts of both the one-component, and the two-component variety have been explored. For instance, $TiCl_2$ (26, 27) is an active catalyst which does not require a co-catalyst and $Ti(Benzyl)_4$ is a polymerization catalyst either alone, supported on Mg(OH)Cl with aluminum co-catalysts (21), or supported on oxides (28) without co-catalysts.

1.6 The Transition Metal-Carbon Bond

An impressive number and variety of catalysts are now known to polymerize olefins and di-olefins: traditional Ziegler-Natta two-component catalysts, oxide-supported Ziegler-Natta catalysts either of the one-

component metal-alkyl free type or those requiring a co-catalyst, and a large number of transition metal complexes either supported or unsupported and with or without an added aluminum alkyl. This diverse composition of transition metal compounds presents a seemingly overwhelmingly complex picture of polymerization. In many of these systems, the number of transition metal atoms present and the steps required to transform the initial transition metal complex into the active center are unclear. However, in each of these diverse systems, it is now clear that the active center is a transition metal-carbon bond. It appears that the mechanism of olefin polymerization by all solid catalysts is basically the same. Chain propagation involves two distinct steps: coordination of the monomer to the metal and insertion of the complexed olefin into an adjacent metal-carbon bond (16, 21, 29, 30).

It now appears that the oxide polymerization catalysts like the Phillips Petroleum Co. catalyst (CrO_3 on oxides) and the Standard Oil Co. catalyst (MoO_3 on Al_2O_3) may differ only from α-$TiCl_3$ Ziegler-Natta catalysts in the manner of formation of the propagation centers - the surface compounds with an active metal-carbon bond. In the Ziegler-Natta systems, the transition metal-carbon bond can be formed by alkylation of the transition metal salt by the added metal alkyl co-catalyst as in reaction 6.

(6) $LxMCl + AlR_3 \text{ -------> } LxM\text{-}R + AlR_2Cl$

Additionally, the co-catalyst may act as a reducing agent, as a stabilizing agent for the metal center by completing the coordination sphere

of the metal or via the formation of halogen or alkyl bridges, or by scavenging impurities that may poison the center. It may also participate in chain transfer reactions and control the stereochemical behavior of the catalyst. In metal alkyl-free systems it is not always clear if the starting material or some species derived from it is the active species. In some cases not all molecules are simultaneously active. The slow first addition of monomer may account for the low activity found in certain cases. However, most catalysts exhibit varying degrees of reactivity depending on the monomer to be polymerized.

1.7 Formation of the Propagation Centers

The extent of polymerization thus depends on the mechanism of propagation center formation and the number of centers formed. The transformation of the surface complexes to propagation centers has been proposed to proceed via the following routes (3, 31, 32): insertion of monomer into the metal-organic ligand bond, shown in reaction 7 where R is the organic ligand and Lx represents the other ligands of the surface compound; formation by oxidative addition to low valent ions, as in reaction 8; and formation of hydride complexes followed by monomer insertion, shown in reaction 9.

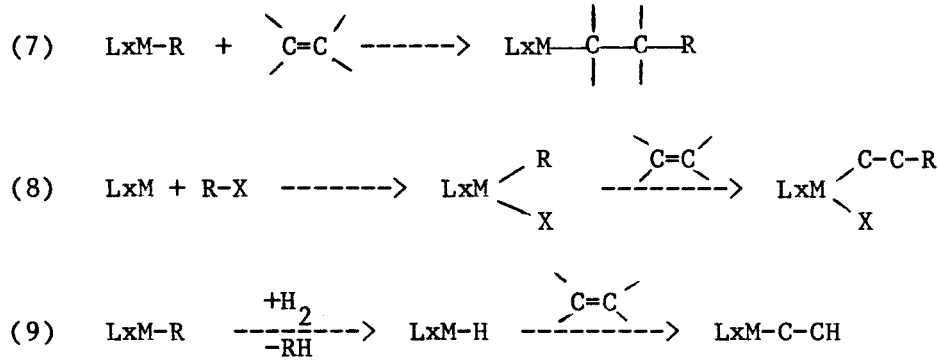

For some systems (31), such as supported tetrakis-π-allyl zirconium, treatment of the initial surface complexes with hydrogen produces surface hydrides which are direct precursors of the propagation centers for ethylene polymerization. For Ti(III) and Zr(III) centers, the propagation reaction appears to involve a two-step process (33), shown in reactions 10 and 11:

$$\text{(10)} \quad \text{LxM=P} + \text{C}_2\text{H}_4 \xrightarrow{\text{H}_2\text{C=CH}_2} \text{LxM-P}$$

$$\text{(11)} \quad \text{LxM-P} \xrightarrow{\text{H}_2\text{C=CH}_2} \text{LxM-CH}_2\text{-CH}_2\text{P}$$

For these catalysts, the elementary stages of the polymerization process include coordination of the monomer, insertion of the monomer into the M-H bond, hydride transfer, hydrogenation of the metal-carbon bond, and regeneration of the propagation centers as the result of olefin insertion into the metal-H bond.

1.8 Monomer Coordination and the Propagation Reaction

The formation of the active propagation center is followed rapidly by olefin insertion into the metal-carbon bond as shown in reaction 12, where P represents the growing polymer chain:

$$\text{(12)} \quad \text{LxM-CH}_2\text{P} + \text{n}(\text{C}_2\text{H}_4) \longrightarrow \text{LxM-}(\text{CH}_2\text{-CH}_2)_n\text{-CH}_2\text{P}$$

Until recently, coordination of the monomer to the metal was thought to result in a π-complex and the insertion of the complexed olefin into an adjacent metal-carbon bond was thought to proceed possibly via intra-nucleophilic attack on the olefin. However, this view of the propagation step mechanism has been challenged.

Cossee's original treatment (34) of the propagation reaction in Ziegler-Natta catalysts postulated that back-bonding of the monomer with the metal ion was an important contribution in the formation of the π complex. Theoretical studies have since shown that such an interaction is small (35-39). In fact, Zr(IV) and Ti(IV) centers which have no d electrons and are unable to backbond into the olefin, nonetheless have high catalytic activity. In considering the reactions of these transition metals without d electrons, one is reminded that Ziegler-Natta polymerization, or coordination polymerization as it is also known, is a special type of anionic polymerization in that the charge on the intermediate can be written (24) as in reaction 13. It may be that for these

(13) $\text{polymer}^- \text{——} M^+$

systems the coordination of the monomer to the metal is best thought of as a Lewis acid-base type interaction, as opposed to the Chatt-Duncanson type (13, 40).

This is supported by Ballard's work on various zirconium derivatives obtained with silanols (41, 42). He speculated that ligands derived from stronger acids would provide more electronegative oxygen atoms that would in turn make the ZrO bond more ionic and intensify the electropositive

charge on the metal. This would not only enhance the coordination of the olefin to the zirconium but would make the Zr-C bond more polarized and more active for insertion of the coordinated olefin. This was supported by showing that Zr derivatives of α-pinacol, a weak acid, were inactive whereas those of perfluoro-α-pinacol, a strong acid, formed active catalysts as shown in structures 9 and 10.

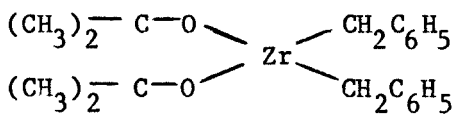

(9) inactive

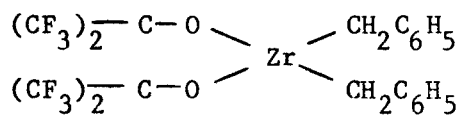

(10) active

One feature of these catalysts which any mechanism must account for is their ability to form highly isotactic polymers from α-olefins, especially propylene. This reflects the very high degree of stereochemical control which is present at each insertion step. The origin of this precise control is believed to be the asymmetry in the coordination sphere of the catalyst center which leads to a highly favoured complexion of the α-olefin. Additionally, it should be noted that the stereospecific characteristics of the traditional Ziegler-Natta systems are also present in the new metal-alkyl free systems and metal complex catalysts.

Ballard (2, 16, 45) has postulated the existence of a 4-center transition state based on the equilibrium between olefin insertion into the M-H bond and β-H abstraction as shown in reaction 14. The olefin insertion reaction is the reverse of this process.

(14) 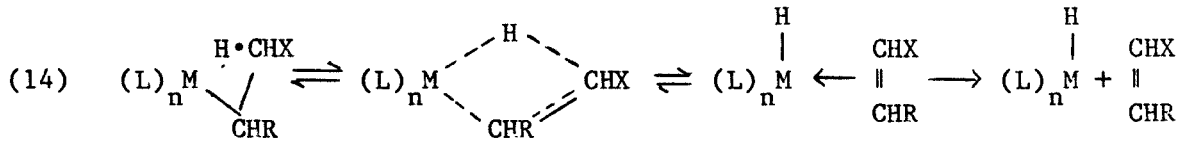

Ballard generalized the reaction to include metal alkyls as well as hydride species. One of the central points of this reaction is that the intermediate is similar to a π-allyl complex. The three C atoms lie in a plane nearly at right angles to the plane of the transition metal and the bond lengths are intermediate between C-C single and double bonds. This resonant specie is shown in structure 11. This intermediate also accounts for the asymmetric synthesis of polymers. Structure 12 is the isotactic intermediate and structure 13 is the syndiotactic intermediate.

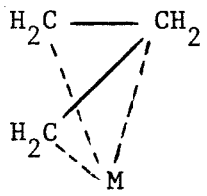

11

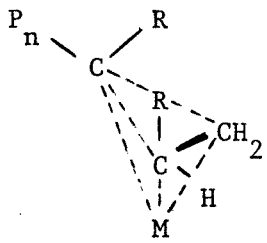

12

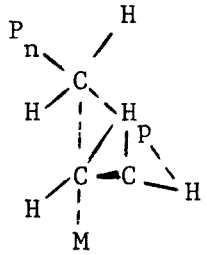

13

1.9 Similarities of Polymerization and Metathesis

Recent work on the mechanistic details involved in the propagation step have focused on unifying the mechanistic pathways of polymerization, oligomerization, and metathesis by proposing a common metal-carbene or metallocyclobutane intermediate (**44, 45**). Results from research on

alkene metathesis reactions led to a re-examination of the polymerization reaction and the proposal of a new mechanism because of the similarity of the metathesis and polymerization reactions. In particular, the metathesis of some cyclic olefins was found to result in ring opening polymerization and some Ziegler-Natta systems catalyze both ring opening and normal polymerization (46).

Recent work on alkene metathesis reactions has shown that the catalytic chain is propagated by two different odd-carbon-number species, metal-carbenes and metallocyclobutanes. The reaction mechanism originally proposed by Bradshaw (47) involved pairwise exchange of alkylidene units at the catalytic center and has since been disproven. Herisson and Chavin (48) proposed a mechanism which involved a metal-carbene intermediate in 1970:

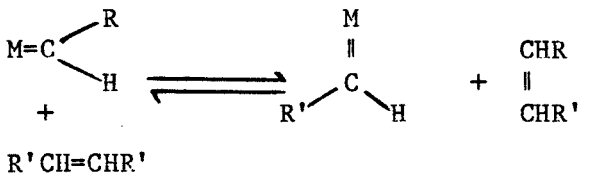

In recent years studies have focused on isolating a recoverable metal carbene catalyst that would catalyze metathesis and on demonstrating the participation of metallocyclobutanes in catalytic reactions.

A unifying mechanism for metathesis and polymerization has been proposed by Ivin et al. (49) in which R represents the growing chain:

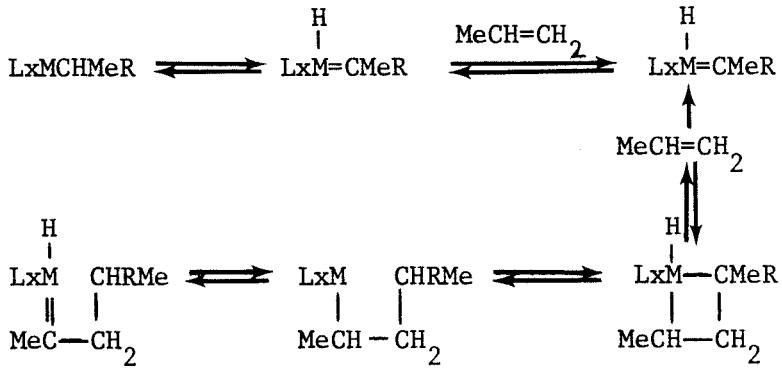

Two main routes for the formation of metal-carbenes and metallocyclobutanes have been proposed: α-elimination and η^3-allyl-metallocyclobutane interconversion. The α-elimination pathways for homogeneous and heterogeneous systems are shown in reactions 7 and 8, respectively:

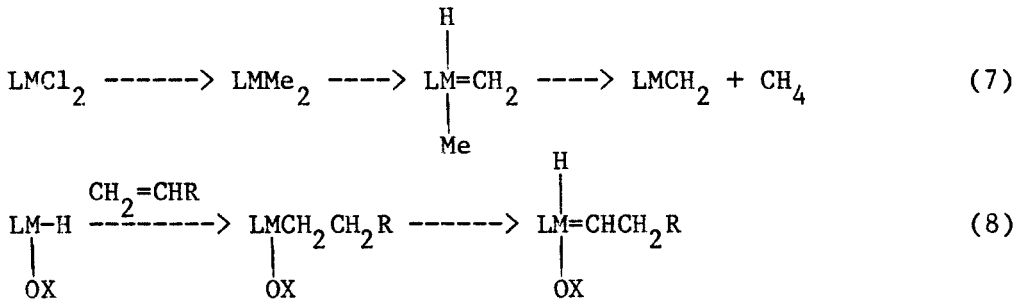

(7)

(8)

In situations where there is no obvious route via metal alkyls or hydrides a η^3-allyl-metallocyclobutane interconversion may be possible as shown in reaction 9:

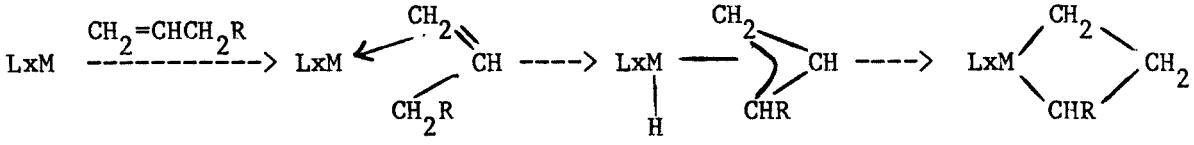

The recent studies of reaction mechanisms in metathesis, oligomerization and polymerization systems demonstrate that the same

fundamental processes are operative in each: molecular complexation, addition and elimination. Recent studies are designed to isolate well-characterized catalysts that are slow enough that chain growth may be monitored. An example of this was provided by the work of Turner and Schrock (50) who reported on the polymerization of ethylene by a tantalum alkylidene hydride complex. Other studies have been concerned with preparing and isolating metallacyclobutanes and metal-carbene complexes. A recent example of this is provided by Gilliom and Grubbs (51) who reported the preparation of a titanocyclobutane precursor to alkyl-substituted titanium-carbene complexes.

1.10 The Role of the Support.

It may be that in supported organotransition metal polymerization catalysts, the mechanism is governed largely by the presence of the bulky surface through proximity and electronic effects, as well as by the other ligands in the coordination sphere.

The choice of support has been shown to have an important effect on the formation of propagation center precursors and hence on the number of propagation centers formed. A good example is provided by the $Zr(allyl)_4$ system which has a propagation rate constant which is an order of magnitude higher when Al_2O_3 is used as the support as compared to SiO_2. A similar effect has been observed with chromium oxide catalysts (29, 52). Studies of $Zr(BH_4)_4$ adsorbed on Al_2O_3 and SiO_2 have also shown different proportions of surface decomposition products are formed as the catalyst is heated depending on the support used (53).

The proximity of the transition metal to the surface implies that an electronic effect of the surface is to be expected and that changes in the electronegativity of the substrate element E in the E-O-M portion of the propagation center should definitely change the electronic density of the metal. The estimation of this effect on the propagation rate constant is, however, not straightforward. One would also expect to find a steric effect generated by the surface since the surface is considered to be a ligand in these complexes. Changes in selectivity have in fact been demonstrated in olefin metathesis with tungsten complexes acting as either homogeneous catalysts or supported on alumina (54). It is also expected that replacement of the oxygen as a surface ligand by other elements should have a profound effect on the properties of the catalyst, but this has not been investigated.

Much remains to be done with these systems before the coordination sphere of the supported complexes is completely understood. In any case, the support in these systems seems to play an important role; by rendering the catalyst insoluble, by dispersing the active centers, and by acting as a co-catalyst or activating agent.

2.0 Inelastic Electron Tunneling Spectroscopy

Inelastic electron tunneling spectroscopy (IETS) was discovered 20 years ago by Jaklevic and Lambe (55). IETS is a surface vibrational spectroscopy which is characterized by its high sensitivity and resolution. Most of the studies conducted to date have used either Al-Al_2O_3-Pb or Mg-MgO-Pb junctions and a compilation of IET spectra has recently

appeared (56). Since IETS has been used exclusively to study the interactions of cyclic hydrocarbons with the Al_2O_3-supported polymerization catalyst, $Zr(BH_4)_4$, as reported in this thesis, a brief summary of this technique is warranted. Several reviews of tunneling spectroscopy, as well as details concerning the application and interpretation of IETS, are available elsewhere (57-61).

Inelastic electron tunneling spectra result from the absorption of energy by molecules adsorbed in the insulating layer of a metal-insulator-metal junction from electrons which tunnel inelastically through the junction. Figure 1 shows a typical junction. As a dc bias voltage, V, is applied, the Fermi levels of the metal 1 and 2 are separated by eV. The horizontal line corresponds to elastic tunneling of the electrons and the dashed oblique line corresponds to inelastic tunneling in which the electrons lose energy $\hbar\omega_o$, to excite an oscillator in the insulating region. In order for the tunneling electron to find an empty state in the right-hand metal, the applied voltage eV must be greater than or equal to $\hbar\omega_o$, where ω_o is the excitation frequency of the oscillator or adsorbate in the junction. As the bias voltage is increased, new inelastic channels will result as higher vibrational frequencies become accessible to the tunneling electrons and are able to be excited. These small increases in the availability of inelastic channels result in a small change of slope in the current versus voltage plot as shown in Figure 2. The first derivative of the current versus voltage will then exhibit a small step. However, since approximately only 1% of the electrons tunnel inelastically, the second derivative of the current with

respect to voltage, d^2I/dV^2, is usually recorded instead since this allows a clearer display. The baseline of the d^2I/dV^2 versus V curve is not flat. When the second electrode is superconducting, the typical energy gap, labelled as 2Δ in Figure 1, will appear as expected. This results in a small offset between the applied voltage and the accessibility of empty states in metal 2 since tunneling into the superconducting gap is forbidden.

Scalapino and Marcus (62) were the first to develop a theory showing that the d^2I/dV^2 versus V spectrum of IETS is analogous to an infrared absorption spectrum. They demonstrated that the selection rules operable in IR spectroscopy also apply to IETS, that electron dipole interactions are allowed and observed. The theory of Scalapino and Marcus was extended by Lambe and Jaklevic (63) to include the polarizability of the molecule. They demonstrated that Raman active transitions are observed in IETS. In practice, most adsorbates studied by IETS do not have sufficient symmetry to have separate Raman and IR active modes. However, a study of anthracene (64) demonstrated that the IR and Raman modes are separate in the IET spectrum of this molecule and that they occur with nearly equal intensity.

IET junctions are thin film devices and are fabricated at the time of an experiment. The steps followed in the fabrication are presented schematically in Figure 3. All experiments are conducted in a high or ultra-high vacuum environment since the fabrication process requires the evaporation of the metal electrodes as well as a clean contaminant-free environment. The IET junctions used for the studies presented in this

thesis were all prepared in an oil diffusion-pumped bell jar with a base pressure of 5×10^{-8} Torr. Before beginning an experiment an oxygen plasma discharge was run to help clean the system of hydrocarbon contaminants (65). Aluminum strips approximately 800 Å in thickness are evaporated onto glass slides. Electrical contacts to the films are made using In/Sn solder as shown in Figure 3. The simultaneous heating and temperature measurement technique developed by Bowser and Weinberg (66) was used for all heating operations. After evaporation, the aluminum strips are annealed to 520 K to ensure that the integrity of the oxide barriers will be preserved in any subsequent heating operations during the experiment. After annealing, thin oxide barriers are formed by oxidizing the aluminum in a plasma discharge of O_2 containing a trace of H_2O vapor. The resulting oxide is 20 - 25 Å in thickness and provides the surface upon which the experiments of interest are carried out. The nature of the oxide barrier is important since modeling commercial alumina catalysts with IETS is highly desirable. Studies have shown that the oxide barriers formed are physically, chemically and catalytically similar to γ-alumina (67, 68).

The adsorbate of interest is next exposed to the oxide film as a vapor or a dilute solution. In some cases, the junctions are heated or cooled during or after this step in order to promote reaction or adsorption. In the case of the $Zr(BH_4)_4$ studies preserved in this thesis, the junctions were first exposed to the $Zr(BH_4)_4$ in order to form the Al_2O_3 supported catalyst. After forming the immobilized catalyst in this manner, the junctions were allowed to interact with the cyclic hydro-

carbon adsorbate over a range of temperatures and exposures.

The junctions are completed by evaporating a counter electrode of Pb approximately 1000 to 2000 Å in thickness in a crossed strip geometry which allows the current-voltage characteristics of the junction to be measured by using a four-point probe geometry. Pb is chosen as the counter electrode because of its inertness, large ionic radius and low melting point which makes it easy to use. Lead also has a relatively high superconducting transition temperature which ensures that it is superconducting at the temperature at which the IET junctions are measured. This increases the resolution (69).

The IET spectra are measured using a harmonic detection scheme as shown in Figure 4 which has been previously described (57). The electronics actually measure d^2V/dI^2 which is equal to $-(dI/dV)^{-3}d^2I/dV^2$. In most cases, dI/dV is essentially constant over the spectral range so the measured quantity is proportional to d^2I/dV^2. Measurements are carried out with the junctions submerged in LHe over the spectral range of 240 - 4000 cm^{-1}. The region below 240 cm^{-1} is not measured because of the magnitude of phonon excitations due to the Pb superconducting counter electrode. Recording the data at 4.2 K or below ensures not only that the Pb will be superconducting but also reduces thermal broadening.

3.0 Objectives

IETS has great applicability to studies of chemisorption and heterogeneous catalysis. Tunneling spectroscopy has been used to study the molecular structure of adsorbates, adsorbate orientation, surface

concentration, absorbate-adsorbate interactions, surface reactions and supported metal catalysts. A great number of adsorbates, especially carboxylic acids and alcohols, have been studied by IETS (56). Many of these past studies used IETS to merely survey a group of adsorbates rather than study the surface reactions of the absorbates in any detail.

One of the objectives of the work presented in this thesis was to study in detail one particular adsorbate system in the hope of extensively characterizing its temperature and exposure dependent reactivity. The system chosen for this in-depth study was cyclohexene interacting with $Zr(BH_4)_4$ adsorbed on Al_2O_3. $Zr(BH_4)_4$ on Al_2O_3, a known olefin polymerization catalyst, has been successfully studied by IETS previously (70-72). It is a nearly ideal choice for a supported catalyst because of its high vapor pressure and the unique spectral features associated with the BH_4 ligands. It was hoped by this work to not only learn more about the chemistry and reactivity of the supported $Zr(BH_4)_4$ catalyst but also to demonstrate that IETS can be successfully used for this type of detailed investigation. Chapter 2 presents the results of this study with cyclohexene.

Chapter 3 presents the results of a similar study of the interactions of 1,3-cyclohexadiene with $Zr(BH_4)_4$ supported on Al_2O_3, and demonstrates that IETS may be better suited for the study of some adsorbates than others. Chapter 4 presents the conclusions.

In order to carry out these objectives certain practical considerations had to be addressed. First, the vacuum system used for the

preparation of these junctions required serious upgrading. The many design changes and improvements which were made to the system are presented in Appendix A as well as a detailed description of the fabrication process steps which are actually required for an experiment using this particular vacuum system. The second practical consideration involved developing a reliable method for the accurate assignment of spectral peak positions. The programs originally written (73) were found to require major changes in the method of background subtraction before they could be applied favorably to the cyclohexene and 1,3-cyclohexadiene spectra. Consequently, a number of alterations were made to the program and several new features such as a screen plotting option and the ability to produce graphs of up to 10 spectra were incorporated. The resulting programs are presented in Appendix B.

References

1. J. M. Basset and A. K. Smith, in "Fundamental Research in Homogeneous Catalysis", M. Tsutsui, R. Ugo, Eds, Plenum: New York 1977, pp. 69-98.

2. V. A. Zakharov and Yu. I. Yermakov, Catal. Rev.-Sci. Eng. 19, 67 (1979).

3. D. G. H. Ballard, J. Polymer Science 13, 2191 (1975).

4. Z. M. Michalska and D. E. Webster, Chemtech, 117 (1975).

5. B. C. Gates, J. R. Katzer and G. C. A. Schuit, "Chemistry of Catalytic Processes", McGraw-Hill, New York, 1975, pp. 176-179.

6. K. G. Allum, R. D. Hancock, I. V. Howell, R. C. Pitkethly and P. J. Robinson, J. Organomet. Chem. 87, 189 (1975).

7. K. G. Allum, R. D. Hancock, I. V. Howell, R. C. Pitkethly, S. McKenzie and P. J. Robinson, J. Organomet. Chem. 87, 203 (1975).

8. K. G. Allum, R. D. Hancock, I. V. Howell, R. C. Pitkethly and P. J. Robinson, J. Catal. 43, 322 (1976).

9. K. G. Allum, R. D. Hancock, I. V. Howell, T. E. Lester, S. McKenzie, R. C. Pitkethly and P. J. Robinson, J. Catal. 43, 331 (1976).

10. A. Brenner and R. L. Burwell, Jr., J. Amer. Chem. Soc. 97, 2565 (1975).

11. R. F. Howe, Inorg. Chem. 15, 486 (1976).

12. A. K. Smith, J. M Basset and P. Maitlis, J. Molec. Catal. 2, 223 (1977).

13. J. Chatt and L. A. Duncanson, J. Chem. Soc., 2939 (1953).

14. F. J. Karol and R. N. Johnson, J. Polym. Sci., Polym. Sci., Polym. Chem. Ed. 13, 1607 (1975).

15. V. A. Zakharov, V. K. Dudchenko, A. I. Minkov, O. A. Yefimov, L. G. Chomyakova, V. I. Babenko and Yu. I. Yermakov, Kinet. Katal. 17, 643 (1976).

16. D. G. H. Ballard, in "Coordination Polymerization", J. C. W. Chien, Ed., Academic, New York, 1975, pp. 223-262.

17. D. G. H. Ballard, Advan. Catal. 23, 263 (1973).

18. H. P. Boehm, Advan. Catal. 16, 1979 (1966).

19. J. B. Peri and A. L. Hensley, J. Phys. Chem. 72, 2926 (1968).

20. F. H. Hambleton, J. A. Hockey and J. A. G. Taylor, Trans. Faraday Soc. 6, 794, 801 (1966).

21. J. C. W. Chien, J. T. T. Hsieh, in "Coordination Polymerization", J. C. W. Chien, Ed., Academic, New York, 1975, pp. 305-325.

22. J. C. W. Chien, J. Amer. Chem. Soc. 93, 4675 (1971).

23. R. S. Coffey, J. M. Key, B. T. Kilbourne and U. K. Wright, Application No. 26134/72.

24. J. P. Candlin, in "Catalysis and Chemical Processes", R. Pearce and W. R. Patterson, Eds., John Wiley and Sons, New York, 1981, Chap. 10.

25. L. A. M. Rodriguez and H. M. Van Looy, J. Polymer Sci., Part A-1, 4, 1971 (1966).

26. C. X. Werber, C. J. Benning, W. R. Wszolek and G. E. Ashby, J. Polym. Sci., Part A-1, 6, 743 (1968).

27. A. S. Matlack and D. S. Breslow, J. Polym. Sci. A 3, 2853 (1965).

28. G. A. Nesterov, V. A. Zakharov, E. A. Paukshtis, E. N. Yurchenko and Yu. I. Ermakov, Kinet. Katal. 20, 429 (1979).

29. Yu. I. Yermakov and V. A. Zakharov, in "Coordination Polymerization", J. C. W. Chien, Ed., Academic, New York, 1975, pp. 91.

30. H. Sinn and W. Kaminsky, Adv. Organomet. Chem. 18, 99 (1980).

31. V. A. Zakharov, V. K. Dudchenko, E. A. Paukshtis, L. G. Karakchiyev and Yu. I. Yermakov, J. Molec. Catal. 2, 421 (1977).

32. Yu. I. Yermakov and V. A. Zakharov, Advan. Catal. 24, 173 (1975).

33. V. A. Zakharov, N. G. Maksimov, G. A. Nesterov, V. F. Anufrienko, V. K. Stachastnev and Yu. I. Yermakov, J. Molec. Catal. 4, 167 (1978).

34. P. Cossee, J. Catal. 3, 80 (1964).

35. D. R. Armstrong, P. G. Perkins and J. J. P. Stewart, J. Chem. Soc., Dalton Trans., 1972 (1972).

36. D. R. Armstrong, P. G. Perkins and J. J. P. Stewart, J. Chem. Soc. (A), 3674 (1971).

37. G. Giunchi, E. Clementi, M. E. Ruiz-Vizcaya and O. Novaro, Chem. Phys. Letters 49, 8 (1977).

38. O. Novaro, S. Chow and P. Magnouat, J. Catal. 41, 91 (1976).

39. P. Cassoux, F. Crasnier and J. -F. LaBarre, J. Organomet. Chem. 165, 303 (1979).

40. J. Boor, "Ziegler-Natta Catalysts and Polymerization", Academic Press, New York, 1979.

41. D. G. H. Ballard, N. Heap, P. T. Kilbourn and R. J. Wyatt, Makromol. Chem. 170, 1 (1973).

42. D. G. H. Ballard, Polym. Prepr., Am. Chem. Soc., Div. Polym. Chem. 15, 364 (1974).

43. D. G. H. Ballard, Chemistry in Britain 10, 20 (1974).

44. R. H. Grubbs, in "Comprehensive Organometallic Chemistry", G. Wilkinson, Ed., Pergamon, Oxford (1982), Chap. 54.

45. R. Pearce, in "Catalysis and Chemical Processes", R. Pearce and W. R. Patterson, Eds., John Wiley and Sons, New York, 1981, Chap. 9.

46. G. Natta, G. Dall'Asta and G. Mazzarti, Angew Chem. 76, 765 (1964).

47. C. P. C. Bradshaw, E. J. Howman and L. Turner, J. Catal. 7, 269 (1967).

48. J. L. Herisson and Y. Chauvin, Makromol. Chem. 141, 161 (1970).

49. K. J. Ivin, J. J. Rooney, C. D. Stewart, M. L. H. Green and R. Mahtab, J. C. S. Chem. Comm., 604 (1978).

50. H. W. Turner and R. R. Schrock, J. Am. Chem. Soc. 104, 2331 (1982).

51. L. R. Gilliom and R. H. Grubbs, Organometallics 5, 721 (1986).

52. E. G. Kushnareva, Yu. I. Ermakov and V. A. Zakharov, Kinet. Katal. 12, 359 (1971).

53. G. A. Nesterov, V. A. Zakharov, E. A. Paukshtis, E. N. Yurchenko, V. V. Volkov and K. G. Myakishev, Kinet. Katal. 21, 739 (1980).

54. J. M. Basset, J. L. Biljou, R. Mutin and A. Theolier, J. Amer. Chem. Soc. 97, 7376 (1975).

55. R. C. Jaklevic and J. Lambe, Phys. Rev. Lett. 17, 1139 (1966).

56. D. G. Walmsley and J. L. Tomlin, Prog. Surface Science 18, 247 (1985).

57. W. H. Weinberg, Ann. Rev. Phys. Chem. 29, 115 (1978).

58. P. K. Hansma, Phys. Letters C 30, 145 (1977).

59. "Inelastic Electron Tunneling Spectroscopy", T. Wolfram, Ed., Springer, Berlin (1978).

60. "Tunneling Spectroscopy", P. K. Hansma, Ed., Plenum, New York (1982).

61. S. K. Khanna and J. Lambe, Science 220, 1345 (1983).

62. D. J. Scalapino and S. M. Marcus, Phys. Rev. Lett. 18, 459 (1967).

63. J. Lambe and R. C. Jaklevic, Phys. Rev. 165, 821 (1968).

64. M. G. Simonsen, R. V. Coleman and P. K. Hansma, J. Chem. Phys. 61, 3789 (1974).

65. J. W. Coburn, "Plasma Etching and Reactive Ion Etching", American Institute of Physics, New York, 1982.

66. W. M. Bowser and W. H. Weinberg, Rev. Sci. Instrum. 47, 583 (1976).

67. P. K. Hansma, D. A. Hickson and J. A. Schwarz, J. Catal. 48, 237 (1977).

68. H. E. Evans, W. M. Bowser and W. H. Weinberg, Appl. Surf. Sci. 5, 258, 1980.

69. J. Klein, A. Leger, M. Belin and D. D'efourneau, Phys. Rev. B 7, 2336 (1973).

70. H. E. Evans and W. H. Weinberg, J. Am. Chem. Soc. 102, 872 (1980).

71. H. E. Evans and W. H. Weinberg, J. Am. Chem. Soc. 102, 2548 (1980).

72. H. E. Evans and W. H. Weinberg, J. Am. Chem. Soc. 102, 2554 (1980).

73. M. K. Templeton, Ph. D. Thesis, California Institute of Technology, 1984.

Figure Captions

Figure 1: Schematic energy diagram for elastic (horizontal line) and inelastic (oblique line) electron tunneling through a barrier of width 1. E_1, the initial energy, and E_2, the final energy, are separated by $\hbar\omega_o$, a vibrational excitation energy. E_{F1} and E_{F2} are the Fermi levels in the two metals. $2\Delta_2$ represents the superconducting gap in metal 2 and eV is the bias voltage.

Figure 2: Schematic representation of the effect of a vibrational excitation at energy eV_o on the current-voltage characteristic and the first (dI/dV) and second (d^2I/dV^2) derivatives of the current with respect to voltage (V) of a tunnel junction.

Figure 3: A schematic of the junction fabrication procedure showing (a) a clean glass substrate with attached electrical leads, (b) evaporation of the aluminum strip, annealing of Al, oxidation and exposure to adsorbates, and (c) deposition of top counter electrode.

Figure 4: Schematic of the IETS analog measurement electronics.

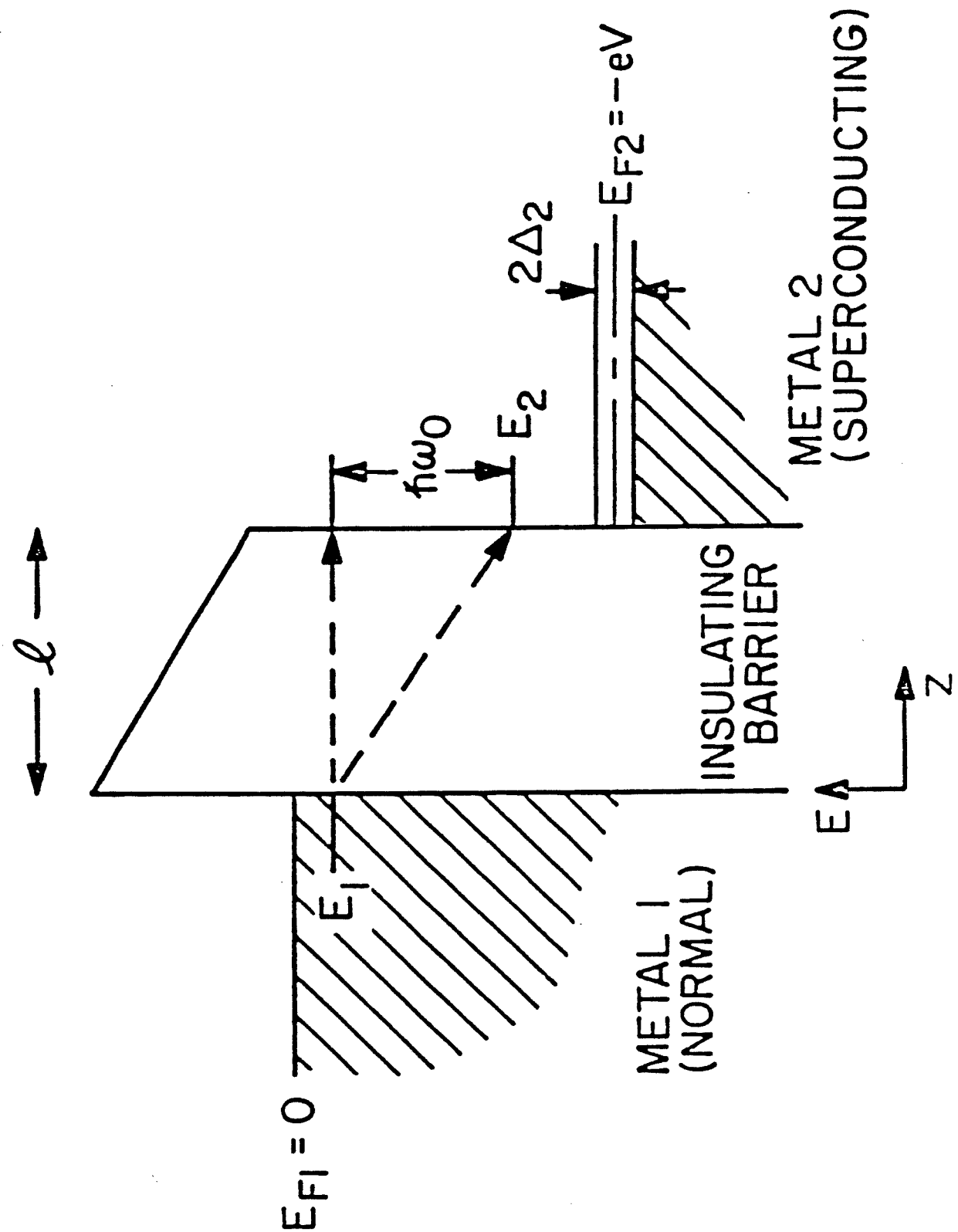
$E_{F1}=0$
E_1
METAL 1
(NORMAL)
INSULATING
BARRIER
METAL 2
(SUPERCONDUCTING)
E_2
$\hbar\omega_0$
$2\Delta_2$
$E_{F2}=-eV$
ℓ
E
Z

Figure 1

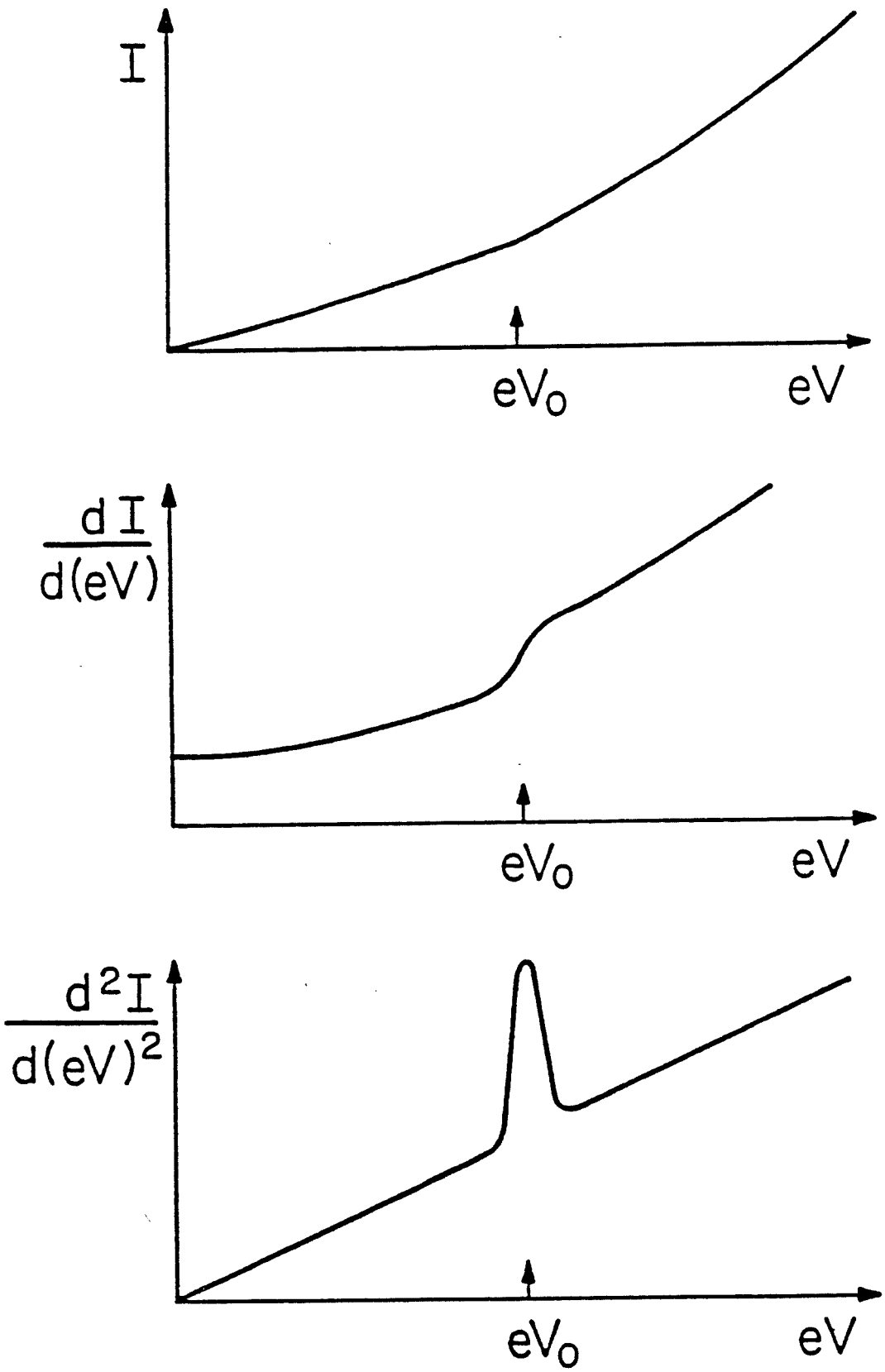

Figure 2

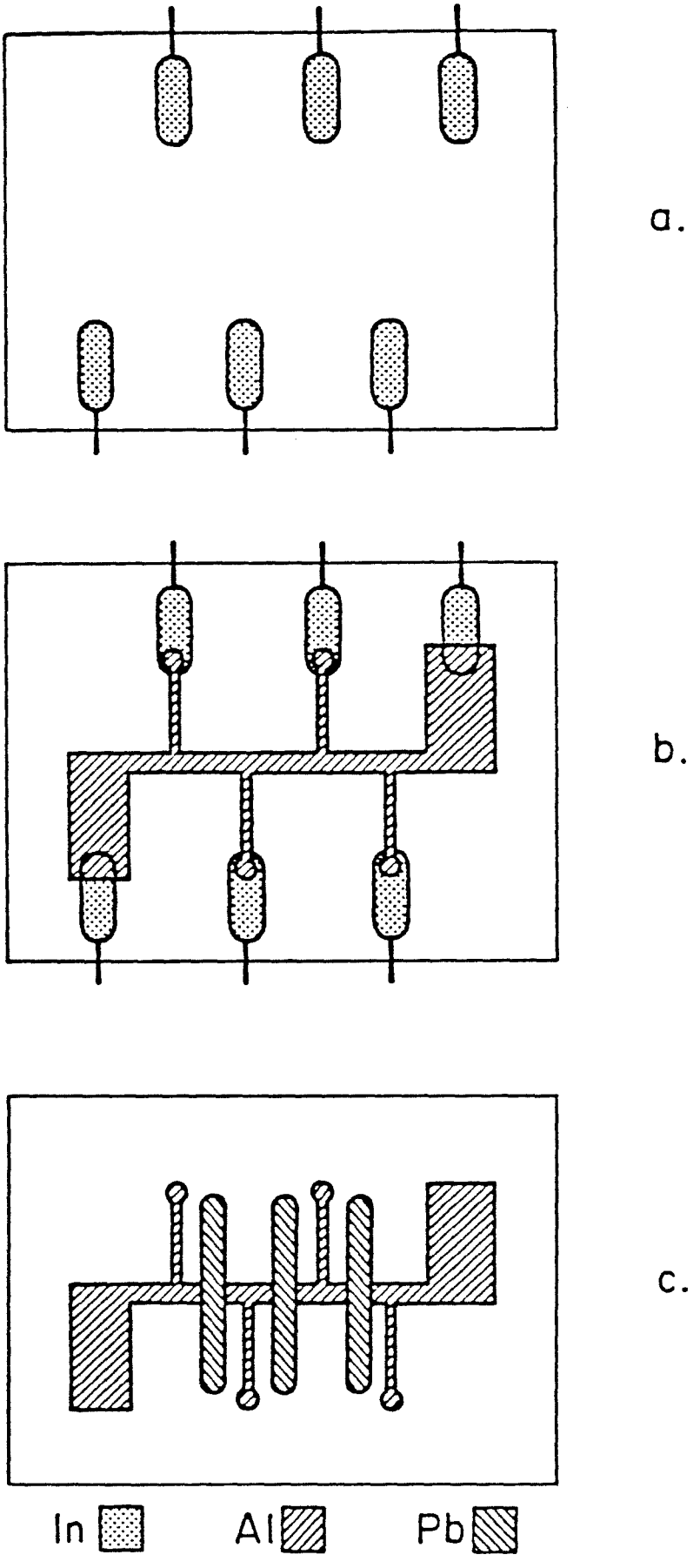

Figure 3

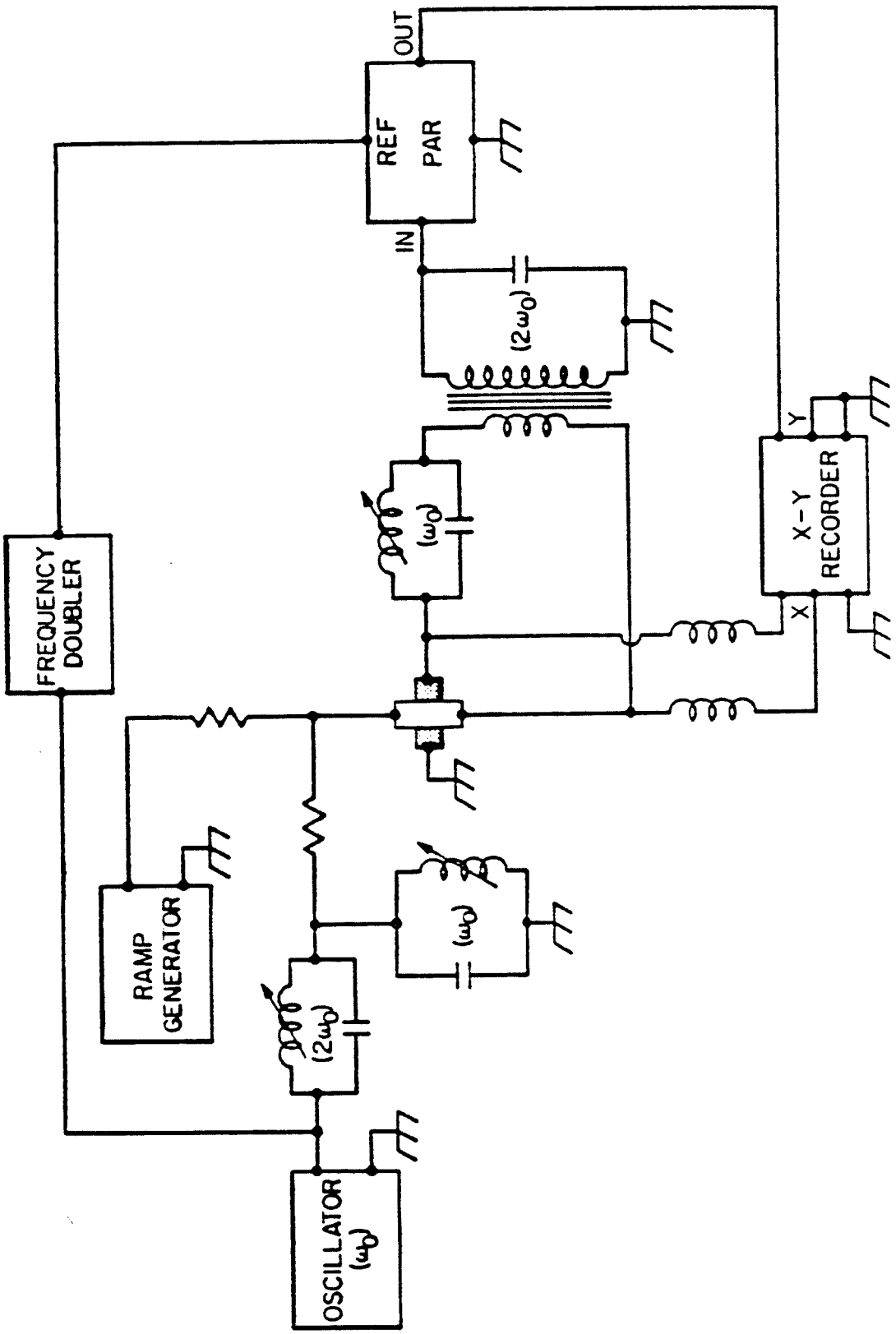
OUT
REF
PAR
IN
$(2\omega_0)$
(ω_0)
Y
X-Y
RECORDER
X
FREQUENCY
DOUBLER
RAMP
GENERATOR
(ω_0)
$(2\omega_0)$
OSCILLATOR
(ω_0)

Figure 4

Chapter 2

The Interactions of Cyclohexene with $Zr(BH_4)_4$ Adsorbed on Al_2O_3

1.0 Introduction

During the past decade there has been a growing interest in homogeneous catalysts supported on aluminum and other inorganic oxide supports (1-3). The observation that the activity of many of the supported catalysts is increased by several orders of magnitude over that of their homogeneous counterparts has provided a significant impetus to this line of research. Supported catalysts are usually more stable than homogeneous catalysts and the fact that in many cases the reaction products may be separated from the catalysts make these new systems commercially attractive. Additionally, they often retain the selectivity found in homogeneous complexes. However, very little information is known about the surface structures of these supported catalytic systems. In order to design and develop new catalytic systems as well as refine the selectivity and activity of presently known complexes, an increased knowledge of surface structure and chemistry is required. The supported systems are not generally amenable to traditional structural studies such as NMR which are routinely used to characterize homogeneous complexes (4).

Our research group has been involved in an ongoing effort to characterize the surface structures and chemistry of known homogeneous catalysts and complexes supported on alumina by means of inelastic electron tunneling spectroscopy (IETS) (5-9). IETS is a type of surface vibrational spectroscopy which is particularly well-suited for studies of model catalytic systems because of its resolution, sensitivity, and spectral range (240 to 4000 cm^{-1}). IETS involves monitoring the current due

to electrons tunneling inelastically through a thin insulating barrier between two electrodes. The junctions are of Al-Al_2O_3-Pb and the Al_2O_3 barrier serves as the oxide support for the catalyst. The nature of the oxide barrier is an important consideration since the applicability of IETS results to commercial γ-alumina catalysts is highly desirable. Hansma et al. (10) have demonstrated that the aluminum oxide that grows at room temperature is similar physically, chemically, and catalytically to γ-alumina. X-ray photoelectron spectroscopy (11) has been used to characterize a number of different types of alumina thin films used in inelastic electron tunneling spectroscopy. One of the most important conclusions of this study is that the chemical nature of thermally oxidized alumina films is similar to that of alumina films prepared via an O_2 plasma discharge. This allows direct comparison of studies employing these different fabrication techniques and demonstrates that alumina films grown in a plasma discharge may also be compared to commercial γ-alumina. For these reasons, IETS is especially suitable for studies modelling supported catalysts.

In the present study, IETS has been used to investigate the interactions of $Zr(BH_4)_4$ absorbed on Al_2O_3 with cyclohexene at moderate and high exposures over a wide range of temperatures. Previous papers have reported on the interaction of $Zr(BH_4)_4$ with the Al_2O_3 surface (7), the interactions of the adsorbed catalyst with D_2, D_2O, and H_2O (8) and with ethylene, propylene, and acetylene (9). In the latter study the vibrational spectra revealed polymer formation upon interaction with acetylene at elevated temperatures. This finding has provided additional impetus

for the study of the interactions of this unique catalytic system with cyclic hydrocarbons.

There are several reasons why $Zr(BH_4)_4$ was chosen for these studies. First, $Zr(BH_4)_4$ supported on Al_2O_3 is a known polymerization catalyst for olefins and has generated a great deal of commercial interest. Phillips Petroleum Co. holds a patent on supported $Zr(BH_4)_4$ (12). Imperial Chemical Industries (ICI) is very active in this area and holds a number of patents (13-15) on zirconium, chromium, and titanium alkyl catalysts supported on γ-Al_2O_3. Dupont de Nemours and Company has also been active in studying this and related catalysts (16,17). The catalytic properties of $Zr(BH_4)_4$ supported on Al_2O_3 and SiO_2 have been studied also by Nesterov et al. at the Institute of Catalysis in Novosibirsk (18).

$Zr(BH_4)_4$ is especially suited for IETS studies because of its high vapor pressure as compared to other similar catalysts such as the zirconium alkyls. This allows for easy introduction of the catalyst into the bell jar. Of more importance though is the presence of the borohydride ligands as compared to alkyl ligands. These ligands serve as a very sensitive source of information regarding the structure of the supported catalyst because their vibrational frequencies are well separated from other frequencies observed for the supported catalyst. In contrast, the vibrational spectrum of an adsorbed zirconium alkyl catalyst interacting with a hydrocarbon adsorbate would not allow for separation of the vibrations arising from the ligands and those due to the adsorbate.

$Zr(BH_4)_4$ adsorbed on γ-alumina has been demonstrated to be an active catalyst for the polymerization of ethylene (16,18) and previous IETS studies indicated that it also readily polymerized acetylene (9). Since adsorption of the homogeneous catalyst onto a solid support imparts a significant increase in stability, we were interested in investigating the chemistry of this supported catalyst with cyclic hydrocarbons in order to probe the difference in reactivity and selectivity between the non-supported and the supported catalyst.

The polymerization of cyclic olefins has been the subject of a continuing research effort for many years. Cyclic olefins may polymerize either by ring-opening polymerization resulting in straight-chain hydrocarbon polymers or by homopolymerization in which the cyclic structures remain intact. The polymer product and yield depend on the catalyst, reaction conditions and monomer. In traditional catalytic polymerization systems, cyclohexene has been found to be quite unreactive. In general, ring-opening polymerization is favored for smaller rings where the ring strain is more severe than in cyclohexene. Ring-opening polymerization of cyclohexene does not occur with polymerization catalysts such as $AlBr_3$-WCl_6 (19), although a very low rate of conversion was found with WCl_6 alone (20). Several studies with cyclohexene have shown that it does not form stereoregular polymers upon ring-opening (21).

Homopolymerization of cyclohexene to form polymers with intact C_6 rings has never been achieved with a traditional Ziegler-Natta polymerization catalyst. However, under conditions of high temperature and pressure, cyclic olefins including cyclohexene, as well as internal ole-

fins, have been shown to polymerize (22). The device used was an anvil where pressures up to 65000 atm (65 kbars) and temperatures up to 500°C were produced. The 1,2-addition polymerization was found to occur at 300°C and 65000 atm and was the first reported addition polymer of cyclohexene.

There has been only one reported homopolymerization of cyclohexene under mild conditions (23). This was accomplished using a $Re(CO)_5Cl$ catalyst with an $EtAlCl_2$ co-catalyst at 110°C. This system is a known catalyst for the metathesis of internal and terminal olefins. The cyclohexene homopolymer appears to be a totally saturated polymer made up of either 1,2-cyclohexene units or 1,2-, 1,3-, and/or 1,4- repeating units.

The present study demonstrates that IETS can be used to investigate and identify novel reactions in a supported catalytic system. The vibrational information provided by this study of the pressure and temperature-dependent interactions of cyclohexene with $Zr(BH_4)_4$ adsorbed on Al_2O_3 complements recent studies in catalysis which have been designed to identify reaction intermediates as well as the chemical species which are the true catalysts involved in the basic processes of molecular complexation, addition and elimination reactions.

2.0 Experimental

Inelastic electron tunneling spectroscopy (IETS) is an effective means of monitoring the vibrational modes of molecules adsorbed on or near insulating surfaces. The IETS procedure involves monitoring the current due to electrons tunneling inelastically through a thin insu-

lating barrier between two electrodes. While most of the tunneling current arises from electrons tunneling elastically, some electrons may tunnel inelastically by exciting the vibrational modes of the adsorbates. Inelastic transitions occur only when the bias voltage across the barrier is greater than or equal to a vibrational activation energy. These transitions result in an increase in conductance across the barrier by providing additional channels for electron tunneling. The conductance increases are observed as peaks when d^2V/dI^2, proportional to d^2I/dV^2, is plotted as a function of the bias voltage, V. Peak positions correspond to vibration frequencies. Both infrared and Raman modes are observed in IET spectra. Additional details on the interpretation of IET spectra are available elsewhere (24).

The IET junctions used in this study were prepared in an oil diffusion-pumped bell jar with a base pressure of 5×10^{-8} Torr. Before beginning an experiment, an oxygen plasma discharge was run to help clean the system of hydrocarbons (25). The oxidation voltage was -1000 V, the O_2 pressure was 150 microns and the oxidation time was 1000 seconds. Aluminum strips approximately 800 Å in thickness were evaporated onto Corning 7059 borosilicate glass slides. Film thicknesses were monitored using a quartz crystal microbalance. After evaporation, the aluminum strips were annealed in vacuum by heating them to 520 K for at least 10 minutes. The technique developed by Bowser and Weinberg (26) for simultaneous heating and temperature measurement was used for all heating operations. The annealing step is necessary to preserve the integrity of the thin oxide barriers during subsequent heating operations. After an-

nealing, the thin oxide barriers are formed by oxidizing the aluminum strips in a plasma discharge of O_2 containing a trace of H_2O vapor. The oxidation voltage was -1000 V, the O_2 pressure was 150 microns and the oxidation times varied between 350 and 800 seconds depending on the adsorbate exposure and temperature to be studied. The oxide formed in this manner is between 20 and 25 Å in thickness.

After the oxidation the $Zr(BH_4)_4$ complex was adsorbed onto the oxide surfaces by exposing the samples to 5×10^{-2} Torr of $Zr(BH_4)_4$ for 15 minutes, corresponding to a saturation coverage (7). This produced the supported catalyst. After the excess was evacuated from the bell jar, cyclohexene vapor was introduced into the bell jar and allowed to interact with the samples. Exposures ranged from 1.5×10^{-1} Torr to 5 Torr for 1000 to 1200 seconds. In some experiments, the samples were heated after the cyclohexene had been introduced into the bell jar. Temperatures ranged from 298 K to 623 K. In some experiments, the samples were not exposed to the catalyst and the oxide was allowed to interact with the cyclohexene alone. After the desired period of time had elapsed, heating was discontinued and the cyclohexene was evacuated from the bell jar.

After the bell jar was evacuated to a pressure below 1×10^{-6} Torr, Pb cross strips were evaporated onto the samples. The glass slides were then removed from the bell jar and mounted onto holders used to measure their spectra while immersed in liquid helium. Before the spectra were recorded, the resistance value of each junction was recorded.

Spectral measurements were recorded with PDP 11/10 digitally-controlled electronics (27). Measurements were carried out over the spectral range of 240 to 4000 cm^{-1} using multiple scan averaging. The recorded data were then smoothed, the sloped background was subtracted, peaks were located and peak energies assigned after correcting for the Pb superconducting band gap and for modulation effects (28). Spectra were originally recorded in two sections, from 240 to 2240 cm^{-1} and from 2000 to 4000 cm^{-1}. The two halves of the spectra were then matched and the y-values were scaled using the modulation voltages at which the spectra were recorded. It should be noted that the y-values were further scaled relative to the most intense feature in the spectrum (usually the hydrocarbon stretching peak near 2830 cm^{-1}) in order to fit the spectra onto the graph.

3.0 Results

3.1 General Observations

Spectral measurements of junctions of $Zr(BH_4)_4$ adsorbed on Al_2O_3 exposed to cyclohexene at exposures of 150 Torr s (1.50×10^{-1} Torr for 1000 seconds), 1200 Torr s (1 Torr for 1200 seconds), and 6000 Torr s (5 Torr for 1200 seconds) are shown in Figures 1, 2, and 3 respectively. Substrate temperatures in these figures range from 298 to 623 K.

One of the most striking features of the cyclohexene system as contrasted with previous studies with ethylene and propylene (9) is that there is no apparent saturation coverage of cyclohexene. With ethylene and propylene, saturation coverages were obtained at all temperatures

with exposures of 3×10^3 Torr s as judged by the lack of any further spectral changes with increasing exposure. Additionally, no reproducible shifts in peak positions were observed as a function of coverage. The cyclohexene system is quite different. First of all, no apparent saturation coverage was reached with cyclohexene, even up to exposures of 6000 Torr s. At all exposures studied, increases in temperature were accompanied by significant increases in cyclohexene adsorption as judged by further increases in hydrocarbon peak intensity. With either increasing exposure or substrate temperature, a number of highly reproducible shifts in peak position as well as substantial increases in peak intensity were observed.

Further evidence of the lack of a saturation limit is provided by the resistances of the junctions. Hydrocarbon concentrations can be monitored qualitatively by measuring the resistance of the insulating barrier consisting of the aluminum oxide plus adsorbed species. Junctions producing the best spectra fall in the 30-200 Ω range (for an area of approximately 1 mm^2), because these exhibit the best signal/noise ratios with our electronics. The thickness of the oxide layer can be controlled by varying the length of time of the O_2 plasma discharge. The resistance of the samples can thus be adjusted in an attempt to provide a resistance value in the desired range. In the case of cyclohexene however, there was no limit to the junction resistance that could be obtained when increasing the cyclohexene exposure and/or substrate temperature. In all cases, increases in the cyclohexene exposure correlated with increases in the spectral intensity of key hydrocarbon features as

well as increases in the resistance of the junctions. Resistance values ranged from under 20 Ω for 150 Torr s and 298 K to well over 600 Ω at the highest exposures and temperatures studied. The highest resistance junctions which were able to be measured were between 350 and 400 Ω.

The lack of any apparent saturation limit for cyclohexene is similar to the behavior found when acetylene was the adsorbate (9). In this case, the concentration of hydrocarbon species on the surface increased with no apparent saturation limit at temperatures above 400 K at exposures of 300 Torr s.

The major changes observed in peak position and intensity as a function of cyclohexene exposure and substrate temperature will be discussed below. Figures 4 through 9 show spectra with labelled peak positions. Figure 4 shows the results obtained at 298 K for 150, 1200 and 6000 Torr s cyclohexene exposures. Figure 5 shows the results at 348 K, Figure 6 the results at 403 K, Figure 7 the results at 473 K, and Figure 8 the results at 523 K for all three exposures studied. Figure 9 shows the results obtained at 623 K for the 150 and 6000 Torr s exposures.

3.2 150 Torr s at 298 K

Figure 4, spectrum (A) shows the results obtained at 150 Torr s and 298 K. Peak positions are listed in Table 1. In the upper half of the spectrum, there are two well-resolved very intense features in the 2100-2300 and 2400-2600 cm^{-1} regions with maxima at 2232, 2289, 2493, 2525, and 2562 cm^{-1}. In the 2800-3100 cm^{-1} region, major features are located at 2927 and 3008 cm^{-1} and there appears to be two unresolved shoulders on

the high energy side of the 3008 cm^{-1} peak. A broad feature is located at 3743 cm^{-1}.

The lower half of the spectrum contains a number of peaks. The most intense feature is located at 933 cm^{-1}. The asymmetry of this feature indicates that there is an unresolved shoulder on the high energy side of this peak. In the 1000-1500 cm^{-1} region, there are features located at 1055, 1096, 1134, 1202, 1247, 1293, 1425 and 1494 cm^{-1}. The feature at 1425 cm^{-1} is broad and rounded and has at least one shoulder located near 1360-1370 cm^{-1}. There is also a small broad feature which is not well resolved near 1600 cm^{-1}. Below the 933 cm^{-1} peak, there are two peaks located at 266 and 302 cm^{-1} and a rounded feature exhibiting maxima at 698 and 720 cm^{-1}.

3.3 150 Torr s at 348 K

Figure 5, spectrum (A) shows the results obtained at 348 K. Peak positions are listed in Table 1. A comparison of the results obtained at 348 K with those obtained at 298 K shows that a number of changes in peak position and intensity have occurred.

In the upper half of the spectrum, there is a rounded feature with maxima at 2210 and 2270 cm^{-1} and another intense feature with maxima at 2480, 2510 and 2542 cm^{-1}. In the 2800-3100 cm^{-1} region, there are two main features at 2904 and 2982 cm^{-1} with two unresolved shoulders on the high energy side of the 2982 cm^{-1} feature. A broad, round peak is located near 3730 cm^{-1} and a partially resolved peak is observed at 3613 cm^{-1}.

In the lower half of the spectrum the most intense feature is located at 924 cm^{-1}. This displays the same asymmetry shown in the 298 K spectrum. Features in the 1000-1500 cm^{-1} region occur at 1052, 1083, 1123, 1189, 1230, 1283, 1410 and 1480 cm^{-1}. As at 298 K, the feature at 1410 cm^{-1} is a rounded, broad feature with significant intensity in the 1350-1400 cm^{-1} region. Below the 924 cm^{-1} peak, there are features at 262, 295, 502 and 707 cm^{-1}. As observed in the 298 K spectrum, there is also a broad unresolved feature at approximately 1600 cm^{-1}.

One of the most significant differences between the 298 and 348 K results is the reduced intensity of the features in the 2100-2300 and 2400-2600 cm^{-1} regions. These features are reduced approximately 50% in intensity. The 2800-3100 cm^{-1} region has also changed. First, there is a loss of intensity in the highest energy feature located at 3008 cm^{-1} at 298 K. This broad asymmetric peak has decreased in intensity so that the maximum at 348 K has shifted to 2982 cm^{-1}. The two unresolved shoulders are also decreased in intensity. The feature located at 2926 cm^{-1} at 298 K has also lost intensity so that its maximum is observed at approximately 2904 cm^{-1} at 348 K.

Other changes have occurred in the lower half of the spectrum. The peak found at 266 cm^{-1} at 298 K has shifted to 262 cm^{-1} and is slightly more intense than the adjacent peak at 295 cm^{-1}. The broad feature with maxima at 694 and 720 cm^{-1} at 298 K appears to have a sharper more intense profile at 348 K. There is a small feature found at 502 cm^{-1} which was unresolved at 298 K.

In the 1000-1500 cm^{-1} region, the 1055 cm^{-1} peak seems to be reduced in intensity because it appears as a rounded shoulder on the 1083 cm^{-1} peak. However, this may be an illusion since the peak located at 1096 cm^{-1} at 298 K has increased in intensity and at 348 K has a well-resolved maximum at 1083 cm^{-1} which partially overlaps the feature at 1055 cm^{-1}. The relative intensities of most of the other features in the 1000-1500 cm^{-1} region appear relatively unchanged at 348 K as compared to 298 K.

3.4 150 Torr s at 403 K

Figure 6, spectrum (A) shows the results obtained at 403 K. Peak positions are shown in Table 1. In the upper region of the spectrum, the features located in the 2100-2300 and 2400-2600 cm^{-1} regions are greatly reduced in intensity compared to 298 K and 348 K. At 403 K, there are two rounded features observed at approximately 2172-2210 cm^{-1} and 2260-2285 cm^{-1}. The intense peak with maxima at 2480, 2510 and 2542 cm^{-1} observed at 348 K is greatly reduced in intensity at 403 K and the band shape is considerably different. At 403 K this feature is a rounded, broad peak with partially resolved maxima at 2458 and 2500 cm^{-1}. Of special interest is the great loss in intensity above 2500 cm^{-1} as compared to the lower temperature spectra. This feature no longer has the skewed bimodal appearance which it had at 298 and 348 K.

The 2800-3100 cm^{-1} region has two main peaks at 2896 and approximately 2965 cm^{-1}. The 2965 cm^{-1} peak has maxima at 2957 and 2983 cm^{-1}. These features are considerably more intense than the peaks found in this region at 348 K. The broad feature located at 3730 cm^{-1} at 348 K has

shifted in position so that the maximum of this broad feature is located at approximately 3717 cm^{-1}. An increase in intensity between 3600-3700 cm^{-1} is also evident and partially resolved features are observed at 3613 and 3649 cm^{-1}.

The most intense feature in the lower half of the spectrum is observed at 922 cm^{-1}. Compared to the feature observed at 924 cm^{-1} at 348 K, the 922 cm^{-1} feature is broadened at the top. The 1000-1500 cm^{-1} region has changed considerably. At 403 K features are observed at 1076, 1114, 1189, 1229, 1283, 1399 and 1474 cm^{-1}. When the spectra observed at 348 and 403 K are compared, the peak intensity of the features located between 1000-1320 cm^{-1} is decreased at 403 K with the greatest loss in the 1114 cm^{-1} peak and the least reduction in the 1052 cm^{-1} peak. The features at 1399 and 1474 cm^{-1} have increased in intensity relative to those observed at 348 K. In particular, the 1399 cm^{-1} feature has an increase in intensity between 1350-1399 cm^{-1}. The 1474 cm^{-1} feature has increased considerably and broadened at the base as compared to the 1480 cm^{-1} peak observed at 348 K. At 403 K there is also a broad, rounded feature at approximately 1600 cm^{-1} as was observed in the 298 and 348 K spectra.

Additional features at 403 K are located at 264 and 299 cm^{-1}. Two unresolved features are evident between 400-500 cm^{-1}. The broad peak located at approximately 720 cm^{-1} has increased in intensity and has two small resolved maxima at 708 and 732 cm^{-1}.

3.5 150 Torr s at 473 K

Figure 7, spectrum (A) shows the results obtained at 473 K and peak positions are listed in Table 1. In the upper half of the spectrum, weak features are located at 2166, 2196, 2244 and 2281 cm^{-1} and a broad intense feature is centered at 2465 cm^{-1}. The maxima at 2458 and 2500 cm^{-1} observed at 403 K are not resolved at 473 K. The 2465 cm^{-1} feature, as well as those in the 2100-2300 cm^{-1} region, are significantly reduced in intensity.

In the 2800-3100 cm^{-1} region, there are two main features at 2879 and 2931 cm^{-1} which are of nearly equal intensity. The 2931 cm^{-1} peak is broader than that at 2879 cm^{-1} and several unresolved features are evident on the high energy side of this peak. The feature at 3706 cm^{-1} is broader and less intense than that observed in the lower temperature spectra and has shifted to a lower energy.

In the 1000-1500 cm^{-1} region, peaks are resolved at 1068, 1106, 1184, 1226, 1279, 1391 and 1464 cm^{-1}. A rounded feature is also observed in the 1580-1620 cm^{-1} area. As observed at lower temperatures, the 1391 cm^{-1} peak has considerable intensity in the 1340-1380 cm^{-1} region. The features resolved at 1068 and 1106 cm^{-1} form part of a broad band ranging from 1040-1140 cm^{-1}. Compared to the results at 403 K, the 1068 cm^{-1} peak is considerably reduced in intensity at 473 K.

The asymmetric peak at 919 cm^{-1} is the most intense feature in the spectrum. Features are observed also at 266, 301, 502, and 712 cm^{-1} and correspond to those seen at 403 K. The 502 cm^{-1} peak is more intense

than that observed at lower temperatures. Several new features are resolved at 473 K including peaks at 443, 552, 564 and 808 cm^{-1}. The slope of the 500-800 cm^{-1} region indicates that this region is considerably more intense than that observed at lower temperatures.

3.6 150 Torr s at 523 K

Results obtained for a 150 Torr s exposure of cyclohexene at a substrate temperature of 523 K are shown in Figure 8, spectrum (A). Table 1 lists the peak positions observed at this temperature.

The 2100-2300 cm^{-1} region has only very weak features with one small partially resolved peak at 2280 cm^{-1}. The 2400-2600 cm^{-1} region resembles that seen at 473 K; there is only one broad, rounded feature centered at approximately 2460-2470 cm^{-1}. This feature appears to be approximately as intense at 523 K as that observed at 473 K. The 2100-2300 cm^{-1} region shows a slight reduction in intensity at 523 K.

The 2800-3100 cm^{-1} region shows a number of changes in peak position and intensity at 523 K. The most intense feature in this area is now at 2898 cm^{-1}. The broad band at 2931 cm^{-1} observed at 473 K is considerably reduced in intensity at 523 K and two features are resolved, one at 2944 cm^{-1} and a less intense shoulder at 2978 cm^{-1}. The 3702 cm^{-1} feature observed at 473 K appears to be less well-resolved and somewhat less intense at 523 K.

In the 1000-1500 cm^{1} region, there is a broad band at 1050-1150 cm^{-1} with a maximum at 1123 cm^{-1}. The 1068 cm^{-1} feature which was well-

resolved at 473 K is no longer evident at 523 K. Other features in this region are located at 1079, 1190, 1232, 1287, 1392 and 1474 cm^{-1}. The 1392 cm^{-1} feature is a broad peak similar to that observed at 473 K. As in the lower temperature spectra, there is a weak, rounded peak located at approximately 1600 cm^{-1}. Compared to the 473 K spectrum, this feature appears to be somewhat reduced in intensity at 523 K.

As in the lower temperature results, the most intense spectral feature is the peak located at 924 cm^{-1} at 523 K. Other features are at 263, 299, 440, 502 and 555 cm^{-1}. The broad round feature at 707 cm^{-1} is similar to that observed at 473 K. The 808 cm^{-1} shoulder on the 924 cm^{-1} peak which was first resolved at 473 K is also resolved in the 523 K spectrum with a maximum at approximately 804 cm^{-1}.

3.7 150 Torr s at 623 K

The results obtained at 623 K are shown in Figure 9 spectrum (A) and peak positions are listed in Table 1.

In the upper portion of the spectrum, there are no resolved features in the 2100-2300 cm^{-1} region and only a small change in slope indicates that there is any remaining intensity in this region. The broad, round feature observed in the 523 K results at 2465 cm^{-1} is present also at 623 K. A close comparison of the two features indicates that the 623 K peak is in fact broader than the 523 K feature and the additional intensity is on the low energy side of this peak.

The 2800-3100 cm^{-1} region features are quite different than the features observed at lower temperatures. First, there is a sharp, intense peak located at 2852 cm^{-1} which is not observed in the lower temperature spectra. This new feature is the most intense feature in this region. A second maximum is located at 2898 cm^{-1} and there is an unresolved shoulder on the high energy side of this peak located at approximately 2940 cm^{-1}. The feature at 2981 cm^{-1} which is resolved at 523 K is not observed at 623 K and the results indicate that there is a considerable reduction in intensity of the higher energy features which are observed in this region at lower temperatures. The 3706 cm^{-1} feature observed at 523 K is less intense and downshifted to approximately 3648 cm^{-1} at 623 K.

The 1000-1500 cm^{-1} region is different than that observed at 523 K. Major features are located at 1040, 1100, 1178, 1216, 1270, 1351, 1376 and 1452 cm^{-1}. A careful comparison of the 523 and 623 K results indicates that the following changes have occurred. First, the 1474 cm^{-1} peak observed at 523 K has downshifted to 1452 cm^{-1} and increased in intensity. The broad band containing maxima at 1385 and 1396 cm^{-1} at 523 K has a shifted profile at 623 K; the 1396 cm^{-1} feature is reduced, the 1380-85 cm^{-1} peak is of approximately the same intensity, and the sloping 1350 cm^{-1} region observed at 523 K has resolved into a new feature at 1351 cm^{-1}. The 1287 cm^{-1} feature observed at 523 K is a considerably more intense feature observed at 1270 cm^{-1} at 623 K. The 1050-1150 cm^{-1} region appears as a broad band with a couple of resolved maxima in the lower temperature spectra. At 623 K, there appear to be

two main features in this region: a small but well-resolved peak at 1040 cm^{-1} and a broader, more intense, asymmetric feature with a maximum at 1100 cm^{-1}. A comparison of the spectra indicates a loss of intensity at 1079 cm^{-1}, an increase at 1100 cm^{-1}, a loss at 1140-1160 cm^{-1} and little or no change in intensity at 1122 cm^{-1}. The remaining features are observed at 1190 and 1231 cm^{-1} at 523 K. At 623 K, these features have shifted. The 1190 cm^{-1} peak appears to be nearly as intense at 623 K as at 523 K but has broadened so that the maximum intensity occurs at 1178 cm^{-1} at 623 K. The 1231 cm^{-1} feature at 523 K appears to be as intense at 623 K but an adjacent feature at 1216 cm^{-1} has grown in so that the 1231 cm^{-1} peak appears as a shoulder on the more intense 1216 cm^{-1} peak. The broad feature observed in the 1580-1620 cm^{-1} region in the lower temperature spectra is also observed at 623 K although it is less intense, especially in the 1600-1620 cm^{-1} region.

The intense feature observed at 923 cm^{-1} at 523 K is observed at 909 cm^{-1} at 623 K. Additional features are observed at 257, 295, 439, 499, 541, 698 and 807 cm^{-1}. The 439 and 499 cm^{-1} features show small increases in intensity but the 541 cm^{-1} feature is of approximately the same magnitude as that observed at 523 K. The rounded feature observed at 710 cm^{-1} in the lower temperature results is of approximately the same intensity at 623 K. However, there appears to be a decrease in the 736 cm^{-1} region of this feature so that at 623 K the peak is less broad than at 523 K and the maximum intensity is at 698 cm^{-1}. The 807 cm^{-1} feature appears to be equal in intensity to the feature observed at lower temperatures.

The changes in peak position and intensity which occur at 623 K as compared to 523 K may be ranked as follows: the greatest increases in intensity occur at 2852 > 2898 > 1452 ≥ 1270 > 1351 > 1100 ≥ 439 > 499 cm^{-1}. The greatest losses in intensity may be ranked as well: 2981 > 1474 > 1390 > 1140 > 1079 > 736 ≥ 1620 cm^{-1}.

3.8 1200 Torr s at 298 K

The results obtained at 1200 Torr s are shown in Figure 4 spectrum (B) and peak positions are listed in Table 2.

The 2100-2300 and 2400-2600 cm^{-1} regions resemble those seen at 150 Torr s at 298 K although there is less intensity at 1200 Torr s. The bimodal feature in the 2100-2300 cm^{-1} region has maxima at 2175 and 2243 cm^{-1}. The large intense feature in the 2400-2600 cm^{-1} region has maxima at 2441, 2466, 2508 and 2524 cm^{-1}. The 2800-3100 cm^{-1} region also is similar to that observed at 150 Torr s. There are two main features: a narrow feature at 2872 cm^{-1} and a broader band with a maximum at 2951 cm^{-1}. There are two unresolved shoulders which are evident on the high energy side of the 2951 cm^{-1} peak, occurring at approximately 3008 cm^{-1} and 3050 cm^{-1}. There is also a shoulder at approximately 2925 cm^{-1}. There is a broad feature at 3689 cm^{-1} which is approximately as intense as the feature at 150 Torr s.

The 1000-1500 cm^{-1} region has peaks at 1041, 1075, 1109, 1179, 1221, 1271, 1364, 1395 and 1464 cm^{-1}. A rounded, weak feature is observed in the 1580-1620 cm^{-1} region, similar to that at 150 Torr s. The 915 cm^{-1} feature is the most intense in the spectrum. Additional peaks are

resolved at 257, 296, 495, 549, 601, 695 and a weak shoulder on the 915 cm^{-1} peak is barely visible near 800 cm^{-1}. Compared to the 150 Torr s results, several new features are resolved at 1200 Torr s, including the 495, 549 and 800 cm^{-1} features. The most dramatic change though is the reduction in intensity of the 2100-2300 and 2400-2600 cm^{-1} regions, as well as the loss of intensity at 3008 cm^{-1}.

3.9 1200 Torr s at 348 K

The results obtained at 348 K are shown in Figure 5 spectrum (B) and peak positions are listed in Table 2.

The 2100-2300 cm^{-1} region has several maxima superimposed on a broad background. The bimodal appearance of this region which was well-defined at both 1200 and 150 Torr s at 298 K is less obvious at 1200 Torr s at 348 K. Peaks are resolved at 2153, 2177, 2207 and 2227 cm^{-1}. The 2400-2600 cm^{-1} region has features resolved at 2422, 2449 and 2492 cm^{-1}. A comparison to the results at 1200 Torr s at 298 K shows that the 2400-2600 cm^{-1} region is reduced in intensity at 348 K, especially above 2500 cm^{-1}. The 2800-3100 cm^{-1} region has maxima at 2848 and 2925 cm^{-1}, and as before, the 2925 cm^{-1} feature is broad and asymmetric with at least two high energy shoulders visible at approximately 2980 and 3026 cm^{-1}. The 2800-3100 cm^{-1} features are more intense than those observed at 298 K. There is a broad, rounded feature centered at approximately 3655 cm^{-1} which appears to be of the same magnitude as that observed at 1200 Torr s at 298 K.

The most intense feature in the spectrum is the asymmetric band with a maximum at 908 cm^{-1}. The 1000-1500 cm^{-1} region has maxima at 1040, 1063, 1103, 1168, 1208, 1232, 1260, 1357, 1389 and 1450 cm^{-1}. Compared to the results at 298 K, the 1103 cm^{-1} feature is reduced in intensity and the 1450 cm^{-1} peak is increased. As observed at 298 K, there is a broad, rounded peak at 1580-1620 cm^{-1}. Additional features are resolved at 257, 295, 498, 701, 725 and 798 cm^{-1}. There is also a small, unresolved peak at 400-430 cm^{-1} which is evident at 348 K but not at 298 K.

3.10 1200 Torr s at 403 K

The results obtained at 403 K are shown in Figure 6, spectrum (B) and the peak positions are listed in Table 2. Figure 10 shows the 240-2000 cm^{-1} region in more detail.

The 2100-2300 cm^{-1} region has several weak features at 2142, 2163, 2215, and 2234 cm^{-1}. There appears to be less separation between the 2100-2300 cm^{-1} and the 2400-2600 cm^{-1} features as compared to the results at lower temperatures. At 403 K, there is a large, rounded feature with maxima at 2356, 2410, 2455 and 2482 cm^{-1}. Compared to the results at either 298 or 348 K, the features in this region are considerably reduced in intensity at 403 K.

The 2800-3100 cm^{-1} region at 403 K no longer resembles the features seen at 298 or 348 K and is considerably more intense than any of the features observed at 150 Torr s or at lower temperatures at 1200 Torr s. A narrow, intense feature is observed at 2829 cm^{-1}. A second peak has a maximum at 2878 cm^{-1} with several partially-resolved shoulders evident at

approximately at 2925, 3002 and 3022 cm^{-1}.

The most intense feature in the spectrum is the feature at 2829 cm^{-1}. It appears from the spectrum that the 906 cm^{-1} feature, which was the most intense feature in all the results obtained at lower exposures and/or temperatures, is considerably reduced in intensity at 403 K. This is believed to be an artifact of the computer processing which first scales the two halves of the spectrum based on the sensitivities at which they were measured and then reduces all the y-values so that the most intense feature (in this case the 2829 cm^{-1} peak) will fit onto the computer plot of the spectrum. Virtually all of the major spectral features discussed in this results section will vary in position and intensity as a function of the cyclohexene exposure and as a function of the substrate temperature. The one spectral feature which is expected to undergo the least change in intensity is that due to the Al-O bulk stretch, found at approximately 945 cm^{-1}. In the results presented here, this feature appears as an unresolved shoulder on the more intense 910 cm^{-1} peak, but may still be used as an internal standard when comparing different spectra. Since the computer scaling causes the features in the 240-2000 cm^{-1} region to appear to be less well-resolved at 403 K than at lower temperatures and/or exposures, Figure 10 has been included to display the resolution which is actually obtained for this region.

In the 3600-3750 cm^{-1} region, there is a broad rounded feature centered at approximately 3645 cm^{-1}. Its intensity is analogous to that observed at 348 K.

In the 1000-1500 cm^{-1} region of the spectrum, there are peaks observed at 1032, 1057, 1094, 1168, 1198, 1257, 1339 and 1439 cm^{-1}. There is also a weak feature evident at 1580-1620 cm^{-1}. Compared to the results obtained at 348 K, a number of features are considerably more intense at 403 K. These include features at 1032, 1057, 1168, 1257, 1339 and 1439 cm^{-1}. These last three features display the largest increases in intensity.

Additional features are resolved at 251, 301, 333, 359, 402, 433, 498, 659, 695, 729 and 787 cm^{-1}. Of these, the peaks at 333, 359, 402, 433 and 787 cm^{-1} are new features which were not resolved at 348 K. The largest increases in intensity are observed at 333, 359, 402, 433, 498 and 787 cm^{-1}. The features in the 650-730 cm^{-1} region appear to be approximately as intense as features observed in this region at 348 K.

3.11 1200 Torr s at 473 K

The results obtained for a 1200 Torr s exposure of cyclohexene at a substrate temperature of 473 K are shown in Figure 7, spectrum (B). The 240-2000 cm^{-1} region is shown as well in Figure 11. Peak positions are listed in Table 2.

The 2100-2300 cm^{-1} region at 473 K is considerably reduced in intensity compared to the 403 K results. There are very weak features evident at 2177 and 2231 cm^{-1}. Between 2400-2600 cm^{-1}, there is a broad weak feature with maxima at 2441 and 2487 cm^{-1} which is considerably less intense than the features observed at 403 K. The 2800-3100 cm^{-1} region resembles that observed at 403 K. The most intense spectral feature is

the narrow peak at 2826 cm^{-1}. A second feature is observed at 2871 cm^{-1} and weak shoulders are located at 3004 and 3020 cm^{-1}. A new, weak feature at 2656 cm^{-1} is also resolved at 473 K which was not evident at lower temperatures. The broad feature seen at 3645 cm^{-1} at 403 K is centered at 3640 cm^{-1} at 473 K and is reduced in intensity compared to the results obtained at lower temperatures.

A comparison of the 403 and 473 K results obtained at 1200 Torr s shows that the 240-2000 cm^{-1} features appear to be reduced in intensity at 473 K as compared to 403 K. Keeping in mind the effects of the computer processing on the data, this indicates that at 473 K there is an increase in the adsorption of cyclohexene as based on the intensity of several features, especially those in the 2800-3100 cm^{-1}.

The 1000-1500 cm^{-1} region has features located at 1030, 1083, 1134, 1167, 1203, 1257, 1337 and 1436 cm^{-1}. There is also a weak feature resolved at 1602 cm^{-1} in the 1580-1620 cm^{-1} region. A comparison of the 403 and 473 K results shows that the greatest increases in intensity are observed at 1436, 1337, 1257 and 1203 cm^{-1}. There is a decrease in the feature at 1057 cm^{-1} and in the 1134 cm^{-1} region.

In the low energy region of the spectrum, features are located at 251, 294, 332, 401, 433, 488, 553, 623, 677, 698, 712,785, and 902 cm^{-1}. This region appears to be more intense than that observed at 403 K and the 433, 488 and 785 cm^{-1} features in particular appear to be more intense at 473 K than at 403 K.

3.12 1200 Torr s at 523 K

The results obtained at 523 K are shown in Figure 9, spectrum (B) and in Figure 12. Peak positions are listed in Table 2.

At 523 K, there appears to be little or no intensity remaining in the 2100-2300 cm^{-1} region. The 2400-2600 cm^{-1} region has a broad, rounded feature with maxima at 2396, 2427 and 2458 cm^{-1}. As at 473 K, there is a small peak at 2651 cm^{-1}. In the 2800-3100 cm^{-1} region, there are two features at 2826 and 2873 cm^{-1}. The asymmetry of the 2873 cm^{-1} feature indicates that there are unresolved features on the high energy side of this peak. The 3600-3750 cm^{-1} region has one broad weak feature with maxima at 3613 and 3642 cm^{-1}.

Compared to the 473 K results, the features in the lower half of the spectrum appear to be reduced at 523 K, indicating an increase in the relative intensity of the 2800-3100 cm^{-1} features. The features in the lower half of the spectrum are best displayed in Figure 12. In the 1000-1500 cm^{-1} region, features are observed at 1029, 1082, 1132, 1167, 1205, 1259, 1338 and 1438 cm^{-1}. There is also a weak feature present in the 1580-1620 cm^{-1} region which appears to be less intense than that observed at 473 K. The features at 1082, 1167, 1205, 1259, 1338 and 1438 cm^{-1} appear to be more intense at 523 K than at 473 K. In the lower portion of the spectrum, features are observed at 251, 297, 348, 402, 433, 489, 538, 699, 737, 787 and 907 cm^{-1}. The 907 cm^{-1} peak appears broadened relative to that observed at lower temperatures and a large unresolved shoulder is evident at approximately 850 cm^{-1}. The feature at 787 cm^{-1} appears to be slightly more intense at 523 K than at 473 K.

3.13 6000 Torr s at 298 K

The results obtained at 6000 Torr s and 298 K are shown in Figure 4, spectrum (C) and in Figure 13. Peak positions are listed in Table 3.

The 2100-2300 and 2400-2600 cm^{-1} regions resemble those seen at lower exposures although they are considerably reduced in intensity at 6000 Torr s. Features are resolved at approximately 2167 and 2213 cm^{-1}. The 2400-2600 cm^{-1} region has a large, broad feature with a well-resolved maximum at 2490 cm^{-1}. There is also a weak feature at 2660 cm^{-1} similar to that seen at 1200 Torr s at 473 and 523 K. The 2800-3100 cm^{-1} region is different than that observed at 1200 or 150 Torr s at 298 K. It does however resemble the features seen at 403 K and higher at 1200 Torr s. There is a very intense, narrow peak at 2835 cm^{-1} and a second feature with a maximum at 2882 cm^{-1} and a shoulder at 2912 cm^{-1}. In the 3600-3750 cm^{-1} region, a broad feature is centered at 3639 cm^{-1}.

As explained in section 3.10, the computer processing requires that all peaks be scaled relative to the most intense spectral feature, the peak at 2835 cm^{-1}. This creates the illusion that the other features, especially those in the 240-2000 cm^{-1} region, are less intense and less well-resolved than those observed at lower exposures. However, it is thought that the best choice for an internal standard is the shoulder visible near 945 cm^{-1}, corresponding to the bulk Al-O stretch. It should be kept in mind when reviewing the results at 6000 Torr s at all temperatures studied that the appearance of shrinking resolution in the 240-2000

cm^{-1} region is a result of the computer data analysis rather than reduced resolution at this high exposure.

The 240-2000 cm^{-1} region is shown in Figure 13. The 1000-1500 cm^{-1} region has features at 1033, 1065, 1091, 1166, 1202, 1259, 1345 and 1441 cm^{-1}. There is a broad weak feature at 1580-1620 cm^{-1}. Additional features are observed at 251, 292, 329, 408, 432, 487, 550, 689, 786 and 902 cm^{-1}. When these results are compared to those obtained at 1200 Torr s at 403, 473 and 523 K, that is, to the spectra which display the same intense features in the 2800-3100 cm^{-1} region, a number of similarities in peak position and in the relative intensities of certain features are observed. Most notable are those at 408, 432, 487, 786, 1259, 1345, 1441, 2835 and 2882 cm^{-1}.

3.14 6000 Torr s at 348 K

The results obtained for a 6000 Torr s exposure of cyclohexene at a substrate temperaure of 348 K are shown in Figure 5, spectrum (C) and in Figure 14. Table 3 lists the peak positions.

The 2100-2300 and 2400-2600 cm^{-1} regions are significantly less intense at 348 K than at 298 K. Peak positions are at 2110, 2152, 2190 and 2225 cm^{-1}. In the 2400-2600 cm^{-1} region there is a broad feature with maxima at 2440, 2439, 2467 and 2489 cm^{-1}. A weak feature is also resolved at 2660 cm^{-1}. The 2800-3100 cm^{-1} region resembles that seen at 298 K and at the three highest temperatures studied at 1200 Torr s. There is a narrow, intense feature at 2830 cm^{-1} and a broader, less intense peak at 2875 cm^{-1}. Compared to the 298 K results, which displayed

a shoulder at 2912 cm^{-1}, the 348 K results show a loss of intensity on the high energy side of the 2875 cm^{-1} feature. A weak feature is also resolved at 3020 cm^{-1}. A broad, rounded peak is centered at 3611 cm^{-1}.

The lower half of the spectrum is shown in Figure 14. Features in the 1000-1500 cm^{-1} region are observed at 1031, 1062, 1085, 1136, 1166, 1205, 1233, 1258, 1342 and 1439 cm^{-1}. Compared to results at 298 K, the peaks at 1258, 1342 and 1439 cm^{-1} are considerably more intense at 348 K. Much smaller increases in intensity are observed for the features at 1031, 1062, 1085 and 1166 cm^{-1}. Lower energy features are located at 251, 295, 331, 407, 435, 489, 552, 667, 689, 722, 784 and 903 cm^{-1}. The 903 cm^{-1} peak has an unresolved shoulder on the low energy side near 850 cm^{-1}. The relative intensities of these features are similar to those observed at 298 K. However, the 331 cm^{-1} peak seems slightly more intense as does the shoulder on the 903 cm^{-1} peak.

3.15 6000 Torr s at 403 K

Figure 6, spectrum (C) and Figure 15 show the results obtained at 403 K. Table 3 lists the peak positions.

The 2100-2300 cm^{-1} region is less intense than that observed at 348 K. Weak features are barely evident at 2152 and 2233 cm^{-1}. The 2400-2600 cm^{-1} feature is also reduced in intensity compared to that observed at 348 K and appears as a broad feature centered at 2455 cm^{-1}. A small feature is observed at 2657 cm^{-1}. The 2800-3100 cm^{-1} region resembles that seen at lower temperatures at 6000 Torr s as well as that observed at 403 K at 1200 Torr s. The most intense feature is at

2828 cm^{-1} and a second, broader feature is at 2873 cm^{-1}. A broad, weak feature is observed in the 3600-3750 cm^{-1} region at approximately 3626 cm^{-1}.

Features in the lower half of the spectrum are shown in Figure 15. In the 1000-1500 cm^{-1} region, bands are observed at 1031, 1061, 1085, 1132, 1165, 1198, 1258, 1341 and 1439 cm^{-1}. Compared to the 348 K results, the peaks at 1439, 1341, 1258 and at 1198 cm^{-1} have increased in magnitude at 403 K. The 1439 cm^{-1} peak is nearly as intense as the feature at 903 cm^{-1}. Additional features are observed at 251, 297, 334, 405, 433, 488, 550, 695, 785 and 850 cm^{-1}. The 850 cm^{-1} peak is resolved for the first time at 403 K although a shoulder was evident in this position at 298 and 348 K. Relative to the 348 K results, the features at 433, 488, 785 and 850 cm^{-1} have increased in intensity at 403 K. Similar to the results at lower temperatures, a broad, low intensity feature is observed at 1580-1620 cm^{-1} at 403 K.

3.16 6000 Torr s at 473 K

Spectrum (C) in Figure 7 shows the results obtained at 6000 Torr s at 473 K. The 240-2000 cm^{-1} region is also shown in Figure 16 and Table 3 lists the peak positions.

At 473 K, a number of changes in peak intensity and position have occurred relative to the 403 K results. There are no longer any discernible features in the 2100-2300 cm^{-1} region and only a very weak feature remains near 2465 cm^{-1}. The 2800-3100 cm^{-1} region has two main features at 2823 and 2869 cm^{-1}. A very small feature is also evident at

3024 cm^{-1}. In the 3600-3750 cm^{-1} region, there is no evidence of a broad, round feature as observed at lower temperatures. A small feature is also observed at 2654 cm^{-1}.

In the lower half of the spectrum, the 903 cm^{-1} feature is no longer the most intense feature in this region. Instead, the narrow, sharp feature at 1436 cm^{-1} is the most intense feature at 473 K. As explained previously in section 3.10, this implies that all the features in the lower portion of the spectrum have been scaled accordingly. Thus all the features in this region appear to be less well-resolved at 473 K than at 403 K. Figure 16, however, shows the resolution that was obtained at this temperature in better detail than can be seen in Figure 7.

In the 1000-1500 cm^{-1} region, peaks are resolved at 1027, 1061, 1079, 1133, 1168, 1197, 1256, 1338 and 1436 cm^{-1}. A number of changes in relative intensity are evident when compared to the 403 K results. First, the peak at 1436 cm^{-1} has increased dramatically in intensity as have the features at 1256 and 1338 cm^{-1}. At 403 K, the 1256 cm^{-1} feature was more intense than that at 1338 cm^{-1} but at 473 K the 1338 cm^{-1} feature is observed to be slightly more intense. The peaks at 1027 and 1078 cm^{-1} are also more intense at 473 K but the 1061 cm^{-1} peak resembles that seen at 403 K. The 1166 and 1197 cm^{-1} features are also more intense at 473 K. The weak feature observed between 1580-1620 cm^{-1} at lower temperatures is less well defined at 473 K although some intensity near 1600 cm^{-1} may remain.

In the lower region of the spectrum, peaks are resolved at 251, 313,

339, 411, 432, 486, 550, 703, 729, 781, 852, 885, 907, 954 and 990 cm^{-1}. Several of these features are not observed at lower temperatures and/or exposures including the peaks at 885, 954 and 990 cm^{-1}. Compared to the results obtained at 403 K, the peaks at 251, 339, 411, 432 and 486 cm^{-1} show the greatest increases in intensity at 473 K.

3.17 6000 Torr s at 523 K

Results obtained at 523 K are shown in Figure 8, spectrum (C) and in Figure 17. Table 3 lists the peak positions.

At 523 K there is a weak broad feature in the 2400-2600 cm^{-1} region centered at approximately 2465 cm^{-1}. A small feature is also observed at 2653 cm^{-1}. In the 2800-3100 cm^{-1} region, there are two main features at 2823 and 2869 cm^{-1}. A weak feature is also observed at 3041 cm^{-1}. There is no resolved feature in the 3600-3750 cm^{-1} region as seen at lower exposures and/or temperatures.

In the 1000-1500 cm^{-1} region, features are resolved at 1028, 1076, 1117, 1166, 1201, 1258, 1336 and 1435 cm^{-1}. The 1435 cm^{-1} peak is the most intense feature in the lower half of the spectrum. Compared to the 473 K results, several features in the spectrum are seen to be less intense at 523 K including the features at 1027, 1078 and 1133 cm^{-1}. There is little or no intensity in the 1580-1620 cm^{-1} region at 523 K.

Additional features are resolved at 251, 333, 407, 433, 489, 653, 694, 782, 850, 885 and 898 cm^{-1}. Shoulders on the 898 cm^{-1} peak are evident at 907, 950 and 990 cm^{-1}. Compared to the 473 K results, the

peak at 433 cm^{-1}, as well as the 550 and 729 cm^{-1} regions, is somewhat reduced in intensity at 523 K.

3.18 6000 Torr s at 623 K

The results obtained for a 6000 Torr s exposure of cyclohexene at 623 K are shown in Figure 9, spectrum (C) and also in Figure 18. The peak positions are listed in Table 3.

At 623 K, a slight change in slope of the background in the 2400-2600 cm^{-1} region indicates there is some residual intensity in this area. A weak feature at 2452 cm^{-1} is resolved. A peak is also observed at 2640 cm^{-1}. As at lower temperatures, two very intense features are observed in the 2800-3100 cm^{-1} region at 2819 and 2865 cm^{-1}. A very weak feature is observed at 2998 cm^{-1} as well. The 3600-3750 cm^{-1} region has no resolved features as observed at lower temperatures.

The 1000-1500 cm^{-1} region is shown in Figure 18. Features are observed at 1018, 1069, 1101, 1120, 1172, 1186, 1212, 1259, 1336 and 1434 cm^{-1}. In the lower energy region of the spectrum, features are observed at 251, 323, 335, 361, 407, 435, 489, 678, 782, 852, 875, 913, 955 and 994 cm^{-1}. Many of these features display relative intensities similar to those observed at 523 or 473 K. At 623 K however, there does seem to be a reduction in intensity of the feature located at 910 cm^{-1}.

3.19 Cyclohexene Adsorption on Al_2O_3

The adsorption of cyclohexene on Al_2O_3 without pre-treatment with $Zr(BH_4)_4$ was studied at several exposures and temperatures. The results

indicate that little cyclohexene adsorbs on the Al_2O_3 surface, even at 6000 Torr, the highest exposure studied.

Figure 19 shows the results obtained for a 6000 Torr s exposure of cyclohexene at 403 K. Features are located at 309, 459, 963, 1082, 2855, 2974, 3095 and 3726 cm^{-1}. Figure 20 shows the 2100-4000 cm^{-1} region in greater detail. Features are resolved at 2833, 2970, 3075 and 3096 cm^{-1}. A broad band with partially resolved maxima at 2872 and 2879 cm^{-1} is also evident. A very intense feature is also observed at 3725 cm^{-1}. Good quality spectra from junctions of cyclohexene adsorbed on Al_2O_3 were consistently difficult to obtain, a further indication of the low adsorption of cyclohexene under the conditions employed. The intensity of the features at 965 cm^{-1} and 3726 cm^{-1}, combined with the low intensity of the features in the 2800-3100 cm^{-1} region, indicate also that little cyclohexene is adsorbed on Al_2O_3 which has not been pre-treated with $Zr(BH_4)_4$.

4.0 Discussion

4.1 The Adsorption of $Zr(BH_4)_4$ on Al_2O_3

$Zr(BH_4)_4$ has been studied extensively by a number of techniques, including NMR (29, 30), IR (30-34), Raman (31-35), and photoelectron (36) spectroscopies, as well as by X-ray (37) and electron (38) diffraction. These studies have shown that the BH_4 ligands in $Zr(BH_4)_4$ are tetrahedrally arranged around the central zirconium atom. Each boron atom is bonded to the zirconium atom through three bridging hydrogens (designated H_b), leaving one terminal atom (H_t) in each BH_4 group. This type of tri-

dentate bonding is not found when one or more of the BH_4 ligands are replaced by other groups. For example, in $(C_5H_5)_2Zr(BH_4)_4$ the bonding between the boron atoms and the zirconium atom is bidentate, involving only two bridging hydrogens (39).

When $Zr(BH_4)_4$ is adsorbed onto the Al_2O_3 surface it loses one or more BH_4 ligands. The remaining BH_4 groups do not necessarily retain their tridentate structure and may become bidentate. Monodentate bonding of BH_4 ligands in zirconium complexes has not been demonstrated although Ballard (40) has presented the following scheme for the adsorption of $Zr(BH_4)_4$ on silica in which the bonding is through one bridging hydrogen atom only:

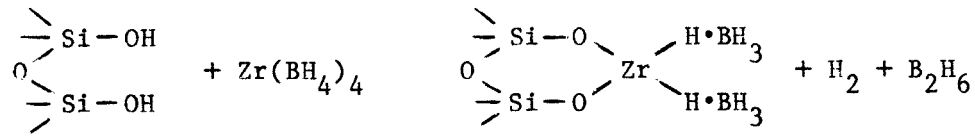

$Zr(BH_4)_4$ may also become either singly or multiply coordinated to the surface oxygen atoms as it adsorbs on the surface. Both of the following species have been shown to be formed when organozirconium complexes containing halogen ligands are adsorbed on silica (2, 3).

Similar results have been obtained with aluminum oxides (2). It has been reported also that the coordination state of Zr can change upon adsorption to yield Zr (II) and Zr (III) complexes in addition to the more

abundant Zr (IV) species (3, 41). H_2 studies of organozirconium compounds adsorbed on silica indicate that each zirconium atom retains on the average only 1.8 of its four original ligands (3).

As $Zr(BH_4)_4$ is adsorbed on the Al_2O_3 surface displaced BH_4 groups may coordinate to surface Al and O atoms instead of desorbing. Studies of diborane (B_2H_6) adsorption on Al_2O_3 have shown that the following surface complexes are formed (42):

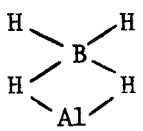

I

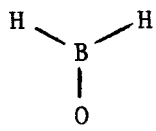

II

BH_4 groups displaced from the zirconium complexes may form similar structures. $Zr(BH_4)_4$ also decomposes slowly at room temperature to yield B_2H_6, another possible source for the above surface species (39). Species II would give rise to B-O vibrations.

Nesterov et al. (18) have studied the adsorption of $Zr(BH_4)_4$ on γ-Al_2O_3 and silica gel. The interaction of the Zr complex with both supports resulted in the evolution of hydrogen and diborane and the mole ratio of boron to zirconium on both supports was close to 3.0. Upon heating of the catalysts to 300°C, the mole ratio of boron to zirconium on SiO_2 was found to be 2.2 whereas for Al_2O_3 the ratio was 2.9. Considerably more hydrogen and diborane was found to be released by the silica-supported system than by the alumina-supported catalyst. The mole ratio of boron to zirconium includes contributions from zirconium com-

plexes singly bound to a surface oxygen, complexes of zirconium multiply bound to surface oxygen atoms, and boron-oxygen complexes formed by the evolution of BH_3 from the supported catalyst. The formation of boron-oxygen complexes was found to be characteristic of $Zr(BH_4)_4$ adsorbed on Al_2O_3 whereas diborane evolution was favored for $Zr(BH_4)_4$ adsorbed on SiO_2. The retention of the high boron content in Al_2O_3 may also be due to the formation of surface zirconium borides as shown below. When zirconium tetrahydroborate is thermally decomposed at temperatures of

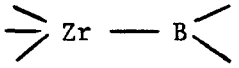

III

200-300°C, zirconium borides are formed (43).

4.2 Spectral Features Associated with Adsorbed $Zr(BH_4)_4$

Evans and Weinberg (7) have identified the vibrational features which result from the adsorption of $Zr(BH_4)_4$ on Al_2O_3. Figure 21 shows the IET spectrum of $Zr(BH_4)_4$ adsorbed on Al_2O_3 (7).

The BH_4 ligands in $Zr(BH_4)_4$ give rise to characteristic vibrations. The $B-H_b$ stretching region is located between 2100-2300 cm^{-1} and the $B-H_t$ stretching region between 2400-2600 cm^{-1}. Tridentate BH_4 ligands give rise to one terminal B-H stretch between 2560-2580 cm^{-1}. Bidentate BH_4 ligands give rise to two peaks, one asymmetric and one symmetric stretch at frequencies between 2350-2450 cm^{-1}. The number of features observed in the $B-H_b$ and $B-H_t$ regions in Figure 21 indicates that more than one type of surface specie is likely for adsorbed $Zr(BH_4)_4$.

Consistent with this is the assignment of features at 693 and 910 cm^{-1} to different types of Zr-O stretching modes. Zirconium complexes multiply coordinated to surface oxygen atoms would be expected to exhibit vibrational frequencies which are similar to those observed in bulk zirconium oxides or in thin zirconium oxide films. Depending on the method of preparation, these have been shown to exhibit a number of bands in the low frequency region (44). Collectively, these values are 730-750, 571, 513, 500, 483, 408 and 357 cm^{-1}, the band at 730-750 cm^{-1} being the most common. In complexes which have only one Zr-O bond or when one of the Zr-O bonds possesses slightly more double-bond character than others in the same complex, vibrational frequencies are expected between 900-1000 cm^{-1} (45). Consequently, Evans and Weinberg (7) have assigned the 693 cm^{-1} mode to stretching of multiply coordinated Zr atoms and the 910 cm^{-1} feature to stretching of singly coordinated Zr. They have also identified the unresolved features in the 480-580 cm^{-1} region as Zr-O modes and a Zr-BH_4 stretch. The peak near 260 cm^{-1} has been assigned as a BH_4-Zr-BH_4 bend or torsion and the 320 cm^{-1} feature has likewise been assigned to a $Zr(BH_4)_4$ torsion or a metal-oxide mode.

BH_4 deformation modes are expected between 1000-1400 cm^{-1}. B-O modes, resulting from dissociated BH_4 ligands which form complexes instead of desorbing, are expected in the 1200-1450 cm^{-1} region. In $Zr(BH_4)_4$ adsorbed an alumina, Evans and Weinberg (7) have identified the features at 1106-1130, 1173 and 1220 cm^{-1} as B-H deformations, the feature at 1260 cm^{-1} as a combination of a B-H and a B-O stretch, and features at 1378 and 1457 cm^{-1} as B-O modes. The small feature at 1030

cm^{-1} as well as the peak near 2930 cm^{-1} are due to contaminant hydrocarbon.

4.3 Cyclohexene Interactions with Supported $Zr(BH_4)_4$

An examination of the spectra presented in Figures 1 through 9 reveals that they can be classified into two types depending on the predominant spectral features observed. The first type (I) is formed at the lowest exposures and temperatures studied and the second type of spectra (II) is formed at the highest exposures and temperatures. In Table 4, a matrix of cyclohexene exposures versus substrate temperatures summarizes the primary type of spectra observed for each set of conditions.

Tentative spectral assignments will be discussed below for representative spectra of both types. Due to the inhomogeneity of the surface, several types of surface specie are expected to be formed at each set of reaction conditions studied. However, to simplify the discussion of the results it is useful to classify the spectra as representing primarily spectra type I or type II.

4.4 Type I

The first spectrum to be discussed in detail is that resulting from a cyclohexene exposure of 150 Torr s at 298 K shown in spectrum (A) Figure 4 and classified in Table 4 as a type I spectrum. A number of features may be readily assigned based on a comparison with undoped Al-Al_2O_3-Pb junctions (46). The feature located near 299 cm^{-1} is due to a phonon in the underlying Al film, the prominent shoulder near 945 cm^{-1}

corresponds to the bulk stretch of the aluminum oxide, the rounded feature near 1860 cm^{-1} is an overtone of the Al-O (bulk) stretch, and the broad feature located between 3600-3750 cm^{-1} is due to the stretch of surface hydroxyl groups.

The infrared stretching frequencies of various types of surface hydroxyl groups have been extensively characterized for both alumina and silica (47). Generally, peaks found above 3700 cm^{-1} correspond to vibrations of free hydroxyl groups while those in the 3600-3700 cm^{-1} region correspond to hydroxyl groups which are involved in hydrogen-bonding on the oxide surface. It has been noted also that adsorbed molecules perturb the surface hydroxyl groups resulting in a downward frequency shift of the O-H stretch, as well as a considerable broadening and decrease in intensity of this feature. At 150 Torr s and 298 K, the O-H stretch is centered at approximately 3743 cm^{-1}.

Based on the previous work of Evans and Weinberg (7), as well as vibrational studies of metal tetrahydroborates (30-35, 48), several of the most intense features in Figure 4 may be assigned as vibrations of the BH_4 ligands. In particular, the features between 2100-2300 cm^{-1}, located at 2232 and 2289 cm^{-1}, may be assigned to B-H_b stretching arising from BH_4 ligands which contain either two or three bridging hydrogens. The bands at 2493, 2525 and 2562 cm^{-1} may be assigned to B-H_t stretching. The broadness of these features, as well as the fact that there are several modes evident in the B-H_t stretching region indicates that several types of BH_4 ligands are present in the adsorbed catalyst. The bimodal nature of the features indicates the presence of bidentate bridge bond-

ing. However, tridentate BH_4 ligands exhibit B-H_t stretching between 2560-2580 cm^{-1} which correlates well with the sharp peak seen at 2562 cm^{-1}.

The features in the 2800-3100 cm^{-1} region correspond to C-H stretching vibrations of the adsorbed cyclohexene. There are two main features located at 2927 and 3008 cm^{-1}. The highest frequency band may be assigned to =C-H stretching since its position above 3000 cm^{-1} is indicative of unsaturated C-H stretching in non-conjugated olefins. Free cyclohexene exhibits two =C-H stretching frequencies above 3000 cm^{-1}. The highest of these is located near 3059-3067 cm^{-1} and has a weak to medium intensity whereas the second is a very strong peak located at 3021-3026 cm^{-1} (49). CH_2 stretching frequencies have been noted in cyclohexene to occur at 2993 (medium), 2960 (strong), 2940 (very strong), 2929 (very strong), 2898 (very strong), 2882 (very strong), 2860 (very strong) and 2840 cm^{-1} (very strong) (49, 50). All of these have been assigned to symmetric and antisymmetric CH_2 stretching. The peak at 2927 cm^{-1} in Figure 4 may therefore be assigned to CH_2 stretching.

The 933 cm^{-1} peak may be assigned to a Zr-O stretching mode corresponding to singly coordinated Zr atoms and the broad band with maxima at 698 and 720 cm^{-1} may be assigned to multiply coordinated Zr-O. The 266 cm^{-1} feature was assigned by Evans and Weinberg (7) to a BH_4-Zr-BH_4 bend or torsion. The 302 cm^{-1} feature may be assigned to the Al phonon.

Cyclohexene also exhibits a number of vibrations in the low frequency range (49-53). Ring deformation vibrations occur at 876, 810, 640 and 525 cm^{-1} and ring bending modes at 492 and 453 cm^{-1}. At higher

frequency, there is a strong CH_2 rocking mode at 917 cm^{-1} and a Raman active mode at 966 cm^{-1}. Kumar et al. (51) assigned the strong band at 719 cm^{-1} to out-of-plane CH bending in cyclohexene. A medium to strong band at 904 cm^{-1} has been identified by Sakashita (49) as a ring deformation mode. Several of these modes could conceivably contribute to the intensity of the 933 cm^{-1} peak.

In the 1000-1500 cm^{-1} region a number of characteristic frequencies are expected both for the adsorbed $Zr(BH_4)_4$ complex and for cyclohexene. BH_4 deformations are expected between 1000-1400 cm^{-1} and B-O modes are expected in the 1200-1450 cm^{-1} region. In addition, C-C stretching, CH_2 vibrations, and CH modes are expected.

Cyclohexene exhibits a number of vibrations in the 1000 to 1500 cm^{-1} region. A very strong band at 1037 cm^{-1} has been assigned as a ring stretching vibration (51) and alternatively, as a CH_2 deformation (49). Sakashita (49) has assigned the very strong band at 1138 cm^{-1} to a CH_2 deformation vibration and Kumar et al. (51) has assigned it to a ring deformation. Other features include two wagging modes of the CH_2 group at 1241 and 1266 cm^{-1}, three CH_2 twisting modes at 1307, 1323 and 1351 cm^{-1} and one CH_2 scissoring mode at 1435 cm^{-1}. A strong Raman band at 1222 cm^{-1} has been assigned to a =CH deformation and a very strong band appearing at 1450 cm^{-1} has been assigned to a CH_2 deformation (49). A band near 1007 cm^{-1} has also been assigned as a CH_2 deformation and a Raman active band near 1068 cm^{-1} has been identified as a ring stretching vibration. A band near 1150 cm^{-1} has also been previously assigned to a CH_2 deformation mode.

Referring to figure 4, the 1055 cm^{-1} feature is probably best assigned as either a CH_2 deformation mode or a ring breathing mode although bidentate and tridentate BH_4 ligands, which have only very weak bands in this region, do exhibit a medium to weak band at 1058 cm^{-1} (33). Evans and Weinberg (7) also assigned a feature at 1030 cm^{-1} to hydrocarbon contamination.

The 1096 cm^{-1} feature may be assigned as a deformation mode of the BH_2 terminal group. Smith et al. (39) state that this feature is one of the most strikingly characteristic features of doubly-bridged BH_4 groups. The 1134 cm^{-1} feature could be assigned to either the strong CH_2 deformation vibration band assigned by Sakashita (49) to the 1138 cm^{-1} band, the cyclohexene ring deformation mode assigned by Kumar et al. (51) to the same band, or to a B-H deformation mode (7). However, the assignment of this band to a B-H deformation mode is the best choice based on a comparison of spectra which exhibit greatly reduced BH_4 features.

Studies of $Zr(BH_4)_4$ report a strong band at 1213-1217 cm^{-1} and a medium intensity feature at 1170-1178 cm^{-1}. Bidentate BH_4 ligands in $(C_5H_5)_2Zr(BH_4)_4$ do not exhibit a band in this region (39). The small feature at 1202 cm^{-1} may therefore be assigned to a tridentate BH deformation mode. The strong Raman band at 1222 cm^{-1} in cyclohexene, assigned to a =CH deformation, may also contribute to intensity in this region.

The peak at 1293 cm^{-1} may be assigned to a combination of CH_2 twisting and M-BH_4 deformation. $Zr(BH_4)_4$ has a strong HBH bend at 1285 cm^{-1} (33, 34) while bidentate M-BH_4 groups exhibit a weak or medium intensity

band at 1294-1300 cm^{-1} (39). Cyclohexene exhibits a CH_2 twisting mode at 1307 cm^{-1}.

The next feature to be discussed is that at 1425 cm^{-1}. This feature is very broad and clearly has a shoulder on the low energy side near 1360-1370 cm^{-1}. Possible assignments include B-O, B-H or C-H modes. B-O modes have been reported at 1370 and 1330 cm^{-1} (42). Evans and Weinberg (7) assigned a peak at 1378 cm^{-1} to a B-O mode. However, this feature is not particularly intense in the spectrum of $Zr(BH_4)_4$ adsorbed on Al_2O_3 and therefore cannot account alone for the intense feature located in this region. A B-H deformation mode has been assigned to a feature at 1345 cm^{-1} in the IR spectrum of a hafnium borohydride complex (48). The most probable assignment of this feature is to the strong CH_2 scissoring mode reported at 1435 cm^{-1}. (49, 51).

The feature observed at 1494 cm^{-1} may be assigned to a cyclohexene mode based on a comparison of its intensity in Figure 4 with that seen for $Zr(BH_4)_4$ adsorbed on Al_2O_3 alone. Matsuda and Kawashima (42) have identified the peak found at 1470 cm^{-1} in their studies as a B-H deformation of the Al-BH_4 surface specie as has Maschenko (54). A very strong band in cyclohexene at 1450 cm^{-1} has been assigned to a CH_2 deformation (49). Generally, CH_2 deformation vibrations are expected in the 1465 $\pm$ 20 cm^{-1} region (55).

Another possible assignment for the 1494 cm^{-1} band which must be considered is a combination of CH_2 deformation and C=C stretching modes. Cyclohexene exhibits a medium intensity feature at 1652-1658 cm^{-1}.

Figure 4 shows that there is only a very weak feature located from 1600-1650 cm^{-1} in this region although the C-H stretching features clearly indicate that the adsorbed specie is unsaturated. Studies of the C=C shift in $[(C_5H_5)Fe(CO)_2Olefin]PF_6$ (56) found that the C=C bond of cyclohexene shifted to 1515 cm^{-1}, a shift of 140 cm^{-1}. Studies of Zeise's salt have assigned the weak mode near 1520 cm^{-1} to the C=C stretch of ethylene which occurs at 1623 cm^{-1} in free ethylene (57, 58). In complexes of (cyclohexene-Ag)$^+BF_4^-$ the C=C stretch occurs at 1583 cm^{-1} as a sharp intense feature (59). A low temperature infrared study of ethylene adsorption on Al_2O_3-supported Pt, Pd and Rh found that the C=C stretch shifted downfield 113 cm^{-1} for Pd and approximately 125 cm^{-1} for Pt and Rh and that the CH_2 scissoring vibrations shifted 143 cm^{-1} for Pt, 128 cm^{-1} for Rh, and 101 cm^{-1} for Pd (60). It is also known that the C=C stretching mode of an olefin often couples to other modes such as CH_2 scissoring and that the magnitude of the shift cannot be used as a quantitative measure of the strength of the coordination bond (58). In fact, Hiraishi (61) assigned the strong Raman band at 1243 cm^{-1} in Zeise's salt to C-C stretching and the band at 1520 cm^{-1} to a CH_2 scissoring mode although he stated that there was mixing of both modes in each band.

Powell et al. (59), in a study of Ag and Pt olefin complexes, found that the perturbation of other CH modes such as the CH_2 scissoring vibration is much more pronounced in ethylene complexes than it is for other types of olefin complexes and that the extent of perturbation also depends on the metal to which the olefin is coordinated. Silver forms weaker complexes with olefins than platinum and the silver complexes

showed much less shift of the coupled C=C and CH vibrations. In the silver cyclohexene complex, the C=C band shifted 4.5% and the CH in-plane deformation did not shift at all. It was noted also that in complexes in which the perturbation of the C=C stretching mode is small, this mode usually appears with an intensity equal to that found in the free molecule, but in complexes in which the mixing of this mode with a CH mode is greater, this bond usually appears with much less intensity than in the free molecule.

Another possible assignment of the 1494 cm^{-1} feature is to the C-C stretching mode of an allylic ligand. Diallyldicyclopentadienyl zirconium and related complexes have been characterized by infrared and NMR (65). Complexes such as $Cp_2V(C_3H_5)$ with a σ-bonded allylic group show a strong C=C band in the 1650-1580 cm^{-1} range but in complexes with π-bonded allylic ligands the corresponding band (the asymmetric CC stretch) is in the range 1550-1450 cm^{-1}.

A number of comments may be made concerning the feature located between 1600-1650 cm^{-1}. Although this band is near in frequency to that observed for free cyclohexene, its lack of intensity and broadness may indicate the presence of more than one type of surface specie as cyclohexene coordinates with the adsorbed $Zr(BH_4)_4$ complexes through the C=C bond. This is expected based on the diversity of possible Zr bonding to the oxide support and is indicated also by the evidence of both bidentate and tridentate BH_4 bonding.

An alternate assignment for this weak band would be to a Zr-H stretch. $Cp^*_2Zr(H)NC(H)C_6H_4Me$ has a broad IR adsorption at 1500 cm^{-1} which is characteristic of a Zr-H bond (62). The hafnium complex $\{Hf[N(SiMe_2CH_2PMe_2)_2]\}_2(H)_3(BH_4)_3$ exhibits a strong band at 1545 cm^{-1} which has been assigned to B-H and Hf-H modes (48). Additional Zr hydrides $(\eta^5\text{-}C_5H_5)_2W{=}CHOZr(H)(\eta^5\text{-}C_5Me_5)_2$, $(\eta^5\text{-}C_5H_5)_2Mo{=}CHOZr(H)\text{-}(\eta^5\text{-}C_5Me_5)_2$ and $(\eta^5\text{-}C_5H_5)_2(H)N_b{=}CHOZr(H)(\eta^5\text{-}C_5Me_5)_2$ also exhibit Zr-H stretching at 1560, 1543 and 1567 cm^{-1} respectively (63). The tantalum complexes, $Ta(CCMe_3)(H)(dmpe)_2(ClAlMe_2Cl)$ and $Ta(CCMe_3)(H)(dmpe)_2\text{-}(CF_3SO_3)$ exhibit Ta-H stretches at 1595 and 1610 cm^{-1} respectively (64).

The spectral features resulting from a cyclohexene exposure of 150 Torr s at 298 K to $Zr(BH_4)_4$ supported on alumina indicate that the adsorbed cyclohexene is clearly an unsaturated hydrocarbon. At this exposure, cyclohexene coordination to the Zr catalyst does not appear to require an appreciable displacement of BH_4 ligands as evidenced by the magnitude of the characteristic BH_4 stretching vibrations. There is evidence of both bidentate and tridentate BH_4 bonding but less evidence of B-H vibrations arising from B-O complexes since no B-O vibrations were able to be conclusively assigned in the spectrum. Cyclohexene coordination to the catalyst is presumed to be through the double bond as evidenced by the lack of a C=C mode which corresponds closely to that seen in cyclohexene. The features indicate that the C=C mode is either downshifted in frequency or very weak. An alternate assignment for the weak broad feature at 1600-1650 cm^{-1} is to a zirconium hydride specie. The spectral features indicate that there are several types of adsorbed zir-

conium species and the position of the hydroxyl stretch is characteristic of free hydroxyls rather than hydroxyls which are involved in hydrogen bonding.

4.5 Type II

The type II spectra are characterized by several features which are not observed in type I spectra. Figure 4 spectrum (C), a 6000 Torr s exposure of cyclohexene at 298 K to $Zr(BH_4)_4$ supported on Al_2O_3, is an example of a type II spectrum. It should be noted that this spectrum exhibits well-resolved features in both the $B-H_b$ and $B-H_t$ regions indicating that bridging BH_4 ligands still remain coordinated to the Zr. Consequently, the 1000-1500 cm^{-1} region still exhibits B-H deformation modes which complicates the assignment of hydrocarbon modes. In spectra resulting from junctions in which the substrate was heated however, very few indications of B-H features remain and these spectra are therefore useful in assigning the hydrocarbon bands.

At 6000 Torr s and 298 K, the BH_4 stretching features are greatly reduced over those seen at 150 Torr s. Two $B-H_b$ modes are evident at 2167 and 2213 cm^{-1} and a broad feature with a maximum at 2490 cm^{-1} is observed in the $B-H_t$ region. Compared to the 150 Torr s spectrum, there is a loss of intensity around 2560 cm^{-1}, assigned to $B-H_t$ stretching in tridentate BH_4 ligands. This implies that there is less tridentate BH_4 bonding at the high cyclohexene exposure and that most of the coordinated BH_4 groups are involved in bidentate bridge bonding.

The CH stretching region exhibits a very intense feature at 2835

cm^{-1} which was not present in the 150 Torr s spectrum. Two additional features are observed at 2882 and 2912 cm^{-1}. Compared to the 150 Torr s spectrum, the 6000 Torr s spectrum displays a greatly reduced intensity at frequencies near 3000 cm^{-1}. The presence of the new 2835 cm^{-1} peak, as well as the fact that the major stretching features are below 3000 cm^{-1}, indicates that the primary type of surface specie is a saturated hydrocarbon. There is also a very weak feature located at approximately 2650 cm^{-1} which is seen in all the type II spectra.

Features in the 1000-1500 cm^{-1} region may be assigned primarily to hydrocarbon modes although some B-H deformation modes as well as B-O modes may contribute to the intensity of several features in this region. However, most modes are easily assigned as hydrocarbon features based on their increased intensity in other type II spectra which involved substrate heating. The feature at 1091 cm^{-1} may be assigned to the deformation mode of terminal BH_2 groups observed near 1102 cm^{-1} (39). The unresolved intensity near 1370-1390 cm^{-1} may be assigned to a B-O mode. The feature at 1260 cm^{-1} has also been assigned to a combination of B-H and B-O modes (7).

The shoulder on the 1091 cm^{-1} peak may be assigned to a CH mode. Type II spectra from heated junctions do not have large features near 1100 cm^{-1} but consistently exhibit a band near 1080 cm^{-1}. Type II spectra also have features at or near 1030, 1080, 1166, 1202, 1259, 1336 and 1435 cm^{-1}. The 1030 cm^{-1} band may be assigned to either a ring stretching vibration (51) or a CH_2 deformation mode (49). The 1080 cm^{-1} band may correspond to the Raman active band near 1068 cm^{-1} which has been

identified as a ring stretching vibration. The 1167 cm^{-1} peak may be either a CH_2 deformation mode or a ring deformation. The 1205 cm^{-1} feature corresponds to the Raman band at 1222 cm^{-1}, assigned to a =CH deformation (49) and the 1259 cm^{-1} peak is probably due to a CH_2 wagging mode. The 1336 cm^{-1} band may be assigned to -CH- bending and the intense 1435 cm^{-1} feature may be assigned to CH_2 scissoring (55).

Several features in the lower region of the spectrum may be assigned to Zr-O modes: the 902 cm^{-1} peak to singly coordinated Zr and the peak near 690 cm^{-1} to multiply coordinated Zr. However, a medium to strong band at 904 cm^{-1} in cyclohexene has been assigned as a ring deformation mode. The 251 cm^{-1} feature is probably a Zr bend or torsion and is lower in frequency than that observed at 150 Torr s. The feature at 329 cm^{-1} may be a metal oxide or a torsional mode of the Zr.

Several features are found in type II spectra in the low energy range which were not observed in the 150 Torr s spectrum. A strong doublet at 408 and 432 cm^{-1}, a feature at 487 cm^{-1}, a smaller band at approximately 540 cm^{-1}, a new feature near 785 cm^{-1} and a shoulder on the 902 cm^{-1} peak near 850 cm^{-1}. A definitive assignment for all of these new features is difficult. The peaks between 350-500 cm^{-1} are similar to long chain skeletal deformation modes that are typical of all polymer vibrational spectra (66). However, some zirconium oxides exhibit bands at 408 and 483 cm^{-1} (44). One or more features due to Zr-C bonding is also expected but this feature would not be expected to increase in intensity nearly as much as the CH features. A tentative assignment may be made of the 550 cm^{-1} feature, or possibly the 487 cm^{-1} peak, to a Zr-C

mode. A band at 850 cm^{-1} has been observed in polyvinylcyclohexane (67) and polycyclohexylacetylene (68) as well as cyclohexane and is indicative of C_6 rings. The 786 cm^{-1} may be assigned to the ν_β (ring) mode identified in virtually all substituted cyclohexanes (69).

The spectral features discussed above indicate that type II spectra are clearly different than the type I. In type II spectra, the adsorbed cyclohexene is clearly a saturated hydrocarbon. Although the saturated hydrocarbon is formed at a higher exposure of cyclohexene, the spectrum of a 6000 Torr s exposure of cyclohexene to the supported catalyst reveals clearly that BH_4 ligands remain coordinated to the zirconium. There is evidence of both bridging and terminal BH_4 stretching and peak positions indicate that the BH_4 bonding is primarily bidentate. There is some evidence also of B-O stretching. The weak feature seen at 1600-1650 cm^{-1} at 150 Torr s is present also at 6000 Torr s and possibly indicates the presence of Zr-H species. There is little or no evidence of a C=C stretching mode and the great loss of intensity near 3000 cm^{-1} indicates that the predominant type of surface specie is a saturated hydrocarbon. Several new low energy features are observed in type II spectra and may correspond to torsional modes, Zr-C modes, skeletal deformation modes and ring bending of substituted cyclohexane. The hydroxyl stretching peak is also downshifted at 6000 Torr s, indicative of hydrogen bonding.

4.6 Temperature and Pressure Dependence of I and II

Figures 1 through 9 show the temperature and pressure dependence of type I and II and Table 4 summarizes the results.

At 150 Torr s, type I spectra result at all temperatures except perhaps the highest investigated, 623 K. At this temperature the spectrum resembles that of a type II, characterized by a narrow, intense low energy hydrocarbon stretching band, although at this exposure and temperature the hydrocarbon stretching frequencies are not as low as those observed at higher exposures. The two main stretching features at 150 Torr s and 623 K are located at 2852 and 2898 cm^{-1} but at 6000 Torr s and 623 K they are located at 2819 and 2865 cm^{-1}. Although the relative intensities of the two hydrocarbon stretching features are similar, the differences in peak position indicate that they do not represent the same surface specie or, that they reflect differences in the relative amounts of two types of specie present on the surface.

Figures 22, 23 and 24 show the shifts in position of several major spectral features as a function of substrate temperature and exposure to cyclohexene. From this analysis it appears that the major spectral feature present at 623 K at 150 Torr s may be indicative of an "incipient" type II spectra. It should be kept in mind that only some of the major spectral features are shown in Figures 22, 23 and 24; shoulders and other unresolved features are not included.

The peak positions observed at 6000 Torr s and at 1200 Torr s at temperature of 403 K and higher are representative of the type II spectrum. Figures 22, 23 and 24 clearly show the transformation that occurs between 348 and 403 K at 1200 Torr s. It is interesting to note however that shifts of some peak positions also occur at 6000 Torr s as a function of increasing substrate temperature. Since the relative intensity

of the hydrocarbon-related features increases greatly as a function of temperature, these shifts in position correlate with the increase in hydrocarbon adsorption. Not all of the features shift with increased cyclohexene adsorption; the feature at 1259 cm^{-1} is very stable in position from 298 K to 623 K. The feature near 1440 cm^{-1} shifts only 8 cm^{-1} from 298 K to 623 K and the feature near 1345 cm^{-1} shifts 9 cm^{-1}. The CH stretching features shift the most. The narrow feature shifts downward by 16 cm^{-1} and the higher energy feature shifts by 17 cm^{-1}. The origin of these small shifts at high exposures may be physical rather than chemical in nature, especially because all of the shifts are decreases in position. Frequency decreases (red shifts) between IETS and other vibrational spectroscopies such as IRS or HREELS have been studied theoretically and experimentally (70, 71) and are a consequence of the interaction of the charge distribution of a vibration with its induced image in the top metal layer. The frequency decrease is proportional to:

$$\Delta\omega = C(d)(q_1^2/\mu\omega_o d^3)$$

where ω_o is the unshifted frequency, μ is the reduced mass of the oscillator, q_1 is the dipole derivative and d is the distance to the top layer. C(d) depends only slightly on d. It may be that the small red shifts seen in the present case reflect a decrease in the "effective" distance to the top metal layer, d, as the hydrocarbon adsorption increases as a function of temperature. That the CH stretching modes in particular could be effected by this is indicated by previous IETS studies (71).

A chemical origin of these red shifts is possible. It may be that as saturated hydrocarbon builds up on the surface intermolecular interactions are responsible for the decrease in frequency. Hydrogen bonding of the α-hydrogen atom in $Ta(CHCMe_3)(dmpe)_2Cl$ results in a very low energy CH_2 vibration at 2200 cm^{-1} (64), but the small decreases seen in these IET spectra, as well as the narrow width of the CH stretching features, appears to rule out a strict hydrogen bonding interpretation of the shifts. The shifts observed here are probably a result of a change in the dielectric constant as hydrocarbon accumulates on the surface of the junction.

A comparison of the peak positions of type II versus type I spectra reveals that the type II spectral features are very stable compared to the type I. For all the type I spectra, shifts in both peak positions and intensities occur as the substrate temperature or the cyclohexene exposure is increased. For type II spectra, there are few shifts in peak positions but the intensities of the hydrocarbon bands increase as a function of both increasing temperature at constant exposure and as a function of exposure at constant temperature. This behavior implies that type II spectra are representative of one main type of surface specie and that type I spectra represent at least two species. Type I spectra are indicative of the initial adsorbate formed when cyclohexene interacts with the supported $Zr(BH_4)_4$ as well as any intermediate species which may be formed during the conversion of the cyclohexene to a saturated surface hydrocarbon.

The spectra show that the catalyst decomposes as a function of temperature and cyclohexene exposure. At 150 Torr s, the strong B-H_b and B-H_t features are reduced as the substrate is heated. At 473 K, few bridging BH_4 features remain yet the BH_t features are still quite intense, indicating the presence of O-BH_2 surface species and possibly Zr borides (43). The OBH_2 or ZrB species are thermally stable since little change in this feature occurs at 523 or 623 K. The hydroxyl group also decreases in intensity and downshifts as the substrate is heated indicating partial dehydroxylation of the surface. Burwell (72) states that dehydroxylation of hydroxylated γ-alumina begins at 200°C and the results here confirm this observation since the hydroxyl band intensity diminishes with increasing substrate temperature at 200°C and above. Similar results are observed in the 1200 Torr s spectra. At 6000 Torr s there is virtually no hydroxyl feature remaining at 473 K and above.

The decomposition of the catalyst as a function of cyclohexene exposure can be seen in Figure 4 and in Figure 3. As the cyclohexene exposure is increased, the BH_4 features undergo a great reduction in intensity. At 6000 Torr s, the catalyst is further decomposed as a function of temperature so that there is only a very weak feature due to B-H_t stretching at 473 K and above. This indicates that the thermally stable OBH_2 or $ZrBH_2$ formed at 150 Torr s do not form or are not stable when subjected to a 6000 Torr s cyclohexene exposure.

4.7 Identification of the Saturated Specie

The spectral features indicate that two reactions may have occurred:

polymerization or hydrogenation of the adsorbed cyclohexene.

The possibility of hydrogenation is quite likely. Previous studies (41,73) have shown that zirconium hydrides are active hydrogenation catalysts for olefins. By reacting the monohydride, $(C_5H_5)_2Zr(H)Cl$, with cyclohexene, the alkyl complex was formed (54):

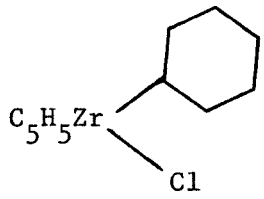

The zirconium dihydride was found to react stoichiometrically to yield an unstable alkyl intermediate which reacted with hydrogen to reform the zirconium hydride and cyclohexane. The monohydride zirconium catalyst also reduces cyclohexene as shown above, but requires longer reaction times or higher temperatures. In the study by Wailes et al. (54) the reaction was carried out at 80°C. It was further noted that the alkyl complexes formed are unstable and decompose slowly in the solid state and more rapidly in solution.

In the present case the BH_4 groups serve as a limited hydrogen supply. Since $Zr(BH_4)_4$ decomposes at room temperature to H and BH_3, each BH_4 ligand may supply one H atom to the double bond of a coordinated cyclohexene molecule to yield the corresponding alkyl ligand. Some zirconium complexes may supply two H atoms to cyclohexene resulting in a small amount of evolved cyclohexane as the reaction proceeds. At 473 K and above, the partial dehydroxylation of the surface may also serve as a limited source of hydrogen. The magnitude of the CH stretching features

indicates that a significant number of alkyl groups remain on the surface and that the amount of saturated hydrocarbon increases without apparent limit as a function of cyclohexene exposure and substrate temperature even when there appears to be no readily available source of hydrogen, as for example at temperatures of 403 K and above at a 6000 Torr s cyclohexene exposure.

This indicates that the saturated hydrocarbon which is formed from the adsorbed cyclohexene may in fact be polycyclohexene. The homopolymerization of cyclohexene under mild conditions has been reported (23, 74) and characterized by NMR and IR spectroscopies. The physical and chemical evidence indicates that the polymer formed is a totally saturated polymer. The 300 MHz NMR spectrum shows only aliphatic proton signals and there are no olefinic proton bands observed. The ^{13}C-NMR spectrum of polycyclohexene shows around 30 signals in the ppm 13.9-35.9 range and its complexity indicates the polymer is not stereoregular.

The IR spectrum also shows only the presence of a saturated hydrocarbon. Several structurally significant bands are observed in the IR spectrum. Aliphatic CH stretching bands are observed at 2960-2800 cm^{-1} and the band at 2650 cm^{-1} indicates that the cyclohexane rings are intact (75). The CH_2 scissoring vibration in the polymer is observed at 1440 cm^{-1}, indicating that the six-membered rings are retained in the polymer since the same vibration in straight-chain alkanes appears at 1470 cm^{-1}. Bands at 890 and 850 cm^{-1} provide further evidence of a polymerized ring system since these same bands have been observed in polyvinylcyclohexane (67) and polycyclohexylacetylene (68) as well as in

cyclohexane. There are no bands observed in the 1600-1700 cm^{-1} region arising from C=C stretching modes.

The evidence indicates that the polymer derived from cyclohexene is an addition type polymer and that the rings are retained. The complex ^{13}C-NMR spectrum seems to indicate that the polycyclohexene is made up of either repeating 1,2- 1,3- and/or 1,4- repeating units as shown:

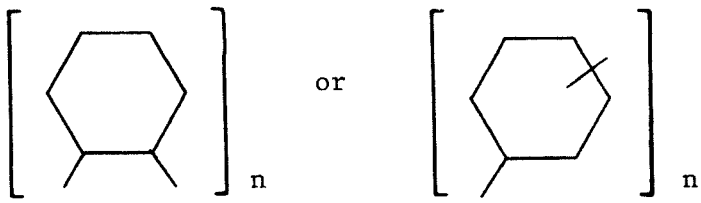

The IR spectrum of polycyclohexene reported by Woon (68) is shown in Figure 25. A comparison of the polycyclohexene spectrum and the type II IET spectra shows that the spectral features are closely matched in terms of peak position and relative intensity. The saturated surface specie produced by the interaction of cyclohexene with $Zr(BH_4)_4$ adsorbed on Al_2O_3 can be identified as polycyclohexene. Additional evidence in support of this conclusion is the apparent lack of a saturation coverage of cyclohexene as judged by the increase in both junction resistance and hydrocarbon peak intensities as a function of cyclohexene exposure and substrate temperature.

4.8 The Cyclohexene Reaction Mechanism

The traditional view of the polymerization reaction has involved initial coordination of the olefin to the transition metal atom via the double bond to form a π-complex. Olefin coordination is thought to be possible without displacing additional ligands from the supported catalyst. This first step in the polymerization process is followed by insertion of the hydrocarbon between the metal atom and one of its remaining ligands. The polymer grows by repeated coordination and insertion of other olefin molecules. It has been postulated that hydrogen ligands form the active polymerization centers (2, 16 - 18, 76).

In recent years however, there has been a growing awareness of the many similarities of polymerization and metathesis reactions (77). Research on alkene metathesis reactions has led to a re-examination of the polymerization reaction. In particular, the metathesis of some cyclic olefins was found to result in ring-opening polymerization and some Ziegler-Natta systems catalyze both ring-opening and normal polymerization (78). Recent work on alkene metathesis reactions indicate that the catalytic chain is propagated by two different odd-carbon-number species; metal-carbenes and metallocyclobutanes.

A unifying mechanism for metathesis and polymerization has been proposed by Ivin et al. (79) where R represents the growing polymer chain:

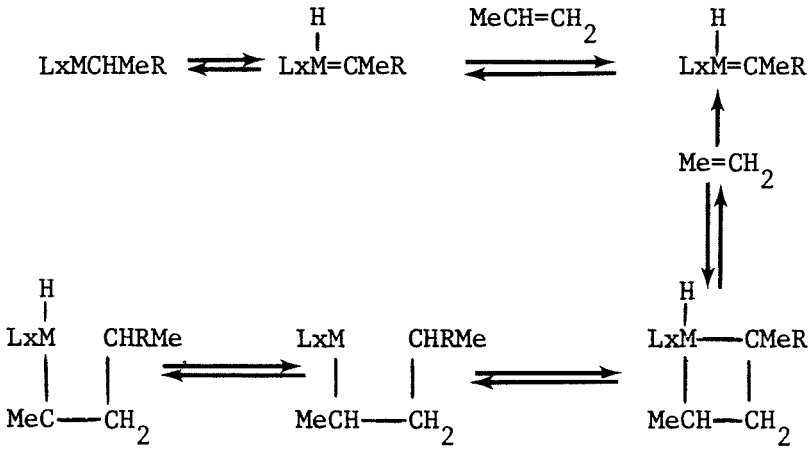

Two main routes for the formation of metal-carbenes and metallocyclobutanes have been proposed: α-elimination and η^3-allyl-metallocyclobutane interconversion. The α-elimination pathway for a heterogeneous system is shown below:

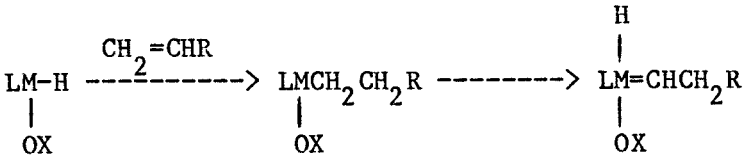

A η^3-allyl-metallocyclobutane interconversion may also be possible in some systems:

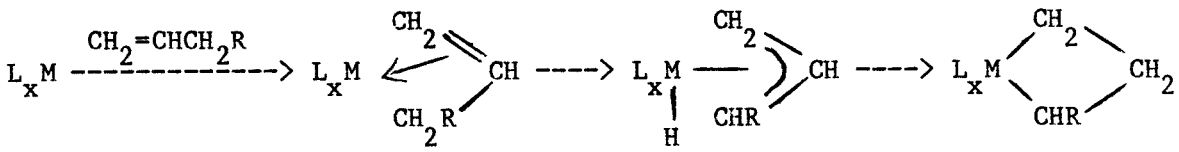

The only previously reported homopolymerization of cyclohexene was catalyzed by a rhenium olefin metathesis catalyst (23, 74). The homogeneous catalyst system is $Re(CO)_5Cl/C_2H_5AlCl_2$, which is known to be an

active catalyst for the metathesis of internal and terminal olefins (80). This system polymerizes 5, 6, 7, and 8-membered rings provided no steric hindrance is encountered. Methyl groups as close to the double bond as the allylic carbon make the cyclic alkene inert to polymerization. Optimum reaction conditions for polymerization are 110°C and extended reaction times. Interestingly, the susceptibility of the monomer to polymerization and the yield of polymer increase as the ring increases in size, although the molecular weight decreases. This contrasts with the observations in other cases that only highly strained cyclic alkenes can form addition polymers (81). When the catalyst system is $Re(CO)_5Cl/C_2H_5AlCl_2$, polymerization of cyclic olefins is enhanced as the ring strain decreases.

The active form of the $Re(CO)_5Cl/C_2H_5AlCl_2$ catalyst has been shown to be $[(CO)_4Re{=}CHCH_2CH^+_3]$, a coordinated propylidene specie (80). Because the only difference in the conditions between metathesis and polymerization of cyclic olefins is the temperature at which reation occurs (90°C for metathesis, 110°C for polymerization), it appears that the same specie is responsible for polymerization. Several studies confirmed this hypothesis (74).

Tsonis and Farona (74) have suggested that the first steps of polymerization are similar to those of metathesis and have proposed the following reaction for the formation of a four-membered metallacycle specie, where M=CHR is the catalyst initiator:

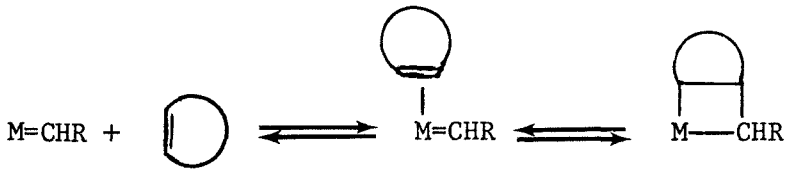

I

Specie (I) is the first step in metathesis. When the second olefin coordinates, an addition polymer, rather than a ring-opening polymer, can arise by a slight modification of the metathesis mechanism:

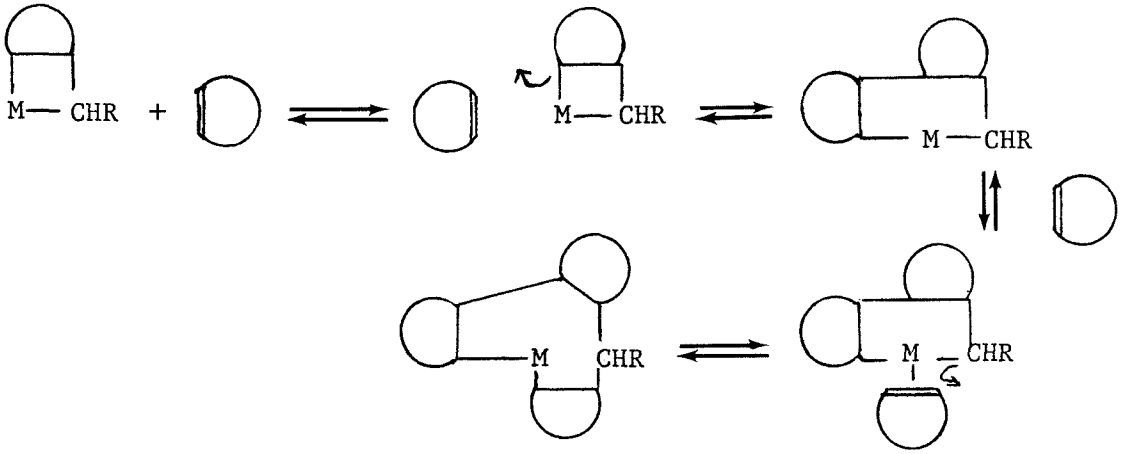

Though this mechanism is speculative, it does account for the formation of an addition polymer by incorporating a metathesis-type initiation and a Ziegler-Natta type polymerization.

In the present study, the initial complex formed by the adsorbed cyclohexene is probably a π-complex. The IET spectra support this conclusion as well as the possibility of conversion to a η^3- allyl ligand. The IET spectra show that the initial complex and possibly one or more reaction intermediates are clearly unsaturated. The results show that the unsaturated species are converted to a saturated hydrocarbon which continues to accumulate on the surface as judged by the increases

in the associated vibrational features. The spectra also show that no olefinic features (such as C=C or =C-H stretching) increase in intensity as either the cyclohexene exposure and/or the substrate temperature is increased.

These results are therefore consistent with the mechanism proposed for cyclohexene polymerization by Tsonis and Farona (74). The conversion to a metallacycle would result in a vibrational spectrum exhibiting features associated with a saturated hydrocarbon and continued coordination and insertion of the cyclohexene molecules into the growing chain would result in increased intensity of the associated spectral features. In the present study, the spectra do not allow a conclusive identification of the adsorbed intermediate but the formation of an intermediate alkylidene specie cannot be ruled out.

4.0 Conclusions

Cyclohexene has been shown to form a saturated polymer consisting of cyclohexane rings formed by homopolymerization. The transformations of the supported catalyst, $Zr(BH_4)_4$, and the surface product, have been studied as a function of both cyclohexene exposure and temperature by inelastic electron tunneling spectroscopy. A tentative reaction mechanism, combining features of metathesis and polymerization reactions, has been considered. This study demonstrates that the unique and sensitive properties of this spectroscopy are highly suited not only for the study of well-understood supported catalytic systems but may also be applied successfully to characterize and identify the nature of new catalytic systems and unexpected new products of reaction.

References

1. J. M. Basset and A. K. Smith, in "Fundamental Research in Homogeneous Catalysis", M. Tsutsui, R. Ugo, Eds. Plenum: New York, 1979, pp. 69-98.

2. D. G. H. Ballard, J. Polymer Science, 13, 2191 (1975).

3. V. A. Zakharov, and Yu I. Yermakov, Catal. Rev.-Sci. Eng. 19, 67 (1979).

4. For a ^{13}C NMR study of $Fe(C_5H_5)(CO)_2CH_3$/Alumina surface chemistry see: P. J. Toscano and T. J. Marks, Organometallics 5, 400 (1986).

5. W. M. Bowser and W. H. Weinberg, J. Am. Chem. Soc. 102, 4720 (1980).

6. W. M. Bowser and W. H. Weinberg, J. Am. Chem. Soc. 103, 1453 (1981).

7. H. E. Evans and W. H. Weinberg, J. Am. Chem. Soc. 102, 872 (1980).

8. H. E. Evans and W. H. Weinberg, J. Am. Chem. Soc. 102, 2548 (1980).

9. H. E. Evans and W. H. Weinberg, J. Am. Chem. Soc. 102, 2554 (1980).

10. P. K. Hansma, D. A. Hickson and J. A. Schwarz, J. Catal. 48, 237 (1977).

11. H. E. Evans, W. M. Bowser and W. H. Weinberg, Appl. Surf. Sci. 5, 1980.

12. D. R. Witt, Phillips Petroleum Co., U.S. 3, 166, 536.

13. D. G. H. Ballard, P. A. Robinson, R. J. Wyatt, E. Jones and A. J. P. Pioli, Imperial Chemical Industries, Ltd. Ger. Offen, 2, 209, 219 (1972).

14. R. J. Wyatt, Imperial Chemical Industries, Ltd. Ger. Off. 2, 235, 960 (1973).

15. D. G. H. Ballard, et al., Imperial Chemical Industries, Ltd. Ger. Offen. 2, 209, 220 (1972).

16. L. E. Firment and R. A. Setterquist, Symposium on Immobilized Homogeneous Catalysts, Am. Chem. Soc. Kansas City Meeting, Sept. 12-17, 1982.

17. L. E. Firment, J. Cat. 77, 491 (1982).

18. G. A. Nesterov, V. A. Zakharov, E. A. Paukshtis, E. N. Yurchenko, V. V. Volkov, and K. G. Myakishev, Kinet. Katal. 21, 739 (1980).

19. P. R. Marshall and B. J. Ridgewell, Eur. Polymer J. 5, 29 (1969).

20. A. J. Amass, T. A. McGourtney and C. N. Tuck, Eur. Polymer J. 12, 93 (1976).

21. G. Natta, I. W. Bassi and G. Fagherazzi, Eur. Polymer J. 5, 239 (1969).

22. B. C. Onderson, C. L. Hoover and O. Vogl, Macromolecules, 2, 686 (1969).

23. M. F. Farona and C. Tsonis, J.C.S. Chem. Comm., 363 (1977).

24. W. H. Weinberg, Ann. Rev. Phys. Chem. 29, 115 (1978).

25. J. W. Coburn, "Plasma Etching and Reactive Ion Etching", American Institute of Physics, New York, 1982.

26. W. M. Bowser and W. H. Weinberg, Rev. Sci. Instrum. 47, 583 (1976).

27. W. M. Bowser, Ph.D. Thesis, California Institute of Technology, Pasadena, CA, 1980.

28. J. Kirtley and P. K. Hansma, Phys. Rev. B 13, 2910 (1976).

29. T. J. Marks and L. A. Shimp, J. Am. Chem. Soc. 94, 1542 (1972).

30. B. D. James, R. K. Nanda and M. G. H. Wallbridge, J. Chem. Soc. A, 182 (1966).

31. T. J. Marks, W. J. Kennelly, J. R. Kolb and L. A. Shimp, Inorg. Chem. 11, 2540 (1972).

32. N. Davies, M. G. H. Wallbridge, R. E. Smith and B. D. James, J. Chem. Soc., Dalton Trans. 162 (1973).

33. B. D. James, B. E. Smith and H. F. Shurvell, J. Mol. Struct. 33, 91 (1976).

34. B. E. Smith, H. F. Shurvell and B. D. James, J. Chem. Soc., Dalton Trans. 710 (1978).

35. B. E. Smith and B. D. James, Inorg. Nucl. Chem. Lett. 7, 857 (1971).

36. A. J. Downs, R. G. Egdell, A. F. Orchard and P. D. P. Thomas, J. Chem. Soc., Dalton Trans. 1755 (1978).

37. P. H. Bird and M. R. Churchill, Chem. Commun. 403 (1967).

38. V. Plato and K. Hedberg, Inorg. Chem. 10, 590 (1971).

39. B. E. Smith, B. D. James and J. A. Dilts, J. Inorg. Nucl. Chem. 38, 1973 (1976).

40. D. G. H. Ballard, in "Coordination Polymerization", J. D. W. Chien, Ed., Academic, New York, 1975, pp. 223-262.

41. T. J. Marks and J. R. Kolb, J. Am. Chem. Soc. 97, 3397 (1975).

42. T. Matsuda and H. Kawashima, J. Catal. 49, 141 (1977).

43. K. N. Semenko, O. V. Kravchenko and V. B. Polyakova, Usp. Khim. 42, 8 (1973).

44. T. Markawa and M. Terada, Trans. Jpn. Inst. Met. 4, 57 (1963).

45. G. A. Ozin in "Vibrational Spectroscopy of Trapped Species", H. E. Hallum, Ed., Wiley, New York, 1973, pp. 237-244.

46. W. M. Bowser and W. H. Weinberg. Surface Sci. 64, 377 (1977).

47. L. H. Little, "Infrared Spectra of Adsorbed Species", H. E. Hallum, Ed., Wiley, New York, 1973, pp. 237-244.

48. M. D. Fryzuk and H. D. Williams, Organometallics 2, 162 (1983).

49. K. Sakashita, J. Chem. Soc. Japan 77, 1094 (1955).

50. N. Neto, C. DiLauro, E. Castellucci and S. Califano, Spectrochim. Acta 23A, 1763 (1967).

51. S. Kumar, V. D. Gupta and P. C. Jain, Acta Ciencia Indica 5, 8 (1979).

52. S. J. Cyvin and O. Gebhardt, Monatsheffe fur Chemie 105, 1374 (1974).

53. F. F. Cleveland, J. Chem. Phys. 11, 301 (1943).

54. A. I. Mashchenko, Kinet. Katal. 15, 903 (1974).

55. L. J. Bellamy, "The Infra-Red Spectra of Complex Molecules", John Wiley and Sons, New York, 1966, pp. 13-33.

56. E. O. Fischer and K. Fichtel, Chem. Ber. 95, 2063 (1962).

57. M. J. Grogan and K. Nakamoto, J. Amer. Chem. Soc. 88, 5454 (1966).

58. M. J. Grogan and K. Nakamoto, J. Amer. Chem. Soc. 90, 918 (1968).

59. D. B. Powell, J. G. V. Scott and N. Sheppard, Spectrochim. Acta (28A), 327 (1972).

60. Y. Soma, J. Catal. 59, 239 (1979).

61. J. Hiraishi, Spectrochim. Acta. 25A, 740 (1969).

62. J. E. Bercaw, D. L. Davies and P. T. Wolczanski, Organometallics 5, 443 (1986).

63. P. T. Wolczanski, R. S. Threlkel and J. E. Bercaw, J. Am. Chem. Soc. 101, 218 (1979).

64. M. R. Churchill, H. J. Wasserman, H. W. Turner and R. R. Schrock, J. Am. Chem. Soc. 104, 1711 (1982).

65. H. A. Martin, P. J. Lemaire and F. Jellinek, J. Organomet. Chem. 14, 149 (1968).

66. D. O. Hummel, Polymer Rev. 14, 8 (1966).

67. J. P. Kennedy, J. J. Elliott and W. Naegele, J. Polymer Sci. Part A 2, 5029 (1964).

68. P. Woon. Ph.D. Dissertation, The University of Akron, 1974.

69. H. A. Szymanski, in "Interpreted Infrared Spectra", Plenum, New York, 1964, pp. 230-293.

70. J. Kirtley and P. K. Hansma, Phys. Rev. B 13, 2910 (1976).

71. M. Liehr, P. A. Thiry, J. J. Pireaux and R. Caudano, Phys. Rev. B 31, 000 (1985).

72. R. L. Burwell, Jr., J. Catal. 86, 301 (1984).

73. P. C. Wailes, H. Weingold and A. P. Bell, J. Organomet. Chem. 43, C32 (1974).

74. C. Tsonis and M. F. Farona, J. Polymer Sci.: Polymer Chemistry 17, 185 (1979).

75. G. Dall'Asta, G. Mazzanti, G. Natta and L. Porri, Makromol. Chem. 56, 224 (1962).

76. V. A. Zakharov, V. K. Dudchenko, E. A. Paukshtis, L. G. Karakchiev and Yu. I. Yermakov, J. Mol. Cat. 2, 421 (1977).

77. R. H. Grubbs , in "Comprehensive Organometallic Chemistry", G. Wilkinson, Ed., Pergamon, Oxford (1982) Chap. 54.

78. G. Natta, G. Dall'Asta and G. Mazzanti, Angew. Chem. 76, 765 (1964).

79. K. J. Ivin, J. J. Rooney, C. D. Stewart, M.L.H. Green and R. Mahtab, JCS Chem. Comm., 604 (1978).

80. W. S. Greenlee and M. J. Farona, Inorg. Chem. 15, 2129 (1976).

81. N. Calderon, J. Macromol. Sci. Rev. Macromol. Chem. C7, 105 (1972).

Figure Captions

Figure 1: Comparative view of IET spectra of cyclohexene at an exposure of 150 Torr s interacting with $Zr(BH_4)_4$ supported on Al_2O_3. Substrate temperatures during the cyclohexene exposure were (A) 298 K, (B) 348 K, (C) 403 K, (D) 473 K, (E) 523 K and (F) 623 K.

Figure 2: Comparative view of IET spectra of Cyclohexene at an exposure of 1200 Torr s interacting with $Zr(BH_4)_4$ supported on Al_2O_3. Substrate temperatures during the cyclohexene exposures were (A) 298 K, (B) 348 K, (C) 403 K, (D) 473 K, (E) 523 K and (F) 623 K.

Figure 3: Comparative view of IET spectra of cyclohexene at an exposure of 6000 Torr s interacting with $Zr(BH_4)_4$ supported on Al_2O_3. Substrate temperatures during the cyclohexene exposures were (A) 298 K, (B) 348 K, (C) 403 K, (D) 473 K, (E) 523 K and (F) 623 K.

Figure 4: IET spectra (240 - 4000 cm^{-1}) of cyclohexene interacting with $Zr(BH_4)_4$ supported on Al_2O_3 at a surface temperature of 298 K during cyclohexene exposures of (A) 150 Torr s, (B) 1200 Torr s and (C) 6000 Torr s.

Figure 5: IET spectra (240 - 4000 cm^{-1}) of cyclohexene interacting with $Zr(BH_4)_4$ supported on Al_2O_3 at a surface temperature of 348 K during cyclohexene exposures of (A) 150 Torr s, (B) 1200 Torr s and (C) 6000 Torr s.

Figure 6: IET spectra (240 - 4000 cm^{-1}) of cyclohexene interacting with $Zr(BH_4)_4$ supported on Al_2O_3 at a surface temperature of 403 K during cyclohexene exposures of (A) 150 Torr s, (B) 1200 Torr s and (C) 6000 Torr s.

Figure 7: IET spectra (240 - 4000 cm^{-1}) of cyclohexene interacting with $Zr(BH_4)_4$ supported on Al_2O_3 at a surface temperature of 473 K during cyclohexene exposures of (A) 150 Torr s, (B) 1200 Torr s and (C) 6000 Torr s.

Figure 8: IET spectra (240 - 4000 cm^{-1}) of cyclohexene interacting with $Zr(BH_4)_4$ supported on Al_2O_3 at a surface temperature of 523 K during cyclohexene exposures of (A) 150 Torr s, (B) 1200 Torr s and (C) 6000 Torr s.

Figure 9: IET spectra (240 - 4000 cm^{-1}) of cyclohexene interacting with $Zr(BH_4)_4$ supported on Al_2O_3 at a surface temperature of 623 K during cyclohexene exposures of (A) 150 Torr s and (B) 6000 Torr s.

Figure 10: IET spectrum (240 - 2000 cm^{-1}) of cyclohexene interacting with $Zr(BH_4)_4$ supported on Al_2O_3 at a surface temperature of 403 K and a cyclohexene exposure of 1200 Torr s.

Figure 11: IET spectrum of (240 - 2000 cm^{-1}) of cyclohexene interacting with $Zr(BH_4)_4$ supported on Al_2O_3 at a surface temperature of 473 K and a cyclohexene exposure of 1200 Torr s.

Figure 12: IET spectrum (240 - 2000 cm^{-1}) of cyclohexene interacting with $Zr(BH_4)_4$ supported on Al_2O_3 at a surface temperature of 523 K and a cyclohexene exposure of 1200 Torr s.

Figure 13: IET spectrum (240 - 2000 cm^{-1}) of cyclohexene interacting with $Zr(BH_4)_4$ supported on Al_2O_3 at a surface temperature of 298 K and a cyclohexene exposure of 6000 Torr s.

Figure 14: IET spectrum (240 - 2000 cm^{-1}) of cyclohexene interacting with $Zr(BH_4)_4$ supported on Al_2O_3 at a surface temperature of 348 K and a cyclohexene exposure of 6000 Torr s.

Figure 15: IET spectrum (240 - 2000 cm^{-1}) of cyclohexene interacting with $Zr(BH_4)_4$ supported on Al_2O_3 at a surface temperature of 403 K and a cyclohexene exposure of 6000 Torr s.

Figure 16: IET spectrum (240 - 2000 cm^{-1}) of cyclohexene interacting with $Zr(BH_4)_4$ supported on Al_2O_3 at a surface temperature of 473 K and a cyclohexene exposure of 6000 Torr s.

Figure 17: IET spectrum (240 - 2000 cm^{-1}) of cyclohexene interacting with $Zr(BH_4)_4$ supported on Al_2O_3 at a surface temperature of 523 K and a cyclohexene exposure of 6000 Torr s.

Figure 18: IET spectrum (240 -2000 cm^{-1}) of cyclohexene interacting with $Zr(BH_4)_4$ supported on Al_2O_3 at a surface temperature of 623 K and a cyclohexene exposure of 6000 Torr s.

Figure 19: IET spectrum (240 - 2000 cm^{-1}) of cyclohexene interacting with Al_2O_3 at a surface temperature of 403 K and a cyclohexene exposure of 6000 Torr s.

Figure 20: IET spectrum (2000 - 4000 cm^{-1}) of cyclohexene interacting with Al_2O_3 at a surface temperature of 403 K and a cyclohexene exposure of 6000 Torr s.

Figure 21: IET spectrum of $Zr(BH_4)_4$ supported on Al_2O_3 at 300 K over the energy range (a) 240 - 2000 cm^{-1} and (b) 2000 - 4000 cm^{-1}. Reproduced from H. E. Evans and W. H. Weinberg (7).

Figure 22: Graph showing shift of resolved IET spectral features in the 2800 - 3100 cm^{-1} range as a function of surface temperature for cyclohexene interacting with Al_2O_3-supported $Zr(BH_4)_4$ at cyclohexene exposures of 150 Torr s (▲), 1200 Torr s (●) and 6000 Torr s (■).

Figure 23: Graph showing shift of resolved IET spectral features in the 1300 - 1500 cm^{-1} range as a function of surface temperature for cyclohexene interacting with Al_2O_3-supported $Zr(BH_4)_4$ at cyclohexene exposures of 150 Torr s (▲), 1200 Torr s (●) and 6000 Torr s (■).

Figure 24: Graph showing shift of resolved IET spectral features in the 1180 - 1300 cm^{-1} range as a function of surface temperature for cyclohexene interacting with Al_2O_3-supported $Zr(BH_4)_4$ at cyclohexene exposures of 150 Torr s (▲), 1200 Torr s (●) and 6000 Torr s (■).

Figure 25: Infrared spectrum of polycyclohexene reproduced from P. Woon (68).

Table 1

Peak positions, Relative Intensities and Assignments for IET Spectra of $Zr(BH_4)_4$ Adsorbed on Al_2O_3 Interacting with Cyclohexene at an Exposure of 150 Torr s.

298K	348K	403K	473K	523K	623K	Assignments
3743(.10)	3730(.09) 3613(.03)	3717(.10)	3706(.06)	3702(.06)	3648(.05)	ν(OH)
3008(.77) 2927(.49)	2982(.51) 2904(.32)	2980 sh 2957(.73) 2896(.62)	2931(.61) 2879(.59)	2978(.38) 2944(.41) 2898(.44)	2940 sh 2898(.57) 2852(.72)	ν(CH)
2562(.89) 2525(.84) 2493(.85)	2542(.45) 2510(.42) 2480(.43)	2500(.29) 2458(.30)	2465(.20)	2460(.19)	2465(.24)	$\nu(B\text{-}H_t)$
2289(.39) 2232(.37)	2270(.18) 2210(.18)	2260(.11) 2200(.09)	2281(.04) 2244(.04) 2196(.03) 2166(.02)	2280(.03) 2212(.02)	2293(.03) 2235(.03)	$\nu(B\text{-}H_b)$
1600 w ⊥ ∥	1600 w ⊥ ∥	1600 w ⊥ ∥	1600 w ⊥ ∥	1600 w ⊥ ∥	1600 w ⊥ ∥	ν(C=C)
1494(.15)	1480(.17)	1474(.27)	1464(.33)	1474(.24)	1452(.30)	CH_2 scissoring
1425(.11) 1365 sh 1293(.17) 1247(.11) 1202(.16) 1134(.28)	1410(.13) 1370 sh 1283(.20) 1230(.13) 1189(.17) 1124(.30)	1399(.14) 1283(.13) 1229(.07) 1189(.11) 1114(.15)	1391(.18) 1360 sh 1279(.18) 1226(.11) 1184(.14) 1106(.18)	1392(.12) 1287(.11) 1232(.07) 1190(.10) 1123(.13)	1376(.12) 1351(.13) 1270(.18) 1216(.09) 1178(.10) 1100(.14)	CH deformations B-H deformations B-O modes

Table 1, continued

298K	348K	403K	473K	523K	623K	Assignments
1096(.20)	1083(.26)	1076(.21)	1068(.20)			CH modes
1055(.16)	1052(.18)				1040(.09)	
933(1.0)	924(1.0)	922(1.0)	919(1.0)	924(1.0)	909(1.0)	Zr-O stretch[1]
			808(.29)	804 sh	807(.25)	Zr-C
720(.08)	707(.12)	732(.15)	712(.21)	707(.19)	698(.18)	metal oxide modes
698(.08)		708(.16)				
			552(.06)	555(.05)	541(.04)	CH skeletal deformations
	502(.02)		502(.04)			
			443(.03)		439(.04)	
302(.24)	295(.23)	299(.31)	301(.11)	299(.25)	295(.23)	Al phonon
266(.24)	262(.25)	264(.26)	266(.03)	263(.23)	257(.22)	Zr-B bend or torsion

1. Al-O (bulk) stretch appears as a shoulder on the Zr-O peak.

Table 2

Peak positions, Relative Intensities and Assignments for IET Spectra of $Zr(BH_4)_4$ Adsorbed on Al_2O_3 Interacting with Cyclohexene at an Exposure of 1200 Torr s.

298K	438K	403K	473K	523K	Assignments
3689(.09)	3655(.10)	3645(.21)	3640(.16)	3642(.15) 3613(.16)	ν(OH)
3051(.08) 2951(.52) 2872(.45)	3026(.07) 2925(.58) 2848(.52)	3022(.07) 3002(.15) 2878(1.34) 2829(1.64)	3021 sh 3004(.13) 2871(1.79) 2826(2.22) 2656(.09)	2873(2.26) 2826(3.03) 2651(.12)	ν(CH)
2526(.44) 2508(.43) 2465(.42) 2441(.42)	2492(.34) 2449(.34) 2422(.34)	2482(.29) 2455(.32) 2410(.32) 2356(.21)	2487(.21) 2441(.24)	2458(.24) 2427(.22) 2396(.19)	ν(B-H_t)
2245(.17) 2172(.14)	2227(.16) 2207(.16) 2177(.15) 2153(.15)	2234(.14) 2215(.12) 2163(.16) 2142(.10)	2231(.06) 2177(.06)		ν(B-H_b)
1600 w, br	1600 w, br	1600 w, br	1602(.08)	1600 w, br	ν(C= C)
1464(.18)	1450(.24)	1439(.49)	1436(.72)	1438(.72)	CH_2 scissoring

Table 2, continued

298K	348K	403K	473K	523K	Assignments
1395(.11)	1389(.14)				
1364(.10)	1357(.14)	1339(.27)	1337(.40)	1338(.43)	CH deformations
1271(.20)	1260(.21)	1257(.33)	1257(.45)	1259(.55)	BH deformations
1221(.11)	1232(.11)				
	1208(.12)	1198(.14)	1203(.21)	1205(.28)	B-O modes
1179(.16)	1168(.17)	1168(.22)	1167(.22)	1167(.27)	
			1134(.07)	1132(.13)	
1109(.27)	1103(.26)	1094(.21)	1083(.23)	1082(.30)	CH modes
1075(.23)	1063(.29)	1057(.24)			
		1032(.21)	1030(.24)	1029(.24)	
915(1.0)	908(1.0)	906(1.0)	902(1.0)	907(1.0)	Zr-O stretch[1]
				850 sh	CH modes
	798(.21)	787(.26)	785(.34)	787(.37)	
	725(.13)	729(.13)	712(.13)	737(.15)	
695(.15)	701(.15)	695(.11)	698(.13)	699(.14)	Zr-O stretch
		659(.10)	677(.13)		
601(.07)			623(.04)		
549(.05)			553(.05)	538(.04)	Zr-C modes
495(.06)	498(.03)	498 w	488(.11)	489(.11)	metal oxide modes
	430 sh	433(.07)	433(.20)	433(.22)	CH skeletal deformations
		402 w	401(.11)	402(.10)	
		359(.08)		348(.26)	
		333(.15)	332(.30)		

1. Al-O (bulk) stretch appears as a shoulder on the Zr-O peak.

Table 2, continued

298K	348K	403K	473K	523K	Assignments
296(.22)	295(.24)	301(.19)	294(.28)	297(.26)	A1 phonon
257(.23)	257(.26)	251(.26)	251(.41)	251(.32)	C-Zr-C bend or torsion

Table 3

Peak positions, Relative Intensities and Assignments for IET Spectra of $Zr(BH_4)_4$ Adsorbed on Al_2O_3 Interacting with Cyclohexene at an Exposure of 6000 Torr s.

298K	348K	403K	473K	523K	623K	Assignments
3639(.12)	3611(.11)	3626(.23)	3636(.16)	3699(.09)	3654(.34)	ν(OH)
		3050(.09)	3053(.32)	3041(.16)	3040(.26)	ν(C-H)
	3020(.11)		3024(.31)			
2912(1.47)						
2882(1.60)	2875(1.38)	2873(2.57)	2869(4.51)	2869(2.64)	2865(5.41)	
2835(2.06)	2830(1.85)	2828(3.49)	2823(5.80)	2823(3.48)	2819(7.02)	
2660(.11)	2660(.10)	2657(.12)	2654(.32)	2653(.16)	2640(.35)	
2490(.52)	2489(.26)					ν(B-H_t)
	2467(.26)	2455(.15)	2465(.36)	2465(.23)	2452(.36)	
	2439(.23)					
	2410(.23)					
2213(.17)	2225(.10)	2233(.09)				ν(B-H_b)
	2190(.10)					
2167(.15)	2152(.08)	2152(.09)				
	2110(.06)					
1600 w	1600 w	1600 w	1615(.10)			ν(C= C)
1441(.49)	1439(.64)	1439(.86)	1436(1.26)	1435(1.34)	1434(1.44)	CH_2 scissoring

Table 3, continued

298K	348K	403K	473K	523K	623K	Assignments
1345(.24)	1342(.36)	1341(.47)	1338(1.0)	1336(.92)	1336(1.05)	CH deformations
1259(.36)	1258(.47)	1258(.54)	1256(.92)	1258(.95)	1259(1.05)	BH deformations
	1233(.14)				1212(.46)	B-O modes
1202(.16)	1205(.14)	1198(.17)	1197(.47)	1201(.46)	1186(.41)	
1166(.22)	1166(.25)	1165(.22)	1168(.58)	1166(.45)	1172(.37)	
		1132(.27)	1133(.39)	1117(.22)	1120(.33)	
1091(.29)	1085(.33)	1085(.28)	1079(.60)	1076(.48)	1101(.32)	
1065(.27)	1062(.34)	1061(.27)	1061(.43)		1069(.52)	CH modes
1033(.23)	1031(.28)	1031(.27)	1027(.64)	1028(.41)	1018(.40)	
			990(.22)	990 sh	994(.24)	
			954(.54)		955(.61)	Al-O (bulk) stretch
902(1.0)	903(1.0)	903(1.0)	907(1.0)	907 sh	913(1.0)	Zr-O stretch[1]
			885(1.0)	898(1.0)	875(.96)	
	850 sh	850(.51)	852(.65)	850 sh	852(.78)	CH modes
786(.24)	784(.29)	785(.32)	781(.51)	782(.51)	782(.59)	
	722(.08)		729(.28)			
689(.10)	689(.13)	695(.10)	703 sh	694(.15)	678(.21)	Zr-O
	667(.09)			653(.11)		

1. Al-O (bulk) stretch appears as a shoulder on the Zr-O peak.

Table 3, continued

298K	348K	403K	473K	523K	623K	Assignments
550 w	552 w	550 w	550(.20)			
487(.11)	489(.14)	488(.13)	486(.31)	489(.31)	489(.30)	Zr-C modes
432(.10)	435(.13)	433(.15)	432(.51)	433(.45)	433(.52)	CH skeletal deformations
408(.07)	407(.11)	405 w	411 w	407(.36)	407(.48)	metal oxide modes
					361(.62)	
329(.24)	331(.29)	334(.27)	339(.51)	333(.60)	335(.50)	
			313(.47)			
292(.28)	295(.28)	297(.17)				Al phonon
251(.41)	251(.48)	251(.49)	251(.94)	251(.88)	251(.51)	Zr-C bend or torsion

Table 4

OBSERVATION OF TYPE I AND II SPECTRA
AS A FUNCTION OF TEMPERATURE AND EXPOSURE

	298 K	348 K	403 K	473 K	523 K	623 K
150 Torr s	I	I	I	I	I	II?
1200 Torr s	I	I	II	II	II	--
6000 Torr s	II	II	II	II	II	II

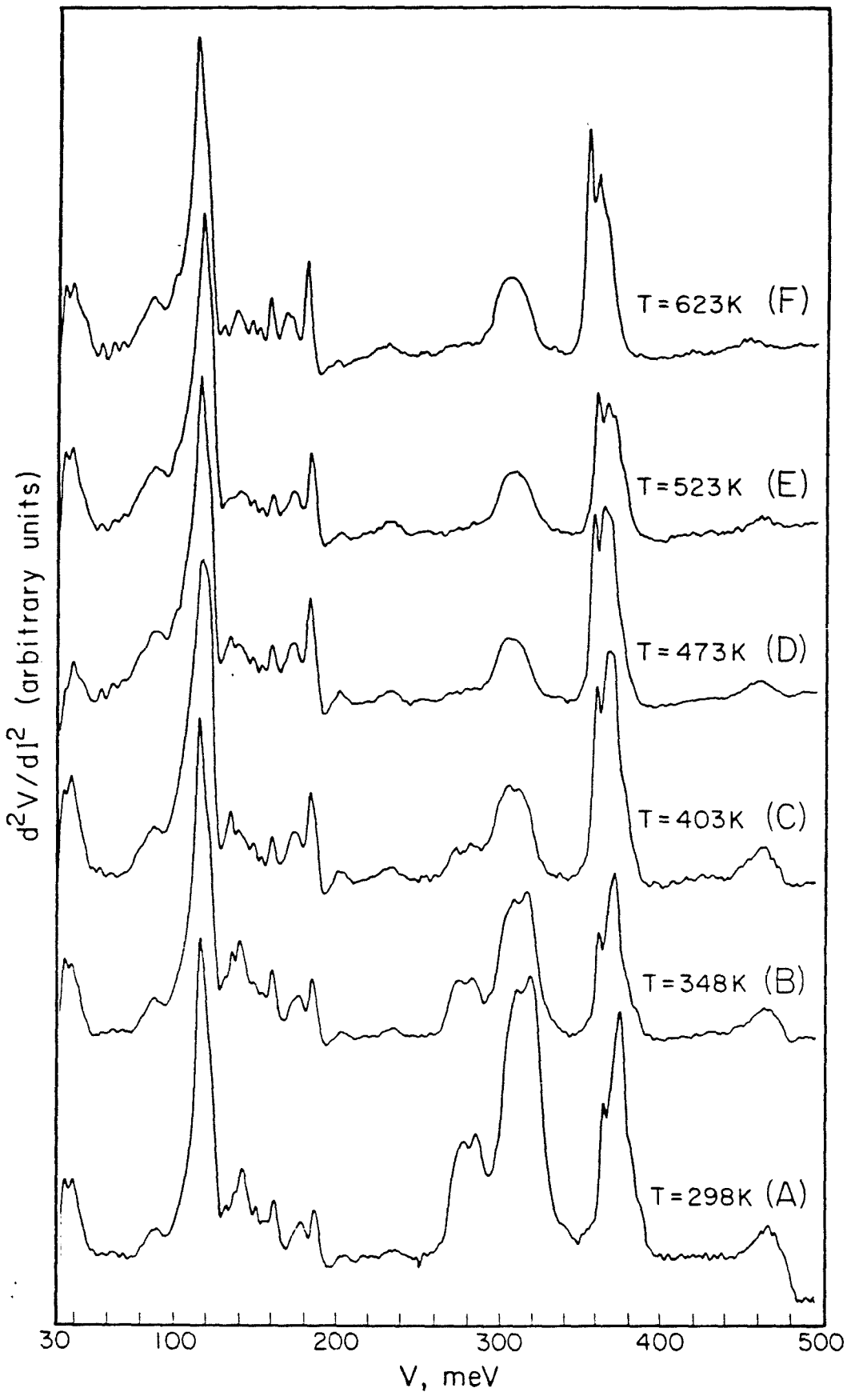
T=623K (F)
T=523K (E)
T=473K (D)
T=403K (C)
T=348K (B)
T=298K (A)
d^2V/dI^2 (arbitrary units)
30
100
200
300
400
500
V, meV

Figure 1

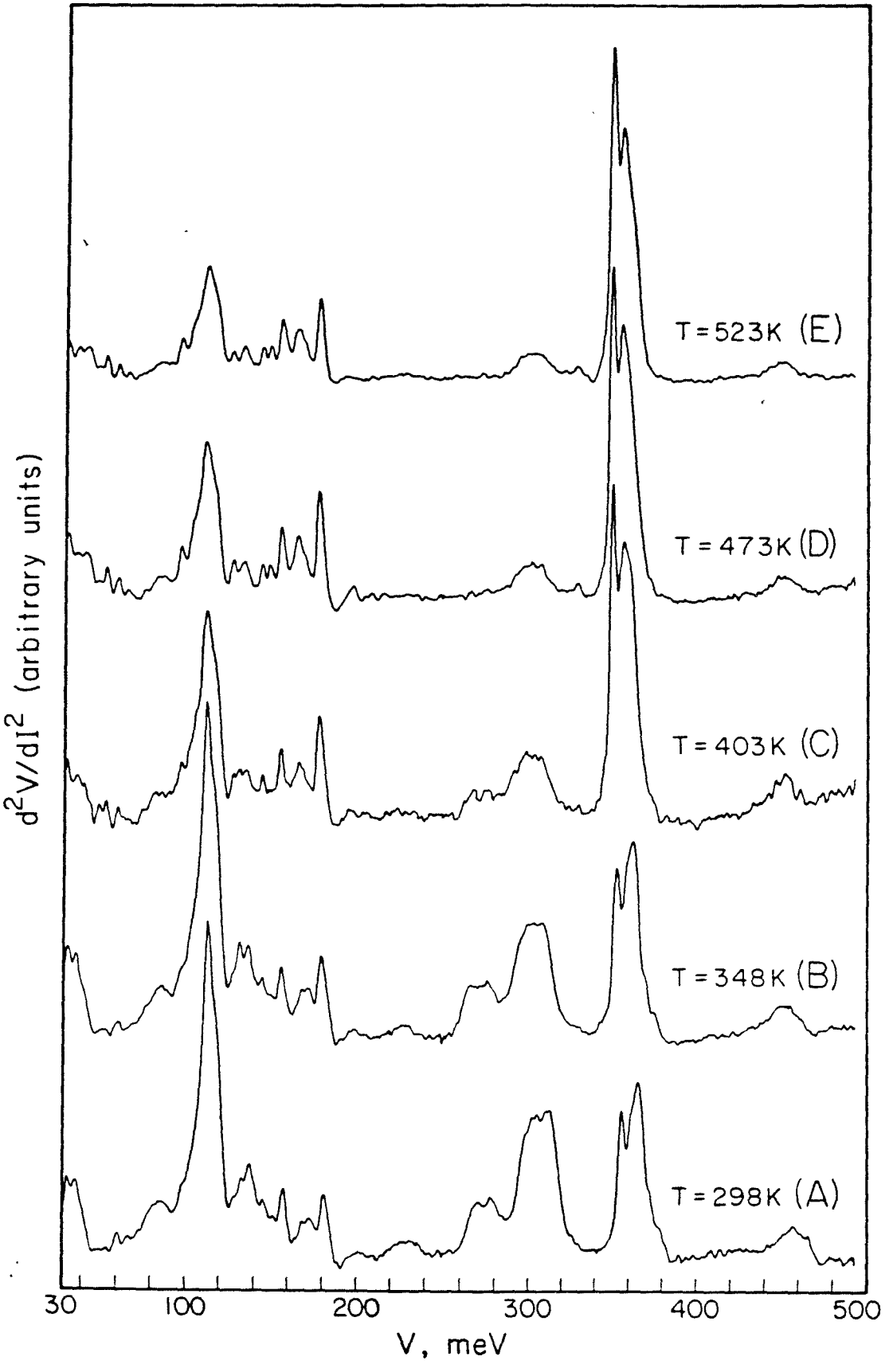
T = 523K (E)
T = 473K (D)
T = 403K (C)
T = 348K (B)
T = 298K (A)
d^2V/dI^2 (arbitrary units)
30
100
200
300
400
500
V, meV

Figure 2

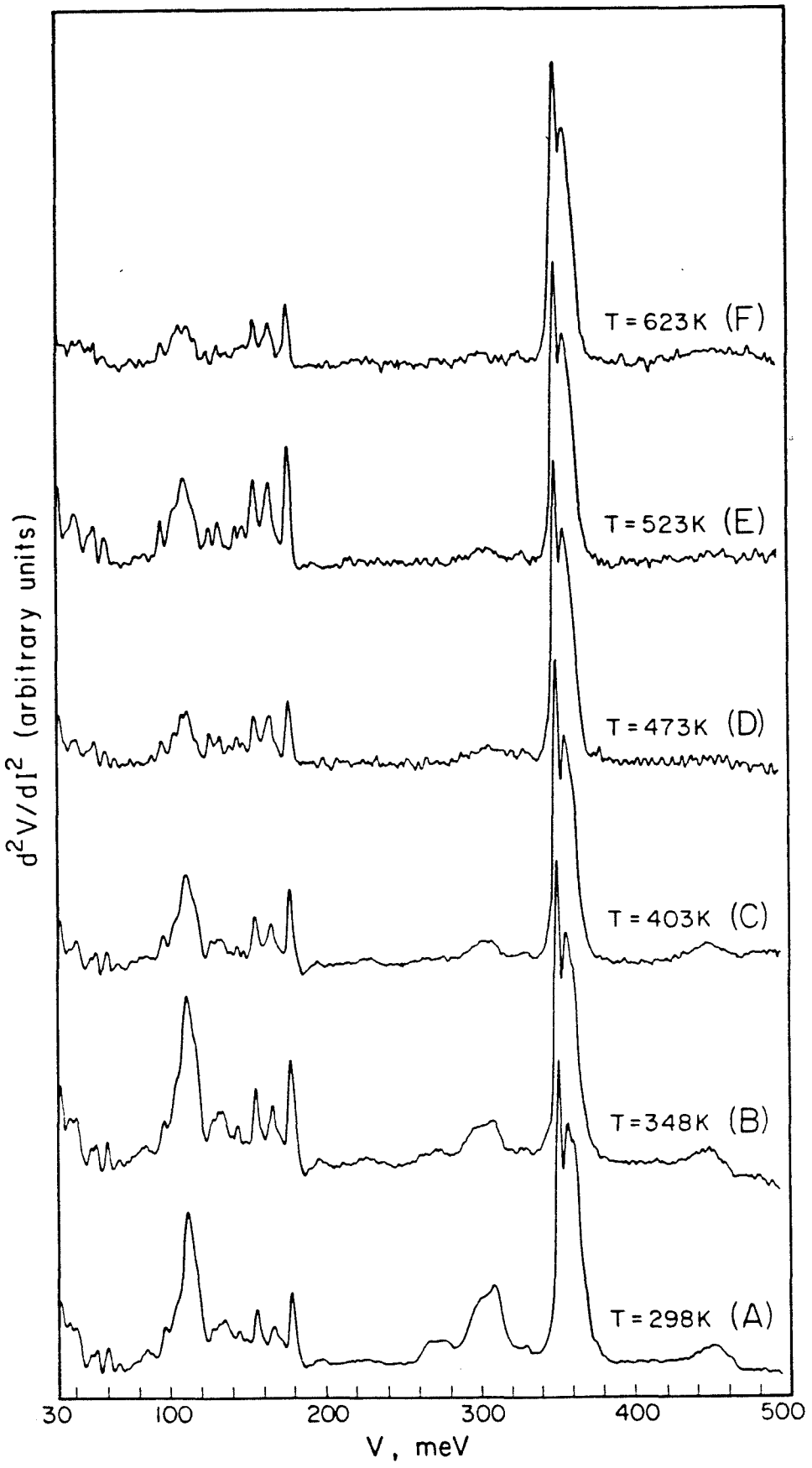
T = 623K (F)
T = 523K (E)
T = 473K (D)
T = 403K (C)
T = 348K (B)
T = 298K (A)
d^2V/dI^2 (arbitrary units)
30
100
200
300
400
500
V, meV

Figure 3

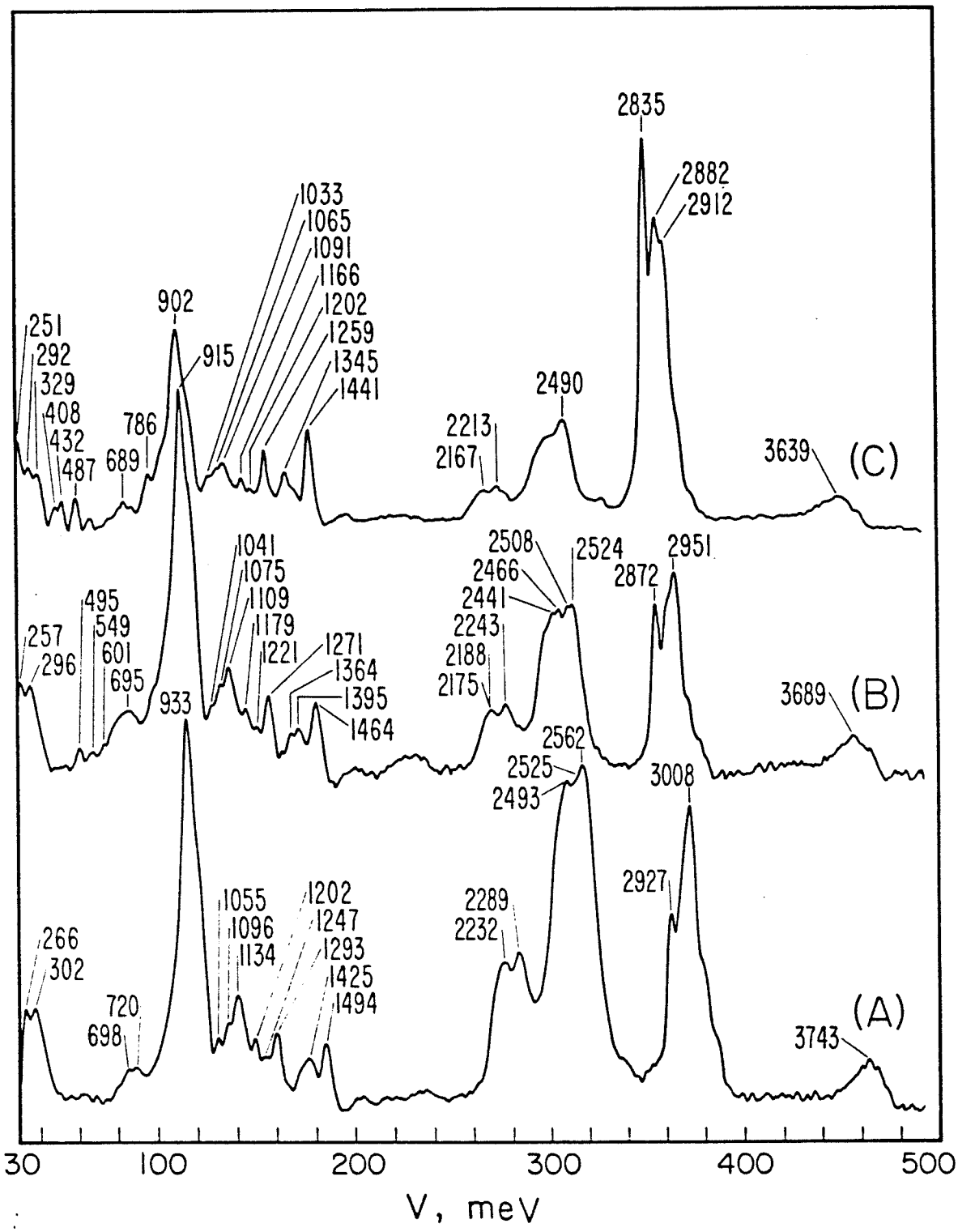
2835
2882
2912
1033
1065
1091
1166
1202
1259
1345
1441
902
915
251
292
329
408
432
487
786
689
2213
2167
2490
3639
(C)
1041
1075
1109
1179
1221
1271
1364
1395
1464
933
257
296
495
549
601
695
2508
2524
2466
2441
2243
2188
2175
2872
2951
3689
(B)
2562
2525
2493
3008
1055
1096
1134
1202
1247
1293
1425
1494
266
302
720
698
2289
2232
2927
3743
(A)
30
100
200
300
400
500
V, meV

Figure 4

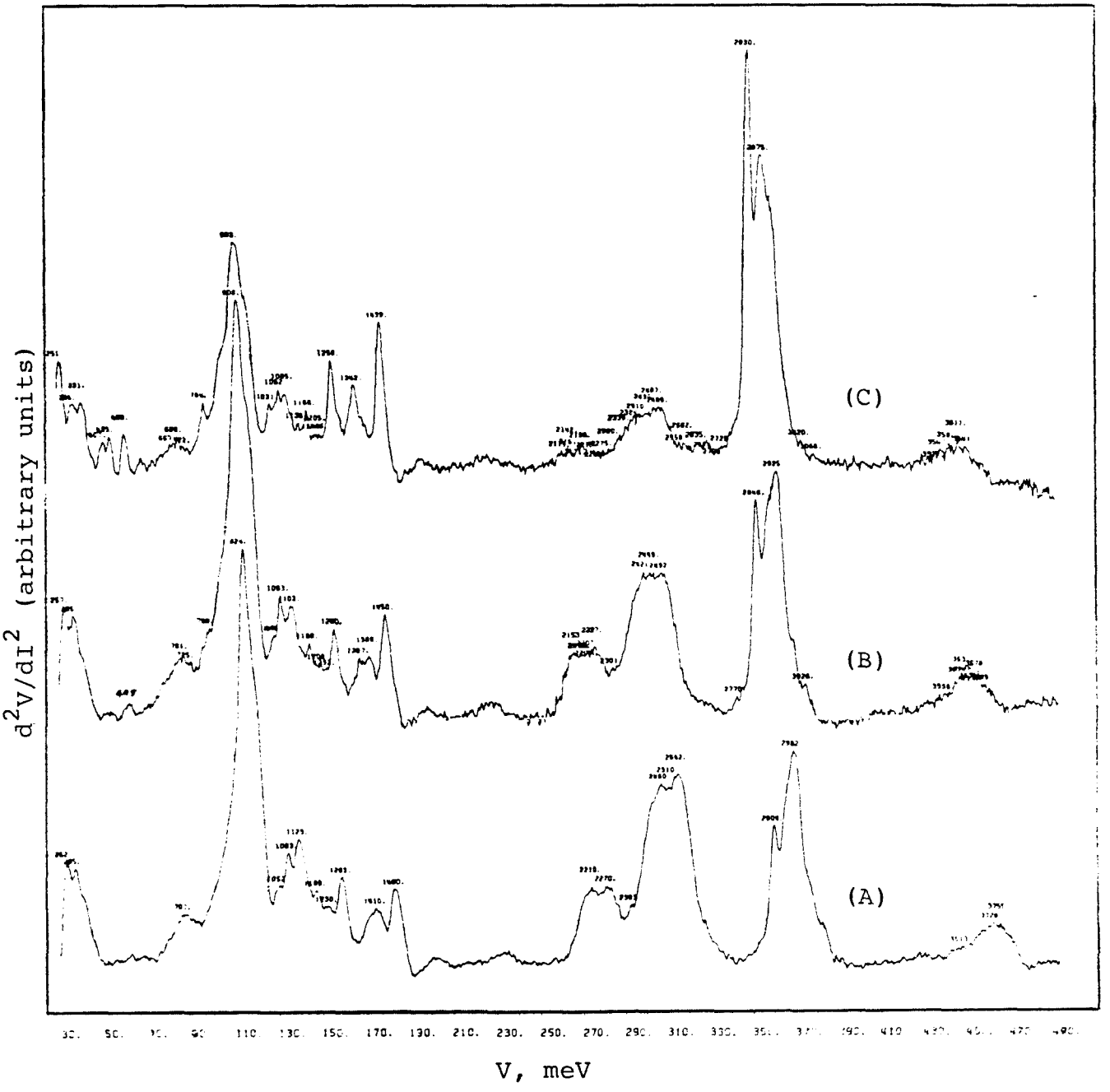

Figure 5

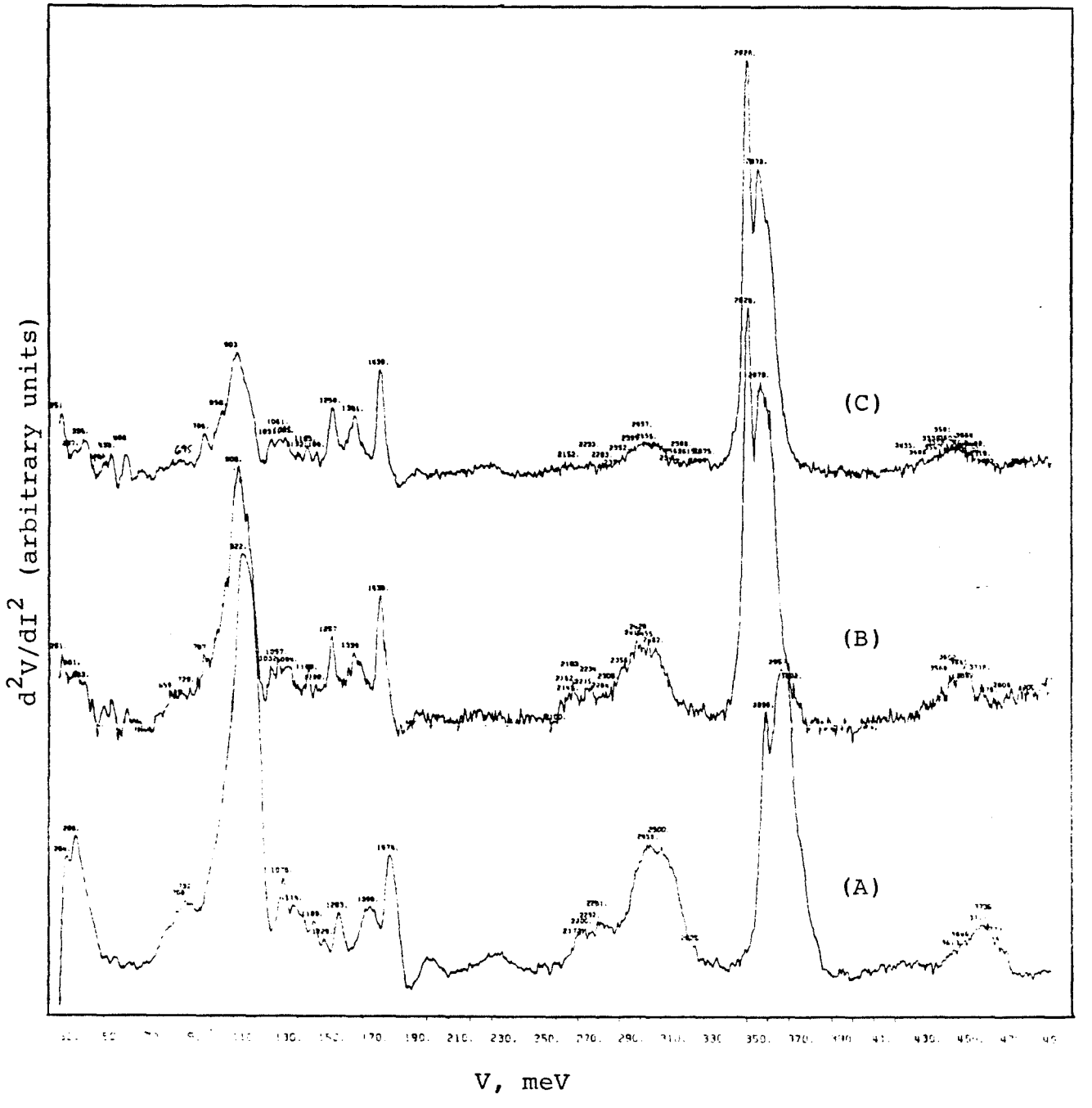

Figure 6

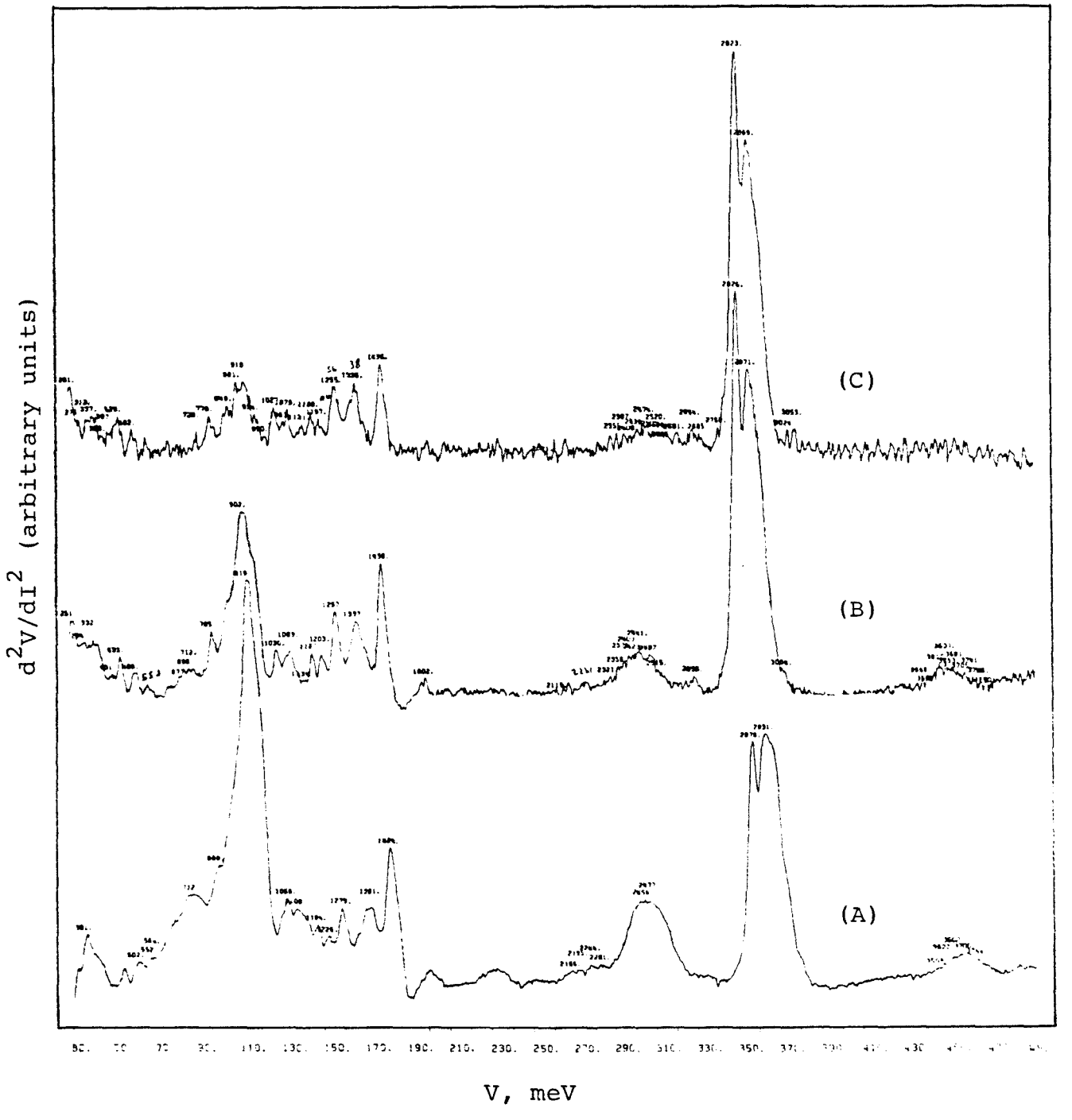

Figure 7

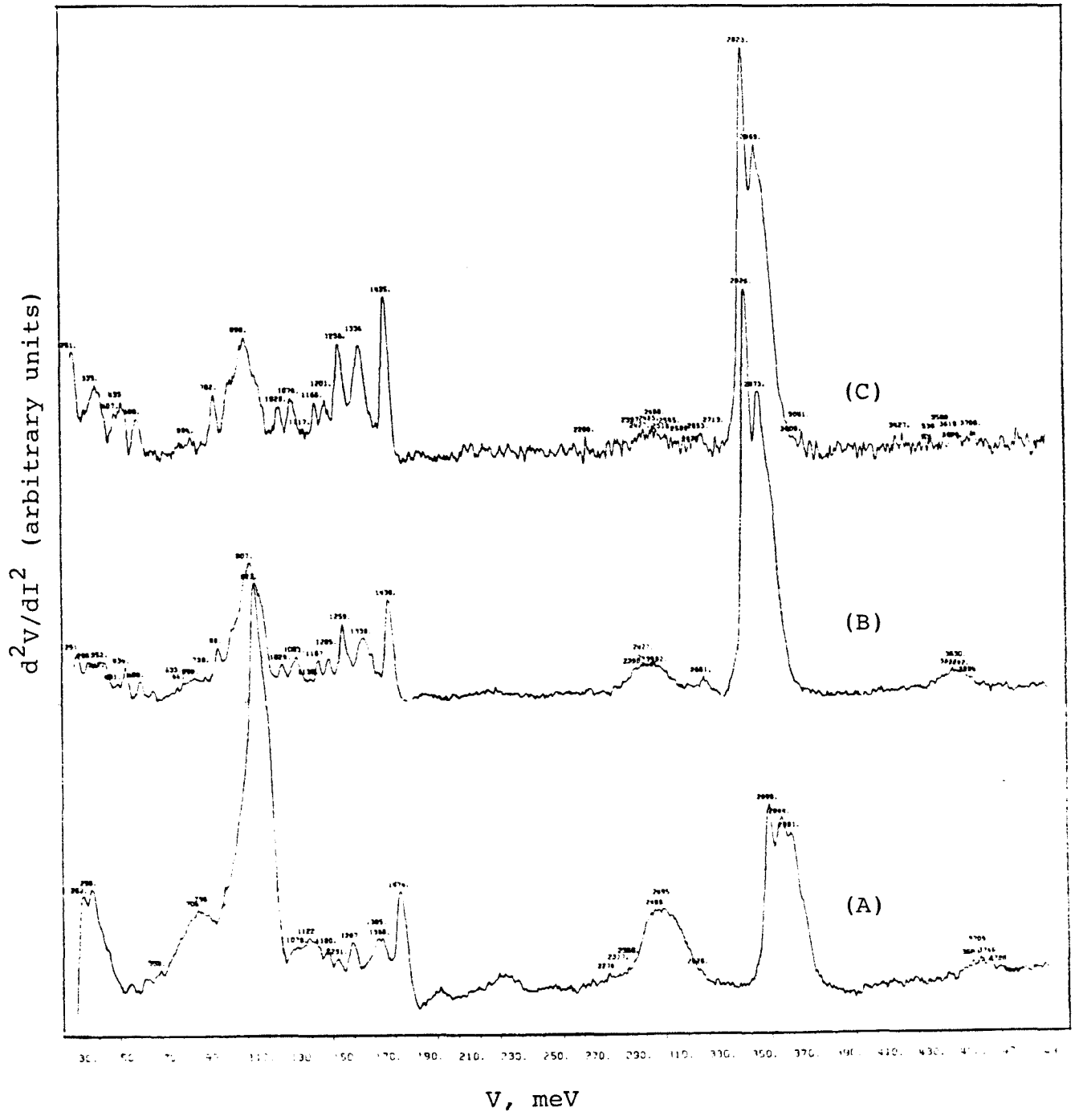

Figure 8

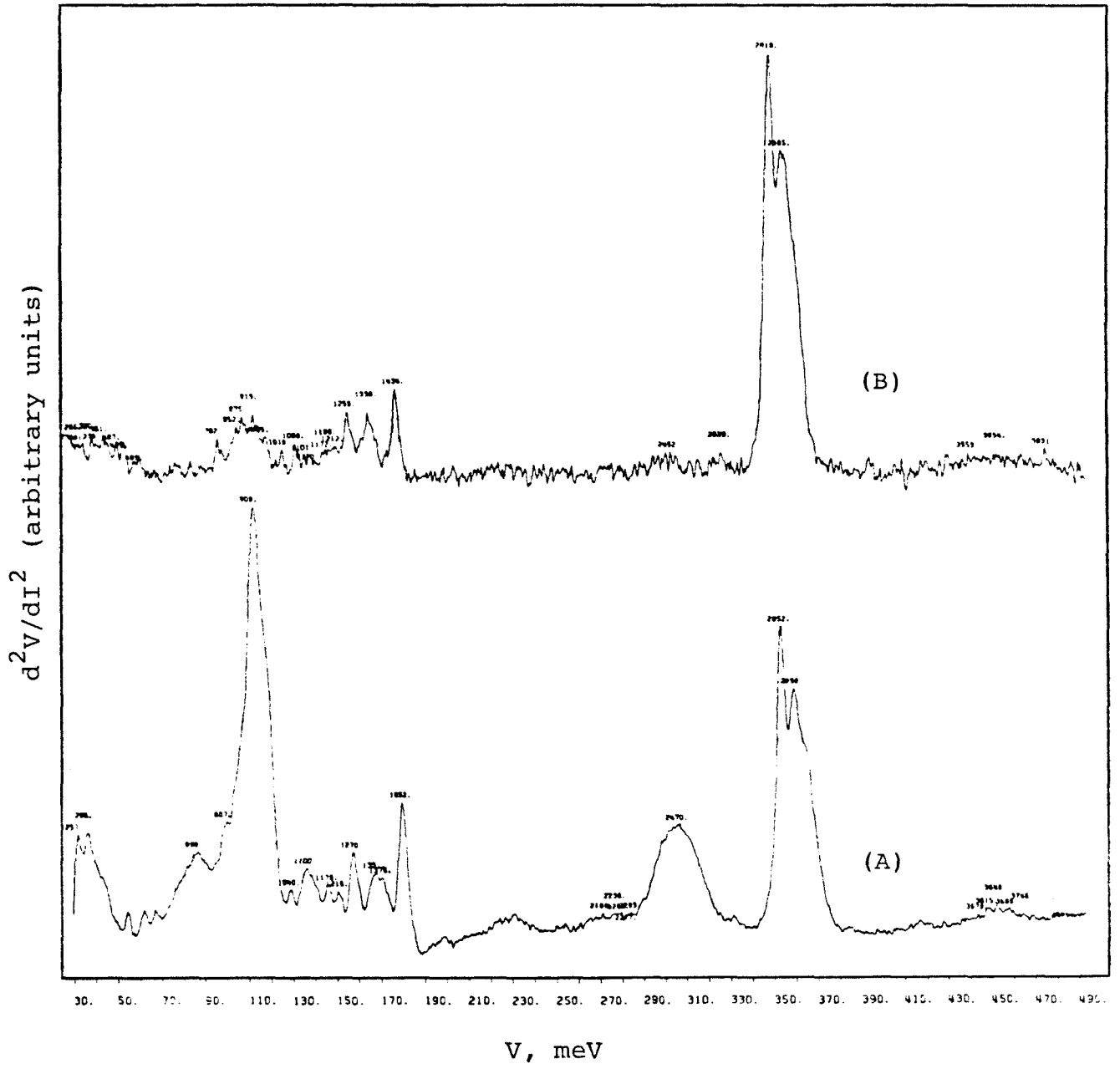
(B)
(A)
d^2V/dI^2 (arbitrary units)
30. 50. 70. 90. 110. 130. 150. 170. 190. 210. 230. 250. 270. 290. 310. 330. 350. 370. 390. 410. 430. 450. 470. 490.
V, meV

Figure 9

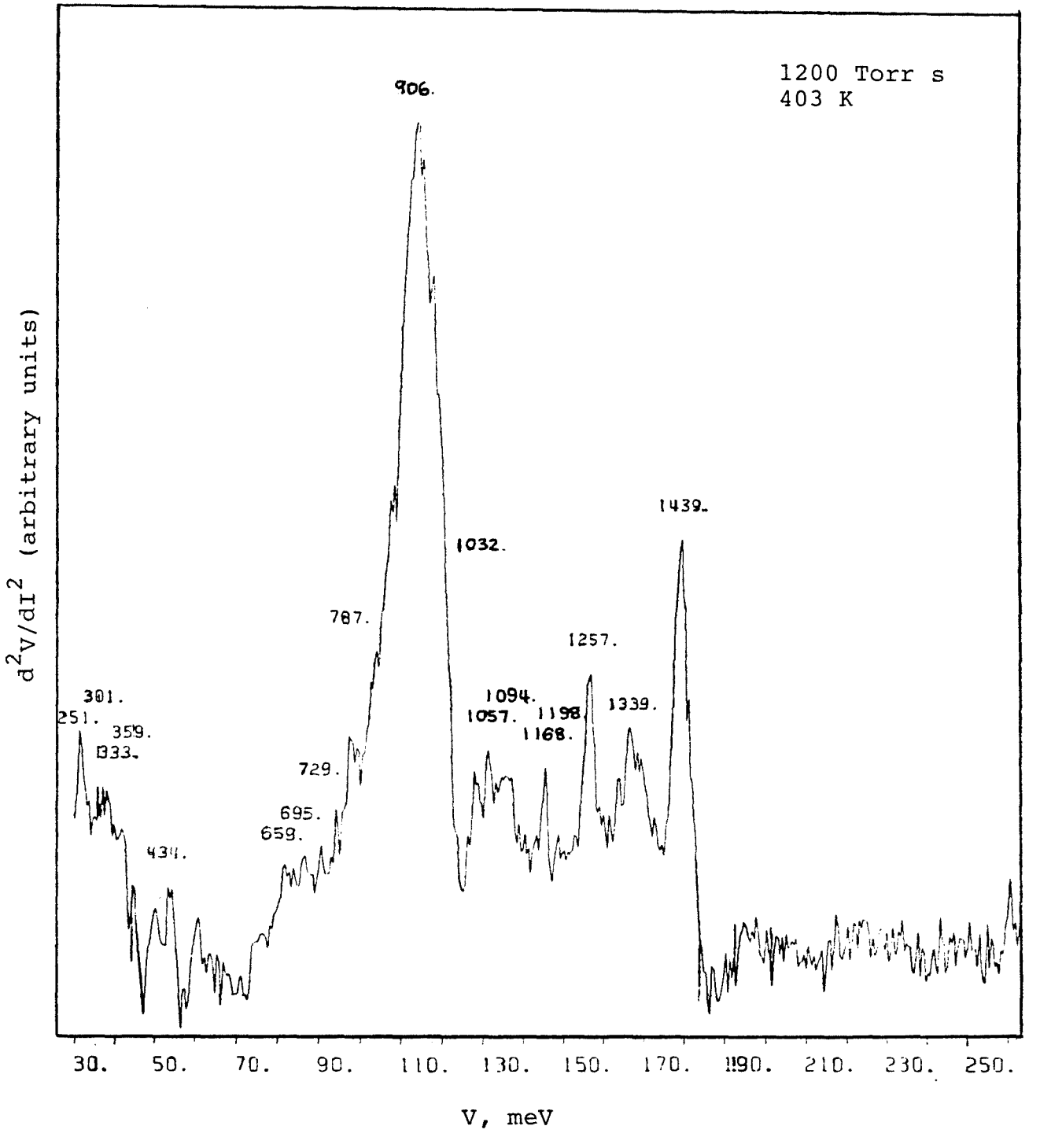
1200 Torr s
403 K
906.
1032.
1439.
787.
1257.
1094.
1057.
1198.
1168.
1339.
729.
695.
659.
301.
251.
359.
333.
434.
d^2V/dI^2 (arbitrary units)
30.
50.
70.
90.
110.
130.
150.
170.
190.
210.
230.
250.
V, meV

Figure 10

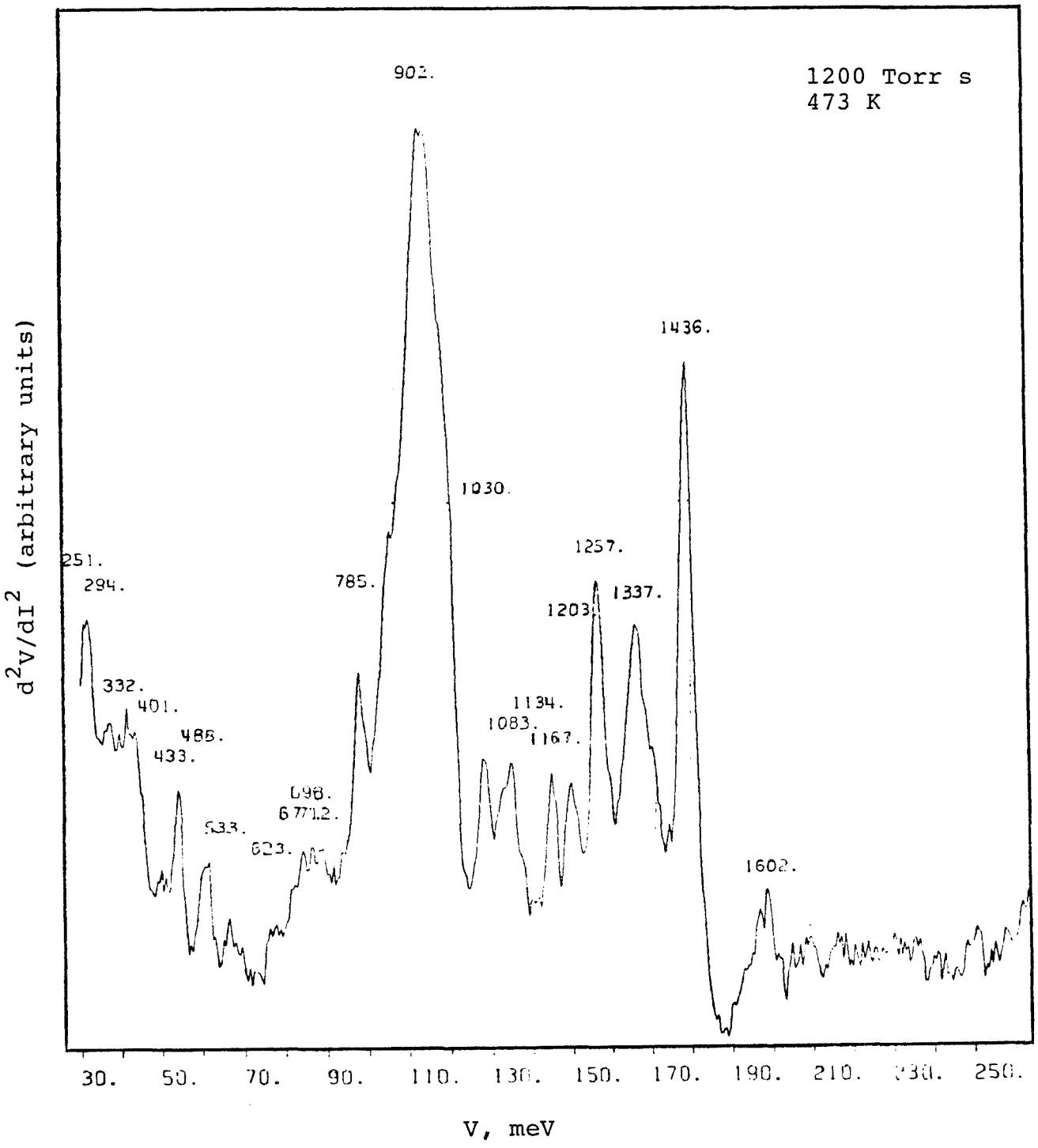
1200 Torr s
473 K
902.
1436.
1030.
1257.
1337.
1203.
785.
251.
294.
332.
401.
486.
433.
533.
623.
698.
677.2.
1134.
1083.
1167.
1602.
30.
50.
70.
90.
110.
130.
150.
170.
190.
210.
230.
250.
V, meV
d²V/dI² (arbitrary units)

Figure 11

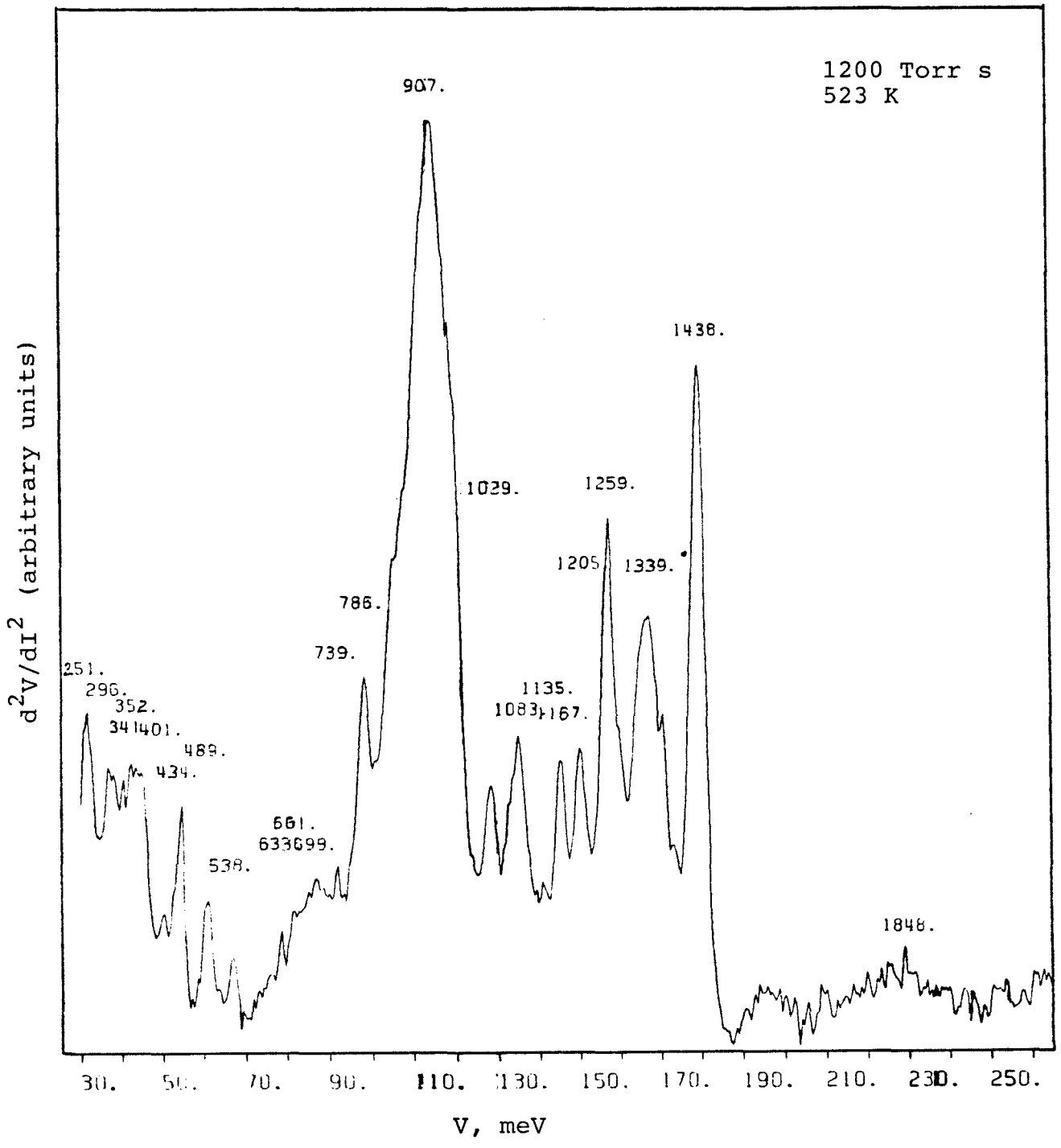
1200 Torr s
523 K
907.
1438.
1029.
1259.
1205
1339.
786.
739.
251.
296.
352.
341401.
489.
434.
661.
633699.
538.
1135.
1083.1167.
1848.
30.
50.
70.
90.
110.
130.
150.
170.
190.
210.
230.
250.
V, meV
d²V/dI² (arbitrary units)

Figure 12

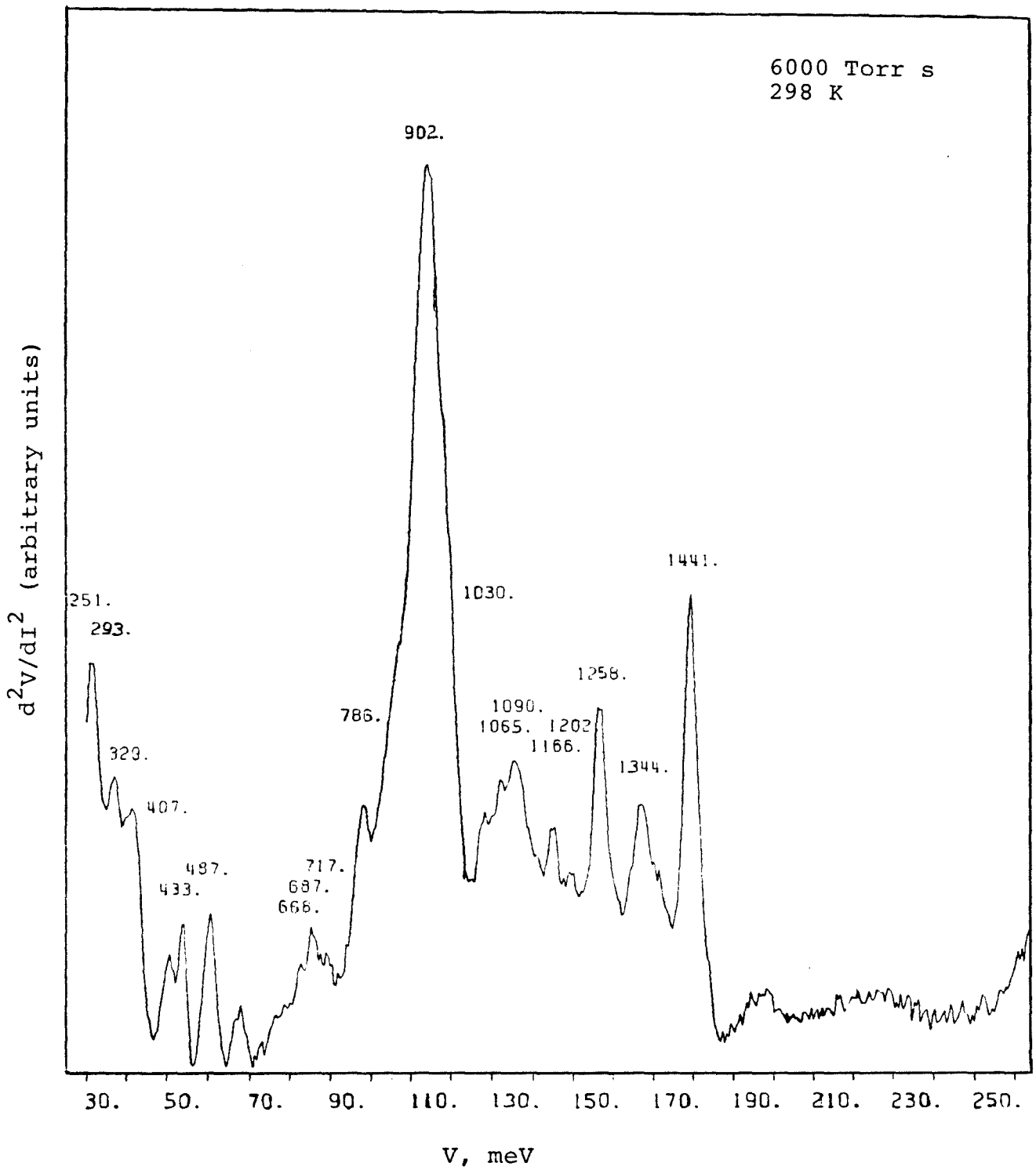
6000 Torr s
298 K
902.
1441.
1030.
251.
293.
1258.
786.
1090.
1065.
1202
1166.
1344.
329.
407.
487.
433.
717.
687.
668.
30.
50.
70.
90.
110.
130.
150.
170.
190.
210.
230.
250.
V, meV
d²V/dI² (arbitrary units)

Figure 13

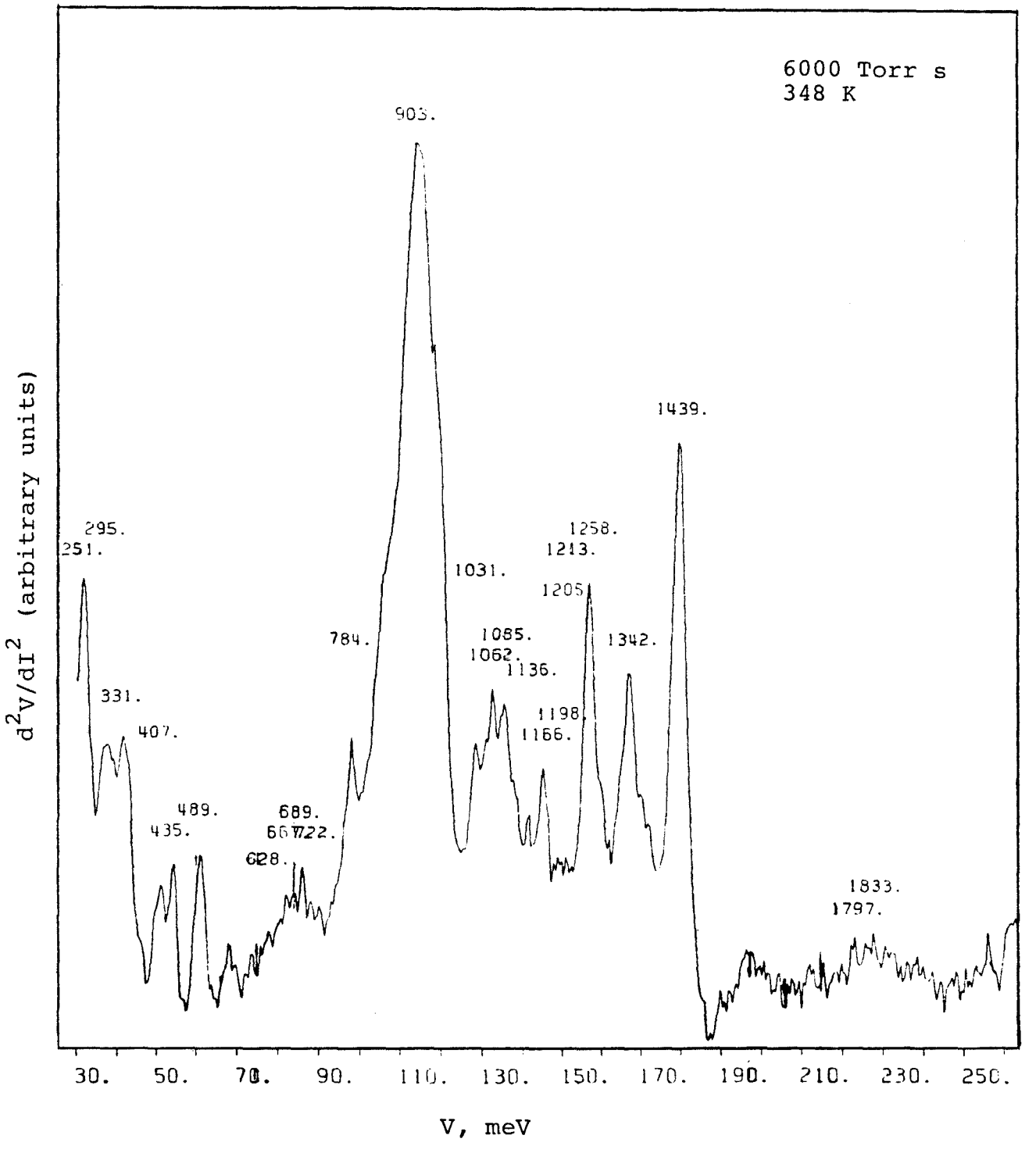
6000 Torr s
348 K
903.
1439.
295.
251.
1258.
1213.
1031.
1205
784.
1085.
1062.
1342.
1136.
331.
1198.
1166.
407.
489.
435.
689.
628.
1833.
1797.
30.
50.
90.
110.
130.
150.
170.
190.
210.
230.
250.
V, meV
d²V/dI² (arbitrary units)

Figure 14

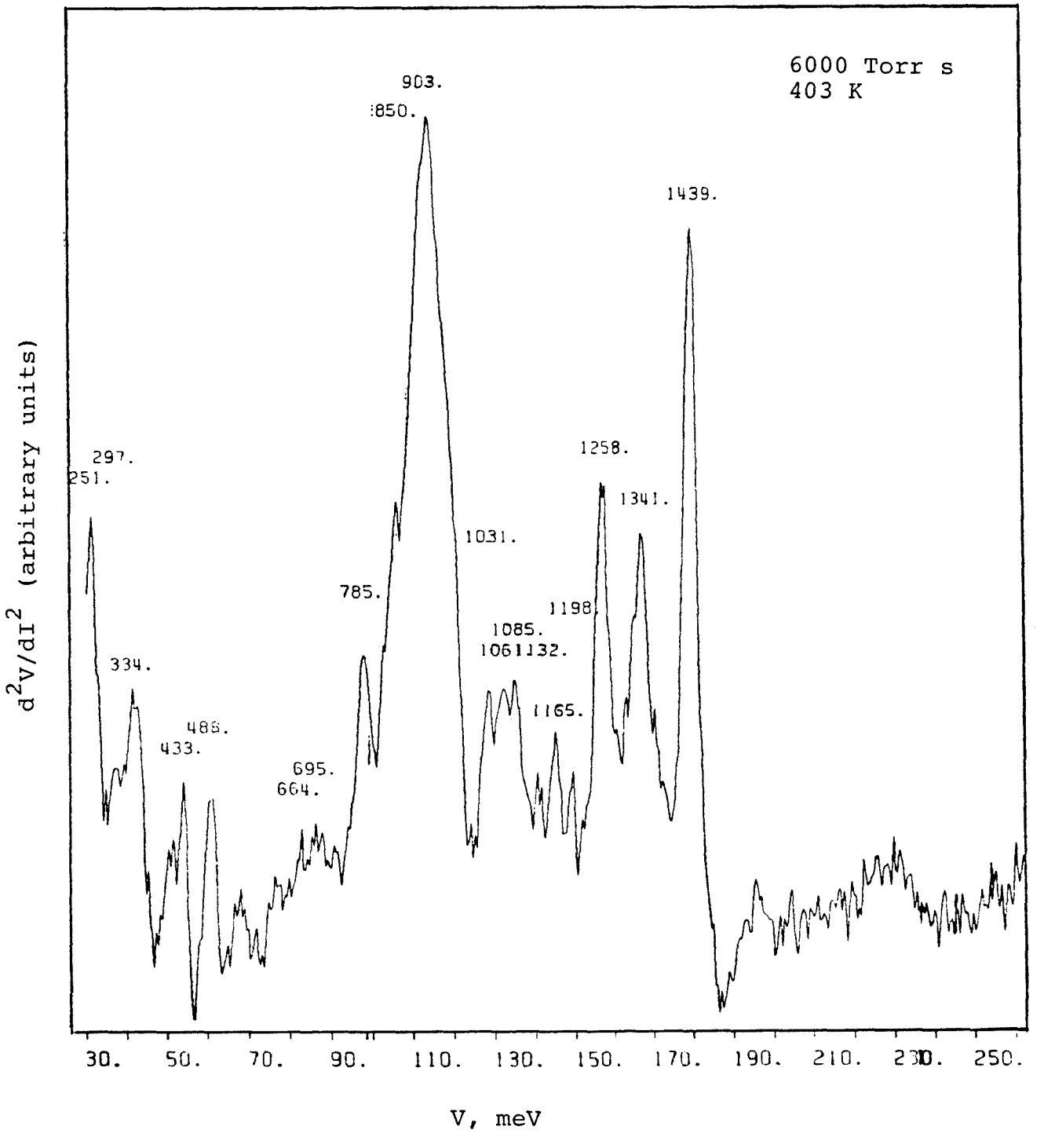
6000 Torr s
403 K
903.
850.
1439.
1258.
1341.
1031.
785.
1198
1085.
1061132.
1165.
334.
486.
433.
695.
664.
297.
251.
d^2V/dI^2 (arbitrary units)
30. 50. 70. 90. 110. 130. 150. 170. 190. 210. 230. 250.
V, meV

Figure 15

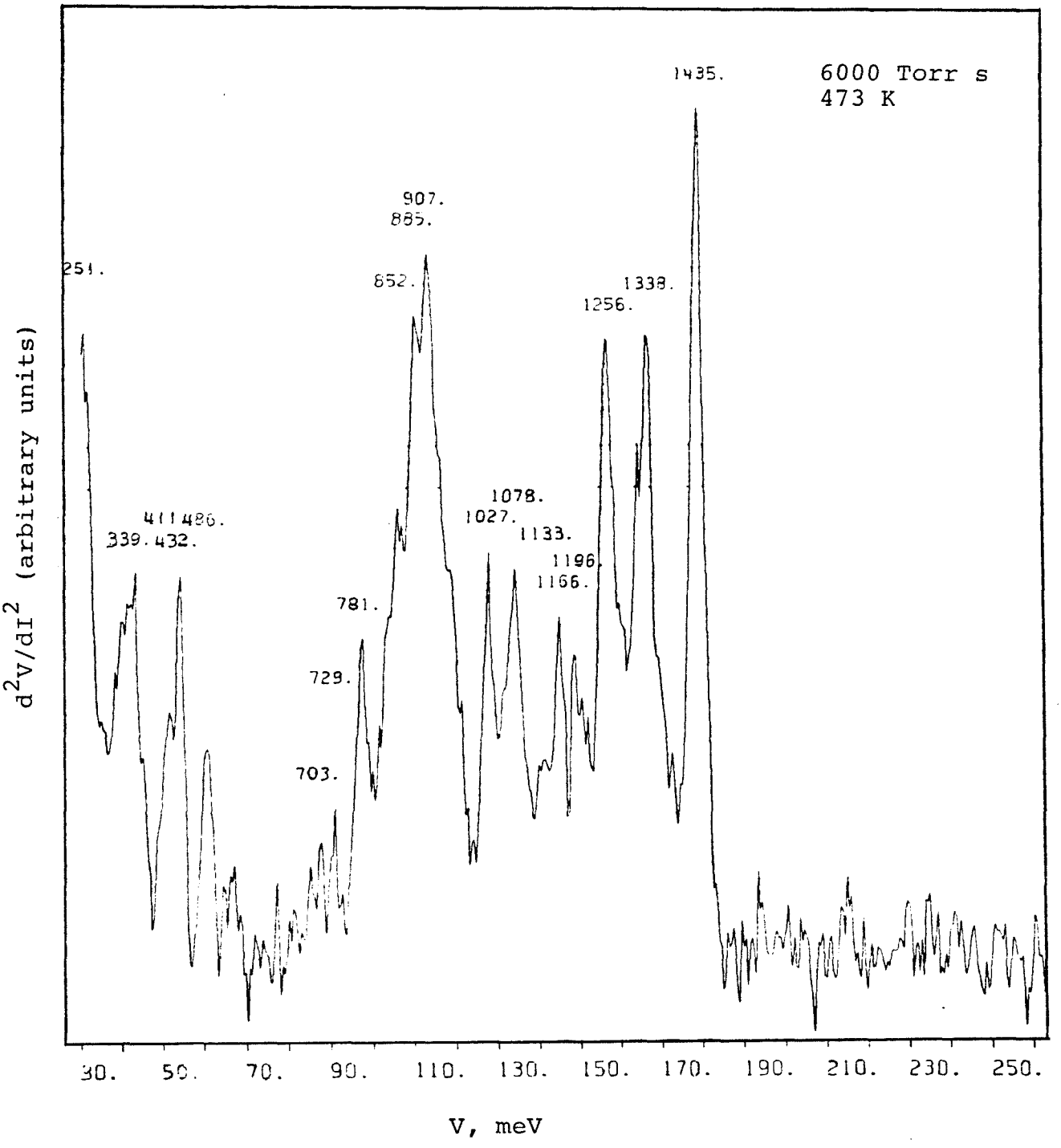
6000 Torr s
473 K
1435.
907.
885.
852.
251.
1338.
1256.
1078.
1027.
1133.
1196
1166.
781.
729.
703.
411 486.
339. 432.
d^2V/dI^2 (arbitrary units)
30. 50. 70. 90. 110. 130. 150. 170. 190. 210. 230. 250.
V, meV

Figure 16

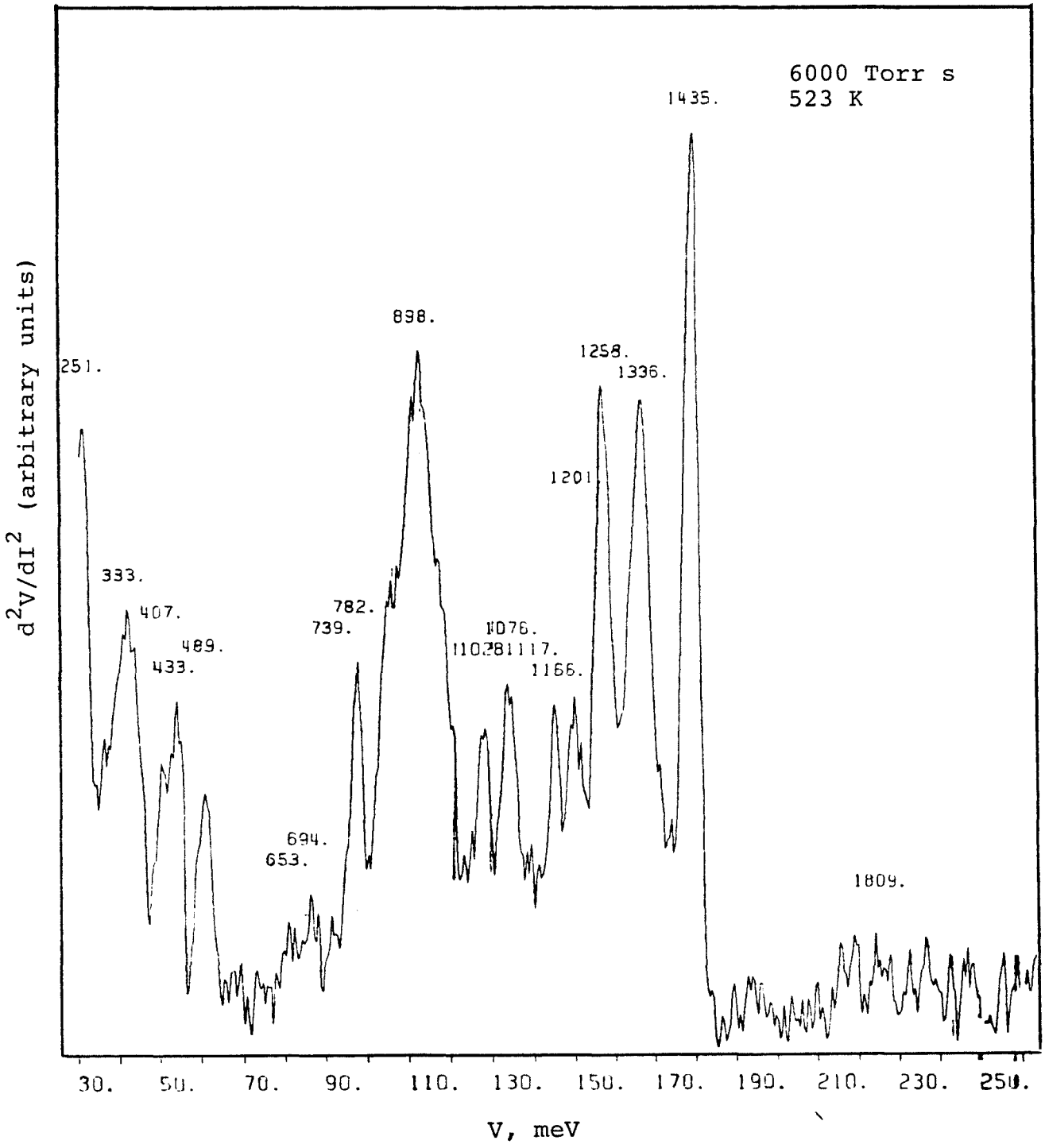
6000 Torr s
523 K
1435.
898.
1258.
1336.
251.
1201
333.
407.
489.
433.
782.
739.
694.
653.
1166.
1809.
30.
50.
70.
90.
110.
130.
150.
170.
190.
210.
230.
250.
V, meV
d²V/dI² (arbitrary units)

Figure 17

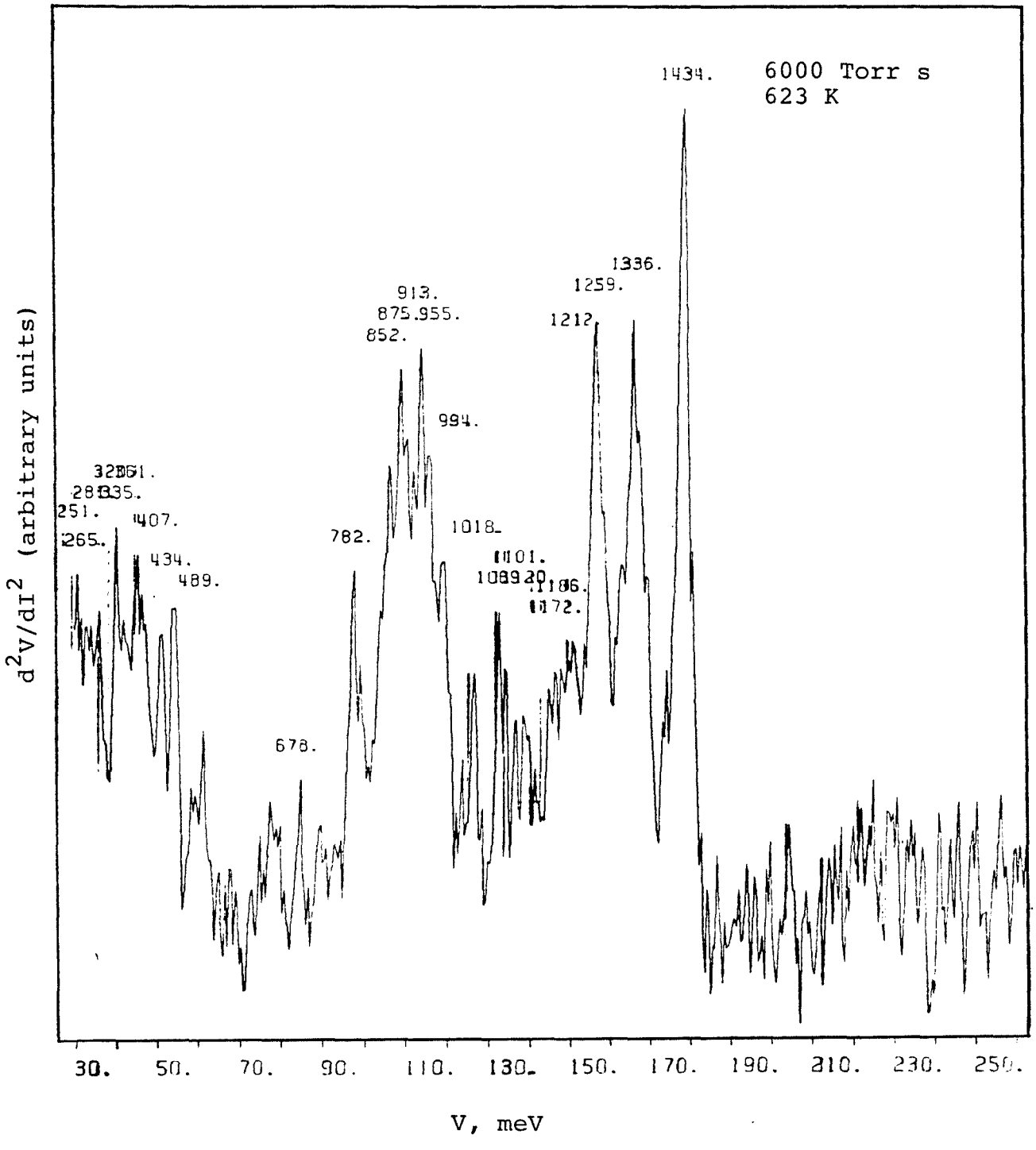
6000 Torr s
623 K
1434.
1336.
1259.
1212.
913.
875.955.
852.
994.
782.
678.
1018.
1101.
1089.20
1186.
1172.
407.
434.
489.
251.
265.
30.
50.
70.
90.
110.
130.
150.
170.
190.
210.
230.
250.
V, meV
d2V/dr2 (arbitrary units)

Figure 18

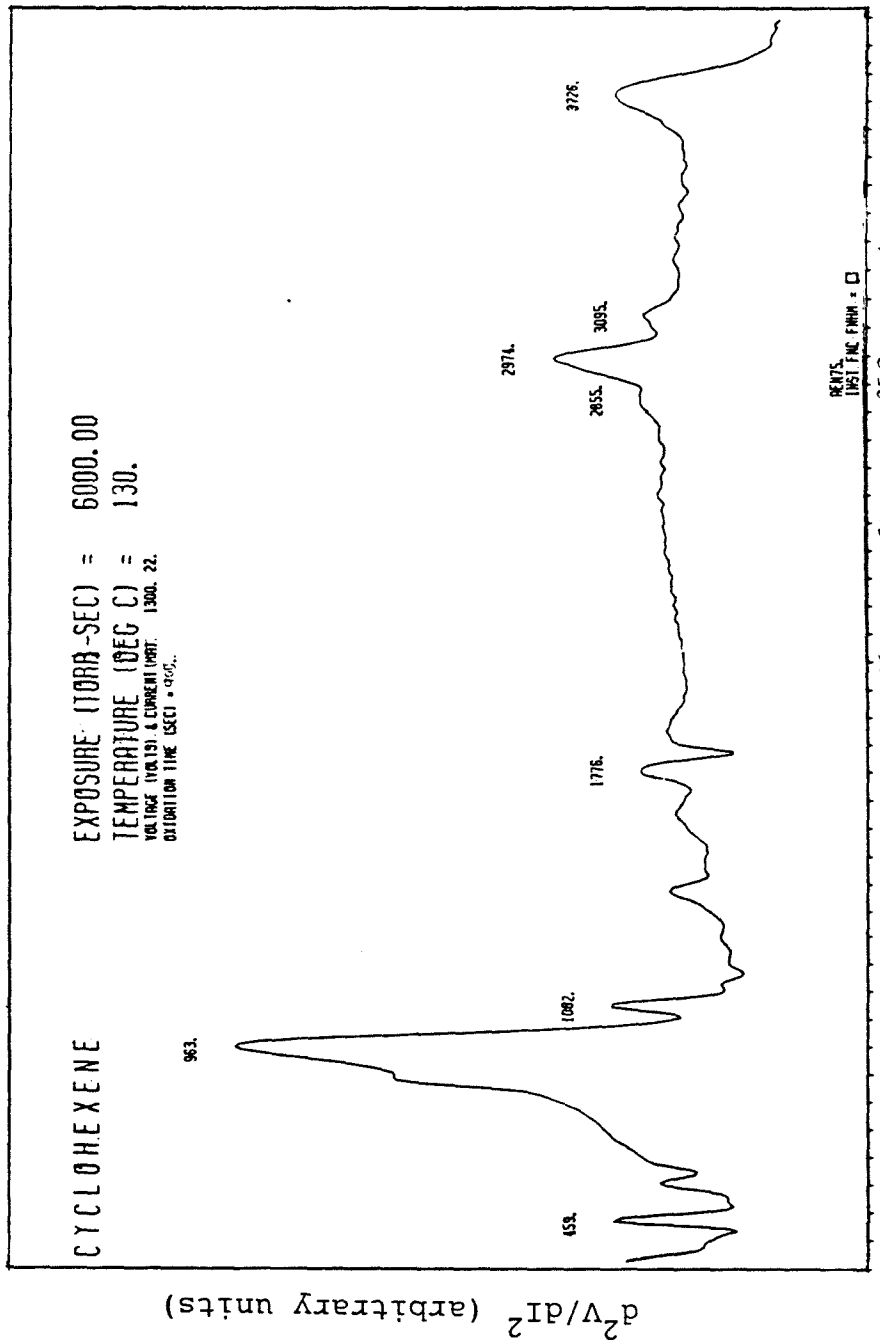
CYCLOHEXENE
EXPOSURE (10RR-SEC) = 6000.00
TEMPERATURE (DEG C) = 130.
963.
1082.
1776.
2974.
2855.
3095.
3226.
459.
50
100
150
200
250
300
350
400
450
V, meV
d^2V/dI^2 (arbitrary units)

Figure 19

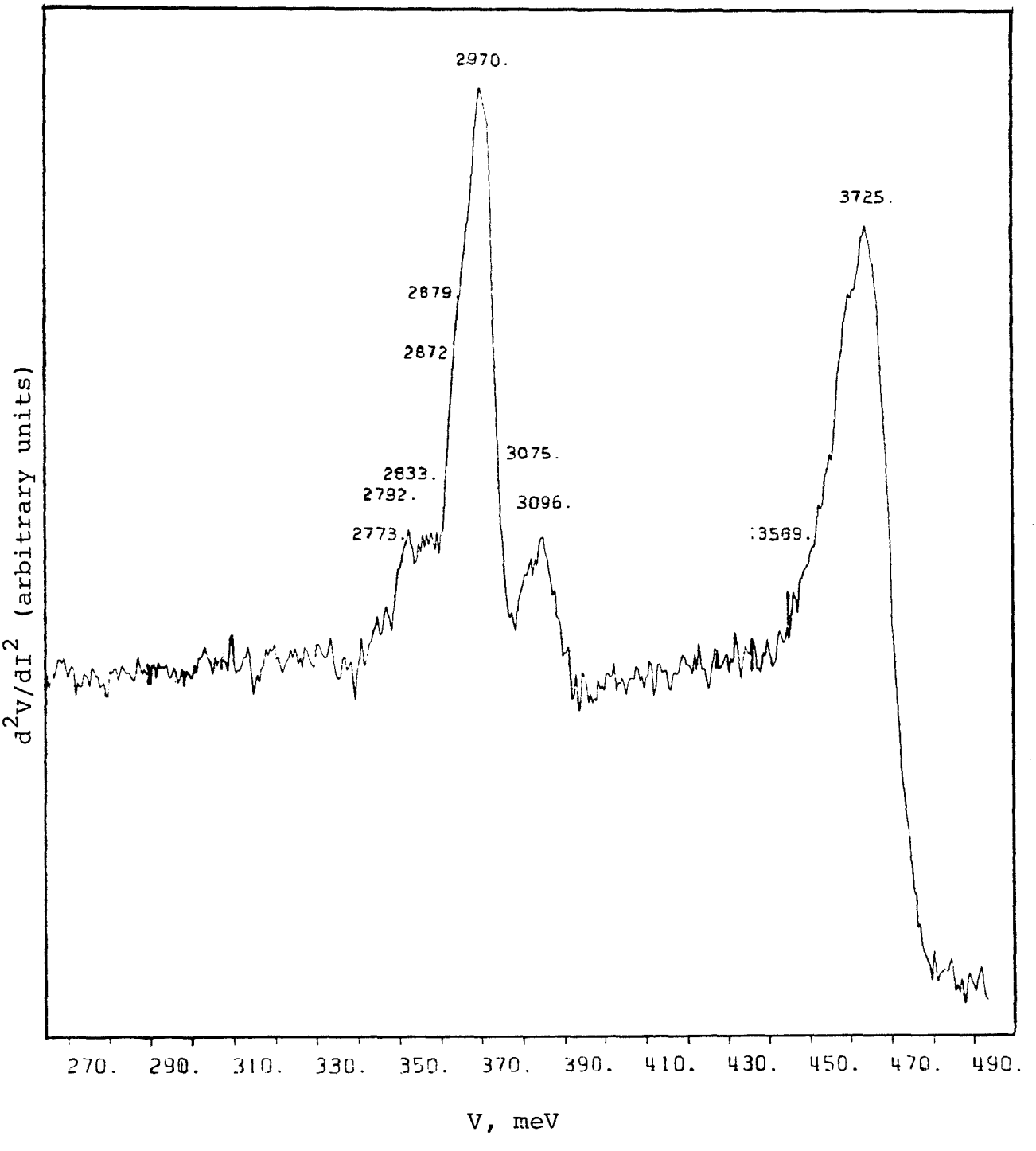
2970.
3725.
2879
2872
3075.
2833.
2792.
3096.
2773.
3589.
d^2V/dI^2 (arbitrary units)
270. 290. 310. 330. 350. 370. 390. 410. 430. 450. 470. 490.
V, meV

Figure 20

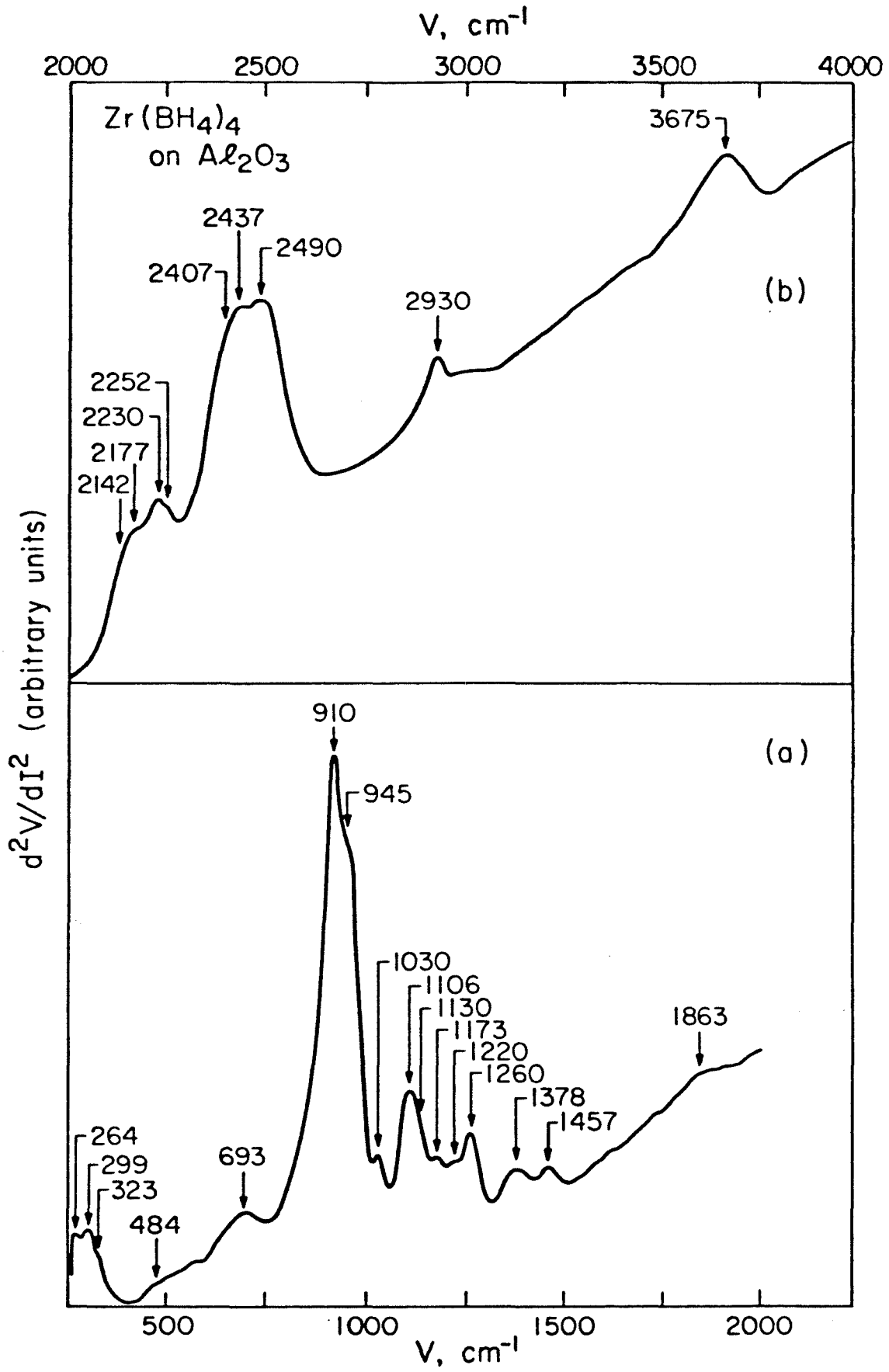
V, cm⁻¹
2000
2500
3000
3500
4000
Zr(BH4)4
on Aℓ2O3
3675
2437
2490
2407
2930
(b)
2252
2230
2177
2142
d²V/dI² (arbitrary units)
910
(a)
945
1030
1106
1130
1173
1220
1260
1378
1457
1863
264
299
323
484
693
500
1000
1500
2000
V, cm⁻¹

Figure 21

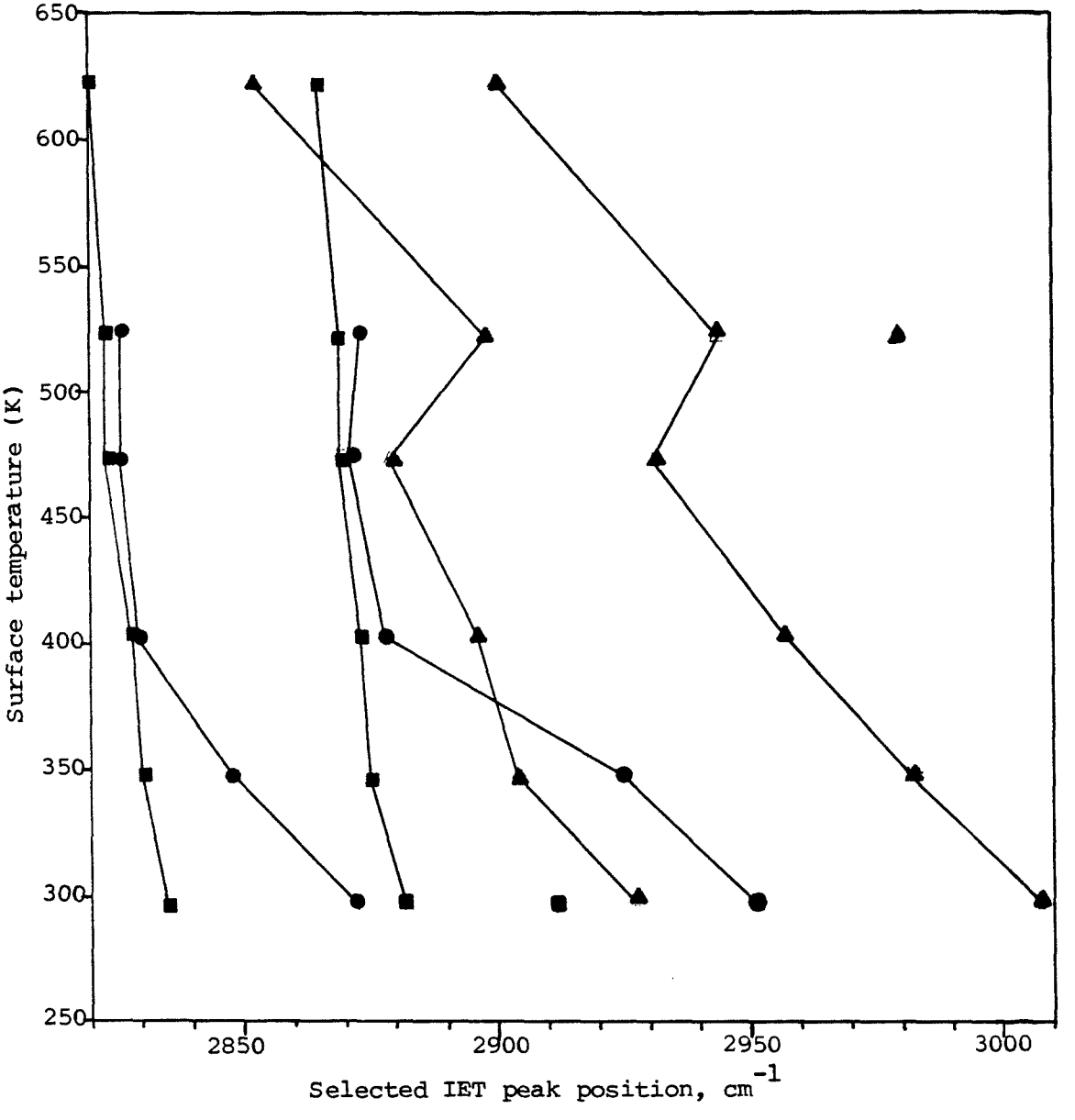
650
600
550
500
450
400
350
300
250
Surface temperature (K)
2850
2900
2950
3000
Selected IET peak position, cm-1

Figure 22

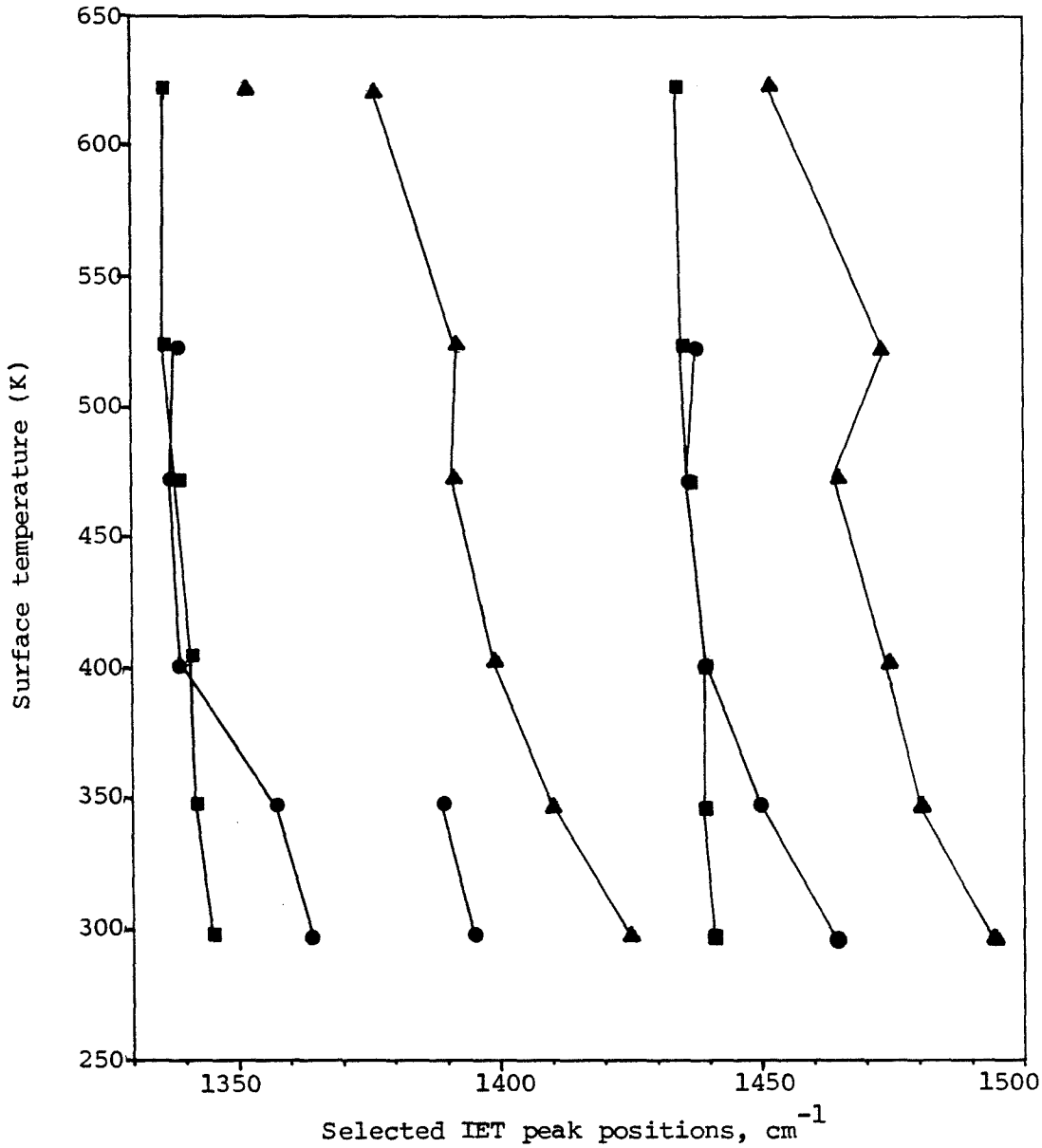
650
600
550
500
450
400
350
300
250
Surface temperature (K)
1350
1400
1450
1500
Selected IET peak positions, cm-1

Figure 23

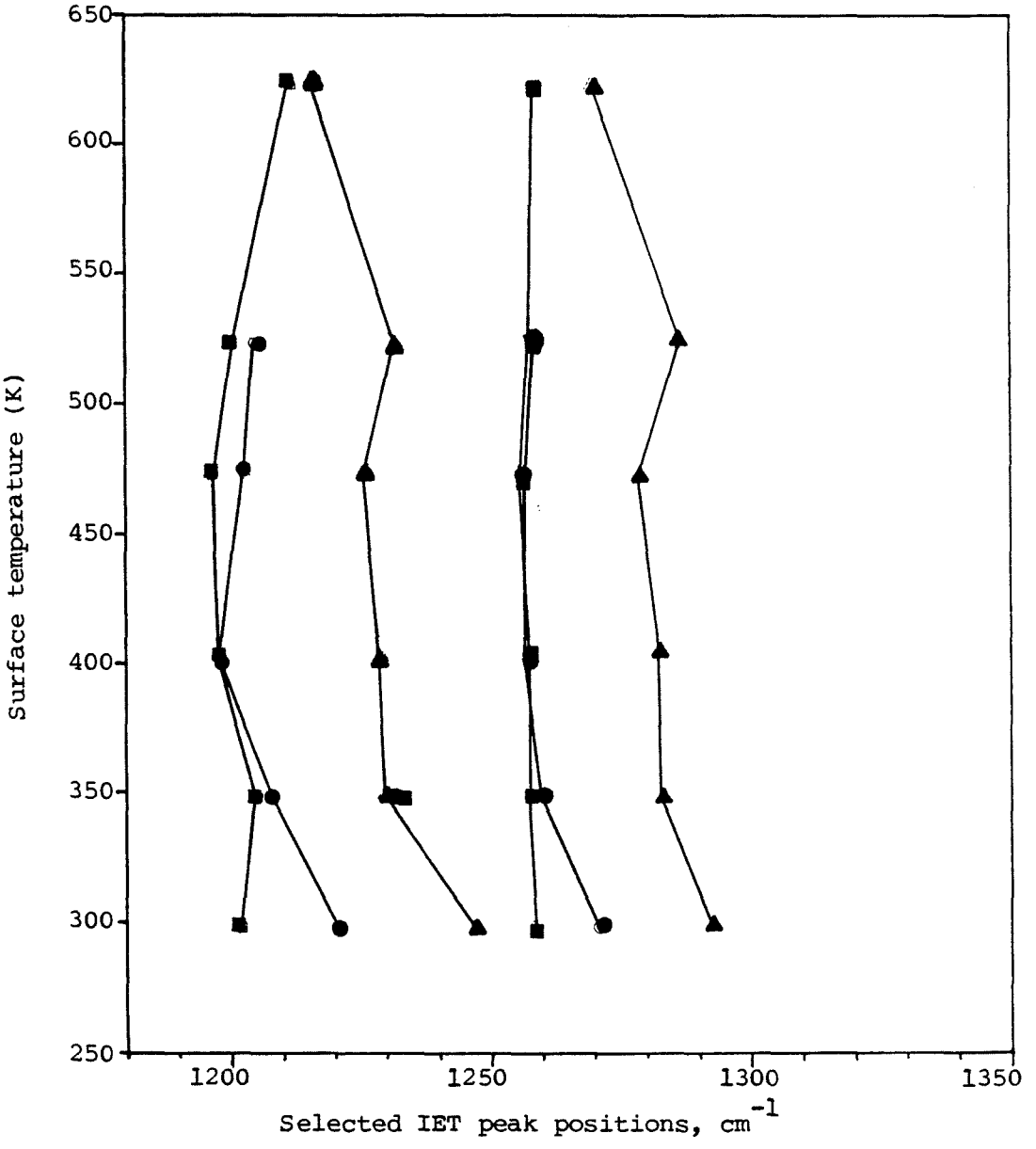
650
600
550
500
450
400
350
300
250
Surface temperature (K)
1200
1250
1300
1350
Selected IET peak positions, cm-1

Figure 24

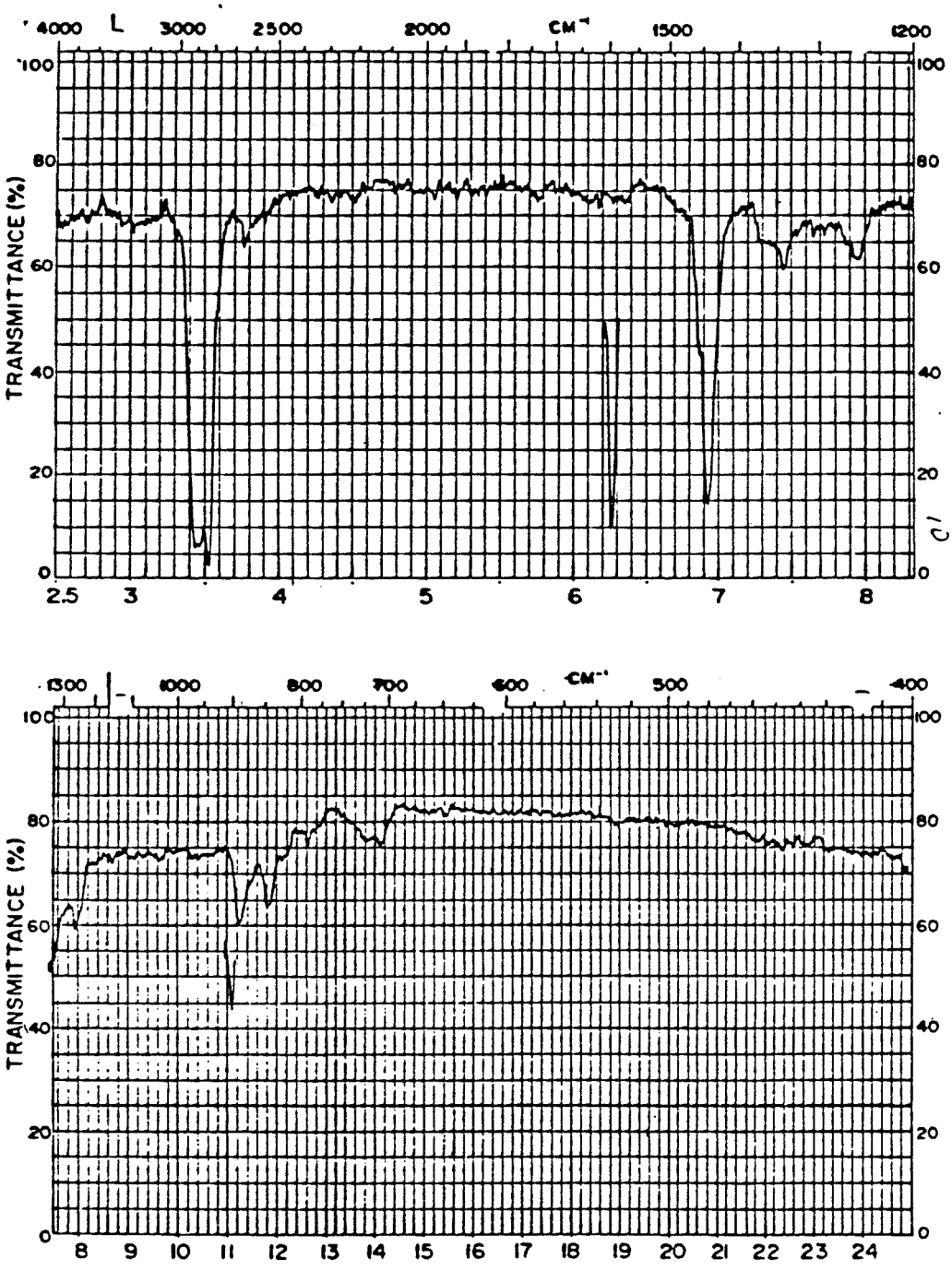

Infrared Spectrum of Polycyclohexene.

Figure 25

Chapter 3

The Interactions of 1,3-Cyclohexadiene with $Zr(BH_4)_4$ Adsorbed on Al_2O_3

1.0 Introduction

Inelastic electron tunneling spectroscopy (IETS) has been used to investigate the temperature and pressure dependent reactivity of 1,3-cyclohexadiene with the known polymerization catalyst $Zr(BH_4)_4$ supported on Al_2O_3. This study is part of a continuing research effort to characterize the structure and catalytic reactivity of supported homogeneous cluster catalysts. Previous papers have reported on the interaction of $Zr(BH_4)_4$ with the Al_2O_3 surface (1), the interactions of the adsorbed catalyst with D_2, D_2O and H_2O (2), and with ethylene, propylene, and acetylene (3). In the latter study the vibrational spectra revealed polymer formation upon interaction with acetylene at elevated temperatures. The interactions of $Zr(BH_4)_4$ supported on Al_2O_3 with cyclohexene have also been studied as a function of temperature and pressure (4).

An extensive effort has been made to polymerize 1,3 and 1,4-cyclohexadiene (5-10), as well as to characterize the polymers by infrared spectroscopy and nuclear magnetic resonance. A great number of catalytic systems have been investigated including $TiCl_4$-$Al(i\text{-}C_4H_9)_3$ (5), $TiCl_4$ (5), $n\text{-}C_4H_9Li$ (6,7), $TiCl_4$-$Al(C_2H_5)_3$ (10), and various π-allyl complexes of nickel (9).

In general, all of the systems catalyzed the 1,4 homopolymerization of 1,3-cyclohexadiene to yield poly-1,3-cyclohexadiene (II):

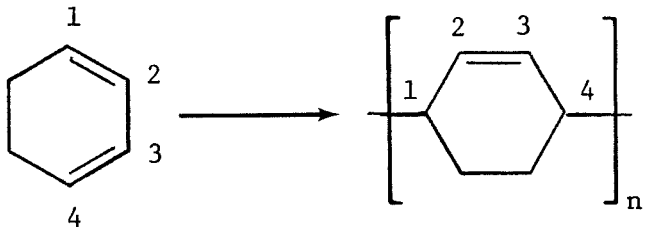

II

Several authors have also reported a much smaller percentage of 1,2 linkages:

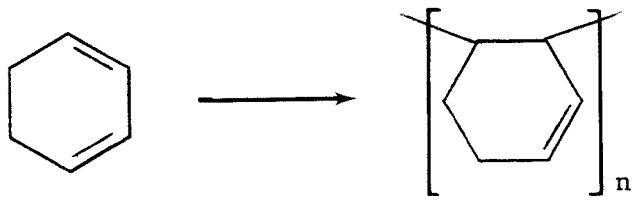

While the Ziegler catalytic systems and the organolithium compounds resulted in amorphous polymers, the nickel π-allyl complexes (9) were reported to yield crystalline stereoregular polymers of 1,3-cyclohexadiene. Several studies of 1,4-cyclohexadiene, in particular the study by Yousufzai et al. (10), have demonstrated that the polymer first isomerizes to 1,3-cyclohexadiene and then undergoes a 1,4 homopolymerization to yield poly-1,3-cyclohexadiene (II) in the presence of Ziegler catalysts.

Many of the polymerization studies of 1,3-cyclohexadiene have ultimately been concerned with the aromatization (dehydrogenation) of the rings to yield p-polyphenyl (III):

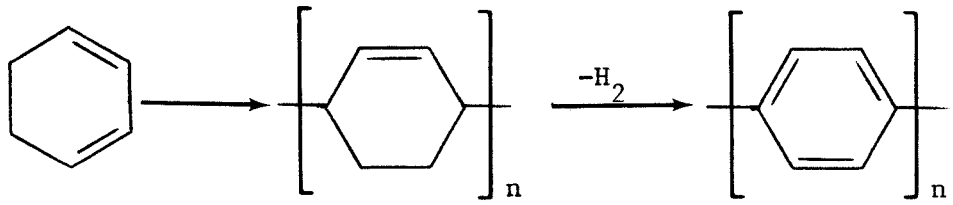

These polymers have interesting physical properties being conductive and their extremely high melting points make them commercially highly desirable. The dehydrogenations have been carried out chemically and catalytically (8).

It is hoped that the vibrational information provided by this study of the interaction of 1,3-cyclohexadiene with $Zr(BH_4)_4$ supported on Al_2O_3 will lead to a greater knowledge of the surface species formed in these industrially important catalytic systems and to a greater understanding of the polymerization mechanism of cyclic olefins by heterogeneous systems.

2. Experimental

Inelastic electron tunneling spectroscopy (IETS) is an effective means of monitoring the vibrational modes of molecules adsorbed on or near insulating surfaces. The IETS procedure involves monitoring the current due to electrons tunneling inelastically through a thin insulating barrier between two electrodes. While most of the tunneling current arises from electrons tunneling elastically, some electrons may tunnel inelastically by exciting the vibrational modes of the adsorbates.

Inelastic transitions occur only when the bias voltage across the barrier is greater than or equal to a vibrational activation energy. These transitions result in an increase in conductance across the barrier by providing additional channels for electron tunneling. The conductance increases are observed as peaks when d^2V/dI^2, proportional to d^2I/dV^2, is plotted as a function of the bias voltage, V. Peak positions correspond to vibration frequencies. Both electron-dipole and electron-induced dipole interactions, analogous to infrared and Raman modes, are observed in IET spectra. Additional details on the interpretation of IET spectra are available elsewhere (11, 12).

The IET junctions used in this study were prepared in an oil diffusion-pumped bell jar with a base pressure of 5×10^{-8} Torr. Before beginning an experiment, an oxygen plasma discharge was run to help clean the system of hydrocarbon contaminants (13). The oxidation voltage was -1000 V, the O_2 pressure was 150 microns and the oxidation time was 1000 seconds. Aluminum strips approximately 800 Å in thickness were evaporated onto Corning 7059 borosilicate glass slides. Film thicknesses were monitored using a quartz crystal microbalance. After evaporation, the aluminum strips were annealed in vacuum by heating to 520 K for at least 10 minutes. The technique developed by Bowser and Weinberg (14) for simultaneous heating and temperature measurement was used for all heating operations. The annealing step is necessary to preserve the integrity of the thin oxide barriers during subsequent heating operations. After annealing, thin oxide barriers are formed by oxidizing the aluminum strips in a plasma discharge of O_2 containing a trace of H_2O

vapor. The oxidation voltage was -1000 V, the O_2 pressure was 150 microns and the oxidation time varied between 350 and 800 seconds depending on the adsorbate exposure and temperature to be studied. The oxide formed in this manner is 20 to 25 Å in thickness.

After the oxidation, the $Zr(BH_4)_4$ complex was adsorbed onto the oxide surfaces by exposing the samples to 5×10^{-2} Torr of $Zr(BH_4)_4$ for 15 minutes, corresponding to a saturation coverage (1). This produced the supported catalyst. After the excess was evacuated from the bell jar, 1,3-cyclohexadiene was introduced as a vapor into the bell jar and allowed to interact with the supported catalyst. Exposures ranged from 1.5×10^{-1} Torr for 1000 seconds to 5 Torr for 1200 seconds. In some experiments, the slides were heated after the 1,3-cyclohexadiene was introduced into the bell jar. Temperatures ranged from 198 K to 473 K. In some experiments, the slides were not exposed to the catalyst and the oxide was allowed to interact with the 1,3-cyclohexadiene alone.

After the bell jar was evacuated to a pressure below 1×10^{-6} Torr, Pb cross strips were evaporated onto the samples. The glass slides were then removed from the bell jar and mounted onto holders used to measure their spectra while immersed in liquid helium. Before the spectra were recorded, the resistance value of each junction was measured.

Spectral measurements were recorded with PDP-11/10 digitally-controlled electronics (15). Measurements were carried out over the spectral range of 240 to 4000 cm^{-1} using multiple scan averaging. The recorded data were then smoothed, the sloped background was subtracted,

peaks were located and peak energies assigned after correcting for the Pb superconducting band gap and for modulation effects (16). Spectra were originally recorded in two sections, from 240 to 2240 cm^{-1} and from 2000 to 4000 cm^{-1}. The two halves of the spectra were then matched and the y-values were scaled using the modulation voltages at which the spectra were recorded. It should be noted that the y-values were further scaled relative to the most intense feature in the spectrum (usually a hydrocarbon stretching peak) in order to fit the spectrum onto the graph.

3.0 Results

3.1 General Observations

Spectral measurements of junctions of $Zr(BH_4)_4$ exposed to 150 and 6000 Torr s of 1,3-cyclohexadiene are shown in Figures 1 and 2 respectively. Substrate temperatures are 298, 403 and 473 K.

As with previous studies of cyclohexene adsorption, the 1,3-cyclohexadiene system did not reach an apparent saturation coverage at the exposures and temperature studied. Increases in 1,3-cyclohexadiene exposure or substrate temperature resulted in an increased adsorption of 1,3-cyclohexadiene as judged by increases in intensity of the hydrocarbon vibrational modes and by increases in junction resistance. Hydrocarbon concentrations can be monitored qualitatively by measuring the resistance of the insulating barrier consisting of the aluminum oxide plus adsorbed species. Junctions exhibiting the best signal/noise ratios with our electronics fall in the 30-200 Ω range (for an area of approximately

1 mm^2). The thickness of the oxide layer can be controlled by varying the length of time of the O_2 plasma discharge used to form the Al_2O_3 insulating layer. The resistance of the junctions can thus be adjusted in an attempt to provide a resistance value in the desired range. In the case of 1,3-cyclohexadiene however, there was no apparent limit to the junction resistance that could be obtained when increasing the 1,3-cyclohexadiene exposure and/or substrate temperature. Similar behavior was observed when cyclohexene was the adsorbate but with 1,3-cyclohexadiene this effect was even more pronounced.

Studying the interactions of 1,3-cyclohexadiene with the supported catalyst $Zr(BH_4)_4$ proved to be much more difficult than studying other adsorbates, such as cyclohexene. With 1,3-cyclohexadiene, it was very difficult at the higher exposures studied to fabricate junctions which displayed good signal/noise ratios. It may be that this is due to the unsaturated nature of the hydrocarbon barrier formed from 1,3-cyclohexadiene as opposed to the essentially saturated hydrocarbon barrier formed at high exposures of cyclohexene.

3.2 150 Torr s at 298 K

Figure 1, spectrum (A) shows the result obtained for a 150 Torr s exposure of 1,3-cyclohexadiene at 298 K. Peak positions are listed in Table 1.

In the upper region of the spectrum, there are two small rounded features near 2170 and 2256 cm^{-1}. A more intense broad feature centered at approximately 2450 cm^{-1} displays several small maxima at 2386, 2422

and 2477 cm^{-1}. In the 2800-3100 cm^{-1} region, there is an intense feature with two well-resolved maxima at 2856 and 2917 cm^{-1}. On the high energy side of the 2917 cm^{-1} peak there are at least two unresolved shoulders located at approximately 2950-2970 cm^{-1} and 3010 cm^{-1}. There is also a broad feature located at approximately 3640 cm^{-1}.

The most intense feature in the spectrum is the asymmetric peak at 914 cm^{-1}. The lower region of the spectrum displays several features. There is a well-resolved intense feature at 1061 cm^{-1} superimposed on a broad feature with several very small peaks at approximately 1115, 1140 and 1166 cm^{-1}. Another rounded, broad band has a maximum at 1271 cm^{-1}. A somewhat better resolved feature is located between 1340-1390 cm^{-1} with a maximum at 1387 cm^{-1}. An intense feature located at 1454 cm^{-1} is approximately as intense as the feature located at 1061 cm^{-1}. A broad, rounded feature is centered at 1610 cm^{-1}.

The lower region of the spectrum displays a feature at 292 cm^{-1} and there is also a broad band centered near 727 cm^{-1}. Two other very weak features are observed at 390 cm^{-1} and at approximately 450 cm^{-1}.

3.3 150 Torr s at 403 K

The results obtained for a 150 Torr s exposure of 1,3-cyclohexadiene at 403 K are shown in Figure 1, spectrum (B) and peak positions are listed in Table 1.

The upper half of the spectrum shows weak features at 2122 and 2178 cm^{-1} and a broad, round feature exhibiting maxima at 2309, 2366, 2423 and

2457 cm^{-1}. The 2800-3100 cm^{-1} region has two main features located at 2822 and 2866 cm^{-1}. The 2866 cm^{-1} feature appear to have shoulders located near 2900 and 3010 cm^{-1}. A broad feature is centered near 3576 cm^{-1}.

The most intense spectral feature is located at 917 cm^{-1}. Additional features in the lower spectral region are located at 1047, 1334, 1377 and 1437 cm^{-1}. Much weaker features are observed at 1119 1158, 1232 and 1273 cm^{-1}. There are also two well-resolved broad features at 1563 and 1602 cm^{-1}. In the low energy region, features are observed at 292, 680, and 732 cm^{-1}. Several unresolved, weak peaks are seen in the 350-550 cm^{-1} region as well. Compared to the results obtained at 150 Torr s at 298 K, there appears to be a loss of intensity in the 1070-1170 cm^{-1} region at 403 K. The features at 1334 and 1377 cm^{-1} are also much better resolved than at 298 K, as are the features in the 670-740 cm^{-1} range. An interesting observation is the splitting of the broad feature located near 1610 cm^{-1} at 298 K into two separate modes at 1563 and 1607 cm^{-1}. The 2800-3100 cm^{-1} region is also different at 403 K than at 298 K. The bands located at 2822 and 2866 cm^{-1} at 403 K are closer in intensity than the two features located at 2856 and 2917 cm^{-1} at 298 K.

3.4 150 Torr s at 473 K

Results obtained by exposing the adsorbed $Zr(BH_4)_4$ catalyst to 150 Torr s of 1,3-cyclohexadiene at 473 K are shown in Figure 1 spectrum (C) and peak positions are listed in Table 1.

The 2100-2300 cm^{-1} region appears to be much reduced in intensity at 473 K. There are no discernible features in this region and only a broad, rounded feature in the 2400-2600 cm^{-1} region centered at 2449 cm^{-1}. The features in the 2800-3100 cm^{-1} range are the most intense features in the spectrum. There are two main peaks located at 2859 and 2904 cm^{-1}. A broad feature is also resolved at 3635 cm^{-1}.

The lower half of the spectrum appears to be reduced in intensity compared to the results obtained at 298 and 403 K. However, it should be noted that this is due to the computer processing of the spectra which first scales each half of the spectrum according to the modulation voltage at which it was recorded and then further reduces the y-values relative to the most intense spectral feature. Since many of the spectral features change in position and/or intensity as a function of either the 1,3-cyclohexadiene exposure and/or the substrate temperature, the best choice for an internal standard in these IET spectra is the Al-O bulk stretch, located at approximately 945 cm^{-1}. In the present study, this feature appears only as an unresolved shoulder on the more intense feature near 914 cm^{-1} but is nonetheless useful when comparing the relative intensities of spectral features observed at different 1,3-cyclohexadiene exposures or substrate temperatures.

In the lower region of the spectrum several features are much better resolved at 473 K than at 403 K. The features at 914 and 1061 cm^{-1} are both well-resolved, as at lower temperatures. In the 1130-1170 cm^{-1} region there is a more intense band at 473 K with a maximum observed at 1147 cm^{-1}. There is also increased intensity in the 1240-1390 cm^{-1} range

with several features evident at 1248, 1279, 1325 and 1381 cm^{-1}. The feature located at 1453 cm^{-1} is much more intense than that observed at lower temperatures. At 473 K, it is considerably more intense than the 1061 cm^{-1} peak. The broad band at 1603 cm^{-1} is also much more intense at 473 K and the band shape is much narrower than that observed at 298 K or 403 K.

Additional features are observed at 262, 294, 393, 692 and 730 cm^{-1}. As at 403 K, several unresolved features are observed in the 350-550 cm^{-1} range.

3.5 6000 Torr s at 298 K

Figure 2, spectrum (A) shows the results obtained for a 6000 Torr s exposure of 1,3-cyclohexadiene at 298 K. Peak positions are listed in Table 2.

The upper region of the spectrum has only one very weak feature in the 2100-2300 cm^{-1} region at 2252 cm^{-1}. In the 2400-2600 cm^{-1} region there is a broad, weak feature centered at 2445 cm^{-1}. There are three very intense peaks in the 2800-3100 cm^{-1} region at 2848, 2922 and 2960 cm^{-1}. A weak feature is also observed at approximately 3626 cm^{-1}.

In the lower half of the spectrum, the feature at 923 cm^{-1} is the most intense. There is an unresolved shoulder which is evident on the low energy side of this peak near 850 cm^{-1}. Other features are observed at 1057, 1135, 1340, 1370 and 1446 cm^{-1}. A broad feature is also resolved at 1272 cm^{-1}. The relatively narrow feature at 1603 cm^{-1}

observed at 150 Torr s at 473 K is broader at 6000 Torr s. Features are resolved at 1583, 1604 and 1641 cm^{-1}. In the low energy region of the spectrum, features are observed at 278, 385, 450, 650, 696 and 724 cm^{-1}. The feature at 450 cm^{-1} was not well resolved at 150 Torr s. Compared to the results obtained at 150 Torr s, several new features are evident at 6000 Torr s, in particular, the features at 1135, 1340 and 1370 cm^{-1} are much more intense. Also the features in the 2800-3100 cm^{-1} region have increased in intensity, the band shape has changed and a new feature near 2960 cm^{-1} is resolved.

3.6 6000 Torr s at 403 K

The results obtained for a 6000 Torr s exposure of 1,3-cyclohexadiene at a temperature of 403 K are shown in Figure 2 spectrum (B). Table 2 lists the peak positions.

Compared to the results obtained at lower exposures and temperatures, heating the junctions to 403 K or 473 K results in spectra with considerably noisier baselines. Another difference which is observed in the 6000 Torr s spectra at 403 and 473 K is the variability in a number of spectral features, primarily in terms of the intensity but also in position or resolution for some features, even in junctions fabricated on the same slide. This is in sharp contrast to the spectra obtained at high exposures of cyclohexene which were highly reproducible from experiment to experiment over the long period of time that this adsorbate was studied.

In the upper region of the spectrum only a weak feature remains in the 2400-2600 cm^{-1} region, centered near 2425 cm^{-1}. The 2800-3100 cm^{-1} region is very intense. Features are resolved at 2837 and 2915 cm^{-1}. There are two shoulders evident on the 2915 cm^{-1} peak, one on the low energy and one on the high energy side. There appears to be a weak feature in the 3650 cm^{-1} area although the noisy baseline complicates this.

The lower region of the spectrum has a number of intense features. The 922 cm^{-1} feature has a well-resolved shoulder located at 865 cm^{-1} which was not resolved at 298 K and not observed in any of the 150 Torr s spectra. Other features are the broad band at 1055 cm^{-1} and the sharp feature at 1135 cm^{-1}. New features are resolved at 1242 and 1272 cm^{-1}. A doublet is observed at 1341 and 1361 cm^{-1} which is more intense relative to the feature at 1442 cm^{-1} than at 298 K. There are two broad features in the 1550-1650 cm^{-1} region located at 1584 and 1631 cm^{-1}. In the low energy portion of the spectrum, features are resolved at 258, 282, 378, 450, 687, 711 and 732 cm^{-1}. A few other unresolved peaks are observed in the 350-650 cm^{-1} range as well. A comparison to the results obtained at 298 K shows that the feature at 1055 cm^{-1} is reduced in intensity whereas several other features are more intense at 403 K. Relative to the 922 cm^{-1} peak, the feature at 1422 cm^{-1}, as well as the features in the 2800-3100 cm^{-1} region, are more intense at 403 K.

3.7 6000 Torr s at 473 K

Figure 2 spectrum (C) shows the results obtained at a 1,3-cyclohexa-

diene exposure of 6000 Torr s at 473 K. Peak positions are shown in Table 2.

The 2100-2300 and 2400-2600 cm^{-1} regions display only a couple of very weak features at 2428 and 2455 cm^{-1}. In the 2800-3100 cm^{-1} region, three major very intense features are resolved at 2837, 2916 and 2949 cm^{-1}. There doesn't appear to be any discernible feature remaining in the 3600-3700 cm^{-1} region.

The lower half of the spectrum displays a number of intense features. Peaks are located at 924, 1059, 1136, 1244, 1265, 1337, 1368 and 1442 cm^{-1}. The 924 cm^{-1} peak has two shoulders located at 815 and 865 cm^{-1}. Compared to the results observed at lower temperatures, the 1442 cm^{-1} band is more intense at 473 K. There is also a broad band observed near 1609 cm^{-1}.

The low energy region displays several features. Peaks are observed at 278, 391, 443, 472, 688 and 727 cm^{-1}. These are considerably more intense than at 403 K. There also appears to be a shoulder near 350 cm^{-1}.

3.8 1,3-Cyclohexadiene Adsorption on Al_2O_3

Several attempts were made to fabricate measurable junctions of Al_2O_3 exposed to moderate and high pressures of 1,3-cyclohexadiene without pre-adsorption of $Zr(BH_4)_4$. Unfortunately, none of these junctions produced measurable spectra. In most cases, the spectra that resulted were subject to glitches and showed that little or no adsorption of 1,3-

cyclohexadiene occurred on junctions which had not been exposed to the $Zr(BH_4)_4$ catalyst. A previous IETS study (17) also investigated the adsorption of cyclohexadiene on Al_2O_3 and reported that despite numerous attempts at a variety of partial pressures, vapor doping was unsuccessful.

4.0 Discussion

4.1 Spectral Assignments for the 150 Torr s Results

A number of features in the spectra may be readily assigned based on a comparison with undoped Al-Al_2O_3-Pb junctions (18). These include the feature located near 299 cm^{-1} due to a phonon in the underlying aluminum film; the prominent shoulder near 945 cm^{-1} assigned to the Al-O (bulk) stretch; the weak, broad feature near 1860 cm^{-1} which is an overtone of the Al-O (bulk) stretch; and the broad feature located between 3600 - 3750 cm^{-1} due to the stretch of surface hydroxyl groups.

Evans and Weinberg have identified the vibrational features which result from the adsorption of $Zr(BH_4)_4$ on Al_2O_3 (1). These assignments as well as the surface structures which are expected from the adsorption of $Zr(BH_4)_4$ on Al_2O_3 have been discussed elsewhere (1, 2, 4). Based on these results, several of the features in Figure 1, spectrum (A), may be assigned to vibrations of the BH_4 ligands. In particular, the features between 2100 - 2300 cm^{-1}, located at 2170 and 2256 cm^{-1}, may be assigned to B-H_b stretching and the broad peak located between 2400 - 2600 cm^{-1} may be assigned to B-H_t stretching. BH_4 deformation modes are expected in the 1000 - 1400 cm^{-1} range. In $Zr(BH_4)_4$ adsorbed on Al_2O_3, Evans and Weinberg (1) identified features at 1106 - 1130, 1173 and 1220 cm^{-1} as B-H deformations. In the present study, the weak features in the 1115 -

1167 cm^{-1} range may be assigned as B-H deformation modes. B-O modes, resulting from disassociated BH_4 ligands which form surface complexes instead of desorbing, are expected in the 1200 - 1450 cm^{-1} region. In the present work, the rounded, broad band with a maximum at 1271 cm^{-1} may be due in part to B-O modes. Other features are expected from ZrO stretching modes. Evans and Weinberg (1) have assigned the intense feature near 910 cm^{-1} to the stretching of singly coordinated Zr atoms and a broad feature near 690 cm^{-1} to multiply coordinated Zr atoms.

The most intense spectral features resolved at 298 K at a 150 Torr s exposure of 1,3-cyclohexadiene may be assigned as features associated with the adsorbed 1,3-cyclohexadiene rather than features associated with the $Zr(BH_4)_4$ catalyst. This is supported by the observation that the stretching features due to the BH_4 ligands of the catalyst are rather weak, especially in comparison with studies done at comparable exposures of other adsorbates, for example, cyclohexene. Additionally, most of the resolved features are observed to grow in intensity as the 1,3-cyclohexadiene exposure or the substrate temperature is increased.

The CH stretching region from 2800 - 3100 cm^{-1} displays two resolved features at 2856 and 2917 cm^{-1}. At least two unresolved features are evident near 2950 - 2970 cm^{-1} and 3010 cm^{-1}. These unresolved features may be assigned as =C-H stretching modes which are expected to be higher in frequency than the CH_2 stretching modes. The 2917 cm^{-1} feature may be due to either =CH or CH_2 stretching and the 2856 cm^{-1} feature may be assigned as CH_2 stretching. A second feature due to CH_2 stretching is expected near 2875 cm^{-1} but is not resolved in the present study. These

assignments are in agreement with reported IR and Raman vibrational studies of 1,3-cyclohexadiene and 1,4-cyclohexadiene (19 - 22). The main features in the CH stretching region are expected at 3042, 2938, 2873, 2854, and 2822 cm^{-1} (20). Several weaker features are also seen and several of these bands shift by 10 - 15 cm^{-1} depending on the physical state of the 1,3-cyclohexadiene.

Features in the 1000 - 1400 cm^{-1} region may be assigend to CH_2 wag, twists and rocks as well as CH in-plane and out-of-plane bending modes. Features have been reported at 1059, 1165, 1178, 1243, 1330, and 1377 cm^{-1} (19). Additional features have been assigned as CH_2 scissoring modes at 1444 and 1435 cm^{-1} and a ring C-C stretch has been assigned to a feature at 1408 cm^{-1}. Based on these findings, the feature at 1454 cm^{-1} may be assigned to CH_2 scissoring and the other features to CH_2 and CH deformation modes.

Several strong bands are expected at 657, 671 and 745 cm^{-1} and may contribute to the broad feature observed in this region.

The broad feature centered near 1610 cm^{-1} may be assigned to C=C stretching of the adsorbed 1,3-cyclohexadiene. Weak to medium features in this region, assigned to ring C=C stretching, have been reported at 1581 and 1602 cm^{-1} in Raman and IR studies of 1,3-cyclohexadiene (19, 20).

The spectra obtained at 150 Torr s indicate that the adsorbed 1,3-cyclohexadiene is an unsaturated hydrocarbon specie as judged by the position of the CH stretching features and perhaps more importantly, by

the presence of the broad ring C=C stretching feature.

4.2 Temperature Dependence of the 150 Torr s Results

Figure 1 shows the spectral changes which result from increasing the substrate temperature during the 1,3-cyclohexadiene exposure. Several interesting changes are evident. Most important is the increase in intensity of the ring C=C stretching features located in the 1500 - 1650 cm^{-1} region. At a surface temperature of 403 K, this feature splits into two main bands, at 1563 and 1602 cm^{-1}. Other spectra obtained at 403 K, not shown here, displayed variable splitting of this feature, but in all cases increased intensity in the ring C=C stretching region. At 473 K, the ring C=C stretching feature is seen to be even more intense and the band shape appears narrower than at lower surface temperatures.

Several other features increase in intensity as a result of increasing the substrate temperature during the 1,3-cyclohexadiene exposure. The CH stretching features greatly increase in intensity as can be seen in the 473 K spectrum shown in Figure 1. The 1450 cm^{-1} peak also increases and features begin to be resolved in the 1130 - 1160 cm^{-1} range. The 1240 - 1380 cm^{-1} range also increases in intensity as several features are resolved. Most of these features do not display shifts of peak position as the temperature is increased, only increases in intensity. However, the results at 403 K do show a downward shift of the CH stretching features in particular. The observed values are nonetheless consistent with reported values for 1,3-cyclohexadiene and the increased ring C=C stretch indicates that the surface complex formed at 403 K is still

primarily an unsaturated hydrocarbon. A comparison of the peak positions observed at 298 K and 473 K shows that they are nearly identical.

The B-H stretching features also are reduced in intensity as the surface temperature is increased, corresponding to further disassociation of the adsorbed catalyst. At 473 K, there is little or no evidence of B-H bridging stretching and the broad, rounded band in this spectral region is due primarily to B-H terminal stretching. The hydroxyl stretch located in the 3600 - 3750 cm^{-1} region also undergoes only a small reduction in intensity, if at all, as the surface temperature is increased.

The spectra indicate that the primary surface specie formed by 1,3-cyclohexadiene at 298 K continues to accumulate on the surface as the temperature is increased to 473 K and that the hydrocarbon specie is unsaturated as evidenced by the C=C stretching region.

4.3 Spectral Assignments for the 6000 Torr s Results

The spectra obtained for a 6000 Torr s exposure of 1,3-cyclohexadiene interacting with $Zr(BH_4)_4$ adsorbed on Al_2O_3 show several new features not evident at lower exposures. Figure 3 compares the 150 and 6000 Torr s results at 298 K.

At 6000 Torr s, there is only a very weak feature in the B-H bridging stretching region located at 2252 cm^{-1} and a rounded, weak feature in the B-H terminal stretching region. These features are greatly reduced in intensity compared to the results at 150 Torr s.

The CH stretching features located in the 2800 - 3100 cm^{-1} region

have dramatically increased in intensity compared to the 150 Torr s results and a major new feature is observed at 2960 cm^{-1} which was not resolved at 150 Torr s. Additional features are located at 2848 and 2922 cm^{-1} which compare favorably with the two features observed at 150 Torr s at 2856 and 2917 cm^{-1}. There is also evidence of a shoulder on the low energy side of the 2922 cm^{-1} peak near 2860 - 2880 cm^{-1}. Based on previous studies (19 -22), the feature at 2960 cm^{-1} masy be assigned to =C-H stretching and the feature at 2848 cm^{-1} as well as the shoulder near 2870 cm^{-1}, may be assigned to CH_2 stretching. The assignment of the 2922 cm^{-1} feature has been made to either =CH stretching (20) or CH_2 stretching (5).

Features in the 1000 - 1500 cm^{-1} region may be assigned primarily to hydrocarbon modes although some B-H deformation modes as well as B-O modes may contribute to the intensity of several features in this region. Most modes may be assigned as hydrocarbon modes based on their increased intensity at higher 1,3-cyclohexadiene exposures and substrate temperatures. The feature at 1272 cm^{-1} is similar to that observed at 1271 cm^{-1} at 150 Torr s and may be assigned as the combination B-H and B-O mode observed by Evans and Weinberg at 1260 cm^{-1} (1).

Several new features are resolved at 6000 Torr s that were not major features in the spectra at 150 Torr s. Among these is the intense feature located at 1135 cm^{-1} which may be assigned to the CH_2 deformation band observed by Sakashita (23) at 1138 cm^{-1} in cyclohexene or to the ring deformation mode assigned by Kumar *et al.* to this same feature (24). Additional features are resolved at 1340 and 1370 cm^{-1}. The 1370 cm^{-1}

feature corresponds to the strong band observed at 1372 cm^{-1} in 1,3-cyclohexadiene which is probably a CH_2 twisting mode (19). The 1340 cm^{-1} band may be another CH_2 twisting mode or a -CH bending mode (20).

The C=C stretching region is considerably more intense at 6000 Torr s than at 150 Torr s and several features are resolved at 1583, 1604, and 1641 cm^{-1}. The band shape appears to be somewhat broader than observed at 473 K at 1500 Torr s.

Several new features are observed in the low energy region of the spectrum. The 650 cm^{-1} feature may correspond to the IR band at 658 cm^{-1} in 1,3-cyclohexadiene. 1,3-cyclohexadiene also exhibits a strong band at 924 cm^{-1} (19) and a ring breathing mode at 850 cm^{-1} which can be assigned to the strong shoulder seen on the 923 cm^{-1} peak near 860 cm^{-1}. A new feature near 450 cm^{-1} may be a ring bending mode (20).

The spectra show that a great deal more 1,3-cyclohexadiene is adsorbed at 6000 Torr s than at 150 Torr s. The surface specie formed is unsaturated as indicated by the position of certain CH stretching features and the well-resolved C=C stretching region. The ring structure of the adsorbed specie is retained as ring breathing and ring bending modes are observed in the IET spectra. The stretch of surface hydroxyl groups is reduced at the 6000 Torr s 1,3-cyclohexadiene exposure and the BH stretching region indicates further decomposition of the catalyst at this exposure as compared to 150 Torr s.

4.4 Temperature Dependence of the 6000 Torr s Results

As the surface temperature is increased, several features evident at 298 K continue to increase in intensity and several new features are observed. At 403 and 473 K, several features display an increased variability in peak intensity and a number of bands in the low energy region of the spectrum split or shift in position.

At 403 and 473 K features assigned to ring deformation modes increase greatly in intensity. At 403 K a new feature, evident only as a shoulder at 298 K, has been resolved at 864 cm^{-1}. At 473 K, there is a new feature at 815 cm^{-1} and the 865 cm^{-1} feature appears as a shoulder on the 924 cm^{-1} peak. Several new low energy features are observed at 403 K including features at 258 and 398 cm^{-1}. The 690 - 732 cm^{-1} region also displays increases in intensity at both 403 and 473 K. Several unlabeled peaks are observed in the 500 - 650 cm^{-1} region.

The C=C stretching region is split into two main peaks at 403 K, located at 1584 and 1631 cm^{-1}. At 493 K, a broad band is centered at 1609 cm^{-1}.

Several spectral features indicate that more hydrocarbon is adsorbed on the surface as the surface temperature is increased. In particular, the increased intensity of the ring deformation modes in the 880 - 800 cm^{-1} region and of the 1442 cm^{-1} CH_2 scissoring mode relative to the 924 cm^{-1} feature show that the adsorbed hydrocarbon is accumulating on the surface. The relative intensities of the CH stretching features also change. At 403 and 493 K, the high energy feature near 2930 cm^{-1} has

increased in intensity relative to the 2837 cm^{-1} feature.

The CH stretching features also show small red shifts as the surface temperature is increased. At 473 K, the feature observed at 2848 cm^{-1} at 298 K has shifted to 2837 cm^{-1}, a shift of 11 cm^{-1}; the 2922 cm^{-1} peak shifts down 6 cm^{-1} to 2916 cm^{-1} and the 2960 cm^{-1} feature shifts 11 cm^{-1} to 2949 cm^{-1}. Other features show lesser shifts, for example, the 1446 cm^{-1} feature observed at 298 K only shifts 4 cm^{-1} to 1442 cm^{-1} at 473 K. The red shifts may be the result of molecular association of the adsorbed 1,3-cyclohexadiene, similar to the shifts observed in IR spectra for liquid versus vapor states (25). They probably reflect slight changes in the dielectric constant in the adsorbed hydrocarbon layer.

The BH stretching region displays only a very weak feature at 403 K and there is no evidence of $B-H_b$ stretching. At 473 K, there is even less intensity in the $B-H_t$ region indicating that few BH_4 or BH_2 groups remain on the surface. The hydroxyl stretching peak is also reduced in intensity as the surface temperature is increased to 403 and 473 K.

4.5 Identification of the Adsorbed Species

1,3-cyclohexadiene interacts much more with the adsorbed $Zr(BH_4)_4$ catalyst and promotes its decomposition more readily than other adsorbates such as cyclohexene. Figure 4 shows a comparison of the 150 Torr s results for cyclohexene and 1,3-cyclohexadiene interacting with adsorbed $Zr(BH_4)_4$ at 298 K. Cyclohexene clearly perturbs the catalyst much less than 1,3-cyclohexadiene. The spectra show that at 150 Torr s the 1,3-cyclohexadiene has interacted with the adsorbed catalyst much more

extensively than has cyclohexene. Figure 5 shows a comparison of the 6000 Torr s results for cyclohexene and 1,3-cyclohexadiene interacting with adsorbed $Zr(BH_4)_4$ at 298 K. As at 150 Torr s, the 1,3-cyclohexadiene spectra indicate that the $Zr(BH_4)_4$ catalyst has dissociated a great deal more in the presence of 1,3-cyclohexadiene than when interacting with cyclohexene. These comparisons illustrate that the surface species formed by these two adsorbates are quite different. At 6000 Torr s, the cyclohexene specie forms a saturated hydrocarbon and the adsorbed 1,3-cyclohexadiene is unsaturated.

The spectral evidence indicates that 1,3-cyclohexadiene readily interacts with the adsorbed $Zr(BH_4)_4$ to form a coordinated cyclohexene complex, using the BH_4 groups as a limited source of hydrogen. The spectra show that the unsaturated hydrocarbon which results does not continue to add hydrogen to become a totally saturated species. If such species do in fact form, they must desorb from the surface rather than stay coordinated to the catalyst since there is no spectral evidence that such species occur. Instead, there is limited evidence that the coordinated 1,3-cyclohexadiene may start to polymerize, forming a chain of cyclohexene rings as new 1,3-cyclohexadiene molecules coordinate and insert at the metal center.

In sharp contrast to the cyclohexene IET spectra, the 1,3-cyclohexadiene spectra do not exhibit dramatic peak shifts and new features assigned to the growing polymer because in the case of 1,3-cyclohexadiene all of the surface species are unsaturated hydrocarbons whereas with the cyclohexene polymerization the dramatic spectral changes result from the

conversion of the unsaturated monomer to a completely saturated hydrocarbon. The spectral changes that occur in the 1,3-cyclohexadiene adsorbate system are much more subtle.

Marvell and Hartzell (5) reported that the IR spectra of poly-1,3-cyclohexadiene films show absorption maxima corresponding to =C-H stretching at 3010 cm^{-1}, $-CH_2-$ stretching at 2925 and 2850 cm^{-1}, C=C stretching at 1647 cm^{-1} and $-CH_2-$ deformation at 1450 cm^{-1}. Lefebvre and Dawans (8) investigated the polymerization of 1,3-cyclohexadiene by several types of catalyst and found that the IR spectra of the resulting polymers showed several spectral features which shifted in position and intensity depending on the catalyst and media employed. An IR spectrum of polycyclohexadiene synthesized with n-BuLi in hydrocarbon is reproduced from their work and shown in Figure 6. Yousufzai et al. (10) studied the monomer-isomerization polymerization of 1,4-cyclohexadiene to yield poly-1,3-cyclohexadiene through initial isomerization of 1,4-cyclohexadiene to 1,3-cyclohexadiene followed by polymerization. An IR spectrum showing that the polymer formed in this manner was identical to the polymer obtained from 1,3-cyclohexadiene is reproduced in Figure 6. An examination of the two IR spectra in Figure 6 shows they are similar but not identical.

A comparison of the 6000 Torr s results with these published spectra of poly-1,3-cyclohexadiene reveals some similarity in the band shape of the CH stretching region if the feature observed in the IET spectra near 2950 cm^{-1} corresponds to the sharp feature observed in the IR spectra near 3000 cm^{-1}. Several other features differ in intensity although the

general positions of many of the bands are similar.

The 6000 Torr s results show that the C=C stretching region broadens and increases in intensity as the surface temperature is increased. In some cases the C=C stretching features split into two or three bands. The ring breathing modes located in the 800 - 880 cm^{-1} region also increase dramatically at 6000 Torr s and their variability provides evidence of different types of substituted rings. The 150 and 6000 Torr s results demonstrate that there is no apparent saturation limit for 1,3-cyclohexadiene adsorption as based on the increasing intensity of the unsaturated hydrocarbon stretching feature, as the 1,3-cyclohexadiene exposure is increased. As previously mentioned, this is further supported by the increases in junction resistance which occurred for this adsorbate system. The available evidence indicates that the polymerization of 1,3-cyclohexadiene may in fact be initiated by $Zr(BH_4)_4$ supported on Al_2O_3.

5.0 Conclusions

The temperature and pressure dependent reactions of 1,3-cyclohexadiene with $Zr(BH_4)_4$ have been investigated with IETS. Adsorbed 1,3-cyclohexadiene has been shown to form an unsaturated hydrocarbon similar to cyclohexene at moderate exposures and evidence has been presented that the catalyst may initiate the polymerization of 1,3-cyclohexadiene at high exposures to form poly-1,3-cyclohexadiene. Adsorption of 1,3-cyclohexadiene also perturbs the catalyst much more than other adsorbates such as cyclohexene, promoting the disassociation of the BH_4 ligands. This

study demonstrates that inelastic electron tunneling spectroscopy is well suited for investigations of supported catalytic systems.

References

1. H. E. Evans and W. H. Weinberg, J. Am. Chem. Soc. 102, 872 (1980).

2. H. E. Evans and W. H. Weinberg, J. Am. Chem. Soc. 102, 2548 (1980).

3. H. E. Evans and W. H. Weinberg, J. Am. Chem. Soc. 102, 2554 (1980).

4. Presented in Chapter 2 of this thesis.

5. C. S. Marvel and G. E. Hartzell, J. Am. Chem. Soc. 81, 448 (1959).

6. P. E. Cassidy and C. S. Marvel, Macromolecular Synthesis 4, 7 (1972).

7. P. E. Cassidy, C. S. Marvel and S. Ray, J. Polymer Sci. A 3, 1553 (1965).

8. G. Lefebvre and F. Dawans, J. Polymer Sci. A 2, 3277 (1964).

9. B. A. Dolgoplash, S. I. Beilin, Yu. V. Korshak, G. M. Chernenko, L. M. Vardanyan and M. P. Teterina, Eur. Polymer J. 9, 895 (1973).

10. A. H. K. Yousufzai, K. Endo and T. Otsu, J. Polymer Sci. Polym. Chem. 13, 1601 (1975).

11. W. H. Weinberg, Ann. Rev. Phys. Chem. 29, 115 (1978).

12. "Tunneling Spectroscopy", P. K. Hansma, Ed., Plenum, New York (1982).

13. J. W. Coburn, "Plasma Etching and Reactive Ion Etching", American Institute of Physics, New York, 1982.

14. W. M. Bowser and W. H. Weinberg, Rev. Sci. Instrum. 47, 583 (1976).

15. W. M. Bowser, Ph.D. Thesis, California Institute of Technology, Pasadena, CA 1980.

16. J. Kirtley and P. K. Hansma, Phys. Rev. B 13, 2910 (1976).

17. N. M. D. Brown, W. E. Timms, A. J. Turner and D. G. Walmsley, J. Catal. 64, 101 (1980).

18. W. M. Bowser and W. H. Weinberg, Surface Sci. 64, 377 (1977).

19. C. Di Lauro, N. Neto and S. Califano, J. Mol. Structure 3, 219 (1969).

20. L. A. Carreira, R. O. Carter and J. R. Durig, J. Chem. Phys. 59, 812 (1973).

21. H. D. Stidham, Spectrochim. Acta 21, 23 (1965).

22. H. Gerding and F. A. Haak, Rec. Trav. Chim. 68, 293 (1949).

23. K. Sakashita, J. Chem. Soc. Japan 77, 1094 (1955).

24. S. Kumar, V. D. Gupta and P. C. Jain, Acta Ciencia India 5, 8 (1979).

25. L. J. Bellamy, "The Infra-Red Spectra of Complex Molecules", John Wiley and Sons, New York, 1966, pp. 378-380.

Figure Captions

Figure 1: Comparative view of IET spectra of 1,3-cyclohexadiene at an exposure of 150 Torr s interacting with $Zr(BH_4)_4$ supported on Al_2O_3. Substrate temperatures during the cyclohexadiene exposure were (A) 298 K, (B) 403 K and (C) 473 K.

Figure 2: Comparative view of IET spectra of 1,3-cyclohexadiene at an exposure of 6000 Torr s interacting with $Zr(BH_4)_4$ supported on Al_2O_3. Substrate temperatures during the cyclohexadiene exposure were (A) 298 K, (B) 403 K and (C) 473 K.

Figure 3: Comparative view of IET spectra of 1,3-cyclohexadiene interacting with $Zr(BH_4)_4$ supported on Al_2O_3 at a substrate temperature of 298 K during 1,3-cyclohexadiene exposures of (A) 150 Torr s and (B) 6000 Torr s.

Figure 4: Comparative view of IET spectra of $Zr(BH_4)_4$ adsorbed on Al_2O_3 interacting with (A) cyclohexene and (B) 1,3-cyclohexadiene at exposures of 150 Torr s and substrate temperatures of 298 K.

Figure 5: Comparative view of IET spectra of $Zr(BH_4)_4$ adsorbed on Al_2O_3 interacting with (A) cyclohexene and (B) 1,3-cyclohexadiene at exposures of 6000 Torr s and substrate temperatures of 298 K.

Figure 6: IR spectra of poly-1,3-cyclohexadiene. Spectrum (A) is the IR spectrum of poly-1,3-cyclohexadiene synthesized with n-BuLi in hydrocarbon reproduced from reference (8). Spectrum (B) shows two spectra of poly-1,3-cyclohexadiene synthesized from (A)

1,3-cyclohexadiene and (B) 1,4-cyclohexadiene which was first isomerized to 1,3-cyclohexadiene by the catalyst employed. Reproduced from reference (10).

Table 1
Peak positions, Relative Intensities and Assignments for IET Spectra of $Zr(BH_4)_4$ Adsorbed on Al_2O_3 Interacting with 1,3-Cyclohexadiene at an exposure of 150 Torr s.

298K	403K	473K	Assignments
3640(.11)	3576(.16)	3635(.11)	ν(OH)
3010 sh	3010 sh		ν(CH)
2960 sh	2900 sh		
2917(.70)	2866(.69)	2904(1.38)	
2856(.55)	2822(.62)	2859(1.24)	
2477(.16)	2457(.07)	–	ν(B-H_t)
2422(.18)	2423(.10)	2449(.23)	
2386(.16)	2366(.09)		
	2309(.07)	–	
2256(.05)	2178(.05)		ν(B-H_b)
2170(.07)	2122(.04)		
1610(.04) br	1602(.08)	1603(.12)	ν(C= C)
	1563(.06)		
1454(.27)	1437(.24)	1453(.50)	CH_2 scissoring
1387(.18)	1377(.17)	1381(.31)	CH deformations
1350 sh	1334(.14)	1325(.20)	
1271(.10)	1273(.06)	1279(.16)	
	1232(.04)	1248(.17)	BH deformations
1166(.10)	1158(.06)		B-O modes
1140(.12)		1147(.14)	
1115(.12)	1119(.04)		
1061(.29)	1047(.25)	1061(.27)	CH mode
914(1.0)	917(1.0)	914(1.0)	Zr-O stretch[1]
727(.21)	732(.26)	730(.23)	metal oxide, Zr-C and Zr-B modes
	680(.26)	692(.20)	
390(.03)		393(.04)	
292(.30)	292(.29)	294(.40)	Al phonon
		262(.35)	Zr-C bend or torsion

1. Al-O (bulk) stretch appears as a shoulder on the Zr-O peak.

Table 2
Peak positions, Relative Intensities and Assignments for IET Spectra of $Zr(BH_4)_4$ Adsorbed on Al_2O_3 Interacting with 1,3-Cyclohexadiene at an Exposure of 6000 Torr s.

298K	403K	473K	Assignments
3626(.06)	3650(.16)		ν(OH)
2960(1.43)	2955 sh	2949(1.77)	ν(CH)
2922(1.96)	2915(2.28)	2916(2.30)	
2848(1.33)	2837(1.42)	2837(1.56)	
2445(.12)	2425(.16)	2428(.13)	$\nu(B-H_t)$
2252(.09)			$\nu(B-H_b)$
1641(.10)	1631(.16)		ν(C= C)
1604(.10)		1609(.12) br	
1583(.09)	1584(.16)		
1446(.71)	1442(.79)	1442(.87)	CH_2 scissoring
1370(.54)	1361(.59)	1368(.67)	CH deformations
1340(.42)	1341(.56)	1337(.58)	BH deformations
1272(.18)	1272(.23)	1265(.32)	BO modes
	1242(.27)	1244(.30)	
1135(.32)	1135(.40)	1136(.42)	
1057(.35)	1055(.22)	1059(.31)	CH mode
923(1.0)	922(1.0)	924(1.0)	Zr-O stretch[1]
850 sh	865(.68)	865(.61)	CH modes
		815(.40)	
724(.19)	732(.17)	727(.20)	
	711(.18)		
696(.17)	687(.16)	688(.14)	Zr-O stretch
650(.10)		472(.12)	Zr-C modes metal oxide modes CH skeletal deformations
450(.12)	450(.15)	443(.17)	
385(.07)	378(.15)	391(.19)	
278(.43)	282(.53)	278(.57)	
	258(.50)		

1. Al-O (bulk) stretch appears as a shoulder on the Zr-O peak.

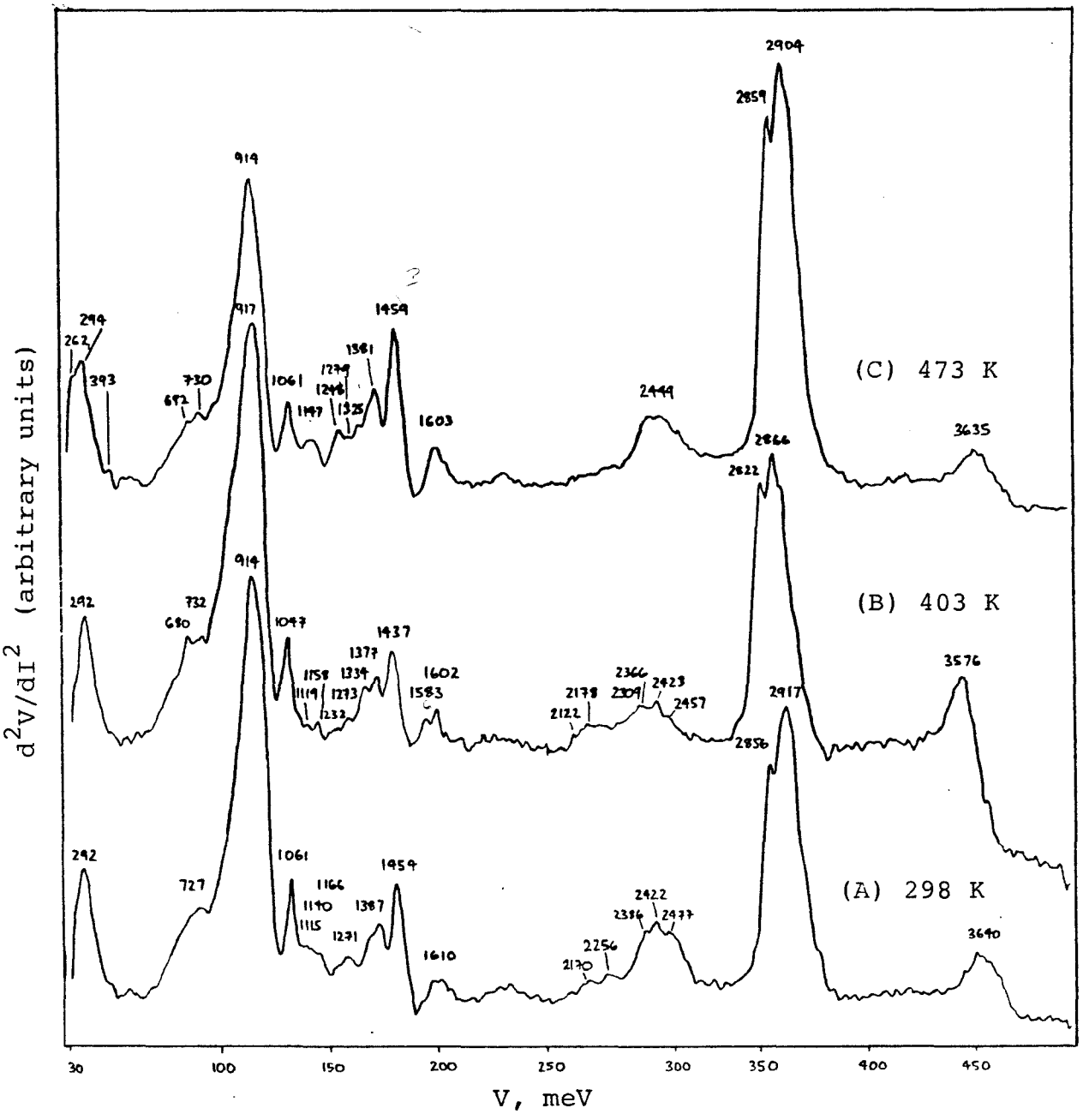
(C) 473 K
(B) 403 K
(A) 298 K
d^2V/dI^2 (arbitrary units)
V, meV
30
100
150
200
250
300
350
400
450
262
294
393
692
730
914
917
1061
1147
1299
1298
1325
1381
1459
1603
2449
2859
2904
3635
292
690
732
914
1097
1158
1119
1233
1293
1339
1377
1437
1583
1602
2122
2178
2309
2366
2423
2457
2822
2866
3576
292
727
1061
1115
1166
1190
1231
1387
1459
1610
2170
2256
2396
2422
2437
2856
2917
3690

Figure 1

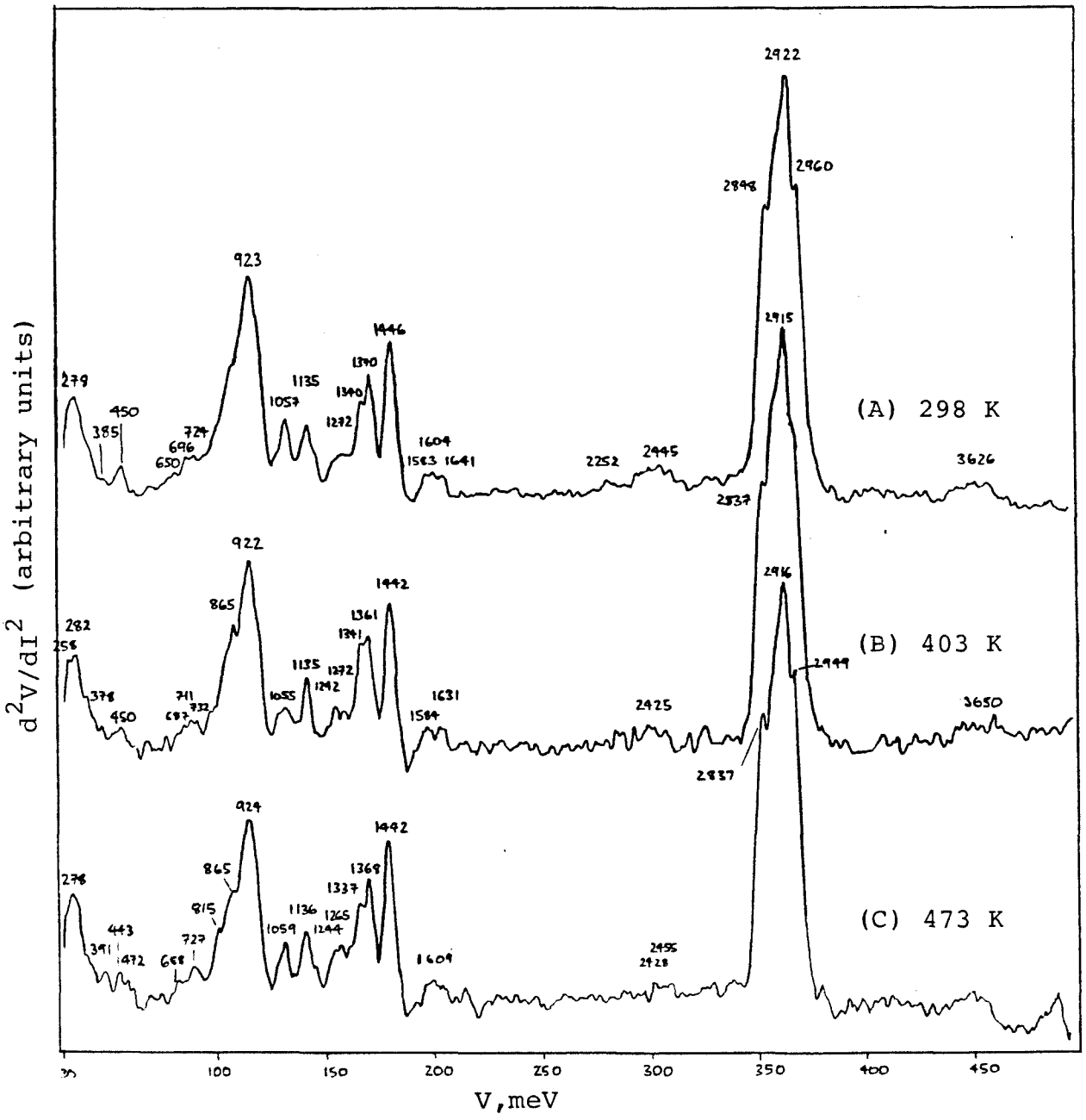
d²V/dI² (arbitrary units)
V,meV
(A) 298 K
(B) 403 K
(C) 473 K
279
385
450
650
696
724
923
1057
1135
1340
1390
1446
1584
1609
1641
2252
2445
2848
2915
2960
3626
282
378
450
697
711
732
865
922
1055
1135
1242
1272
1341
1361
1442
1584
1631
2425
2837
2916
2949
3650
278
391
443
472
668
727
815
865
924
1059
1136
1244
1265
1337
1369
1442
1609
2428
2455

Figure 2

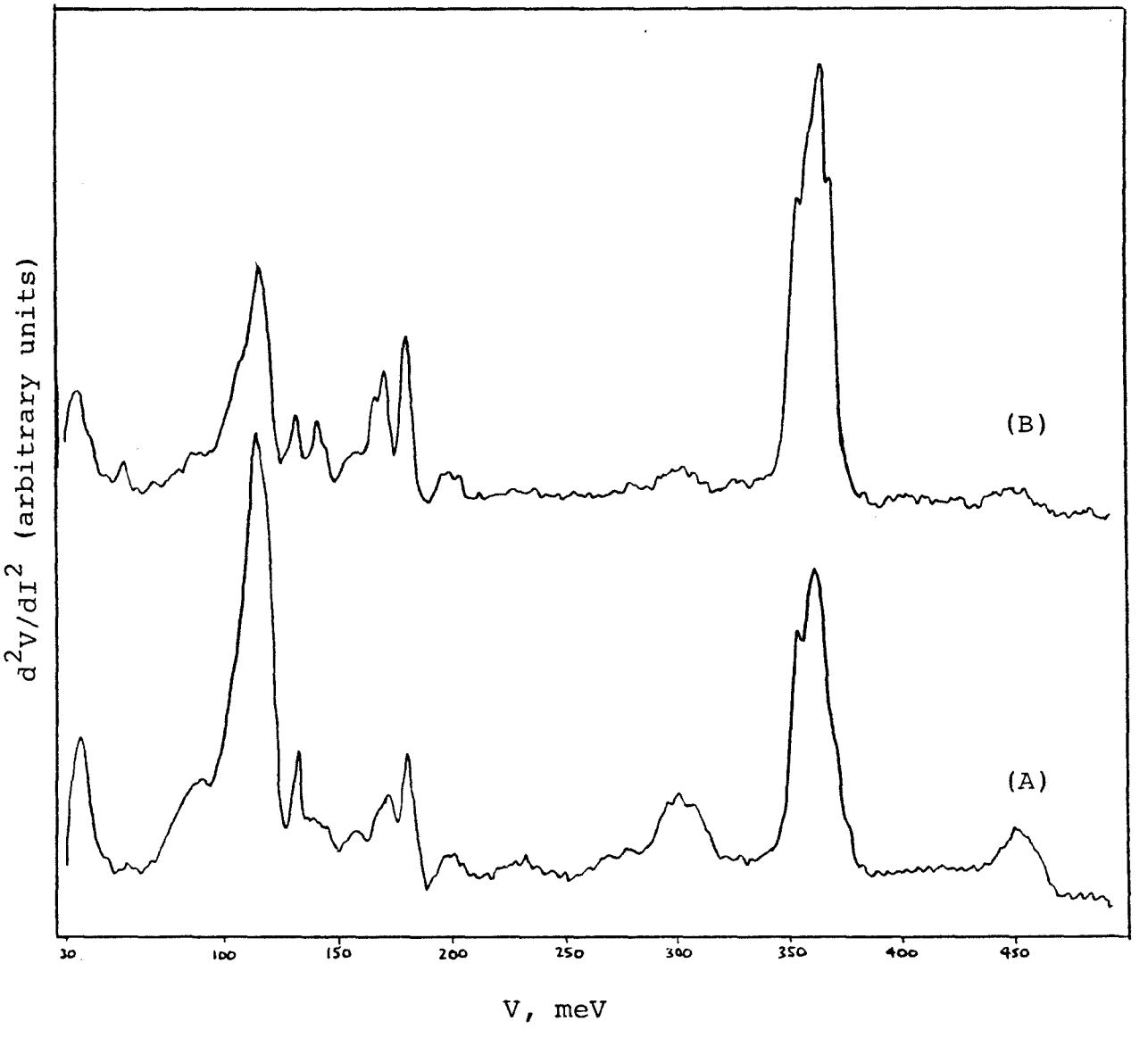
d^2V/dI^2 (arbitrary units)
(B)
(A)
30
100
150
200
250
300
350
400
450
V, meV

Figure 3

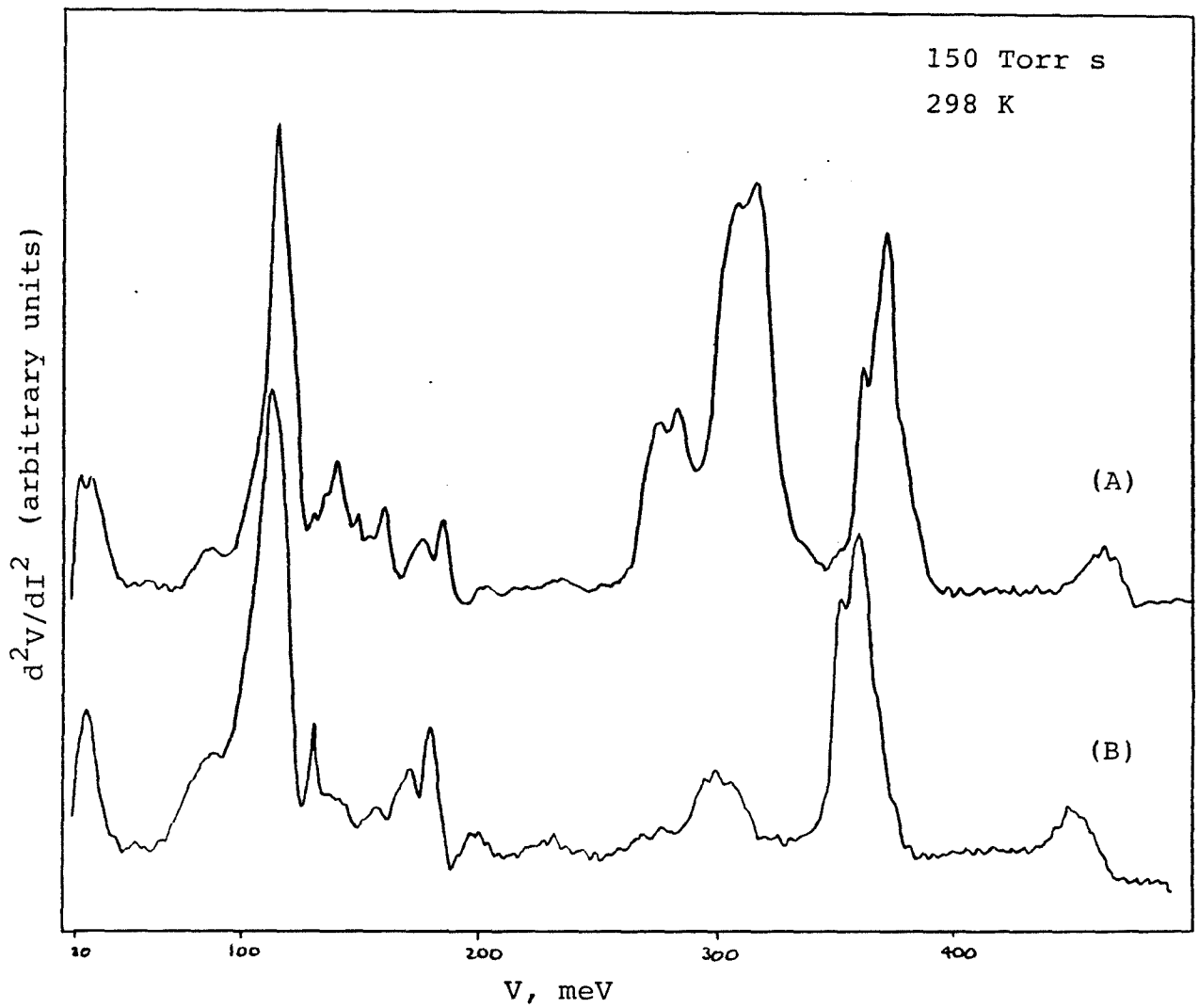
150 Torr s
298 K
(A)
(B)
d^2V/dI^2 (arbitrary units)
10
100
200
300
400
V, meV

Figure 4

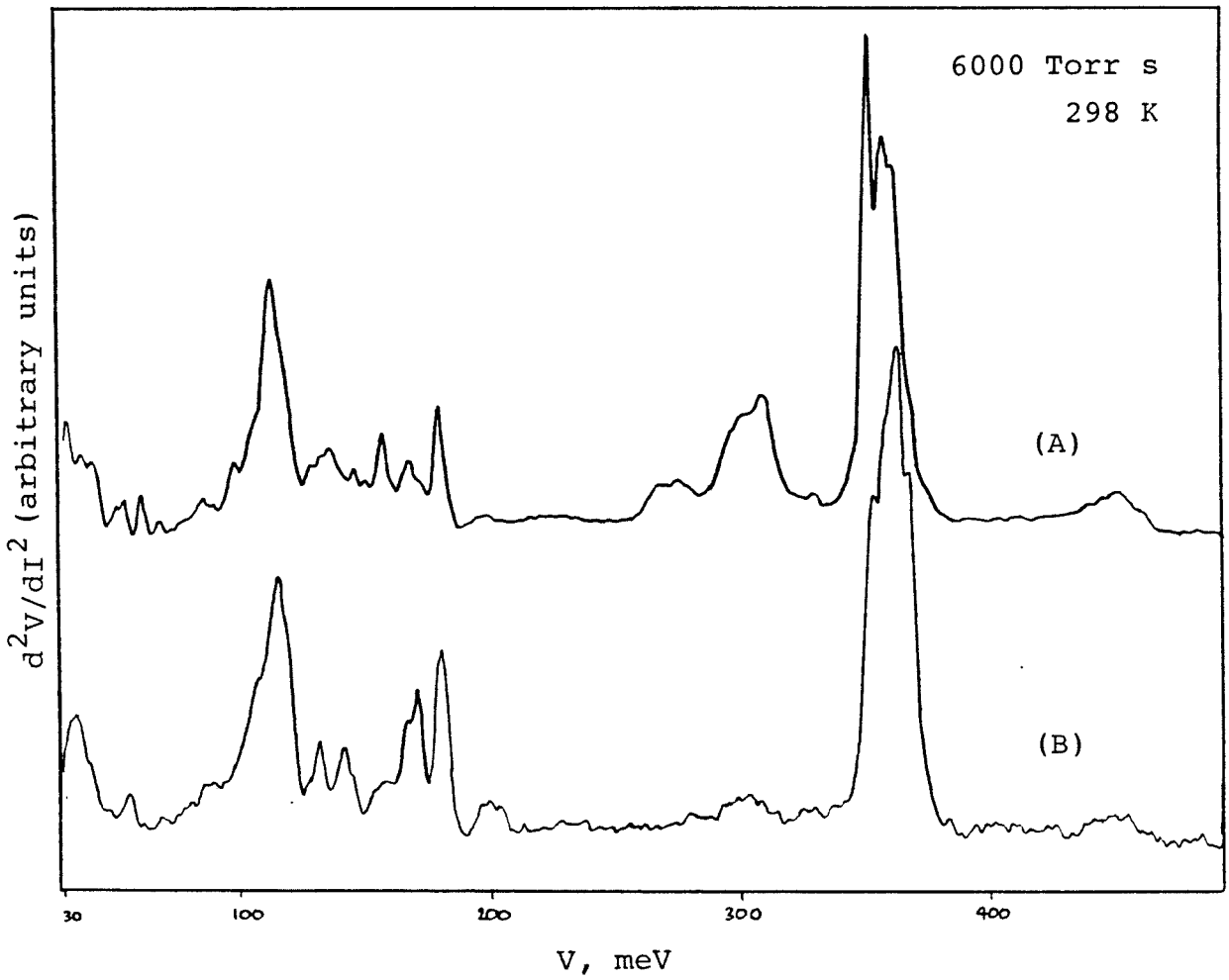
6000 Torr s
298 K
(A)
(B)
d^2V/dI^2 (arbitrary units)
30
100
200
300
400
V, meV

Figure 5

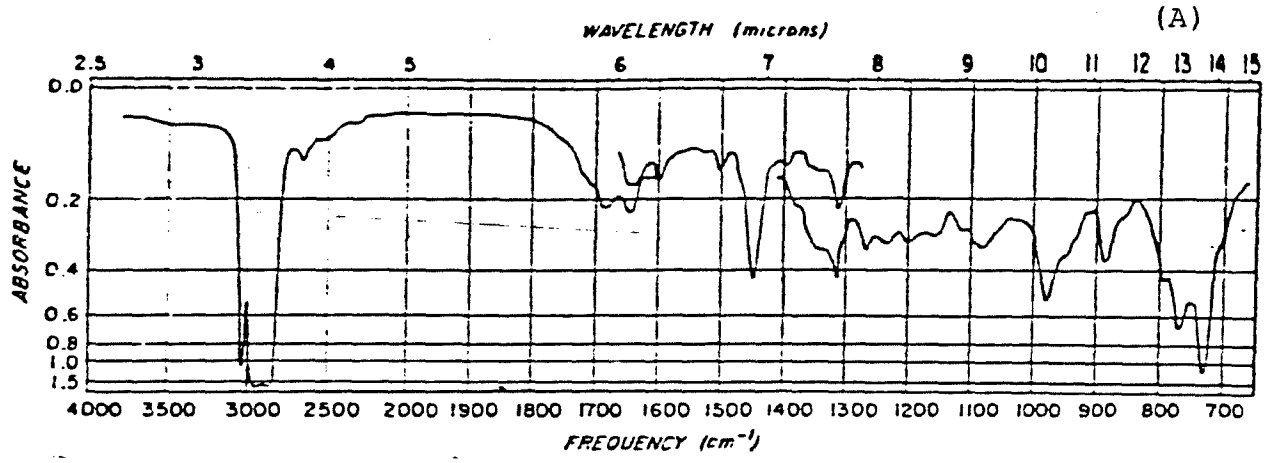

Infrared spectrum of polycyclohexadiene synthesized with *n*-BuLi in hydrocarbon.

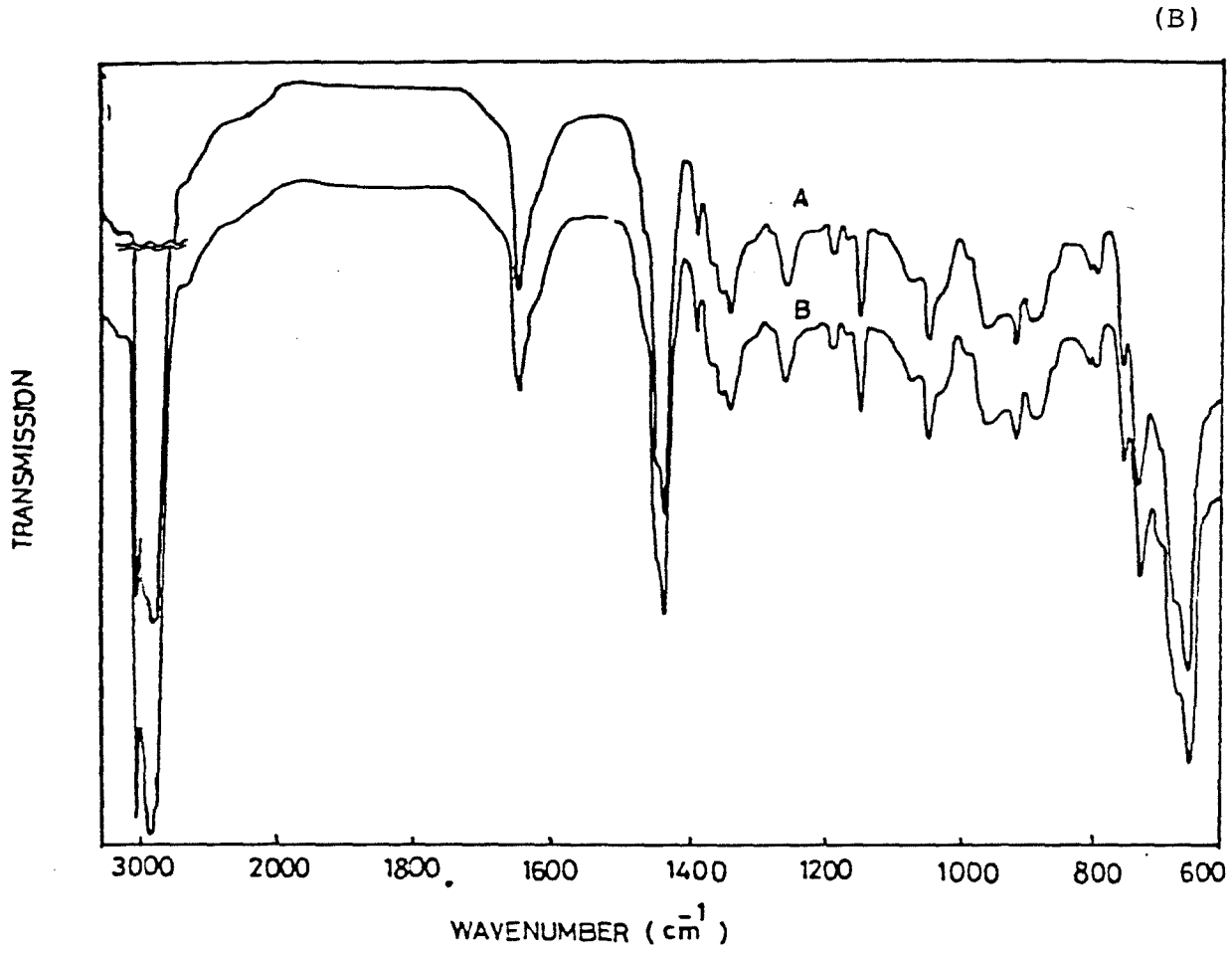

Infrared spectra of polymers obtained from (*A*) 1,3-CHD and (*B*) 1,4-CHD

Figure 6

Chapter 4

Conclusions

Inelastic electron tunneling spectroscopy is a vibrational surface spectroscopy which is well suited for the study of certain chemical reactions and supported complexes. This thesis has demonstrated that it is possible to use IETS to investigate complicated experimental systems over a wide range of adsorbate exposures and substrate temperatures by obtaining detailed IET spectral "snapshots". In the case of cyclohexene interacting with $Zr(BH_4)_4$ adsorbed on Al_2O_3, IETS was used to successfully characterize and identify unexpected new products of reaction as well as monitor the disassociation of the catalyst as a function of adsorbate exposure and substrate temperature.

Cyclohexene was a very successful adsorbate to study with IETS because it provided some interesting chemistry as well as junctions which were electrically insulating at high surface concentrations. The investigation of the interactions of 1,3-cyclohexadiene with $Zr(BH_4)_4$ provided an interesting contrast to the cyclohexene work because it showed that IETS can be used to investigate chemical systems which by their nature provide more complex reaction products. The polymer produced by 1,3-cyclohexadiene was not only chemically complicated, displaying evidence of various types of substituted rings but also produced junctions with poor electrical characteristics, presumably because of the unsaturated nature of the barrier formed at high surface concentrations.

With the proper choice of adsorbate, IETS can be a very rewarding type of surface vibrational probe. Some general guidelines can be proposed. First, the adsorbate system should be chosen such that the expected reaction products are chemically distinct from the adsorbate.

Several questions have arisen in studying polymerization reactions with IETS. How is the vibrational spectrum of a monomer different from an oligomer or a polymer? How will the vibrational spectra reflect the incremental addition of monomer? From this point of view, the cyclohexene adsorbate was a successful system to choose for study but the 1,3-cyclohexadiene adsorbate was a much poorer choice.

A further consideration is the paradox presented by studying polymerization reactions with IETS. A really successful catalyst for the polymerization of a particular monomer could easily produce a barrier too thick for the tunneling electrons to penetrate. A similar consideration regards the rate of the reaction to be studied. Slow reaction rates are preferred when attempting to observe the adsorbed reaction intermediates with IETS. In the work presented here, the reaction of cyclohexene with the adsorbed catalyst turned out to be quite sluggish- and allowed spectra to be obtained which showed that the catalyst was still intact on the surface at the low exposure studied. However, the 1,3-cyclohexadiene system reacted so readily with the catalyst that most of the features due to the BH_4 ligands were lost.

Certain other considerations apply when choosing a system for study with IETS. Since the assignment of spectral features is made primarily by comparison with the reported IR and Raman data of an adsorbate, it is important that such information be available. For example, most polymer chemists do not publish extensive IR spectra of their work. For this thesis, the IR spectrum of polycyclohexene, which was never published in the literature, turned out to be important. An additional source of

information which may be used to identify the reaction products of some adsorbates is to fabricate IET junctions using compounds similar to the expected products of reaction in order to compare their IET spectra. However, not all chemical systems can benefit from this approach, especially studies which investigate the reactions of adsorbed complexes with other adsorbates rather than with the aluminum oxide support.

A last considerations involves the chemical nature of the support and the known sensitivity of IETS to particular chemical groups. Certain vibrations suffer from weak electron vibration coupling constants and the spectra of these systems often display only very weak features. On the other hand, IETS is known to be very sensitive to CH vibrations and these types of reactions can be studied very easily. The known sensitivities can be exploited when choosing experimental systems to study with IETS.

Despite limitations, IETS is a sensitive and unique surface analytical tool which can be successfully employed to study a wide range of adsorbate systems. This thesis has shown it may be employed successfully to investigate the nature of new catalytic systems and unexpected products of reaction.

Appendix A

Experimental Apparatus and Procedures

Joy in the lab

The O-ring fits!

It was in, the O-ring box!

It's even made of Viton

And greased with Apiezon

Its outgassing rate is low

Its form will restrict all flow

It's an O-ring, of Viton,

du Pont's trademark!

To be sung to the tune of

"Joy to the World"

I. Experimental Apparatus

Table of Contents

1. General Description and Capabilities

The vacuum system used for the IETS sample preparation consists of an 18" Pyrex bell jar which houses the interior assemblage, a foreline connected to a mechanical pump, a main pumping stack which has a liquid nitrogen cooled diffusion pump, and a gas-handling manifold.

The bell jar seals onto a polished stainless steel 1" baseplate by means of a Viton gasket and a counter-weighted pulley system. All of the feedthrough ports are located in the baseplate. The bell jar is protected by a steel guard.

The foreline is separated from the bell jar by the valve labeled V1 in Fig. 1. When V1 is open, the bell jar can be evacuated to below 10^{-4} Torr by the 1397 Welch Duo-Seal pump which has a pumping capacity of 500 l/sec. This pressure region is monitored with an NRC Alphatron vacuum gauge.

To further decrease the bell jar pressure, the roughing line is isolated from the bell jar and the main pumping stack is used. This consists of a liquid nitrogen (LN_2) cooled CVC 6" diffusion pump which is backed by a second model 1397 Welch Duo-Seal mechanical pump. This allows maximum throughput, which can be important for some of the experiments which involve adsorbate exposures in the 1 Torr range. This low pressure regime is monitored by a Varian Bayard-Alpert type ionization gauge. A gate valve isolates the bell jar from the diffusion pump when it is not in use.

The mechanical pump is capable of bringing the system to below 10^{-4} Torr in less than five minutes and continued pumping with the new diffusion pump will result in a pressure of less than 5×10^{-6} Torr in approximately 15 minutes. With continued evacuation, the base pressure of the system is on the order of 1×10^{-8} Torr.

It should be noted that this is a vast improvement in pumping time. The diffusion pump which was originally employed as part of this system was a CVC 4" diffusion pump with a maximum pumping speed of 690 l/sec for air. The new pump, CVC model PMC-6B, has a pumping speed of 1,400 l/sec for air. With the smaller pump, at least one day of pumping was required to bring the bell jar into the proper pressure range for an experiment. This turn-around time was especially unproductive because it was often coupled with equipment malfunctions which necessitated bringing the bell jar back to atmospheric pressure before the attempted experiment could be resumed. The new pump virtually eliminates these problems. It is now possible to pump down, go back up to atmospheric pressure if necessary, pump down again and still do an experiment all in one day.

The new system design differs also in that two Welch Duo-Seal Vacuum pumps are in use, each one dedicated to a particular function. Previously, one pump was used for both roughing the system and backing the diffusion pump. This required a complicated sequence of opening and closing valves which increased the likelihood that the diffusion pump would be exposed accidentally to an overly high pressure. This situation could be critical if the sudden pressure increase is large enough to force the pump oil out of the pump and into the vacuum lines since the only way to recover from this type of error is to dismantle the system and thoroughly clean the inside of the lines. The new design eliminates this potential error. The new 6" diffusion pump also has a much better tolerance for moderate pressures than the 4" pump because of its faster pumping speed which helps further reduce the time required to perform an experiment.

Another design change which has been implemented is to run both 1397 pumps off of 220 V rather than 110 V. This keeps the motors cooler under

continuous operation. Each pump is plugged into its own circuit on the south side of the lab and each outlet is equipped with a "Motor Watchman" which allows the pumps to be turned off at the outlet rather than unplugged. The "Motor Watchmen" were installed by Physical Plant and prevent the motors from drawing excessive power and burning out when they are first switched on.

2. Pump Oils

New pump oils are also used in both the diffusion and the two 1397 Welch Duo-Seal pumps. The diffusion pump oil is Santovac 5 polyphenylether, made by Monsanto. Previously, Dow Corning's DC705 was used which is a silicon-based oil rather than being an organic. The change to Santovac 5 was made because if the pump is accidentally left on while not under vacuum, a silicon-based oil will bake itself into a rock-hard substance which is very difficult to remove from the heating fins.

The oil now used in the mechanical pumps is Inland 21, available from Kurt Lesker. It is a highly distilled pure hydrocarbon mineral oil which has a lower vapor pressure than the traditional pump oil. It also contains an antioxidant and is especially formulated for applications which involve repeated cycling between atmospheric pressure and high vacuum.

3. Main Pumping Stack and Foreline

The main pumping stack consists of a CVC gate valve, a LN_2 trap, an adapter flange and the diffusion pump. The pump is followed by a right-angle valve, a molecular sieve trap, and the model 1397 Welch Duo-Seal pump. Pressure in this line is monitored with a thermocouple gauge placed before the right-angle valve. This position was chosen so that the pressure in the pump could still be monitored if it is necessary to turn off the mechanical pump when the diffusion

pump is still running. The right-angle valve was included so that the diffusion pump would be isolated and kept under vacuum.

A small back-to-air valve before the molecular sieve trap allows one to turn off the mechanical pump and bring the entire line back to atmospheric pressure quickly and easily without having to wrestle with the hose connections to the pump. The line should be vented immediately after switching off the pump to ensure that none of the pump oil is forced up into the line as the pressure gradually rises.

The foreline is separated from the bell jar by a valve and consists of copper tubing, a molecular sieve trap and the Welch Duo-Seal 1397 mechanical pump. Preceding the trap is a double-sided flange which serves as the inlet for a 1/4" copper line which serves to differentially pump the gate valve housing and the rotary-linear motion feedthrough used to operate the mask and shuttle assembly. Also mounted on this flange is a thermocouple gauge used to monitor the pressure in the foreline.

The sealing edge of the bell jar is provided by an L-shaped Viton gasket which fits against the polished stainless steel baseplate. The baseplate has 15 ports arranged around a large centrally-located pumping port. The gate valve is located under the pumping port and isolates the diffusion pump from the bell jar. The gate valve provides only a one-way seal; it will not seal when the diffusion pump is not under vacuum because the O-ring seal is on the lower side of the valve. The gate valve is closed whenever the bell jar is open to the atmosphere or at a pressure above 10^{-3}–10^{-4} Torr. However, the gate valve can be opened slowly at pressures up to 5×10^{-1} Torr if the thermocouple gauge pressure in the diffusion pump line is kept at approximately 200 microns or below. This is especially useful when evacuating hydrocarbons which can be pumped

out at only a moderate rate by a mechanical pump as compared to a LN_2-trapped diffusion pump, which will pump them away nearly as quickly as the gate valve can be opened.

4. Ports and Feedthroughs

The port and feedthrough arrangement on the baseplate has changed from what was used previously **(1)**. There is no longer a feedthrough for cooling fluids. These lines were used occasionally to cool the samples during certain fabrication steps. When cooling with LN_2, the contraction of the O-ring seals used in these lines caused them to leak extensively and freeze up. Additionally, the Swagelok fittings used to construct these lines were not sufficiently leak-tight for this application and were also located in the bell jar interior.

There are now four high-current feedthroughs and one high voltage feedthrough. Three feedthroughs are used for pressure monitors; the Alphatron gauge, the ionization gauge and a seldom-used thermocouple gauge. Additional feedthroughs are the rotary-linear motion feedthrough (used to operate the mask and shutter assembly), a multi-pin electrical feedthrough, an inlet for the manifold, a port for the $Zr(BH_4)_4$ trapline, and three blank ports (labeled as 1, 2 and 3 in Fig. 2). Port 2 has been used to accommodate a second rotary/linear motion feedthrough which is used for handling solid samples which cannot be introduced into the system through the manifold. A heating wire is used to sublime the solid after it is in position under the slides. Other feedthroughs are available for special purposes.

In addition to the ports located in the baseplate, another very large port is located on the side of the bell jar. This is blanked off with a 6" diameter Pyrex flange. Originally, this port permitted the use of an auxiliary custom-built titanium sublimation pump which was encased in a protective shield next to the

bell jar but was removed because it was too cumbersome and time-consuming to use on a regular basis. To use the pump required removing it from the protective shield, attaching it to the bell jar before pumpdown and removing it before the bell jar could be raised. This procedure added approximately 1.5 hours to an already lengthy experimental procedure. The Ti sublimation pump was useful though because it could lower the base pressure of the system an order of magnitude or more to a level not readily obtained with the diffusion pump. With the new diffusion pump, however, the base pressure of the system is now even lower than that obtainable with the Ti sublimation pump.

5. Manifold

An extensive manifold system located to the left of the bell jar is used to handle the wide range of gases and vapors used in tunneling experiments. A schematic of the manifold connections is shown in Fig. 3. The manifold is evacuated by a Welch Duo-Seal #1376 vacuum pump with a pumping speed of 300 l/min which is connected to a custom-made molecular sieve trap used to prevent pump oil contamination in the manifold.

6. Bell Jar Interior Assemblage

The interior of the bell jar contains provisions for three samples, or slides. (Each sample has three junctions.) One innovation which has helped make the tunneling experiments easier is to use pre-cut high temperature glass slides. In the past, regular glass laboratory slides were bought from one of the campus stockrooms and cut to size with a diamond scribe, a tedious and time-consuming process. Sometimes this glass cracked when the slides were heated or submerged in LHe. The new glass slides have never cracked. They are pre-cut and cleaned, and individually wrapped in tissue. They save a great deal of time and trouble. They are available by special order from Corning Glass in Danville,

VA (glass #7059; .438" x 1.020" x .032" in thickness; 400 units/box).

The slides are mounted first on sample holders outside of the system using In/Sn solder from Indium Corporation of America. Four teflon-coated 22 awg wires are attached to the surface of each slide. After mounting, the three sample holders are then mounted inside the vacuum system on a tripod framework so that the slides face downward. The four soldered wires serve to hold the slide in place as well as provide the four electrical contacts to the aluminum film which are used during the 4-point resistance measurement and the temperature monitoring/sample heating procedure **(2)**. The 4-point resistance measurement is used to monitor the Al film growth during deposition and the completion of the Al annealing procedure. Each wire is soldered permanently to a miniature gold-plated banana plug to make or break electrical connections easily.

A. Sample Holders

A number of alterations have been made to the slide holders **(3)**. A drawing of one of the redesigned holders is shown in Fig. 4. Each holder consists of a 6mm x 16mm x 38mm copper block milled out on one side to accommodate the glass slide. The electrical leads are supported on each side of the copper by Macor strips (6mm x 6mm x 38mm) (a machinable ceramic made by Corning Glass) attached to the two long sides of the copper block. The changes in the sample holder design are concerned primarily with how the electrical connections are supported by the Macor strips. The electrical wires are now positioned in the Macor parallel to the position they will be soldered on the slide. In the past, these were offset in such a way that stress in the solder often resulted in broken electrical connections during an experiment. The new simplified blocks also wear better because fewer connections are made with set screws which wear away the tapped Macor every time they are positioned.

In addition, a second set of three sample holders was made to reduce the "turn-around" time between experiments. During an experiment, the second set of holders can be prepared for mounting so that when the completed junctions are removed the new set can be mounted quickly, reducing the time that the system is at atmospheric pressure.

B. Mask and Shutter Assembly

The mask and shutter assembly is located under the mounted sample holders and is operated by a linear-rotary feedthrough. The design of this feedthrough has been altered to provide more stability and a smoother operation of the assembly. The mask stage is operated separately from the shutter and consists of the Al masks, Pb masks, "blank" mask, and an open area to allow full exposure of the slides.

C. Evaporation Sources

The evaporation sources are located directly under the samples. Although there are provisions for up to four different sources, only three are in use: two for aluminum and one for lead. In the past, the aluminum evaporation source has been a triple-stranded tungsten filament with six coils and the Pb evaporation source has been a tungsten isolated hot zone boat (dimple type) with a small dimple area (7/16" diameter x 1/8" deep). One of the innovations employed successfully is a Pb boat much larger than those used previously. This saves time and effort because the boat no longer needs to be carefully refilled for each evaporation.

D. Al Evaporation Window

The Al evaporation has been one of the most troubleprone procedures required for the sample preparation. Countless experiments have terminated prematurely because of this seemingly simple step. The problems involved

include the following: (1) the Al fails to properly wet the tungsten and drops off of the filament; (2) the filament ages, becomes brittle and cracks during heating thus shorting out the circuit; (3) the Al evaporates but forms a film too thin to ensure its properties will be like those of the thicker films usually employed.

To eliminate these problems, two extremely valuable changes have been made. First, the third evaporation source is now kept permanently ready to provide an emergency backup for the Al evaporation source. In the past, this third source was never used and if the Al evaporation failed, no backup was available.

The most important change however has been to improvise a "window" to monitor visually the progress of the metal evaporation. This "window" is a Pyrex glass plate held in an aluminum frame resembling a candelabra and can be removed from the frame for cleaning. Before the glass candelabra could be used, the metal deposits on the bell jar interior were removed. The "candelabra" is placed between the bell jar wall and the evaporation sources and prevents metal deposits on the walls. After an experiment is completed, the glass can be readily cleaned. Since the bell jar wall is essentially isolated from the evaporation sources, the evaporation process can be observed. The moment the Al melts is crucial because the Al will drop off of the tungsten filament if the power is increased too quickly.

E. The DVM Monitor

The metal deposition rate is monitored by a quartz crystal oscillator located at the same vertical distance from the evaporation source as the three samples and situated immediately in front of the center sample. A new monitor for the Al evaporation has also been adopted: the Hewlett-Packard Digital Multimeter, which was used primarily during the sample heating/temperature measurement

process. As the evaporated Al begins to form a thin film, the DVM can be used to measure the resistance of the film, providing a sensitive monitor of the growth of each of the three samples.

The DVM is also a vital monitor for a new procedure which has become an essential component of every tunneling experiment — annealing the Al films after the evaporation. This step is probably responsible for more successful experiments than any of the other improvements noted thus far, at least for those experiments where the samples were heated above 200°C. Before this step was added, literally every experiment performed at these elevated temperatures failed because the junctions were immeasurable due to shorts in the oxide. It was decided to heat the aluminum before it was oxidized or exposed to adsorbates because it was reasoned that the junction shorted out because the thin oxide barriers cracked as the Al film underwent a thermally-induced rearrangement. Since this procedure was adopted, all experiments conducted at higher temperatures (the highest being 400°) have been successful. The annealing step is done at 250°C for 10-15 minutes using the technique of Bowser and Weinberg **(2)**. Annealing also lowers the resistance of the films by approximately 15% which is indicative of their lower stress after annealing. This reduced stress ensures the thin oxide films remain intact, as for example when the samples are reheated during exposure to an adsorbate.

F. Glow Discharge Apparatus

After annealing, the samples are oxidized, most often using a glow discharge in a background of O_2 with a trace of H_2O vapor. The glow discharge apparatus was completely redesigned* and is located centrally under the three samples

* The previous glow discharge apparatus consisted of a post-type high voltage feedthrough to which three strands of 16 awg untinned copper wires were attached. These wires were enclosed in a single piece of glass tubing and twisted around the end of the electrode which was an Al rod 100mm in length, 75mm of which was exposed to form the glow discharge electrode. This

which are protected from direct line-of-sight by a removable aluminum shield. This new design is a great improvement and is illustrated in Fig. 5. The electrode can now be replaced easily without removing the feedthrough and dismantling the unit. There are no discharges except at the electrode and the new feedthrough prevents any shorting at the base. The Glass Shop is no longer required except in the event of a broken piece of insulation. The entire cost of the new apparatus was under 200 dollars, in addition to a maximum of two hours shop time. The high voltage feedthrough is available from Veeco.

The threaded end of the feedthrough is used to attach a mated copper receptacle made in the Chemical Engineering Shop from OFHC copper. Only one untinned OFHC 17 awg copper wire is used to conduct the high voltage from the feedthrough to the electrode, three wires being unnecessary. The copper wire is crimped into a small piece of machined OFHC copper used to connect the high voltage wire to the Al electrode, forming a better connection than merely wrapping the wire around the electrode. The single piece of glass tubing was replaced by several pieces to conform to the spatial requirements of the bell jar interior. Each piece is more or less a straight rod and the copper wire is threaded easily through it. The separate glass rods are held together by connectors which were machined out of Teflon available from Physical Plant. The Teflon pieces hold the glass tubes snugly and prevent discharge from occurring other than at the electrode. Figure 6 shows the machined Cu pieces.

---

design was unfortunate for a number of reasons. First, the Al rod needed replacing frequently and the old design made no provision for this. To replace the rod, the entire apparatus and feedthrough needed to be removed from the bell jar; this process could only be accomplished by the Glass Shop because the glass tubing rendered the entire contraption inaccessible. Eventually, the glow discharge apparatus succumbed to a problem which developed over a long period of usage. The glass insulator protecting the area near the feedthrough base from discharging had a small leak allowing some glow discharge to occur at the base. This discharge sputtered the metal away at the base thus increasing the leak and the discharge, eventually shorting out the high voltage nearly every time an oxidation was attempted.

Another innovation has been to use the glow discharge as part of a cleaning procedure before the experiment is begun. An O_2 glow discharge can help to clean any hydrocarbon residue off the slides and the bell jar interior.

G. Glow Discharge Shield

The samples are protected from a direct line-of-sight to the glow discharge electrode by an aluminum shield.* The glow discharge shield was redesigned so that two notches in its base now slip directly into place around two screws, and two wing nuts fasten it in place. These wing nuts never need to be completely removed and can be tightened by hand. Also, there are now two shields. Since the shield needs to be removed, polished and cleaned after each experiment, a second shield helps save time.

7. Summary

The vacuum system described here has undergone numerous changes in the past five years. Although challenged by the constraints of a limited budget and the original design of the system, the objective has been to build a vacuum system with greater reliability and a simpler design, thereby improving the up-time and the turn-around time between experiments. My wish as an experimentalist was to have a system which served as a tool rather than as an impediment to science. The changes I made and the many more improvements that could still be made all serve this goal.

---

* Previously, the shield was held in place by fitting two drilled holes in its base over two matching screws in one of the tripod support cross pieces and then tightly fastening two small hexagonal nuts. These also helped hold in place an Al shield located on the left-hand side of the bell jar used to shield part of the bell jar wall from the evaporation sources. This required the nuts to be tightened with a small wrench, difficult to do because of the limited access to this area. (This second shield is now held permanently in place by its own fasteners.)

II. Experimental Procedures

Appendix A.II. Table of Contents

1. Introduction

A tunneling experiment involves the following ten basic procedures: (1) pumping the system down, (2) pre-experimental procedures, (3) evaporating the aluminum, (4) annealing the aluminum, (5) oxidizing the aluminum, (6) exposing the sample to the adsorbate(s), (7) evaporating the lead, (8) bringing the system up to atmospheric pressure, (9) preparing the samples for measurement, and (10) readying the bell jar for the next experiment. The details of each of these is discussed below. The use of $Zr(BH_4)_4$ is also presented.

Two steps have been added to the basic experimental procedures which have not been employed previously. The first is to use a glow discharge to clean up stray contaminants in the bell jar and on the slides prior to beginning an experiment. This is discussed in Sect. 3B. The second new step has revolutionized experiments conducted above 150°C and consists of annealing the freshly evaporated Al films. Before this step was employed, it was virtually impossible to obtain measurable junctions when the experiment involved heating the sample. After this step was adopted, every experiment conducted above 150°C has resulted in measurable junctions, and the highest temperature tested has been 400°C. This step is discussed in Sect. 5.

2. Pumping the System Down

The vacuum system is pumped down from atmospheric pressure by initial pumping with a mechanical pump, followed by continued pumping with a water-cooled oil diffusion pump. Before beginning the evacuation of the bell jar, the Viton gasket which forms the sealing surface of the vacuum chamber should be inspected. This is done with the bell jar in a fully raised position. Two aluminum glide rods prevent the bell jar and its protective metal screen from swinging or twisting and one or two clamps will prevent the bell jar from accidentally

lowering. When the bell jar is raised securely, carefully inspect the bottom sealing surface of the gasket to make sure that it is greased lightly and evenly with Dow Corning High Vacuum Silicon grease; also make sure that there are no paint chips or flakes of evaporated metal stuck onto the sealing surface. (Details on regreasing the gasket as well as other procedures concerning the maintenance of the bell jar are found in Part 11 of this section.)

After checking the gasket, clean the entire baseplate surface with acetone and Kimwipes (or lint-free cloths if they are available), making sure to remove dust as well as the residue of grease left by the gasket. (Try not to get any acetone on the painted surfaces of the vacuum system support table since the acetone will instantly dissolve the paint. Remove the protective coverings from the center pumping port, ion gauge feedthrough, and the $Zr(BH_4)_4$ (ZBH) trap line. Undo the clamp(s) holding the bell jar in the raised position and gently lower the bell jar down onto the baseplate. Make sure the sealing edge of the gasket is seated evenly against the baseplate by pressing down on the top of the metal guard.

Before beginning the evacuation, you may want to adjust the connections to the manifold. Figures 1 and 3 show the vacuum system and manifold valves. The valve closest to the bell jar, M1, is used to introduce various gases and vapors into the bell jar and is a metering type valve which allows the rate of introduction to be controlled, while the pressure rise is monitored visually using one of the various pressure gauges. This valve is a Nupro 4BMG valve which does not provide positive shutoff; that is, even when it is closed it permits a flow of up to 5 Std. cc/min through the valve. Backing valve M1 is a valve labeled H1 in Fig. 3. H1 is a Nupro 4H bellows-sealed valve which is capable of providing a leak-tight seal.

When the manifold is evacuated, H1 can be left open since the flow through M1 does not appear to affect the bell jar pressure. However, the manifold is shared with the adjacent vacuum system and if you even suspect that anyone will be using it during the time you will be pumping the system down, you should close off H1. First of all, a pressure increase in the manifold will raise the pressure in the bell jar if H1 is open. If the manifold is used when H1 is open, the bell jar could be exposed to an unwanted contaminant. If the pressure in the bell jar is being monitored by the ion gauge, this rise in the bell jar pressure could damage the ion gauge because there is some doubt about how well the over-pressure relay on the ion gauge controller works. Lastly, do not rely on other people to remember to check to see if H1 is closed before they begin to use the manifold. If you decide to leave H1 open, place a note on the manifold asking others to close it if they are going to use the manifold.

It is also important to know that the Nupro valves on the manifold do not have to be closed with excessive force. In fact, this will destroy the valve seal and these valves are not inexpensive. Brute force isn't needed to provide a leak tight seal; just close the valve gently, but firmly. The metering valve should be closed gently as well.

To begin pumping out, open valve V1 on the foreline as shown in Fig. 1. The progress may be monitored with the NRC Alphatron Vacuum Gauge by switching the meter to more sensitive scales as the pumping progresses. Occasionally the 1 Torr and the 10^{-1} Torr scales malfunction, and the meter needle will switch rapidly from one side of the scale to another if you try to switch scales. If this happens, just wait for the system pressure to drop and eventually the needle will register on the 10^{-1} Torr scale.

While the mechanical pump continues pumping the system out, fill the metal

reservoir behind the bell jar with liquid nitrogen (LN_2). Go behind the system, remove the cork, hold the rubber hose in place until the line freezes in position, and fill the reservoir. You can tell when the reservoir is full by either (1) hearing the change in sound which occurs as it begins to overflow onto the floor, or (2) seeing the fog created as it overflows onto the floor. After turning off the tank and removing the hose, the easiest way to check to see if the reservoir is full is to remove the lid and quickly dip your hand into the reservoir. Your hand won't freeze, unless of course you leave it there. This is far easier than trying to actually see the LN_2 level which requires that you wait for the mist above it to clear away.

The reservoir requires filling approximately every 2-1/2 hours. If the lab air conditioning is working well, it will usually last three hours. The reservoir has two rubber hose connections to the LN_2 trap located above the diffusion pump in the main pumping stack. If the trap is working properly, the LN_2 will be recirculated from the trap up to the reservoir. The trap should be checked periodically to make sure that the recycle line is recirculating the LN_2. On rare occasions when the system has been pumping down for extended periods of time (over six hours), the rubber lines connecting the trap and reservoir have frozen solid with ice, thereby preventing the LN_2 in the reservoir from refilling the trap. This is why the rubber lines are insulated. If you need to replace the hoses for any reason, be certain to put extra insulation around the hose clamp connections on both ends of the lines and secure them with duct tape. This will usually prevent them from freezing closed.

When the NRC Alphatron Gauge pressure reading drops below the 10^{-4} Torr scale, close valve V1 which will isolate the bell jar from the large mechanical pump used for roughing out the system. Check the pressure on the diffusion pump line by using the thermocouple gauge connected to meter TC2 on the

ionization gauge control unit. The meter should read below 50 microns. If not, this often indicates a faulty connection to the sensor head so try unplugging and reconnecting the sensor head to the TC gauge. Usually this resolves any suspiciously high pressure indication.

To continue pumping the system below the 10^{-4} Torr level, the diffusion pump is used. After the trap is filled, while watching the pressure reading on the TC gauge, slowly open the gate valve until it is fully extended and locked into the open position. The pressure in the diffusion pump line should rise only slightly, if at all. If, however, it does rise, keep the pressure between 100-200 microns by using the gate valve to control the flow rate from the bell jar into the pump. Any large pressure rise will force the oil in the pump out into the lines of the pumping stack. This should be prevented if at all possible, because cleaning the lines of oil requires dismantling the system.

When the valve is fully open and any pressure rise has dissipated, the ionization gauge may be turned on. Make sure the pressure range scale knob is set to 10^{-4}, the power switch is set to ON, the overpressure relay is on, and the range selection knob is on manual not automatic. Next, the small button on the far left of the control panel should be depressed until the ion gauge lights up. When the needle on the pressure meter has settled, the range scale switch may be set to a more sensitive scale as the pressure decreases.

To turn off the meter, turn the range scale switch back to the 10^{-4} Torr scale, and turn the power switch from ON to OFF and back to ON again. The WARM setting is needed only if the control unit has been turned off for awhile. The control unit should always be left on unless you need to change or check the connections to the rear panel. The vacuum tubes in the control unit function better if left on and should always be allowed to warm up before use.

If the range scale switch is turned to a more sensitive scale than the pressure allows, the overpressure relay circuit will turn the gauge off. The purpose of the overpressure circuit is to protect the delicate ion gauge filament from burning out or the electron grid from shorting out. Even if the overpressure circuit is on, never expose the gauge to a pressure burst. If you expect a small pressure rise, you may set the range knob to a less sensitive scale. This will allow for a small pressure increase without requiring that the ion gauge be turned off completely.

The gauge emission can be checked when the multiplier is on the 10^{-4} scale. However, the zero on the meter should be checked first and adjusted if needed. This is done with the zero adjust knob when the gauge is off. Next, turn the gauge on and set the emission pressure knob to emission. Adjust the emission knob so that the needle points to 1 on the multiplier scale. This is the setting for air. Different gases require different emission settings because they ionize more or less readily. Check the ion gauge specifications for the list of gases.

3. Pre-Experimental Procedures

Although the base pressure of the system is approximately 1×10^{-8} Torr, once the pressure has reached 1×10^{-6} Torr there are several pre-experimental procedures which may be performed. These include (A) preparing the ZBH cylinder and trap line, (B) glow discharge cleaning, and (C) melting the Pb.

A. Preparing the $Zr(BH_4)_4$ Hoke Cylinder and Trap Line

$Zr(BH_4)_4$ is a flammable solid that should be handled with great care. Before you begin to work with it, you should familiarize yourself thoroughly with the hazards involved in its use. Exposure of the compound to air presents a serious fire hazard. Rapid hydrolysis produces hydrogen and a temperature rise capable of igniting the hydrogen explosively. In particular, avoid contact of the

$Zr(BH_4)_4$ with air, water, oxygenated or halogenated solvents. Also to be guarded against is exposure of organic materials such as grease and O-rings contaminated with $Zr(BH_4)_4$ to air, water and oxygenated or halogenated solvents. The chemical, physical and toxicological properties of $Zr(BH_4)_4$ are also not fully known.

The procedures for handling $Zr(BH_4)_4$ are outlined here and in part 7A of this section. Any questions regarding the use of these procedures should be clarified before you begin work, and you should not work alone the first time that you run through these procedures.

If you are planning to use the $Zr(BH_4)_4$ (hereafter, ZBH), both the ZBH hoke cylinder and the trap line cylinder should be evacuated before the experiment commences. A schematic of these lines is shown in Figs. 7 and 8. Place LN_2 dewars under both cylinders and fill them with LN_2 until both cylinders are cooled completely.

Venting the trap cylinder is the more tedious process so you may wish to begin with this. Unless you have vented the trap the day before or quite recently and know what sort of pressure rise to expect, you should turn off the ion gauge and probably close the gate valve as well. If the trap hasn't been vented recently, the pressure may rise as high as 10^{-1} Torr and require using the mechanical foreline pump to evacuate the bell jar before the gate valve can be opened again.

The trap line is vented before the trap cylinder. Referring to Fig. 7, leave valves V2 and V3 closed and open V1 very, very slowly. When you first begin to open V1 there will be an initial resistance and then the valve knob will feel loose. Continue to open the valve until you feel a second resistance. This is the critical step. This valve was never designed to be a metering valve but often has to be

used as one, which requires that you turn the knob very slowly. If the gate valve is open and you are pumping out the line through the diffusion pump, you may monitor the pressure rise with the thermocouple gauge which is on the diffusion pump line. Alternatively, you may use the Alphatron gauge. If the pressure rise is too great, it will be impossible to use V1 as a metering valve. In this case you will save both time and trouble if you close the gate valve, open V1 completely and simply let the bell jar pressure rise using the mechanical pump to evacuate it as needed.

After this section of line is evacuated, close V1 again. Open V3 and V4 only if the trap cylinder is cooled in LN_2. Repeat the above procedure using V1 as a metering valve. At this point you can expect a large pressure increase because any excess ZBH in the trap cylinder decomposes to evolve H_2 and B_2H_6. Sometimes V4 is very cold because of its proximity to the LN_2 but it has never frozen open or closed and has always sealed properly even when it is too cold to grasp without a protective cloth.

After the cylinder and line have been evacuated completely with the diffusion pump, close V4, V3 and then V1. The trap line is now vented and ready for use during the experiment. The LN_2 dewar under the trap cylinder should be refilled until it is ready for use. If it turns out you won't be needing it after all, simply remove the dewar and let the cylinder warm up.

Next, the ZBH hoke cylinder and line must be vented. Referring to Fig. 8, there are four valves on this line: the metering valve (V1), a Nupro valve (V2) connecting the ZBH line to the manifold, a ball valve (V3) on the ZBH line, and a Nupro valve (V4) between the line and the ZBH cylinder. First close the Nupro valve (V5) which connects the vacuum system to the manifold if it is not closed already. Next, the line between the Nupro valve (V5) and the metering valve (V1)

should be vented by opening VI until it is fully open. This will usually result in a negligible pressure rise. Now close V1 before beginning the procedure for venting the ZBH line and Hoke cylinder.

Under most circumstances, except when a new Hoke cylinder is being installed or if a full one hasn't been used recently, the ZBH cylinder and line may be evacuated using the diffusion pump with the ion gauge set to the 10^{-4} Torr range. Since V1 is a true metering valve, any pressure rise is much easier to control than it is on the trap line which does not have a metering valve.

When the ZBH cylinder is cooled in LN_2 and the line between V1 and V5 has been vented, close V1 and open V2. Pump out this section of the ZBH line by opening V1 until it is fully open; wait for any pressure rise to dissipate by watching the ion gauge meter, and close V1 again. Next, open V3 and pump out the line again using V1. The ball valve is different from the Nupro valves in use on the rest of the line in that it is either fully closed or completely open, which occurs when the handle is parallel with the copper tubing of the ZBH line. Lastly, the Hoke cylinder itself is vented by opening the Nupro valve and slowly evacuating the line and cylinder by opening V1. After V1 is fully open and the ion gauge pressure is in the 10^{-6} Torr range again, close V4, then V3, V2 and V1. The ZBH line and cylinder are now evacuated and ready for use. Keep the cylinder cooled in LN_2 until ready for use. Valve V5 connecting the manifold to the vacuum system may now be opened.

B. Glow Discharge Cleaning

A glow discharge cleaning helps oxidize any hydrocarbons or other contaminants which may remain in the system from previous experiments or from exposure to the atmosphere. This is a new step which I have incorporated into the experimental procedures and which was not employed previously. It can be

especially useful if one is switching to a new adsorbate after having used a different one for some period of time. Since the vacuum system is not equipped for a full bake-out, any procedure which can help clean things up is very useful. One of the nice things about tunneling spectroscopy as opposed to many other experiments is that if lingering adsorbates are a source of contamination within the system, the spectra will clearly demonstrate their presence. In fact, if the experiments being conducted are critical (and which ones aren't), you may ultimately save time by making a set of "blank" junctions periodically to check the nature of the background contaminants in the bell jar. A "blank" junction consists only of the Al_2O_3 barrier and is not exposed, at least purposefully, to any adsorbates. Although some contaminant sources will not appear in an IET spectrum **(4)**, hydrocarbons do show up very readily.

In a glow discharge the Al electrode is held at a negative voltage and electrons are emitted from it as the surrounding gas is ionized. A cleaning glow discharge can be done in O_2 or in an inert gas like N_2. The glow discharge formed by an inert gas such as N_2 probably helps clean the system by bombarding hydrocarbons off the bell jar walls and interior assemblage. An O_2 glow discharge can getter the hydrocarbons and is probably the best kind of glow discharge to use for cleaning up hydrocarbon contaminants.

The gas pressure and the voltage at which the discharge is maintained are the two variables which must be determined. The progress of the glow discharge is monitored primarily with a Simpson meter which registers the voltage drop across one of the resistors in a resistor network which is used to stabilize the discharge. This resistor circuit is located in a small box which is fastened to the back of the bell jar support table. It consists of three 2.5 kΩ resistors in series. Plug the two banana plug leads into the Simpson meter. The meter is set on the 250 V scale or on any scale which is appropriately sensitive to the voltage drop

to be measured. Actually, the scale you use to read the deflection of the meter needle is not critical. In fact, it is of importance only when the conditions of the glow discharge must be reproduced from one time to another. This is the case when the samples are oxidized, but reproducibility is not a critical issue when a glow discharge is done to clean the slides and the bell jar. Generally, a glow discharge is run at a pre-selected constant voltage, and the gas pressure is adjusted using the metering valve so that the voltage drop registered on the Simpson meter maintains a constant pre-selected value throughout the discharge.

The range of these variables is usually limited because of the following factors. The high voltage is limited because the Al electrode will melt, depending on the gas pressure in the bell jar and to a lesser extent on how long the discharge is run. The gas pressure is limited on the high end because it is desirable to evacuate the bell jar after the discharge using the diffusion pump. If the pressure is above approximately 4×10^{-1} Torr, it is difficult to pump out with the diffusion pump because the gate valve cannot be manipulated carefully enough to control the flow rate out of the bell jar and prevent the pump from exposure to pressures which may be too high. Alternatively, the gas pressure needs to be high enough so that the discharge is easily observed, because the color of the discharge is one of the primary ways to judge if a glow discharge is going well and reproducing previous conditions adequately.

The new glow discharge apparatus is constructed to conduct better the high voltage to the electrode and to prevent any discharge from occurring around the base of the feedthrough (see Fig. 5). For this reason it cannot be run at a voltage as high as that employed previously or the electrode will melt. Instead of the -1300 V used previously, the new electrode is usually run at -1100 V. This value was chosen because although the electrode may be run at higher voltages,

say -1200 V, it was found that this higher value tended to age the electrode faster than -1100 V. The electrodes last through many glow discharges when -1100 V is the high voltage setting.

The first step in preparing to run a glow discharge is to fill the bell jar with the desired background gas. The manifold is used for this purpose, and a schematic of it is shown in Fig. 3. First open valve H1 which separates the manifold from the vacuum system. The manifold should be flushed several times with the gas to be used. Both N_2 and O_2 are attached to the manifold at all times. After opening the cylinder, briefly open the Nupro valve which connects the line to the manifold, close it and let the manifold pump out. When the thermocouple gauge on the manifold reads 60 microns again, which is the base pressure, flush the system once or twice more.

If the ion gauge is on, turn the range select knob to the 10^{-4} Torr range and turn the gauge off. Close the gate valve and make sure that it is locked securely into the closed position. Never close the gate valve when the ion gauge is on, because the gauge might be damaged as the pressure rises. Now the manifold may be filled with the background gas. Close off the Nupro valves (H7 and H8) which separate the manifold from the mechanical pump. Either half of the manifold may also be isolated by closing valves H8 and H13 or H3 and H13. Next, carefully fill the manifold until the Matheson stainless steel test gauge reads 500 mm Hg. Now fill the bell jar by opening the metering valve M1 and monitoring the pressure rise on the Alphatron gauge meter until it reads 1.0-1.5 x 10^{-1} Torr. Close valve M1 firmly but not too tightly.

Occasionally the metering valve will get a pressure "bubble" in it and you should be aware of what this is like. When this happens the valve will respond differently than it does normally. When you open it, it will feel as if there is no

resistance and it will turn freely. Keep opening it until you feel some resistance again and continue turning until you hear a loud "pop", then close it. This will fix it and you can proceed as before.

When the bell jar has been filled with the background gas required for the glow discharge, turn on the high voltage power supply. Make sure the high voltage switch is turned to off, the ± switch is set to -, and all the voltage dials are set to zero. Next, turn on the power switch. When the supply is ready for the high voltage switch to be turned on, it will make a clicking sound and the red light will switch on. Make sure the Simpson meter is hooked into the circuit with the banana plug leads and that the shutter is covering the slides. Now turn on the high voltage switch and turn up the dials to reach the desired voltage, first -500 V, then -1000 V, then -1100 V, using the adjacent knob. Be sure to start the timer when you turn on the high voltage switch. The Data Precision frequency counter is used as the timer.

The glow discharge should be easy to see by -1000 V. As you turn up the voltage, you will notice that the needle on the Simpson meter will jump each time then slowly decrease. After the voltage is at the desired level, you should maintain a steady meter reading by carefully controlling the gas flow through the metering valve.

In N_2, the glow discharge will be reddish purple or a deep violet color, whereas in O_2 it will be a beautiful rich lavender color. Color is an important monitor of how well the discharge is going and also indicates if the glow discharge is stable. When the discharge is stable, you should open the shutter to expose the slides. Usually this takes 60-80 seconds. During a cleaning glow discharge, this is not critical, however. Throughout the discharge you should continue to monitor the Simpson meter reading closely, check the color, and the Alphatron gauge read-

ing to make sure the pressure is at a moderate level. If you find that you have to keep increasing the pressure to maintain a constant reading on the Simpson meter, it's better to choose a lower value on the meter than let the pressure rise too far. I think the best range for the pressure is 1.5-3.0 x 10^{-1} Torr.

When the discharge has run for the desired length of time, 500-3000 sec or more, depending on your patience, close the metering valve if it is still open, turn off the high voltage switch, turn off the power switch, cover the slides with the shutter and record the time when you shut off the high voltage switch. Turn the voltage dials back to zero and open the Nupro valves to allow the manifold to pump out.

Check the pressure reading on the Alphatron gauge and begin to pump out the bell jar by opening the gate valve *extremely slowly*. Monitor the pressure rise in the diffusion pump line by using the thermocouple gauge. If the pressure rises rapidly to 150 microns or above, quickly close the valve. Then begin again more slowly. With the old diffusion pump this took many painstaking minutes; the process is much easier with the larger pump and will take only 1-2 min. Eventually, you will be able to open the gate valve completely. When the pressure has fallen below 10^{-4} Torr, the ion gauge may be turned on.

It is important to use only the diffusion pump to evacuate the bell jar at this stage in the experiment if at all possible. Once you have pumped down the system you should try to avoid using the mechanical pump because this line, even though it has a molecular sieve trap, poses a greater contamination threat than the diffusion pump line equipped with a LN_2 trap. You always want to minimize any possibility of exposing the bell jar to pump oil vapor, especially if you have already started making a set of junctions.

C. Melting the Pb

The last thing that should be done before beginning an experiment is to melt the Pb in order to desorb any contaminants which might adsorb on the samples during the actual fabrication. The controls for the metal evaporation are located to the right of the bell jar on the metal support table. Switch the Cu arm on the control box to the lower right-hand connection and fasten it in place. Make sure the 5-volt dc power supply for the quartz crystal oscillator, located on the shelf next to the Alphatron gauge meter, is on. (This should be left on normally.) Check the frequency reading on the Data Precision frequency counter which should have a reading near 5 MHz. Adjust the trigger knob on the counter if the reading is too high or if it is unstable. Occasionally, you may have to turn the power supply off and on a few times to get a stable reading, especially if the quartz crystal has been subjected to numerous evaporations.

Metal evaporations are always performed with the gate valve open because the pressure rise from the evaporated metal will interfere with the formation of the thin films if the system is not being evacuated. The ion gauge may be switched to the 10^{-4} Torr scale or turned off altogether. The bell jar pressure should be below 5×10^{-5} Torr before you begin. *Make sure that the shutter is covering the slides.*

When you are ready to begin, turn on the power supply switch and record the frequency. Using the lab wall clock as a timer, turn up the Variac 5-10 units every 10-20 sec. For the large Pb boat, the Variac setting will be about 15, which should correspond to an amp meter reading of approximately 80-90. For a small Pb boat, you may probably use lower settings, but they are not critical when you are merely melting the Pb. As soon as the frequency reading begins to decrease, even 2-3 Hz per second, the Pb has melted and you may turn down the Variac and turn off the power switch.

4. Evaporating the Aluminum

After completing the pre-experimental procedures, pump the system back down to below 1 x 10^{-6} Torr before beginning the experiment. The base pressure I usually employ is 1 x 10^{-7} Torr or below, and my working base pressure during an experiment is a minimum of 1 x 10^{-6}. (This is the pressure in the bell jar between each step in the experiment.)

The first step in an experiment is the Al evaporation. To ensure that it is not the last, a number of changes have been made in how the aluminum evaporation is monitored. Previously, evaporations often failed because the Al metal failed to wet the tungsten filament and instead fell into a useless little blob on the bottom of the evaporation box. This often occurred when the Al heating rate was too fast. Unfortunately, this was not possible to monitor as closely as needed with the previous setup because there was no way to visually inspect the filament and the Al metal during the evaporation process. The new setup does allow this by making sure that the bell jar directly in front of the evaporation box remains clear, thus providing a 'window' for visual monitoring. A special quartz shield and holder have been constructed which protect the bell jar wall and are easily removed for cleaning between experiments. This is shown in Fig. 9.

In the past the only monitor used to measure the extent of the evaporation was the quartz crystal oscillator. I prefer to monitor the evaporation using the Hewlett-Packard digital multimeter (DVM) to check the resistance of each of the three samples as they are being formed. This provides an individual monitor of each sample as well as information which is greatly more detailed. With this technique you can also optimize the alignment of each sample with the evaporation source.

Before beginning the evaporation, first put the DVM on the top shelf of the equipment rack, plug in the two dual banana plug leads using the 4-pt probe plug, turn the DVM on and set the function switch to 4-pt resistance. On the heating and temperature control panel, set the functions to R, 4-wire, and V_{1-4}. By turning the sample select switch to 1, 2 or 3 you will now be able to monitor the resistance of the Al films as they are formed. Initially, you won't have any readings at all; there is no film, so there is nothing connecting together the four electrical connections on each slide. As you face the bell jar, slide 1 is on your left, slide 2 is in the middle, and slide 3 is on your right.

Switch the Cu arm of the evaporation control box to the lower left-hand post and tighten it securely. Turn the ion gauge down or off. Leave the gate valve open. Check to make sure that the Al mask is covering the slides, is in proper alignment with the pin, and that the shutter is completely covering the Al mask and slides.

Turn on the evaporation power switch, record the quartz crystal oscillator frequency and, using the lab clock as a timer, turn up the Variac 5 units every 15-20 sec. Very soon you will see that the tungsten filament is glowing bright red, which is normal. If you look carefully through the removable Pyrex shield you should be able to see the four horseshoe-shaped pieces of Al rod hanging on the tungsten filament. Continue turning up the Variac until you have reached 30-35 on the Variac dial. At any moment, the Al will melt. Do not speed up the heating rate at this time because this period is especially critical. As the Al pieces melt, the bright red glow of the tungsten filament will dim and darken which is normal. As this happens, the amp meter needle will suddenly jump up, then start to decrease slowly. At the same time, the reading on the Data Precision frequency meter will begin to decline a few Hz every second.

The trick to the aluminum evaporation is to proceed very slowly once the Al has melted. If you hurry, the Al will usually drop off of the W filament rather than coat it evenly. After the horseshoes have melted and the amp meter needle has jumped, wait the remainder of the 15-20 sec period and then continue turning up the Variac, usually 3-5 units every 10 sec, until the frequency rate of change is 6 Hz/sec or higher. Now open the shutter to expose all of the slides, and as you do, record the frequency reading of the quartz crystal oscillator. Continue to turn up the Variac until the frequency rate of change is at least 8-9 Hz/sec; 10-12 Hz/sec is preferred.

Now use the DVM to monitor the progress of the evaporation. When the resistance of the slides is approximately 7-10 Ω and/or you have evaporated 500-700 Å, corresponding to a frequency change of 500-700 Hz **(1)**, turn the power switch off, quickly cover the slides with the shutter, record the frequency of the quartz crystal oscillator, and turn the Variac to zero. Record the resistances of the three samples using the DVM. Usually, the middle one is slightly lower than the two on either side, which should have approximately equal values. Generally, films between 500-700 Å are preferable to thicker ones because of greater stability.

The pressure in the bell jar should not have risen much above 1 x 10^{-5} Torr during the evaporation. If it has, it may indicate that the evaporation box, which shields most of the system from the evaporation sources, needs to be cleaned.

5. Annealing the Al

The next step in the experiment is to anneal the freshly evaporated Al films. This procedure has revolutionized tunneling experiments which investigate adsorbate-surface interactions at 150°C or above. Before I added this procedure

to the experiment, none of the experiments at elevated temperatures resulted in measurable junctions. Since I began to include this procedure, however, every experiment has produced measurable junctions, and the highest temperature investigated has been 400°C. Heating the Al films causes them to anneal. If this is done after the film is oxidized to form the junction barrier, the thin oxide will crack and the resulting junctions will be unmeasurable because they will have shorted out. However, if the films are annealed before they are oxidized, then the second time they are heated (which is in the presence of an adsorbate after being oxidized) no annealing will occur, the oxide barrier will remain intact, and the resulting junctions will be measurable.

The films are usually annealed for 10-20 min near 250°C. This temperature was chosen because Bowser and Weinberg **(2)** had found that annealing effects in the Al film may still be seen up to 200°C. Many details concerning sample heating and the electrical connections are found elsewhere **(1,3)**. The heating panel has not been changed. Figures 10 and 11 show the panel and the electrical connections. Each slide has its own power supply; the top one on the instrument panel is for slide 1, the middle one for slide 2, and the lower one for slide 3.

To simultaneously heat the slides and monitor the temperatures, you will need some sort of hand-held programmable calculator to compute the temperature of the film. I have used a Texas Instruments Programmable 58C.

The resistive heating technique developed by Bowser and Weinberg **(2)** uses the equation below to determine the temperature:

$$T = T_i + \left[\frac{1 + \alpha T_i}{\alpha}\right]\left[\frac{R - R_i}{R_i}\right]$$

where R is the resistance of the Al film at temperature T, R_i is the initial resistance at the initial temperature T_i, and α is the temperature coefficient of

resistance. During heating, R is calculated from the equations:

$$R = \frac{V_S}{I_S} \quad \text{and} \quad I_S = \frac{V_R}{R_R},$$

where V_S and I_S are the voltage and current across the Al film. V_S is measured directly but I_S is determined by measuring the voltage drop V_R across a resistor with a known resistance R_R in series with the Al film. T_i is usually a constant since the laboratory temperature is regulated. It was found previously **(1,3)** that:

$$\frac{1 + \alpha T_i}{\alpha} = 558.66$$

with a maximum variance of ± 8%. The temperature equation becomes

$$T = T_i + \frac{558.66}{R_i}\left(\frac{V_S R_R}{V_R} - R_i\right)$$

All of the temperatures are in degrees centigrade.

To implement this equation, you must first measure the resistance of each sample [R_R (1), R_R (2), and R_R (3)]. The DVM is set to the 4-pt resistance and the switching panel is set to V_{1-4}, R, and either 1, 2, or 3. Enter these numbers into the program and record their values. Check the thermometer on the manifold to determine the lab temperature. Next, measure the resistance of the three known resistors [R_i (1), R_i (2), and R_i (3)] which are in series with the three Al films. Set the switching panel to either 1 or 10 Ω ; I have always used the 10 Ω resistors. Measure these with the DVM set to 2-wire resistance and the switching panel set at Ohms, R and 1, 2 or 3, and enter the values into the calculator.

Before beginning, move the Al mask away from the slides and the shutter as well, if you wish. Leave the gate valve open. If the power supplies haven't been

used for awhile you should probably let them warm up for a little while, but usually this is not necessary. As you turn on the first power supply and begin the heating procedure, start the timer.

First turn up the voltage knob half-way or more so that the voltage won't limit the current in the films during the heating process. Next turn the current knob up a small amount. First measure V_S, the voltage across the sample. The switching panel is set to V_{1-4}, Sample Heating and either 1, 2 or 3. The DVM is set on V. After measuring, recording and entering this value into the program, measure V_R, the voltage across the known resistor. The switching panel settings are R, Sample Heating and 1, 2 or 3. Record and enter this value; then calculate the temperature of the sample by running the program. Record the temperature and the time and turn up the power supply, unless you have reached the desired temperature, before moving onto the next slide. The DVM and switching panel settings for each measurement are summarized in Table 1.

Unless you encounter a problem, you should be able to measure V_S and V_R, write down and enter their values into the calculator, run the program, record the temperature and time, turn up the power supply and switch to the next slide in approximately 40 sec. The length of time is critical when you are heating junctions in the presence of an adsorbate and have to limit the extent of exposure. However, when you are annealing the films the length of time is not critical.

One other thing should be mentioned in regard to the switching panel. As you can see, there are three buttons labeled V_{1-2}, V_{2-3} and V_{3-4} next to the V_{1-4} button. These were originally intended to provide detailed information on the voltage drop across each section of the aluminum thin film sample, although in practice this was too time-consuming to do and only the V_{1-4} connections were

ever employed. The new sample holders only allow for electrical connections to be made to the sample at the V_{1-4} positions. For future projects however it may be worth remembering that the wires for these extra connections are installed in the vacuum system and in the switching panel.

After the samples have been annealed, their resistance values will be significantly lower than they were before, usually on the order of 15%. The resistance decreases because annealing reduces the stress in the thin film. This reduced resistance is a convenient monitor of the annealing process and can be used to further refine this step in the experiment. In particular there are two factors which could be investigated: the length of time the samples are annealed and the manner in which the annealing step is terminated, either by decreasing the sample temperature gradually or by simply turning off the power supply. Previously the samples were annealed at 250°C for 2000-2500 sec and the slides were cooled gradually to well below 100°C before the power supplies were switched off.

6. Oxidizing the Al

There are several ways that tunneling samples may be oxidized. These include thermal methods, like baking the samples at high temperature, and exposure to an oxidizing atmosphere. For oxidizing aluminum films the method which has proven most reliable for me is a glow discharge in O_2 and H_2O vapor. The water vapor is present only in small amounts and helps make the oxide "sticky" when it is exposed to adsorbates later in the experiment. For thin films of other metals, in particular magnesium, a glow discharge is not the method of choice. For this metal, thermal methods have been shown to produce a more stable oxide.

After the samples have been annealed, cover the slides with the shutter once more. Turn off the ion gauge and close the gate valve after noting the pressure. Prepare the manifold for the glow discharge as before; see Section 3B of these procedures. This time you should flush the system several times with distilled H_2O vapor which is permanently in place on the manifold. Flush once more and when the manifold thermocouple gauge meter reads 100 microns, close off the manifold from the pump. Fill the stainless steel test gauge up to 500 mm Hg as before with the high purity O_2.

Fill the bell jar with the H_2O-O_2 mixture until the Alphatron gauge is between 1.0-1.5 x 10^{-1} Torr. Begin the glow discharge and the timer at the same time. Turn the high voltage to -1000 V or -1100 V. If the high voltage is at -1000 V and the pressure at 1.5 x 10^{-} Torr, the Simpson meter will initially read approximately 35 V. To stabilize at a reading of 30 V the system pressure will be near 1.7 x 10^{-1} Torr at the end of the glow discharge. Different settings may be employed within the limits discussed previously.

The O_2-H_2O glow discharge is an extraordinary lavender color. The longer the discharge runs the richer this shade of color becomes. Every once in awhile, the glow discharge will seem very pale or even "greenish" when it is first started. The cause of this change in color is unknown, but this condition cannot really be considered abnormal since it has been seen many times before. In most cases, the lavender color will develop as the discharge continues.

Once the discharge has stabilized, both in terms of color and the Simpson meter reading, the shutter should be opened to expose the slides. Record the timer reading when the shutter is open. It is preferable to expose the slides after the same period of time has elapsed in each oxidation you perform. I chose 65 sec which meant that in each of my experiments I opened the shutter

after the glow discharge had been running for 65 sec. The length of time is not too critical but experimental reproducibility is extremely important in tunneling experiments. There are several procedures in the junction fabrication process which should be performed in a manner that ensures as much reproducibility as possible. One of these is the oxidation of the aluminum thin films.

The length of time that the oxygen glow discharge is run is a critical experimental parameter. If it's too long the junctions will have resistances so high that it will be difficult if not impossible to record their spectra. If it's too short they won't form an adequate barrier, and the resistances will be too low to produce good spectra or be shorted out altogether. Depending on the adsorbates one is studying and the temperatures at which the exposures are to be performed, the length of oxidation must be adjusted further. Past values have ranged from 450-1300 sec. With experience, one eventually develops some intuition on the proper length of time for a particular adsorbate. 850-950 sec is used most often.

After finishing the glow discharge, the system should be evacuated using the diffusion pump.

7. Exposing the Samples to the Adsorbates

The system pressure should be 1 x 10^{-6} Torr or below before exposing the samples to the adsorbate(s). The manifold is equipped to handle most gases and vapors and a few of the ports on the bell jar have been adapted to accommodate either solid samples or vapors from liquids. Further details on the manifold may be found elsewhere (1).

A. $Zr(BH_4)_4$

If ZBH is one of the adsorbates you are planning to use, you should have

prepared the cylinder and trap line for use in accord with the instructions in part 3A of these procedures. The ZBH and the trap cylinders should both be cooled in LN_2 during this time. The ZBH cylinder is warmed up only prior to use. It is usually convenient to begin this during the oxidation of the aluminum. Remove the LN_2 dewar and pour the LN_2 into the LN_2 reservoir of the diffusion pump. Fill the dewar with hot water and replace it under the cylinder. Alternatively you may also use a heat gun to help the cylinder thaw quickly. I prefer the hot water.

After the oxidation is complete, pump out the bell jar and check the pressure with the ion gauge. However, don't leave the ion gauge on in the period of time just before you are going to expose the samples to the ZBH because the ion gauge filament will decompose the ZBH immediately if it is warm. Leave the ion gauge turned off as much as possible and check it before you begin the exposure to be sure that it isn't hot to the touch. The ZBH cylinder is ready for use when it has thawed but is still cool to the touch.

The ZBH exposure which is used is 5×10^{-2} Torr for 900 sec. Referring to Fig. 3, close the gate valve and isolate the system from the manifold by closing valve H1. Turn the Alphatron gauge to the 10^{-2} scale. Open the valves on the ZBH line approximately halfway, except for the ball valve, and open the metering valve a small amount, perhaps half of one revolution. Wait until you see the pressure begin to rise on the Alphatron gauge meter. This may take up to 30 sec. Then adjust the flow rate with the metering valve. Begin the timer when the pressure is at 2.5×10^{-2} Torr. Close the metering valve just before the pressure reaches 5×10^{-2} Torr so that it doesn't overshoot this value by too much. 5.5×10^{-2} Torr is an acceptable value because as the exposure continues, the pressure will drop, often to about 4.5×10^{-2} Torr, as the ZBH adsorbs on the bell jar interior. The shutter should be moved away from the slides during the exposure.

Once the bell jar is filled with the ZBH, replace the LN_2 dewar under the ZBH cylinder and cool it again in LN_2. Leave all the valves on the line open so that any ZBH in the line will condense back into the cylinder. While the exposure continues, make sure the small LN_2 storage dewar is filled and ready for use since the trap line requires a lot of LN_2 to cool. Place the rectangular styrofoam chest under the trap line and fill it to the top with LN_2 in order to cool the copper line as shown in Fig. 7. This should be started when the timer reads 800 sec or you may not have it ready by 900 sec.

At 900 sec, cover the slides with the shutter and open V1 and V2. The mechanical pump on the trap line will evacuate the bell jar and the excess ZBH will condense onto the cooled lines of the copper tubing. Open the metering valve so that the ZBH line can be evacuated by the trap pump as well, even though this line should already be at a low pressure. When the bell jar pressure falls below 5×10^{-3} Torr the trap line may be isolated from the bell jar and the mechanical pump. Close V1 and V2. Remove the styrofoam LN_2 chest and empty it into the diffusion pump reservoir or back into the storage dewer. Open valve V3 and V4 on the trap line so that the ZBH waste cylinder, still cooled in a LN_2 dewer, is open. As the copper lines warm up the trapped ZBH will condense into the collection cylinder. There is no pressure gauge on the trap line so it is hard to tell when this transfer is complete. Generally, I keep the trap cylinder open and cooled until I've finished the experiment and am straightening up afterwards, which usually takes at least two hours. Certainly, mush less time is actually needed for the transfer.

After the trap line is closed off, open the gate valve and pump out the bell jar and the ZBH line. When the pressure is 5×10^{-6} Torr or below close off the ZBH cylinder and each of the valves on the ZBH line. The cylinder may now be allowed to warm up.

The samples may now be finished off by evaporating the Pb or they may be heated in vacuum or exposed to a second adsorbate.

B. Other Adsorbates and Sample Heating

Many hydrocarbons make lovely IET spectra since IETS seems to be particularly sensitive to C-H vibrations. Most hydrocarbons may be used as the gas or vapor from the manifold although in certain cases liquid doping may be necessary for liquids with low vapor pressures.

For the studies described in this thesis, the hydrocarbon exposures ranged from 1.5×10^{-1} to 5 Torr. As with the other procedures which comprise a tunneling experiment, the reproducibility of the exposure process is more important than the actual things one might do during it. In other words, it's important to choose a way of doing the experiment which you can live with and which you can reproduce as exactly as possible each time you make a new set of junctions. To study a particular adsorbate system in detail requires that you perfect your ability to be internally consistent when you make set after set of junctions over a long period of time. This is true for how you do an exposure, when you begin the timer, how fast the flow rate is into the bell jar, when you heat the junctions and the rate of heating.

Unless you are using unusually low exposures, you should heat the junctions after the adsorbate has been introduced into the bell jar and you should terminate the heating before evacuating the system. Flush the manifold several times with the adsorbate to be used, close the manifold off, be sure the ion gauge is off and the gate valve is shut. Details on the sample heating procedure are found in Part 5 of this procedure. You should remeasure the sample resistances and the known resistor resistances before beginning the exposure and the sample heating. Once you are prepared, fill the bell jar with the adsorbate

and start the timer.

For pressures of 1 Torr or less, use the Alphatron gauge set to the 10^{-1} Torr scale. For higher pressures, you will have to use the 1 Torr scale which doesn't work very well. This will be apparent. As you fill the bell jar, monitor the progress on the 10^{-1} Torr scale. When the needle reads full scale switch to the 1 Torr scale. Now the meter will still read zero even though it should read 1. It will be some time also before the needle on the 1 Torr scale begins to move. Generally, for a 5 Torr pressure I fill the bell jar until the meter reads 4 Torr.

For high exposures using pressures of 5 Torr you will need to use the mechanical pump to evacuate the bell jar. Hydrocarbons pump out very quickly especially with the diffusion pump. For this reason you should be able to bypass the mechanical pump and just use the diffusion pump at pressures at which you would normally use only the mechanical pump if the adsorbate was, for example, oxygen rather than a hydrocarbon. The upper limit on the hydrocarbon pressure which you will be able to evacuate using only the diffusion pump will depend on your manual dexterity in handling the gate valve.

The length of the exposure will depend primarily on whether the samples will be heated during the exposure. For my experiments, I usually chose 1200 sec because this allowed more than sufficient time to reach the desired sample temperature and then continue the exposure while the samples were at the target temperature (usually 900 sec).

8. Evaporating the Pb

After finishing the adsorbate exposures, pump the system down to below 1 x 10^{-5} Torr before evaporating the Pb. These cross-strips serve as the second electrode of the junction and isolate the surface of interest from the atmosphere after the samples are removed from the system. I always pumped the

system back to 1 x 10^{-6} Torr before evaporating the Pb.

Position the Pb mask over the slides and cover them with the shutter. Leave the gate valve open and record the frequency of the quartz crystal oscillator before beginning. Many details regarding this procedure are discussed in Part 3C of this procedure section.

The Pb evaporation is very easy to do compared to the Al evaporation. How quickly you heat the boat is not nearly so critical as how fast you heat the tungsten filament used for the Al evaporation. Usually, 2500 Å of Pb is evaporated which corresponds to a frequency change of about 10,000 Hz **(1)**.

When you begin the evaporation, turn the Variac up 5 units every 10-15 sec. For a large Pb boat a Variac setting of about 15 will cause the Pb to melt and the current reading will be about 85 amps. Raise the Variac steadily until it's set at about 22-23 which should result in a frequency change of approximately 50 Hz/sec, which corresponds to a deposition rate of approximately 20 Å/sec. The amp meter will read about 60. When the frequency rate of change is 30 Hz/sec or greater, open the shutter to expose the slides, recording as you do, the frequency reading. When the evaporation is finished, shut the power off, cover the slides with the shutter, and wait for the Pb to cool.

9. Bringing the System up to Atmospheric Pressure

Nitrogen is used to backfill the bell jar and bring the system up to atmospheric pressure. A cylinder of high purity N_2 gas is always on the manifold and a special metering valve is used to introduce the gas into the bell jar. This procedure may be done with the manifold still under vacuum.

Turn the ion gauge off, close the gate valve, turn the Alphatron Vacuum gauge meter to the 100 Torr scale. Open the N_2 tank and adjust the flow rate into the

bell jar with the metering valve labeled M2 in Fig. 3.

As the bell jar reaches atmospheric pressure, there will be a loud noise as the gasket unseals from the baseplate surface. After this, you may close the N_2 metering valve then close the N_2 cylinder. Vent the regulator and the line through the manifold. Close the regulator valve and the Nupro valve which separates it from the manifold.

10. Preparing the Samples for Measurement

Open the bell jar and secure it in place with the guide rods. Cover all the open ports and the central pumping port with the protective teflon covers to ensure that nothing falls into them. This is very important because even tiny objects like a miniature screw or a piece of Al rod can damage the gate valve seal. Hard objects can embed themselves into the metal of the gate valve next to the O-ring and cause permanent damage to the valve. They can also lodge themselves next to the O-ring and prevent it from sealing when the gate valve is closed.

Now remove the sample holders from the system. Move aside the Pb mask and shutter and unfasten the electrical connections of slide 3 (on the right). The slides are much easier to remove if they are done in order, from right to left. Undo the rear Allen head cap screw before unfastening the front one and carefully remove the sample holder from the system, making sure that the delicate electrical connectors don't get tangled on anything.

After the three samples are removed, the slides have to be unsoldered from the holders, prepared for the measurement connections, then positioned and fastened into the measurement holders. Only In/Sn solder is used for the connections to the glass. The slides are easier to remove from the sample holders if the holders are held in position with the small vise. Use stainless steel tweezers

to lift the electrical wires gently away from the glass when the solder is molten. Grasp the slide with the tweezers and wiggle it out of the holder.

Place the slide on the desk on top of a Kimwipe. With one of the miniature screw drivers available in the lab, scrape away the extra side strips of the evaporated aluminum film. These are usually very close to the Pb cross strips and may short out the samples if the solder connections to the Pb overlap any of them inadvertently. A hard metal object like the end of a screwdriver is needed to remove them because the aluminum films are so hard.

Next the sample is prepared for the electrical connections needed to measure the spectra. The easiest way to do this is to place a small drop of solder on each end of the three Pb strips and on the two ends of the Al film. The soldering iron works best if you don't use the end of the tip but the side of it. Melt some solder on a large glass laboratory slide and roll the sides of the soldering iron tip around in the molten solder. Press the side of the tip onto the place you want to solder, for example, onto the end of one of the Pb cross strips, then slowly move it toward the edge of the glass slide and then up. This will leave a smooth In/Sn bead of the perfect size. It's best if you apply the In/Sn solder in one attempt because the more you have to apply the soldering iron to the slide, the greater the risk of damaging one of the delicate Pb strips. Occasionally, the films will not adhere to the slide surface very well and when you apply the solder, they'll just seem to dissolve away. This is one of the reasons why the glass slides need to be cleaned so thoroughly before an experiment; it affects the film adhesion greatly.

After all of the solder connections have been applied, wiggle the glass slide gently into place on one of the measurement holders, avoiding the wires on either side of the holder and using a pair of tweezers to guide it into place.

While you hold the slide firmly in place, press the wire loops of the holder down onto the previously formed solder beads with the tip of the soldering iron. As you do, the In/Sn bead will melt around the wire loop. Draw the tip of the soldering iron away from the loop toward the edge of the slide and then up.

After you have soldered all three slides in place on one of the measurement holders, you can check the resistances of the junctions. Plug the card connector on the measurement holder into one of the switching boxes which is used to select a particular junction for measurement. Set the DVM on 4-pt resistance and connect the box to the DVM. Measure and record the resistances of all nine junctions. The switch positions on the box are labeled B1, B2, B3, M1, M2, M3, T1, T2 and T3. B denotes the bottom slide, M is the middle slide and T is the top slide, when the samples are immersed in liquid helium. This means that B is on the end farthest away from the wires and T is closest to the wires.

It helps to avoid confusion if you arrange your slides in the same order on the measurement holder each time you make a set of junctions. I always arrange my slides so that B1, 2 and 3 correspond to slide 1; M1, 2 and 3 are slide 2, and T1, 2 and 3 are slide 3. This is especially important when you have heated each sample to a different temperature during an exposure and can't risk getting them mixed up.

Every so often one of the fine wires on the back side of the measurement holder will become unsoldered and the broken connection won't be noticeable from a casual inspection. It's always a good idea to check these before using one of the holders.

Once the resistances have been checked the spectra can be measured. More often than not though, the samples are stored in LN_2 and measured at a later date. There is a storage dewer in the lab that has baskets for holding the sam-

ples. First, wind up the wires connecting the samples and the card connector and use a piece of colored insulated wire to keep the wires from unwinding. Record the color of the wire and the basket number you put it in for future identification. Remember to keep filling the storage dewar because your samples will be ruined if the LN_2 level falls so low that your samples are exposed. If you are going to measure your spectra right away, immerse your samples in one of the small LN_2 dewars until you are ready to put them in LHe. Cooling the samples in LN_2 first also saves a lot of LHe from boiling away. In case your resistances are too low, exposing the samples to dry, high purity O_2 for a day or longer may raise their resistances to satisfactory levels.

Measuring the resistances of your junctions can be a bitter moment of truth. If you feel especially anxious about the outcome of an experiment, it may be better to measure the junction resistances after you have finished preparing the bell jar for the next experiment and already started pumping it down. This way, you can either stand around gloating with self-satisfaction or express your frustration by walking out of the lab in complete disgust.

11. Readying the Bell Jar for the Next Experiment

After you have fabricated a new set of junctions, the bell jar should be prepared for the next experiment and pumped down to at least the 10^{-6} Torr range before you leave. Although you may feel finished, there is still a lot to do: including preparing sample holders with clean slides and putting them in the system, cleaning the removable Al evaporation window shield, polishing the glow discharge protective shield, replenishing the Al and Pb sources, cleaning the baseplate and performing any other preventive maintenance which might be needed.

Quite a few of these things may be done during the experiment. There are several steps which don't require constant attention, in particular, the annealing step after the temperature has stabilized, the ZBH exposure, any adsorbate exposure done only at room temperature, and the Pb evaporation and subsequent cool-down. A lot of time can be saved by using these spare moments. To make this feasible, duplicates of several of the parts mentioned above have been expressly made. There are two complete sets of sample holders, two glow discharge shields, and two Pyrex window shields.

A. Slide Cleaning and Preparation

The slides used in the tunneling experiments are pre-cut to our sample holder specifications and made of high-temperature resistant glass by Corning Glass Inc. They are pre-cleaned and come wrapped in tissue paper. Even so, they should still be cleaned before use.

The cleaning procedure is flexible but usually includes ultrasonic cleaning in detergent, abundant rinsing in distilled H_2O and storage either in alcohol or distilled H_2O. It saves time to clean a number of slides all at once. Be sure not to put your fingers on them when you are unwrapping them. Put them in a beaker with water. I use an all-purpose liquid detergent designed for ultrasonic cleaners. Use only a few drops because it is highly concentrated. Place the beaker on the basket of the ultrasonic, replenish the water so that the beaker is fairly well immersed and turn on the power. Let it run for 30 min. or until you are sick of the noise. Rinse the beaker and slides with copious amounts of tap water and then distilled water. Repeat the ultrasonic cleaning in alcohol or distilled water without detergent. Rinse again generously and store either in distilled water or alcohol. Cover the beaker to protect the slides from dust.

If you use alcohol, wear gloves and avoid contact with your skin. Methanol is

absorbed easily through the skin, damages nerves, and in very high exposures leads to blindness because of optic nerve damage. You should really wear gloves whenever you have extended exposure to any chemical.

Whenever you use the ultrasonic cleaner, always use the basket and never place anything directly onto the bottom of the tank. This can damage or break the ultrasonic cleaner very readily. To be repaired, the ultrasonic has to be packed up and shipped to the manufacturer, which is not only costly but also takes at least a month.

Once the slides have been cleaned, they can be used whenever needed. Before mounting them in the sample holders, they have to be dried using a stream of high purity N_2. One of the manifold valves is connected to a hose and pipette which are used to direct the N_2 stream. Open the N_2 cylinder and get the pipette ready for use. Be sure to have a box or dish lined with a Kimwipe nearby so that you can put the slides on a clean surface after they are dry. Grasp a slide with a large pair of cleaned tweezers and direct a strong N_2 stream toward it until it is thoroughly dry on both sides. Grasp it firmly or it will blow away. Dry three slides. They are now ready to be mounted.

B. Mounting the Slides

Using the soldering iron in the fashion described in Part 10, place four In/Sn solder beads on a freshly-dried, clean glass slide. They should be placed so that they overlap with the Al strip to be evaporated. For accuracy, use a previously made sample as a guide. The beads should be low, small and smooth-looking, especially around the perimeter. After the four beads are applied, the slide can be mounted in a sample holder.

This is easiest to do when the sample holder is held securely in place by the small vise. Wiggle the slide into place with a pair of tweezers. Fasten the four

wire connections to the slide by bending them into place with the soldering iron. Make sure the connections are well made since these wires will provide the electrical connection to the future samples. When the sample holder is held properly in the vise, the banana-plug connector wires will bend to your left.

C. Mounting the Sample Holder

After the slides are soldered in place, the sample holders can be mounted in the bell jar. The three sample holders are not equivalent; the electrical wires are of different lengths. To tell them apart, they have either one, two, or three pieces of transparent teflon tubing around one of the wires.

Slide 1 should be mounted first, then 2 and finally 3. Position the sample holder flush against the copper support block and guide the wires over the arm of the support. Fasten the holder in place with the Allen-head cap screws and plug in the miniature gold-plated banana plugs to make the electrical connections.

D. Cleaning the Al Evaporation Window Shield

After the bell jar is brought up to atmospheric pressure and opened, the Al evaporation window shield should be removed from in front of the evaporation source box. There are two Pyrex shields, so one can be cleaned beforehand if desired.

To remove the evaporated metal, simply clean the glass in the sink with a scrub sponge and some soap. Rinse it well in water and then in acetone. Dry it with Kimwipes and remove any smudges or fingerprints. Slide the glass into the holder and position the teflon inserts in the base, which help the glass fit more snugly. Before closing the bell jar, put the shield back in place. The stem of the holder is wrapped with a piece of thin teflon sheet so that it fits snugly between the copper arms of the current feedthroughs. This prevents it from contacting

either the feedthroughs or the evaporation box and keeps it from rotating. Please see Fig. 9.

E. Polishing the Glow Discharge Protective Shield

After each experiment, the protective shield of the glow discharge is removed and polished. There is a duplicate shield which can be cleaned when the other one is in use.

Loosen the wingnuts which clamp the shield in place and slide the shield out. Be careful to not bump the electrode accidentally. Repositioning it can be time-consuming. Polish the surface of the shield with fine-grade emery cloth, then rinse and dry it carefully with acetone and Kimwipes. When you put it back in the system, be certain to reproduce its position as nearly as you can.

F. Changing the Al Glow Discharge Electrode

After each experiment, you should check the Al glow discharge electrode for signs of aging. Periodically, it needs to be replaced and it's better to do this before it fails during an experiment. When it does fail, the Al rod suffers a sudden irreverisble form of metal fatigue. The end of it will droop, usually touching the shield and causing the glow discharge to short out.

The lifetime of an electrode will depend on how much you use it and at what voltage you run the discharge. Usually, an electrode will last through many discharges. As it ages, the Al rod changes in appearance. The end of it will no longer appear shiny. Instead, it will be dull and even slightly "grainy" in appearance. In contrast to a new Al rod, it will also be very soft and easy to bend.

Before you remove an old electrode, carefully note its position because *you should duplicate this as exactly as possible*. Any change in the position of the electrode or the shield may cause the characteristics of the discharge to

change. To help ensure the reproducibility of the oxidation, you need to be systematic in how you position these parts.

The electrode is held in place by a small machined copper piece as shown in Fig. 6. On one end, the copper has a slotted receptacle which holds the Al rod tightly in place. The other end is crimped onto copper wire. The old electrode can be removed by pulling it out of the copper holder. Select a new electrode from among the Al rods which are also used for the Al evaporation. It should be very straight. You do not have to adjust its length, just force it into the copper holder so that it is inserted firmly and securely. Put the glass insulation back around the copper holder and position the new electrode as needed. Check its alignment from both sides when the glow discharge protective shield is in place. You might want to pump the system down part way and check to see that the new electrode is properly working before you go through all the pre-experimental procedures. However, this is rarely, if ever, a problem.

G. Replenishing the Al and Pb Supplies

The evaporation sources need to be replenished after each experiment. However, if you are using a large tungsten boat for the Pb, it may need to be replenished only every 2-3 experiments.

The Al metal source is an Al rod which is 99.99% pure. The rod is cut into pieces approximately 3/4" long which are bent into horseshoe-shaped loops. An easy way to do this is to grasp one of the Al pieces securely with one of the pairs of square-nosed pliers found in the lab (the ones with the pink handle); then push down against a hard surface (like a desk top), wrapping the wire around the nose of the pliers. Four horseshoes are used each time. When a new tungsten filament is to be used for the first time, hang one horseshoe over each of the centermost filament loops. This will help ensure that the filament gets

coated evenly by the aluminum. If the filament has been used previously, hang two horseshoes on each of the two central loops. This helps the filament last longer by slowing the accumulation of aluminum at the two ends of the filament. Make sure that the horseshoes are not too long since this may cause the ends to melt together more easily than usual, and drop off rather than wet the filament. Use a pair of tweezers to hang the Al rod horseshoes on the tungsten filament.

An extra Al evaporation source is always kept ready for an emergency. This is on the far right-hand side of the evaporation source box. This extra source can also be used for evaporating Mg or other metals to form supported catalysts. In the meantime, it is used as an emergency aluminum backup source in case the first evaporation attempt fails during an experiment. This third source is connected when the copper arm on the source selection box is in the upper right-hand corner.

The Pb metal source is Pb shot. A tungsten boat is used for the evaporation and is refilled easily, but be careful to find and remove any shot which spills on the baseplate. Either a large boat or a small boat may be used.

H. Replacing the Tungsten Evaporation Sources

The tungsten filaments need to be replaced frequently. As a filament is used, aluminum alloys with the tungsten and accumulates on the ends of the filament causing the tungsten to become very brittle. Eventually, the filament will break from the embrittlement.

To replace an old filament, remove the lids and the evaporation box dividers. Undo the Allen-head cap screws and slide the ends of the filament out from underneath the washer. Put a new filament in position, hold it in place and carefully tighten the screws trying to not cause any torque in the filament. If it's too tight the filament will age quickly but it has to be tight enough to make a

good electrical connection.

The Pb boats require changing much less often than the Al filaments and are easier to replace. Use a large pair of scissors or metal cutters to trim the ends of the boat to the correct length.

I. Regreasing the Gasket

The sealing gasket of the bell jar needs to be regreased with Dow Corning High Vacuum Grease every 4-5 times that the bell jar is opened. Spread a small amount of grease evenly around the gasket to form a thin, smooth film. Make sure that the gasket is clean and free of lint or small chips of evaporated metal. Remove any excess grease.

J. Cleaning the Baseplate

The baseplate should always be wiped thoroughly clean of dust and grease before the bell jar is closed. Use acetone and Kimwipes, or lint-free cloths if they are available.

K. Final Points

As you prepare the bell jar for the next experiment, take the time to check out the interior assemblage and make sure everything is in proper working order, including the electrical connections and the rotary feedthrough. Notice when the aluminum foil coverings on the teflon wires and the bell jar shield need replacing or if the evaporation source box has a heavy buildup of evaporated metal. Although these tasks are not part of the routine maintenance procedures, making their examination a routine part of your bell jar preparation can help save time and trouble later by avoiding repairs and ensuring the smooth operation of the system during your experiment.

References

1. H. E. Evans, PhD Thesis, California Institute of Technology (1980).

2. W. M. Bowser and W. H. Weinberg, Rev. Sci. Instrum. **47**, 583 (1976).

3. W. M. Bowser, PhD Thesis, California Institute of Technology (1980).

4. H. E. Evans, W. M. Bowser and W. H. Weinberg, Appl. Surface Sci. **5**, (1980).

Figure Captions

Figure 1: Schematic representation of the vacuum system used in preparing IETS samples.

Figure 2: Diagram of the baseplate ports and feedthroughs.

Figure 3: Schematic representation of the manifold system.

Figure 4: A redesigned sample holder.

Figure 5: The redesigned glow discharge apparatus.

Figure 6: A schematic of the OFHC copper and Teflon parts used in the glow discharge apparatus.

Figure 7: The $Zr(BH_4)_4$ trap line.

Figure 8: The $Zr(BH_4)_4$ Hoke cylinder line.

Figure 9: The Pyrex shield used during the Al evaporation.

Figure 10: Schematic drawing of the heating panel.

Figure 11: Schematic drawing of the electrical circuits used to heat the IETS samples and simultaneously monitor their temperatures.

Table 1

Sample Heating Procedure

	DVM setting	R/V_{1-4} Switch	Ohms/SH switch
R_i	4 wire	V_{1-4}	Ohms
R_r	2 wire	R	SH
V_R	DC volts	R	SH
V_s	DC volts	V_{1-4}	SH

R_i = initial resistance of Al strip
R_r = resistance of precision resistors
V_R = voltage drop across precision resistors
V_s = voltage drop across Al strip

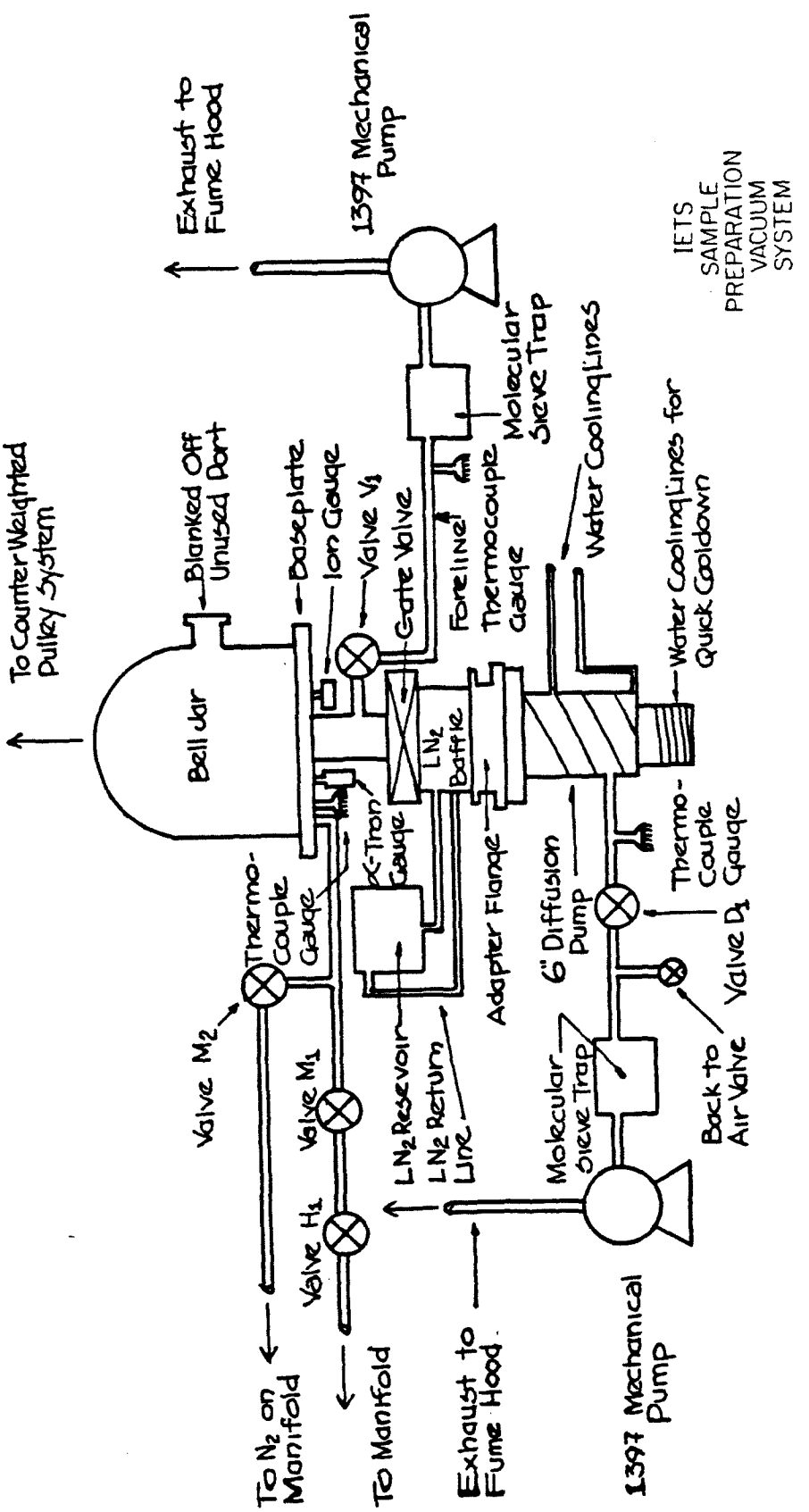
IETS
SAMPLE
PREPARATION
VACUUM
SYSTEM
Exhaust to
Fume Hood
1397 Mechanical
Pump
To Counter Weighted
Pulley System
Blanked Off
Unused Port
Baseplate
Ion Gauge
Valve V1
Gate Valve
Foreline
Thermocouple
Gauge
Molecular
Sieve Trap
Water Cooling Lines
Water Cooling Lines for
Quick Cooldown
Bell Jar
LN2
Baffle
K-Tron
Gauge
Thermo-
Couple
Gauge
Adapter Flange
6" Diffusion
Pump
Thermo-
Couple
Gauge
Valve M2
Valve M1
Valve H1
Valve D1
LN2 Reservoir
LN2 Return
Line
Molecular
Sieve Trap
Back to
Air Valve
To N2 on
Manifold
To Manifold
Exhaust to
Fume Hood
1397 Mechanical
Pump

Figure 1

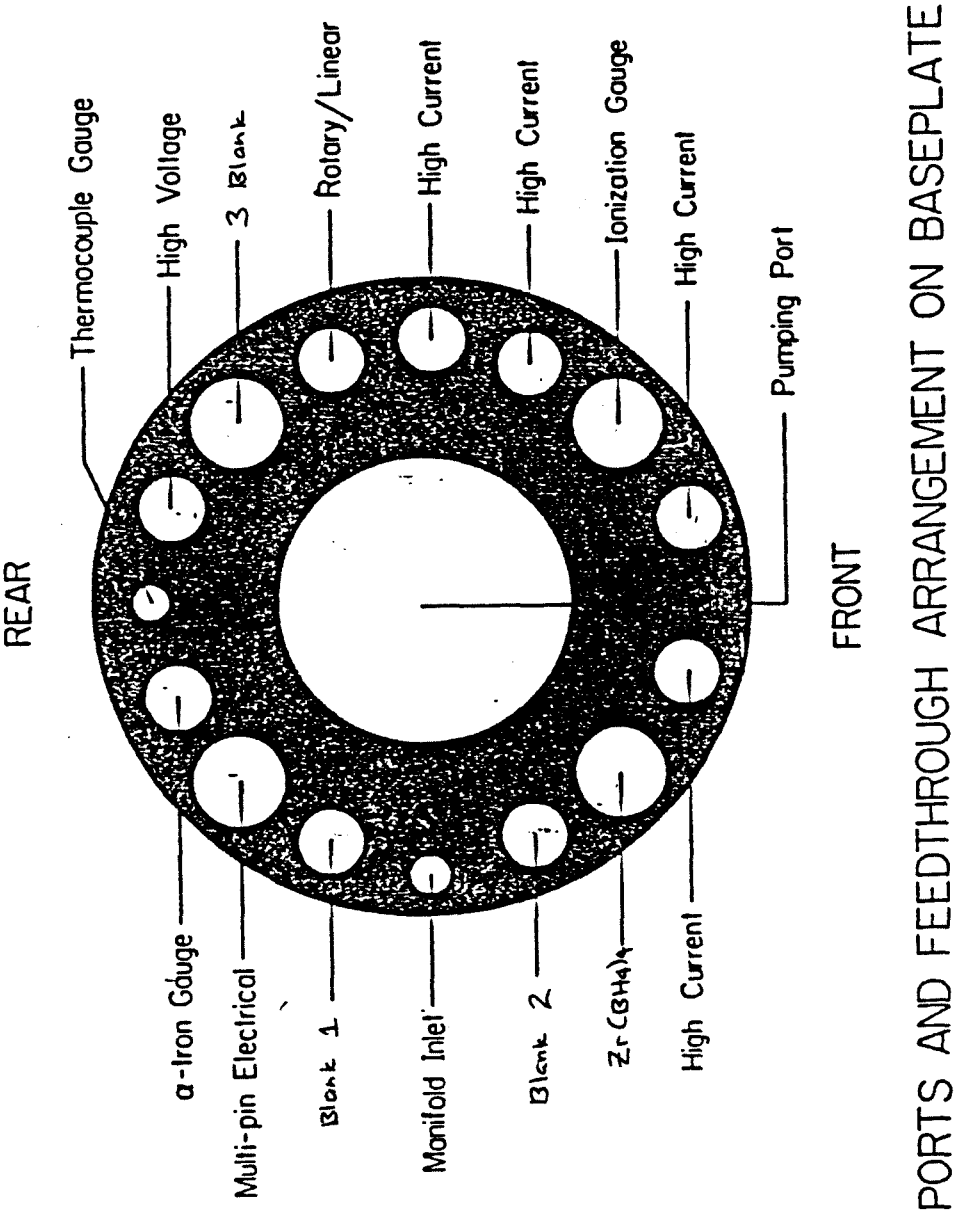
REAR
Thermocouple Gauge
High Voltage
3 Blank
Rotary/Linear
High Current
High Current
Ionization Gauge
High Current
Pumping Port
FRONT
α-Iron Gauge
Multi-pin Electrical
Blank 1
Manifold Inlet
Blank 2
Zr(BH4)4
High Current
PORTS AND FEEDTHROUGH ARRANGEMENT ON BASEPLATE

Figure 2

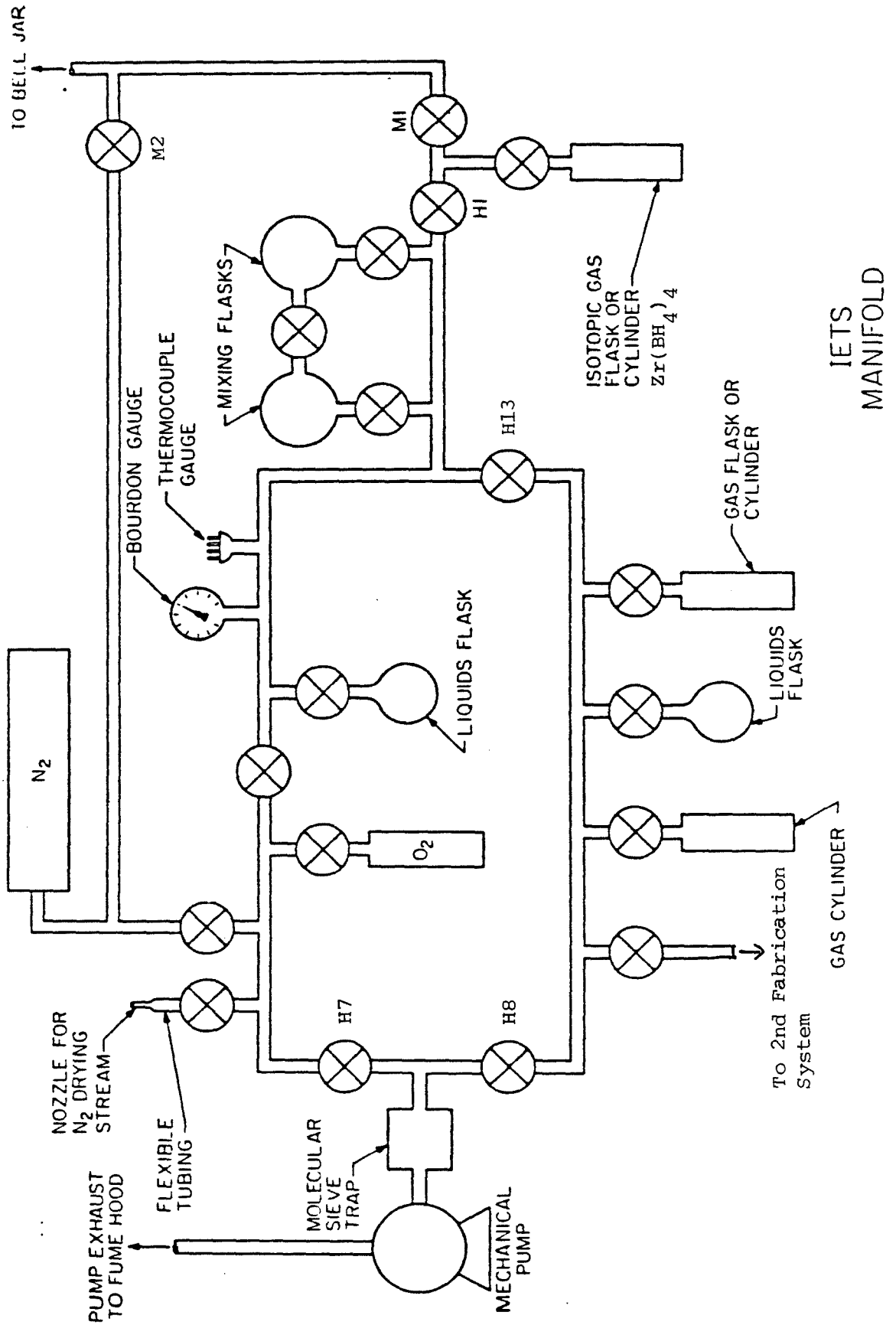
TO BELL JAR
M2
M1
H1
MIXING FLASKS
ISOTOPIC GAS FLASK OR CYLINDER $Zr(BH_4)_4$
BOURDON GAUGE
THERMOCOUPLE GAUGE
H13
GAS FLASK OR CYLINDER
IETS MANIFOLD
LIQUIDS FLASK
N_2
O_2
LIQUIDS FLASK
NOZZLE FOR N_2 DRYING STREAM
FLEXIBLE TUBING
H7
H8
To 2nd Fabrication System
GAS CYLINDER
MOLECULAR SIEVE TRAP
PUMP EXHAUST TO FUME HOOD
MECHANICAL PUMP

Figure 3

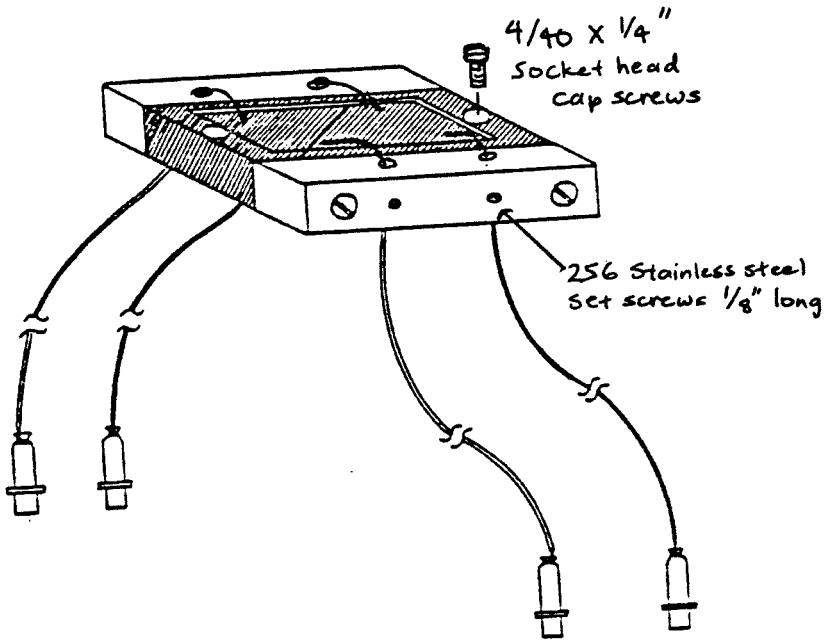
4/40 X 1/4"
Socket head
cap screws
256 Stainless steel
set screws 1/8" long

Figure 4

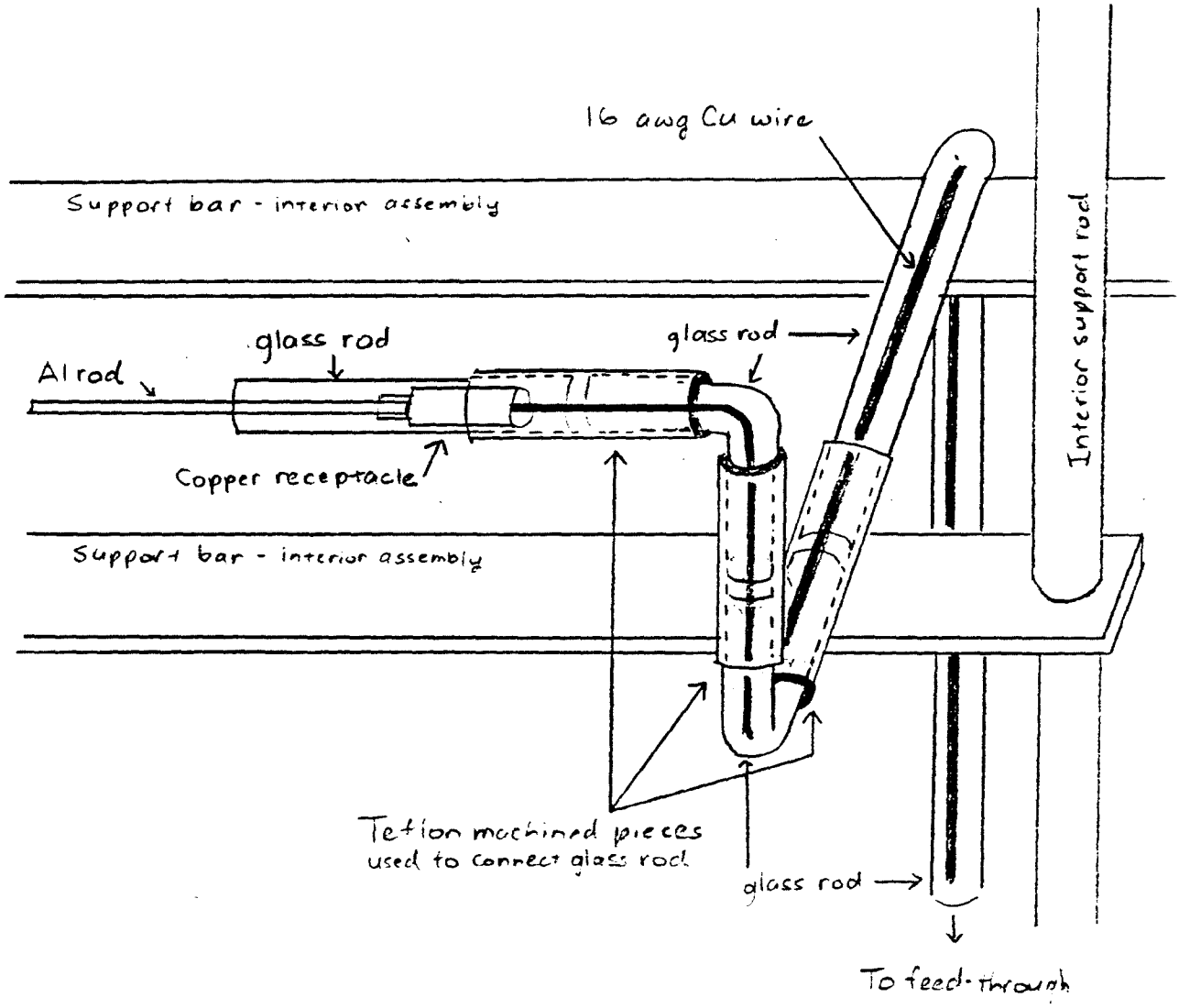
16 awg Cu wire
Support bar - interior assembly
Interior support rod
glass rod
glass rod
Al rod
Copper receptacle
Support bar - interior assembly
Teflon machined pieces
used to connect glass rod
glass rod
To feed-through

Figure 5

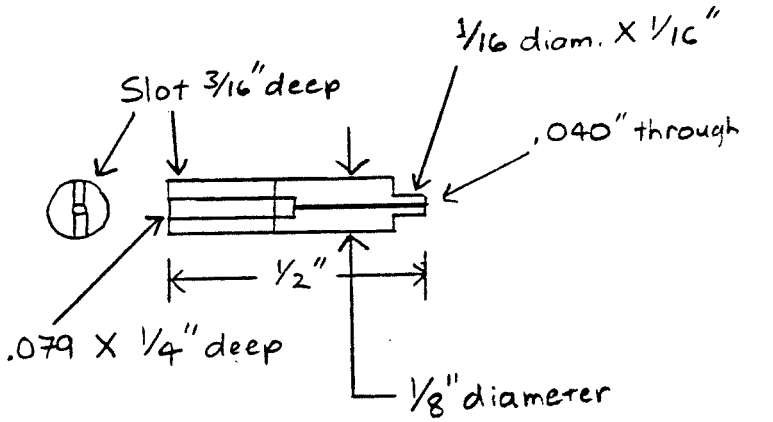

OFHC Cu
Receptacle

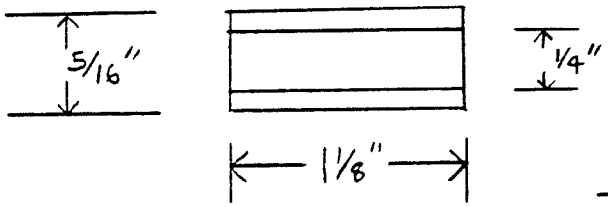

Teflon
Connector

Figure 6

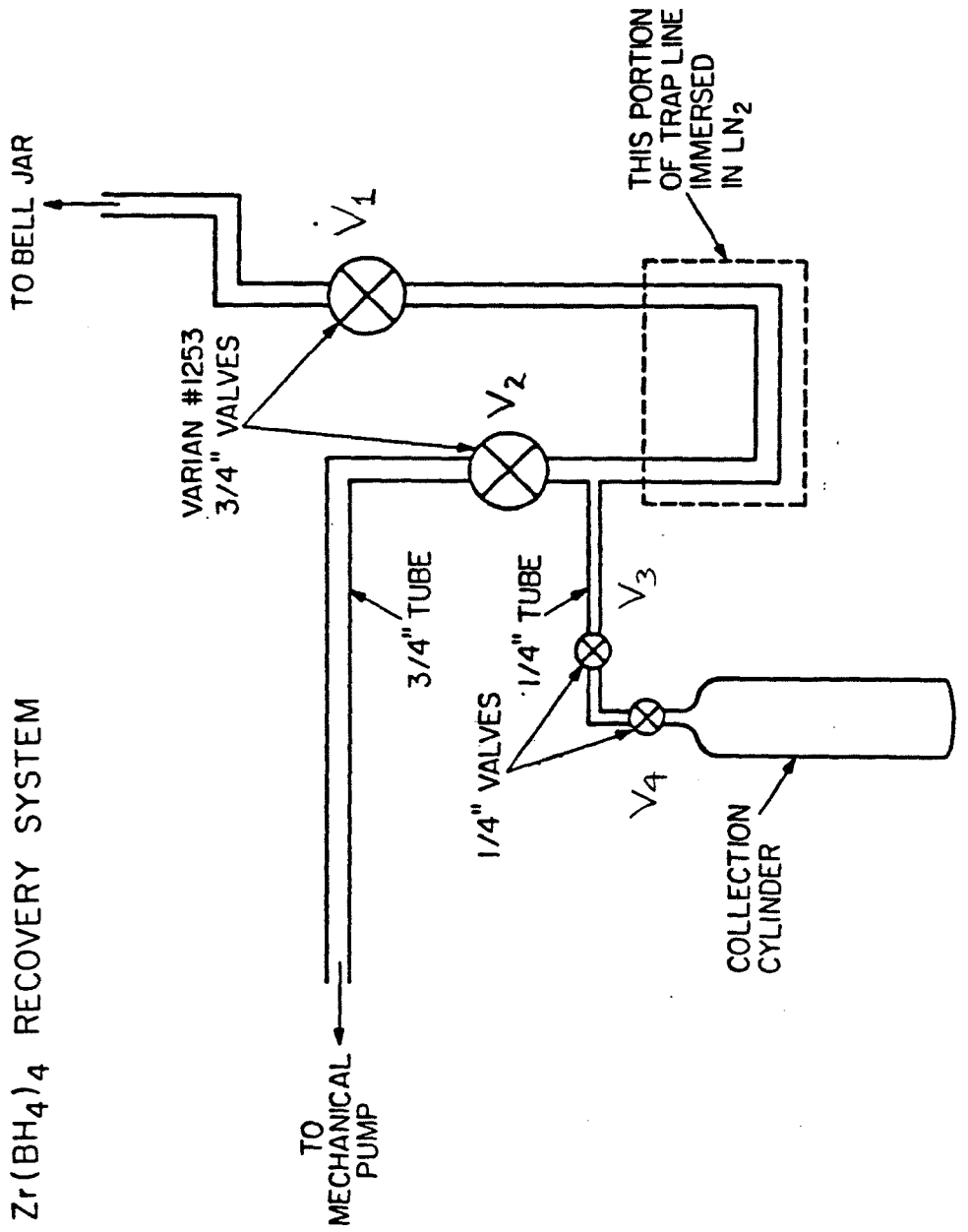
$Zr(BH_4)_4$ RECOVERY SYSTEM
TO BELL JAR
VARIAN #1253
3/4" VALVES
V_1
V_2
V_3
V_4
THIS PORTION
OF TRAP LINE
IMMERSED
IN LN_2
3/4" TUBE
1/4" TUBE
1/4" VALVES
TO
MECHANICAL
PUMP
COLLECTION
CYLINDER

Figure 7

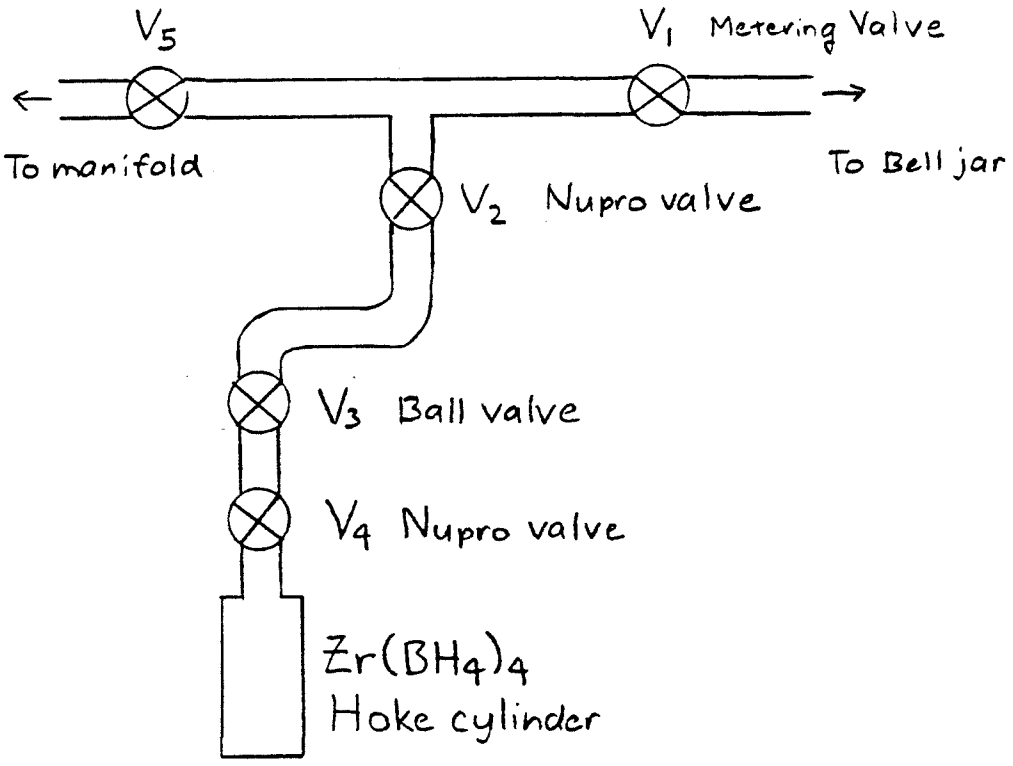
V_5
V_1 Metering Valve
To manifold
To Bell jar
V_2 Nupro valve
V_3 Ball valve
V_4 Nupro valve
$Zr(BH_4)_4$
Hoke cylinder

Figure 8

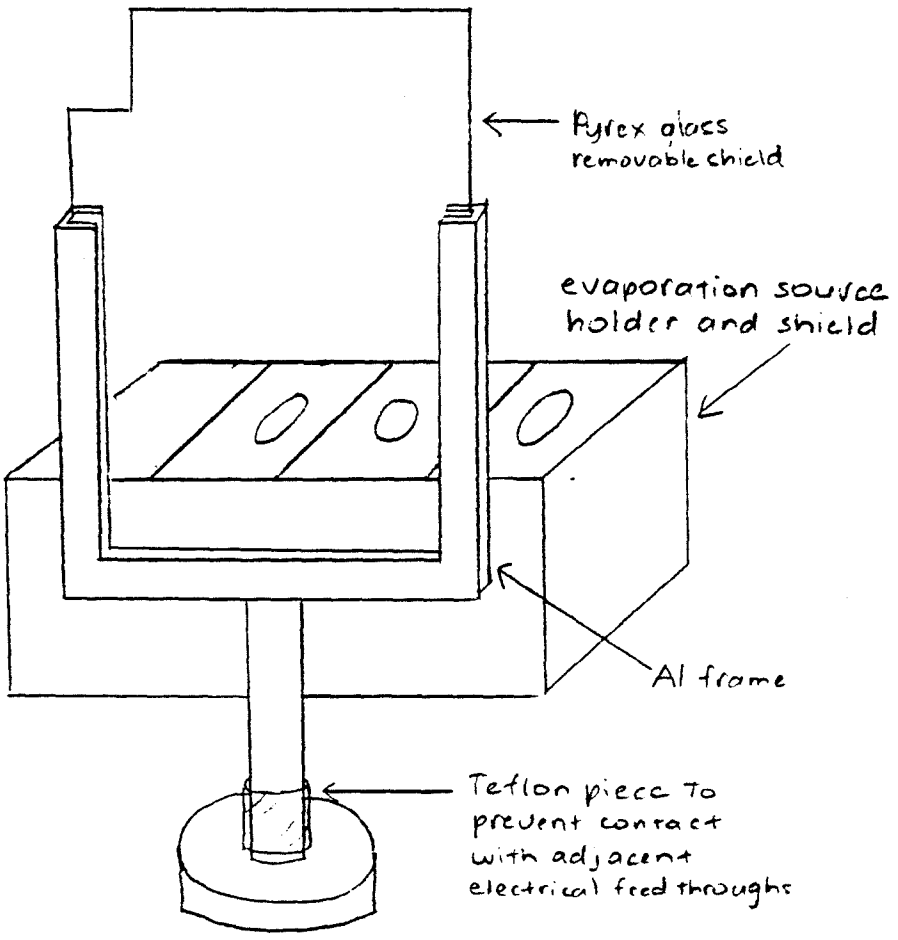
Pyrex glass
removable shield
evaporation source
holder and shield
Al frame
Teflon piece To
prevent contact
with adjacent
electrical feed throughs

Figure 9

Figure 10

(a)

SAMPLE HEATING POWER SUPPLY PANEL

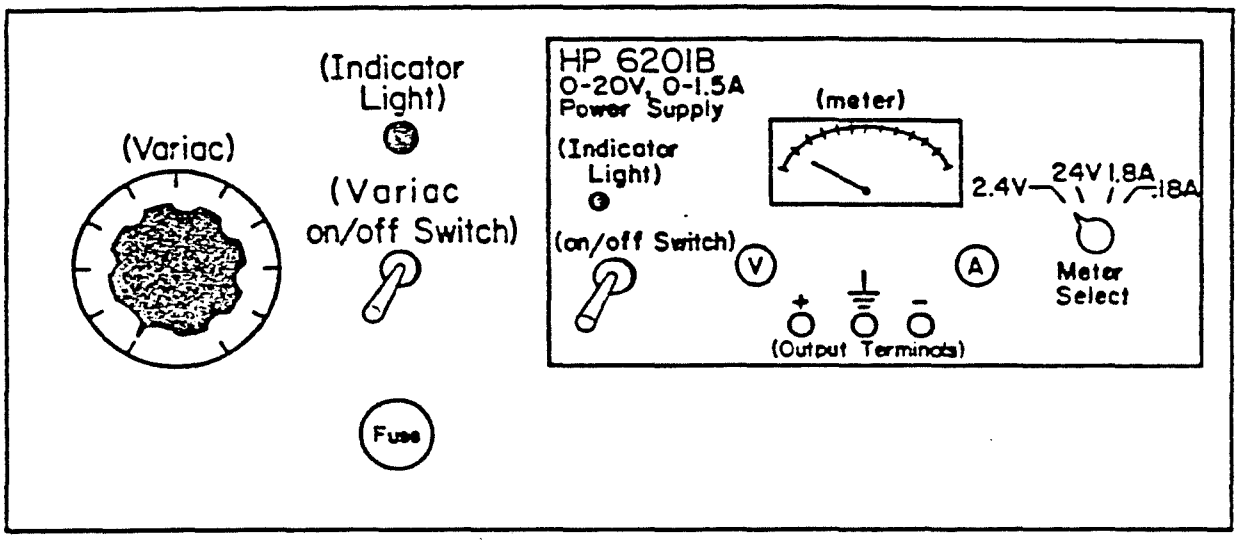

(b)

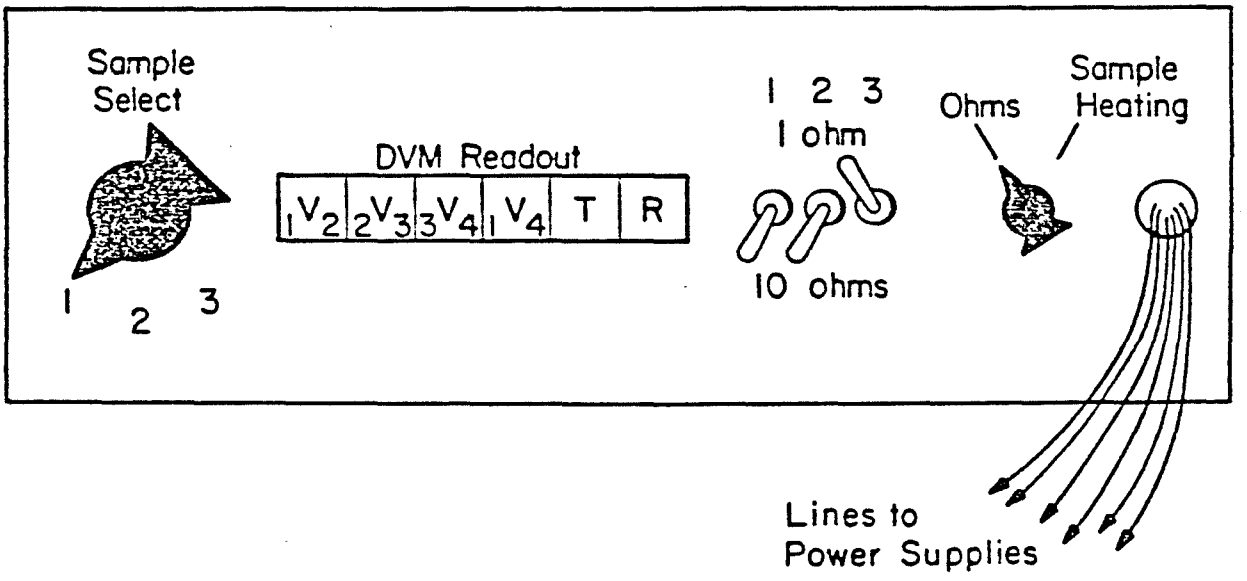

SWITCHING PANEL

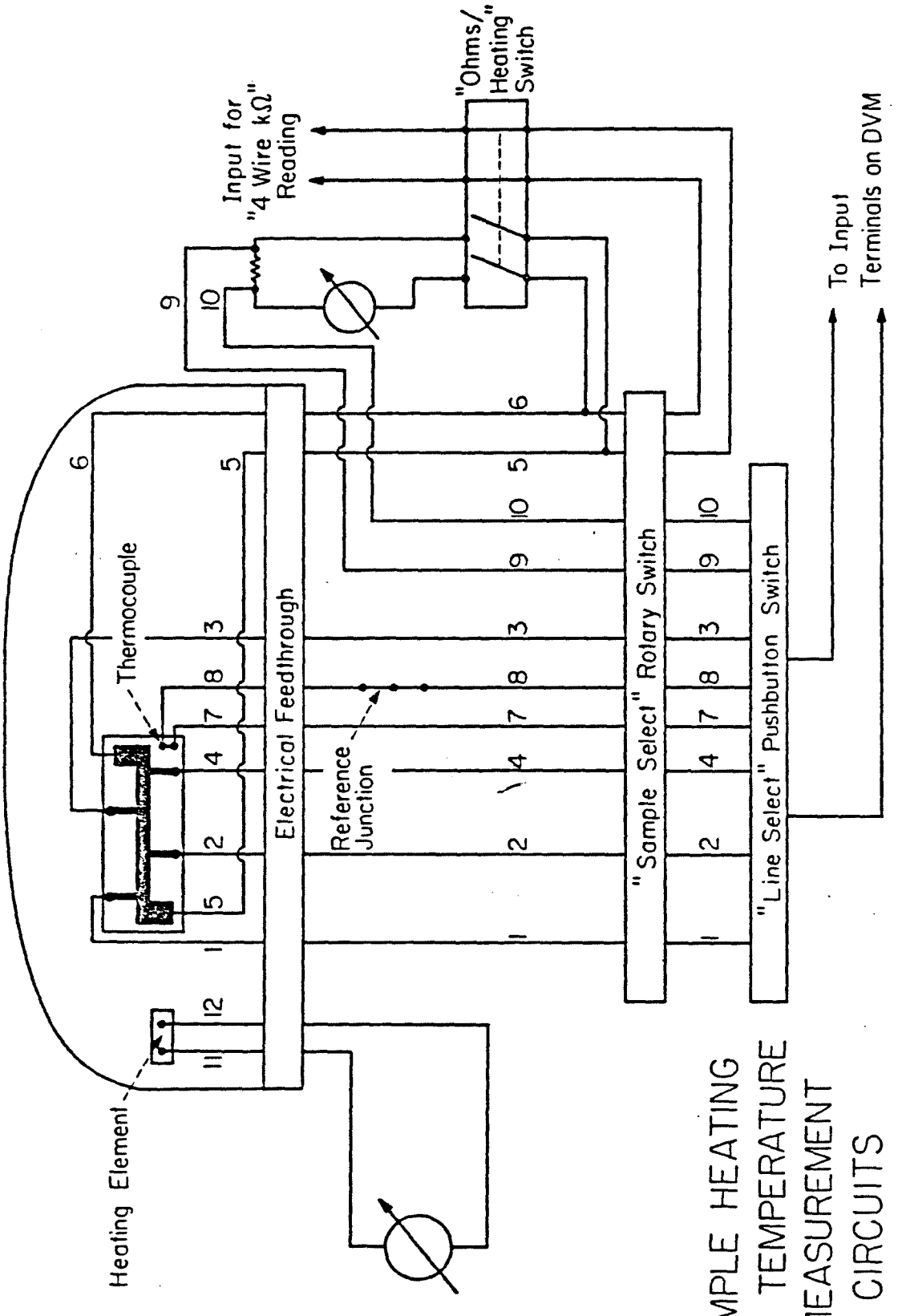
Heating Element
Thermocouple
Electrical Feedthrough
Reference Junction
"Sample Select" Rotary Switch
"Line Select" Pushbutton Switch
Input for "4 Wire kΩ" Reading
"Ohms/" Heating Switch
To Input Terminals on DVM
SAMPLE HEATING AND TEMPERATURE MEASUREMENT CIRCUITS

Figure 11

Appendix B

Computer Spectral Analysis

Table of Contents

1. Introduction

One of the major developments for doing IETS in our laboratory has been the creation of a computer program for plotting and labeling the spectra. The original version of this program **(1)** has been edited and several new programs have been written to allow for further data manipulation. These developments are presented and described in this Appendix.

2. Program capabilities

In our research group, all IET spectral data were recorded using a PDP 11/10 computer. The need for high quality plots and the fact that the spectra are digitally recorded provided the impetus for the development of IETSPLOT. This original program, as well as the programs described here, provides certain basic functions necessary for the IETS data to be presented as a plot. These include: (1) accessing the IETS file, (2) assigning an energy abscissa, (3) removing the sloping background of the spectrum, (4) data smoothing, (5) accurately locating the significant spectral features, and (6) printing the peak position adjacent to the corresponding peak.

The original IETSPLOT accessed the 1623 Zeta plotter in the Dreyfus-NSF Center for Theoretical Chemistry. The programs described here, however, access the Versatec printer/plotter.

Each program is described individually below. Several changes have been made to the original program to enhance its flexibility. These include adding numerous prompts regarding background subtraction, the option to smooth or not to smooth, and the option to view the data on a VT terminal before plotting. The programs described here all use a least-squares fit of the baseline around four reference points which may be selected when the program prompts for the input. The least-squares fit was found to provide "flatter" spectra — for the

chemical systems studied in this thesis —than did the Tschebyshev routine used in the original program. Another program described here can produce a plot with up to ten 'stacked' spectra, which greatly facilitates any comparison between spectral features.

3. Programs

A. Single Spectrum Plot

'HENRY' produces a two-page plot of a single spectrum on the Versatec plotter. The program framework is in HENRY.FOR, the program plotting routines are in HPLOT.FOR, and the program subroutines are in HLIB.FOR, shown on the following pages. An example of the program output is shown in Fig. 1. A full-size spectrum measures 17" x 11".

The program is composed of 'blocks' to facilitate editing. After changes are made to any of the three blocks, the block(s) must be Fortraned and then linked before it can be run. To link the blocks, type SUBMIT LINKH for batch processing or @LINKH for interactive processing.

Each run produces a *.DAT file where * is the name of the input source card (see below), a PARM.PLV and a VECTR1.PLV file. To print the plot on the Versatec, type, MCR RASM (or VPLOT) and the directory will be searched for the most recent .PLV files for plotting.

The program prompts for a number of parameters, many of which are self-explanatory. The other source of input to the program is the 'Input Source Data Card'. This specifies which raw data files are to be used and provides the experimental conditions under which the data were collected, including the temperature, exposure, oxidation time, oxidation voltage and current. For each raw data file, the number of data points in the spectrum minus one, the voltages of

the second datum point and the final datum point in the spectrum, and the modulation voltage at which the spectrum was measured must also be entered.

As many as three files may be used to produce the plot. The first file is usually data recorded for the low energy portion of the spectrum, from 30 to 280 meV, and the second file corresponds to the high energy portion of the spectrum, from 250 to 500 meV. The third file may be used for a reference file, if desired.

When the program is run, the 'Input Source Data Card' is opened to acquire information for the first file. An additional prompt here inquires whether the file is upside down (UPSD), included because the spectra were often recorded upside down. This must be corrected before the spectra can be plotted. Next, the Processfile subroutine is called. This subroutine has a number of prompts allowing the user to choose which points to use as references for the least-squares fit of the baseline. Up to four points may be selected from regions in the spectrum where no major peaks are known or expected to occur. This simplifies the smoothing process greatly because the original IETSPLOT did not prompt for the background subtraction reference points. They were instead included in the program which meant that the program had to be edited to change them, a time-consuming process.

A further improvement to the program is the ability to smooth or not smooth the data. Previously, this was done automatically. The program now asks whether smoothing is desired. It is also possible to plot files without any background subtraction. This is occasionally useful to see the shape of the background or if having trouble subtracting the background nicely. In this case, the program asks how many least-squares fit iterations are desired. If 0 is entered, no background subtraction will be done. The smoothing routine is the original

9-point cubic used in IETSPLOT.

After the Processfile subroutine, the Peak data subroutine is called to find the maximum and minimum peak heights. This subroutine also prints out the maximum height and square deviation, as well as a warning if the baseline seems suspect.

The program then repeats this process for any second or third file. The next section of the program scales the first and second files together so that a single continuous plot is produced. The program asks the user to enter a relative scaling factor to scale the maximum peak in the second file to the maximum peak in the first file. The default value is 1.0. If the first two files overlap, an overlap procedure is also required. The program allows the user to choose which file is to be used in the overlap region of the spectrum. This is a big improvement over the original version of the program which tried to match the two spectra so that they overlapped perfectly. In most spectra, the overlap region turned out looking somewhat sloppy.

It should be noted that the program actually allows for two ways to scale the data. The first way is to use the UPSD prompt when the file is first read. In addition to entering -1 for the case of an inverted file, one can also enter the modulation voltage at which the file was recorded. This is the method used to plot the data shown in this thesis. However, one can also scale the data by entering the relative scaling factor mentioned above, calculated from the ratio of the modulation voltages.

The two files may also be scaled using a third reference file, usually a quick scan taken over the entire spectral range. However, this was found to be inconsistent in some cases depending on the resolution of the peak heights obtained in the full-spectrum file. Ideally, the full spectrum should be measured using a

small step size such as 0.5 meV to avoid the entire problem of relative scaling. With the new measuring system available in our laboratory, this problem is solved (2).

After scaling the files, the subroutine Hscale is called to reduce the height of the peaks to fit on the plotter. Now the data are ready to be plotted. First, the subroutine Labelpos is called to provide a label positioning guide and assign a y-axis location to every x-axis position and establish a center position for the labels corresponding to the x-axis positions. The subroutine Labov then checks the overlap between adjacent labels and shifts the positions if necessary.

Next, the subroutine Plotdata is called. It is located in the third "block" of the single spectrum program, HPLOT.FOR. It contains the plotting instructions for the graph and also incorporates the option to do a VT132 Terminal plot before trying to print the data. The terminal plotting option is a great improvement to the original program. A great deal of time is saved by inspecting the graph before it is plotted to make sure the background subtraction, relative scaling, smoothing and peak positions are all in order. The terminal plot can be done only on the VT132 and some VT100 terminals. The program asks the user if a terminal plot is desired and, if so, to type in 1; if a terminal plot is not desired, the data are plotted on the Versatec. The program next plots the axis twice to make it darker, then the experimental parameters.

The last section of the program produces a file of the peak positions and peak heights both for the reference file, if used, and for the plotted data. This is a very useful improvement to the program because each peak is assigned a y-axis value which can be used to compare the magnitudes of certain spectral features from plot to plot. This is helpful in comparing data from different experiments even though the theory and significance of the peak heights are not well under-

stood in IETS **(3)**. An example of a printout file is shown in Fig. 2. The program also ask the user if sensitivities were used for the UPSD's, and this information is shown in the resulting printout.

HENRY.FOR

```
      CHARACTER*30 FNAME,PLOTFILE*35, title*70,None,filenm
      character*30 datfile1,datfile2,datfile3,reffilenm
      Real uc,sd,ud1,uc2,ngf
      Integer i,j,k,m,nsig1,nsig2,nsig,sens,nsig3
      Integer ndata1,ndata2,ndata3,ncataf
      Diversion xsing(2010),ysing(2010),xit(2CC)
      Diversion icharfname(1),ifname(1),ip1(1C0),ip2(100),ip3(1CC)
      Diversion ixps(1C0),ixps1(100),ixps2(1C0),ixps3(100)
      Double precision xscale,yscale,ytegin,avperin
      Double precision x(2C1C),xf(2C10),x1(2C10),x2(2010),x3(2C10)
      Double precision yps(100),vxpeak(1C0),xt(2C1C)
      Double precision xps(100),xps1(10C),xps2(100),xps3(100)
      Double precision xp1(100),yp1(10C),avpvec(10C),xspace,yspace
      Double precision c,c0,crel,vinc1,vinc2,vinc3,vincf
      Double precision a1,a2,a3,b1,b2,b3,c1,c2,c3
      Double precision yf(2010),y1(201C),y2(2010),y3(2C10)
      Double precision y(2C10),ys(2C10),yd(2C10),ytr(2C10)
      Double precision hmax1,hmax2,hmaxC1,hmax02,hmax31,hmax32
      Double precision hmin,hmax,hminf,hmaxf
      CCMMCN /LABARR/XPL,YPL,APPVEC
      CCMMCN /LABDAT/XSPACE,YSPACE
c           ! program parameters follows
      XSCALE=2C.Cd00          ! i don't think this is used anywhere
      YSCALE=9.5Cd00
      YBEGIN=3C.Cd00
      avperin = 27.90d00

c
c                ****  Inquire TTY for input file  ****
c
      PRINT *, 'INPUT SCURCE DATA FILE'
      READ *,FNAME
c
c
c             create name for peak file
      DO 31 I=1,30
   31 IF(ICHAR(FNAME(I:I)) .EQ. 46 .AND.
     & ICHAR(FNAME(I+1:I+1)) .EQ. 32) GO TC 41
   41 filenm= FNAME
      filenm(I:I+3)= '.DAT'
c
c             now open file with spectra file data
      OPEN(UNIT=8,NAME=FNAME,TYPE='OLD')
c
c
c             first read in TITLE CARD
      READ (8,22) TITLE
   22 FORMAT(A7C)
c             now read in ALL experimental parameters
      READ (8,4) TEMP,EXPSLR,O>TIME,CXYCL,CXCUR
      read (8,4) datfile1
      read (8,4) ndata1,v11,vf1,vmcd1
      read (8,4,end=23) catfile2
      read (8,4) ndata2,v12,vf2,vmcd2
      read (8,4,end=23) catfile3
      read (8,4) ndata3,v13,vf3,vmcd3
   23 read (8,4) ip1(1),ip1(2),ip1(3),ip1(4)
      read (8,4,end=24) ip2(1),ip2(2),ip2(3),ip2(4)
      read (8,4,end=24) ip3(1),ip3(2),ip3(3),ip3(4)
   24 continue
c
cccc
cccccc     ****************************************
cccccc
cccccc               Program Main Body
cccccc
cccccc     ****************************************
cccccc
cccccc     THE FIRST FILE ENTERED MUST BE, WHEN PLOTTED,
cccccc     TO THE LEFT OF THE SECONC FILE ENTERED;
cccccc     THE THIRC FILE, IF ENTERED, IS THE REFERENCE.
cccc
c
      GET DATA FROM FIRST FILE
      print *,'Enter UPSC (C means stop run):'
      read *,ud1              ! uc= -1 if file upside down
      if(ud1.eq.C) then       ! or else ud could = sensitivity
        ndata1 = 0
        go to 9999
      end if
      Call processfile(ndata1,v11,vf1,x1,y1,ud1,ic1,catfile1,
     .  Se21,vinc1,1,vmcd1)
      Call peakcata(ndata1,x1,y1,v11,vf1,vinc1,hmax1,Se21,
     .  xps1,ixcs1,nsig1,vtegin,avperin)
```

```
c
c       GET DATA FOR SECOND FILE
        print *,'Enter UPSC (0 means no second file):'
        read *,uc2
        if(uc2.eq.0) then
          ndata2 = 0
          nsig2 = 0
          go to 4000
        end if
        Call processfile(ndata2,vi2,vf2,x2,y2,ud2,ip2,datfile2,
     .    Se22,vinc2,2,vwcd2)
        Call peakdata(ndata2,x2,y2,vi2,vf2,vinc2,hmax2,Se22,
     .    xps2,ixps2,nsig2,vbegin,avgerin)

c
c       GET DATA FOR THIRD FILE
 4000 print *,'Enter UPSC (0 means no third file):'
        read *,ud3
        if(ud3.eq.0) then
          ndata3 = 0
          go to 17
        end if
        Print *,'Reference file name is? in single quotes.'
        Read *,reffilenm
        Call processfile(ndata3,vi3,vf3,x3,y3,ud3,ip3,datfile3,
     .    Se23,vinc3,3,vwcd3)
        Call peakdata(ndata3,x3,y3,vi3,vf3,vinc3,hmax3,Se23,
     .    xps3,ixps3,nsig3,vbegin,avgerin)
c
c       FIND MAX PEAK HEIGHT IN 1ST & 2ND
c       HALVES OF FILE 3, RESPECTIVELY.    Hope they aren't in overlap
        nd=int(ndata3/2)
        Call Maxwin(1,nd,y3,hwin,hmax31)
        Call Maxwin(nd+1,ndata3,y3,hwin,hmax32)
c
c       DEFAULT VALUE OF RELATIVE SCALING FOLLOWS:
        c0=hmax32/hmax31
d       Print *,'c0= ',c0
c       ASK FOR RELATIVE SCALING (C)
        If(ndata2 .eq. 0) go to 140      ! no scaling needed
17      Print *,'Relative scaling factor? (0 means default)'
        Read *,crel                      ! ratio of hmax2/hmax1 desired
        If(crel .ne. 0.0) then
          c=crel*hmax1/hmax2
          go to 18
        endif
        If(c0 .eq. 0.0) then
d       Print *,'c0=0 '
          c=1.0                  ! default if no reference file is 1.0
          go to 18
        End if
        c=c0*hmax1/hmax2         ! default is reference file scaling
d       Print *,'c=c0*hmax1/hmax2=',c0,'*',hmax1,'/',hmax2,'=',c
18      Continue
d       Print *,'c= ',c
c
c       SCALE Y2 WRT Y1
        Do 140 i=1,ndata2
          y2(i)=y2(i)*c
140     Continue
c
c       ASSIGN YF, XF TO ENTIRE SPECTRUM
c
c       CASE WHERE NO SECOND FILE
        If(ndata2 .eq. 0) then
          do 145 i=1,ndata1
            xf(i)=x1(i)
145         yf(i)=y1(i)
          ndataf=ndata1
          vincf=vinc1
          go to 183
        End if
c
c       CASE WHERE FIRST TWO FILES OVERLAP
c       OVERLAP PROCEDURE FOLLOWS
        a=0.0                            !Will need in ordering xps below
        ovinc=x1(ndata1)-x2(1)
        ovlp1=int(ovlap/vinc1+0.5)+1
        ovlp2=int(ovlap/vinc2+0.5)+1
c       ASK WHICH FILE TO USE FOR OVERLAP REGION
        Print *,'Which file (1 or 2) for overlap region?'
        Read *,w
        If(w .eq. 2) then
          do 150 i=1,ndata1-ovlp1
```

```
          xf(i)=x1(i)
          yf(i)=y1(i)
150     continue
        do 155 i=1,ndata2
          xf(ndata1-ovlp1+i)=x2(i)
          yf(ndata1-ovlp1+i)=y2(i)
155     continue
        ndataf=ndata1+ndata2-ovlp1
c         a=int((x1(ndata1-ovlp1)-x1(1))/vinc1+1.5)
        a=ndata1-ovlp1
      Else
        do 170 i=1,ndata1
          xf(i)=x1(i)
170       yf(i)=y1(i)
        do 180 i=1,ndata2-ovlp2
          xf(ndata1+i)=x2(ovlp2+i)
180       yf(ndata1+i)=y2(ovlp2+i)
        ndataf=ndata1+ndata2-ovlp2
c         a=int((x1(ndata1)-x1(1))/vinc1+1.5-ovlp2)
        a=rdata1-ovlp2    ! # effective points in file 1
      End if
d     Print *,'a=',a
d     Print *,'ndataf=',rdataf
        vincf=(vinc1+vinc2)/2
C     THE VALUE ABOVE FOR VINCF IS ONLY APPROXIMATE
C       BUT DOES NOT AFFECT PEAK ASSIGNMENTS
C     ALSO NOTE a ; IT WILL BE NEEDED BELOW

C       NEED TO ORDER XPS (PEAK POSITIONS)
183   Do 144 i=1,nsig1
        xps(i)=xps1(i)
        ixps(i)=ixps1(i)
144   Continue
      If(ndata2 .eq. 0) go to 245
      Do 245 j=1,nsig2
        xps(nsig1+j)=xps2(j)
        ixps(nsig1+j)=ixps2(j)+a        ! see the a!
245   Continue
      nsig=nsig1+nsig2
C
c       ENTIRE SPECTRUM IN xf(i) AND yf(i)
c
c
C       NEED TO SCALE GRAPH TO PLOTTER SIZE
      Call Maxmin(1,rdataf,yf,hminf,hmaxf)
      Call Mscale(rdataf,xf,yf,vbegin,vperin,yuncin,hminf,hmaxf,yscale)
!       now x(ndataf+1)=vbegin, x(ndataf+2)=vperin, and
!       y(rdataf+1)=hminf(min val. of y), and y(ndataf+2)=yunpin(# of y
!       units per plotter inch)
c
143   Continue
c
C                           new plot out data
      Call labelpos(yf,xps,nsig,yunpin,hwinf,mvperin,vbegin,
     .  v11,vincf)
      Call plotdata(rdataf,xf,yf,nsig,xps,yscale,vf2,fname,vmpc1)
C
c       ASSUME VMPC1 = VMPC2 FOR CALCULATING FWHM
C       (see order subroutine abscissa for reference)
      fwhm = -1.414*vmpc1*.14 + 1.13
c
C             new plot FWHM, and label
      J= LEN(fname)
      DO 67C I=1,J
      Icharfname(I) = ICHAR(fname(I:I))
d     print *,'here is a letter of file label:',icharfname(1)
  67C CALL SYMBOL((VF2-VBEGIN)/MVPERIN-5.+(I-1)*.15,.3,.15,
     .  Icharfname,0.0,0)
      CALL SYMBOL((VF2-VBEGIN)/MVPERIN-5.,.1,.15,
     .  16HINST FNC FWHM = ,0.0,16)
      DO 55 I= 1,2
      CALL PLOT((VF2-VBEGIN)/MVPERIN-5+.15*16,.1,3)
      CALL PLOT((VF2-VBEGIN)/MVPERIN-5+.15*16 + FWHM/MVPERIN,.1,
     .  2)
      CALL PLOT((VF2-VBEGIN)/MVPERIN-5+.15*16 + FWHM/MVPERIN,
     .  .25,2)
      CALL PLOT((VF2-VBEGIN)/MVPERIN-5+.15*16,.25,2)
      CALL PLOT((VF2-VBEGIN)/MVPERIN-5+.15*16,.1,2)
   55 CONTINUE
C                       now plot axis (twice, to make it darker)
      do 665 j=1,2
      Call plot(47C./mvperin,0.,3)
      Call plot(C.,0.,2)
      Do 667 i=1,int(470/10)
        xit(i)=10*(i-1)/mvperin
```

```
        call plot(xlt(i),0.,3)
        call plot(xlt(i),-.07,2)
667   Continue
      Do 668 i=1,int(47C/1C),2
      axispv = vtegin + (i-1)*1C
668   Call rumter(xlb(i),-.3,.12,9xispv,C.C,C)
669   Continue
C
C                          shift origin to plot exp param
      Call plot(C.C,9.6,-3)
      J = ler(title)
      do 666, I=1,J
      ifname(1) = ichar(title(I:I))
 666  call symbol(.5+(i-1)*.3*.9,.1,.3,ifname,0.0,0)
      CALL SYMBOL(6.C,.1,.3,21HEXPOSURE (TORR-SEC) =,0.0,21)
      CALL NUMBER(6.C+.3*24,.1,.3,EXPSUR,0.0,2)
      CALL SYMBOL(6.C,-.4,.3,21HTEMPERATURE (DEG C) =,C.C,21)
      CALL NUMBER(6.C+.3*24,-.4,.3,TEMP,C.C,0)
      CALL SYMBOL(6.C,-.65,.15,2CHVOLTAGE (VOLTS) & CURRENT(MA) ,
     & C.0,3C)
      CALL NUMBER(6.C+.15*33,-.65,.15,CXVOL,C.0,C)
      CALL NUMBER(6.0+.15*39,-.65,.15,CXCUR,C.0,C)
      CALL SYMBOL(6.C,-.9,.15,22HOXIDATION TIME (SEC) =,C.C,22)
      CALL NUMBER(6.0+.15*25,-.9,.15,OXTIME,C.0,0)
 888  CONTINUE
      Call plot(C.0,-10.1,+999)
C
C*****************************************************************
C
C       PRINTOUT OF PEAK POSITIONS AND PEAK HEIGHTS
92C5  CONTINUE
      None='None'
      If(uc3 .eq. 0) ther
        datfile3=None
        go to 92C6
      End if
      Print *,'Reference file name is '//reffilenm
      Call Peakfile(reffilenm,temp,expsur,oxtime,vmod3,nsig3,
     .  ixps3,yf,hmax31,xps3,uc3,0.C,datfile3,None,None,C)
      Print *,'Ref. file of peak positions and heights in '//reffilenm
92C6  Continue
      Print *,'Did you use sensitivities for UPSDs? 0 means no.'
      Read *,sens
      If(uc2 .eq. 0) ther
        datfile2=None
      End if
      Call peakfile(filenm,temp,expsur,oxtime,vmod1,nsig,
     .  ixps,yf,hmax1,xps,uc1,uc2,sens,datfile1,datfile2,datfile3,c)
      Print *,'File of peak positions and heights in '//filenm
9999  END

C
C
```

HLJB.FOR

```
      SUBROUTINE PROCESSFILE(ndata,vi,vf,x,y,uc,ip,datfile,
     .  Se2,vinc,file,vmod)
c
      Dimension ip(100)
      Integer ndata,itimes,file
      Double precision vinc,a,b,c,y(2010),ys(2010)
     > Double precision vi,vf,uc,Se2,x(2010)
      Character*30 datfile
c
C       IF UD = -1.0 :  THE FILE IS UPSIDE DOWN
C       NOW READ IN DATA
7     Print *,'reading data file: '//datfile
      Call Fileread(ndata,datfile,y)
      Do 10 i=1,ndata
      y(i)=ud*y(i)
10    Continue
      Call Atscissa(ndata,vi,vf,x,vinc,vmod)
c
C       SMOOTHING?
      Print *,'Smoothing desired? (0 means no.)'
      Read *, smooth
      If(smooth .eq. 0) then
        call fakesmooth(ndata,y,ys)
      else
        call Smooth5ptcubic(ndata,y,ys)
      endif
c
C       LEAST SQUARE FIT OF BASELINE (QUADRATIC FIT)
C           AND BASELINE SUBTRACTION
      Print *,'Number of Lsqfit iterations?'
      Read *,itimes
      If(itimes .eq. 0) then
        print *,'No baseline subtraction on this file.'
        go to 31
      End if
      Print *,'Selected Points (MV):'
      Print *,IP(1),IP(2),IP(3),IP(4)
      DO 1700 I=1,4
1700  IP(I)=int(MAX(ONE(1.0),ONE((IP(I)-X(1))/VINC+1.0)))
      PRINT *,'Actual Indices are:'
      PRINT *,IP(1),IP(2),IP(3),IP(4)
      PRINT *,'Baseline=apples+bears*x+coconuts*x^2'
      DO 1710 I=1,ITIMES
      CALL LSQFIT(IP,YS,A,B,C,Se2)
      PRINT *,'apples=',A,' bears=',B
      PRINT *,'coconuts=',C
1710  Call flatten(ndata,ys,a,b,c)
2000  Continue
c       RETURN Y VALUES TO Y ARRAY
      Do 2010 i=1,ndata
        y(i)=ys(i)
2010  Continue
c
31    Return
      End
c
c*****************************************************************
c


      Subroutine peakdata(ndata,x,y,vi,vf,vinc,hmax,Se2,
     . xps,ixps,nsig,vbegin,mvcorir)
c
      Integer ndata,num,nsig
      Dimension ixps(100),ivxpeak(100)
      Double precision xps(100),vxpeak(100),x(2010)
      Double precision vinc,y(2010),hmax,hmin
      Double precision vi,vf,vbegin,mvcorir,Se2
c
      Call Maxmin(1,ndata,y,hmin,hmax)
      Print *,'Se. dev.= ',Se2,' hmax= ',hmax
      Print *,'Se. dev./hmax= ',Se2/hmax
      If(Se2 .ge. .1C*hmax) then
        print *,'Deviation considerable.  Baseline may be suspect.'
      Endif
      Call peakloc(ndata,y,x,vxpeak,ivxpeak,num)
      Call sortpeak(vxpeak,ivxpeak,num,xps,ixps,nsig,y,
     .  vinc,vi,Se2,hmax)

      Return
      End
```

```
!*****************************************************************
c
C       SUBROUTINE FOR WRITING PEAK HEIGHTS INTO A FILE
      Subroutine peakfile(yahoo,temp,expsur,extime,vmod,nsig,ixps,
     .  y,hmaxC1,xps,ud1,ud2,sens,catfile1,datfile2,catfile3,c)
c
      Dimension ixps(100)
      Real temp,expsur,extime,vmod,ud1,ud2
      Integer nsig,ndata2,sens
      Character*20 yahoo,catfile1,datfile2,catfile3
      Double precision c,y(2C1C),hmaxC1,xps(10C),fwhm
c
      Open(name=yahoo,unit=17,type='new')
      Write (17,9210) yahoo
9210  Format(12x,a10)
      Write (17,9220) temp,expsur,extime
9220  Format(12x,'Temp=',f1C.2,'  Expos=',f1C.2,'  Oxid. time=',f10.2)
      Write (17,9230)
923C  Format(15x,'xps         y              y/ymax1')
c
      Do 8888 k=1,nsig
      ix=ixps(k)              ! This gives index value of xps(k)
      Write (17,9240) xps(k)*8.C654A,y(ix),y(ix)/hmax01
9240  Format(12x,f10.2,'    ',f1C.2,'    ',f10.6)
8888  CONTINUE
      Write (17,9250)
9250  Format(' ')
      Write (17,9270) ud1
9270  Format(12x,'File 1 was multiplied by a factor of',f10.2)
      If(ud2 .eq. 0) then
        write (17,9275)
9275    format(12x,'There was no second file.')
      Else
        write (17,9280) ud2
9280    format(12x,'File 2 by a factor of               ',f10.2)
      Endif
      If(sens .ne. 0) then
        write (17,9285) Abs(ud1*100)
9285    format(12x,'Sensitivity of file 1 (mV) =',f1C.2)
      if(ud2 .ne. C) then
        write (17,929C) Abs(ud2*10C)
9290    format(12x,'Sensitivity of file 2 (mV) =',f10.2)
      endif
      Endif
      Write (17,9293) catfile1
9293  Format(12x,'First file was      ',a30)
      Write (17,9296) catfile2
9296  Format(12x,'Second file was     ',a3C)
      Write (17,93C0) catfile3
93C0  Format(12x,'Reference file was ',a30)
      Write (17,93C3) c
93C3  Format(12x,'Scaling factor y2 = c*y2;  c = ',f10.6)
9260  Close(unit=17)
      Return
      End
c
!*****************************************************************


C
c       least square fit routines - lsqfit, flatten
c
      subroutine lsqfit (n, ys, a, b, c, Se2)
c       parameters are: c(*) beginning of sample points
c                       ys(*) smoothed data
c
c       returns: a, b, c - the coefficients to fitted parabolic
c                equation of form  a + bx + cx^2
      integer c(100), i, j, k, init
      double precision ys(2010)
      double precision a, b, c, parabla, queen
      double precision dev, Sdev, e2, Se2, Sys
c
c       variables used to solve for  a, b, c
c
      double precision s0, s1, s2, s3, s4, t0, t1, t2, s10, s20
      double precision s21, s31, s32, s42, t00, t11, t22, q(60C)
      double precision s13,s02,s23,s12,s24,s34,t13,t02,t24
c
c       now initialize EVERYTHING
```

```
c
      j=0
      a=0
      b=0
      c=0
      s0=0.0
      s1=0.0
      s2=0.0
      s3=0.0
      s4=0.0
      t0=0.0
      t1=0.0
      t2=0.0
c
c       get constants for equations:
c                a(s0) + b(s1) + c(s2) = t0
c                a(s1) + b(s2) + c(s3) = t1
c                a(s2) + b(s3) + c(s4) = t2
c
c
      init = -1
      incr = 19
      do 8000 i = 1,4
      ibeg = a(i)
      if (init .eq. 0) go to 8050
      init=0
      incr=59
 8050 iend = ibeg+incr
      incr = 19
      do 8100 k = ibeg,iend
      j = j+1
      a(j) = k
 8100 continue
 8000 continue
c
      s0 = j
      do 8200 i = 1,j
      ia=int(a(i))
      queen=c(i)
         s1 = s1+queen
         s2 = s2+(queen**2.0)
         s3 = s3+(queen**3.0)
         s4 = s4+(queen**4.0)
         t0 = t0+ys(ia)
         t1 = t1+queen*ys(ia)
         t2 = t2+(queen**2.0)*ys(ia)
 8200 continue
c
      s10 = s1/s0
      s20 = s2/s0
      s21 = s2/s1
      s31 = s3/s1
      s32 = s3/s2
      s42 = s4/s2
      s13 = s1/s3
      s02 = s0/s2
      s23 = s2/s3
      s12 = s1/s2
      s24 = s2/s4
      s34 = s3/s4
      t00 = t0/s0
      t11 = t1/s1
      t22 = t2/s2
      t13 = t1/s3
      t02 = t0/s2
      t24 = t2/s4


      a=((t13-t02)/(s23-s12)-(t24-t13)/(s34-s23))
     . /((s13-s02)/(s23-s12)-(s24-s13)/(s34-s23))
      b=((t11-t00)/(s31-s20) - (t22-t11)/(s42-s31))
     . /((s21-s10)/(s31-s20) - (s32-s21)/(s42-s31))
      c=((t22-t11)/(s32-s21)-(t11-t00)/(s21-s10))
     . /((s42-s21)/(s32-s21)-(s31-s20)/(s21-s10))
```

```
c
      dev=0
      Sdev=0
      Se2=0
      e2=0
      Sys=0
      do 999 i=1,j
      ic=int(a(i))
      queen=a(i)
      parablem=a+b*queen+c*(queen**2)
      dev=ys(ic)-parablem
      Sdev=Sdev+dev
      e2=dev**2
      Se2=Se2+e2
      Sys=Sys+ys(ic)
c      print *,ic,ys(ic),parablem,dev
999   continue
      Se2=(Se2/(j-1))**.5          ! square deviation
      print *,'avg dev=',Sdev/j,' avg ys=',Sys/j
d     print *,'Tots',t0,t1,t2
d     print *,'Squids',s0,s1,s2,s3,s4
      if(Abs(a*s0+b*s1+c*s2-t0) .ge. Abs(.000001*t0)) goto 8300
      if(Abs(a*s1+b*s2+c*s3-t1) .ge. Abs(.000001*t1)) goto 8300
      if(Abs(a*s2+b*s3+c*s4-t2) .ge. Abs(.000001*t2)) goto 8300
c
8301  return
c
c       oops
c
8300  print *,'oops... lsqfit eqns do not match'
      print *,'both sides of equation:'
      print *, a*s0+b*s1+c*s2, t0
      print *, a*s1+b*s2+c*s3, t1
      print *, a*s2+b*s3+c*s4, t2
      go to 8301
c
      end

c
c       ***********************************************
```

```
c
      SUBROUTINE FLATTEN(NDATA,YS,APPLES,BEARS,COCONUTS)
      Double precision YS(2010)
      double precision apples, bears, cocoruts, parablem, di
      integer i, ndata
c     Subtract least square fit of baseline from YS
      DO 1300 I=1,NDATA
      di=i
      PARABLEM=APPLES+BEARS*dI+COCONUTS*(dI**2.0)
      YS(I)=YS(I)-PARABLEM
1300  CONTINUE
      RETURN
      END
c
cccccc
cccccc
c
```

```
      SUBROUTINE FILEREAD(NDATA,datfile,Y,file)
      INTEGER*2 H,IH,IL
      Double precision Y(2C10)
      CHARACTER*(*) datfile
      print *,datfile
C
C
      If(ud .ec. -595) ther
        open(name=datfile,type='CLD',urit=13)
        do 67P i=1,7
        read(13,*) h
67P   Continue
        do 67C i=1,ndata
        read(13,*) l
        read(13,*) h
        y(i) = h*2**16 + l
67C   Continue
      Close(unit=13)
      Goto ***
      Endif
      OPEN(ACCESS='DIRECT',NAME=datfile,TYPE='CLD',
     & UNIT=6,RECORDTYPE='FIXED')
C
C
C        READ IN FIRST FIVE PARAMETERS
      DO 5C I=1,5
      READ(6'I) H
C       WRITE(7,2C0) H
  2C0 FORMAT(I2C)
   5C CONTINUE
C        THROW AWAY FIRST DATA POINT?
      READ(6'6)H
      READ(6'7)H
C        NOW READ IN WORKING DATA SET
      DO 1CC I=1,NDATA
      READ(6'((I*2+6)) IL
      READ(6'((I*2+7)) IH
      Y(I)= (IH*2**16+IL)
  1C0 CONTINUE
C
C            NOW CLOSE OUT INPUT FILE
C
      CLOSE(UNIT=6)
C
      RETURN
      END
C


      SUBROUTINE ABSCISSA(NDATA,VI,VF,X,VINC,vmod)

      Double precision vinc,X(2C10),vi,vf
      Double precision shift        ! don't really need double precision
      Integer ndata
C
C
C            ** NOW GENERATE ABSCISSA **
C
                        ** VINC= mv/point
      VINC=((VF-VI)/(NDATA-1))
      DO 11C I= 1,NDATA
      X(I)= VI + (VINC*(I-1))
  110 CONTINUE
C
C       now need to calculate the proper energy shift (in mev)
c       to correct Pt energy azo 3 4.2 K for modulation effects
c       Kirtley & Marsha Phys Rev B 13  ,2910 (1976)
c       (In addition, FWHM value is determined for modulation:
c          FWHM= 1.49*VMCD + 0.30)
c                 (see Kirtley's review article)
c               ** VMCD meV rms **
c                     .5 < vmod/delta < 2.
c
      SHIFT= -1.414*VMCD*.14 + 1.13
C                     1 < vmod < 2 meV
c
      do 167 i=1,ndata
        x(i) = x(i) - shift
167   continue
c
      RETURN
      END
```

```
C
      SUBROUTINE FAKESMOOTH(NDATA,Y,YS)
      Double precision y(2C1C),ys(2C10)
C
cc      A fake smooth follows (no smoothing).
c
      do 114 I = 1,ndata
114     ys(i) = y(i)
      Return
      End




c
      SUBROUTINE SMOOTHSPTCUBIC(NDATA,Y,YS)
      Double precision y(2C10),ys(2C10)
C
cc      The real smoothing routine is below.
cc      Also see PLIB.FOR or IETSMCUR.FOR for a 9 pt smooth.
ccc
ccc         SMOOTH DATA (5PT CUBIC/QUADRATIC)
C
      DO 12C I=2,NDATA-2
      YS(I)= (-3*(Y(I-2)+Y(I+2))+12*(Y(I-1)+Y(I+1))
     & +17*Y(I))/35
  12C CONTINUE
      DO 125 I=1,2
      YS(I)= Y(I)
      YS(NDATA-I+1)= Y(NDATA-I+1)
  125 CONTINUE
      RETURN
      END




C
C
      SUBROUTINE HSCALE(NDATA,X,Y,VBEGIN,MVPERIN,YUNPIN,YMIN,
     & YMAX,yscale)

      Double precision y(2C1C),x(2C1C)
      Double precision vbegin,mvperin,yunpin,ymin,ymax,yscale
c
ccc         we went to slightly reduce to scale so everything fits
ccc         plotter y-scale: y-units per inch
C
      YUNPIN= 1.2*(YMAX-YMIN)/YSCALE
      YMIN= .92*YMIN
      IF(YMIN .LT. 0.0) YMIN= 1.1*YMIN/.92
  14C CONTINUE
C
C             ADD SCALE PARAMETERS INTO ARRAYS
      Y(NDATA+1)= YMIN
      X(NDATA+1)= VBEGIN
      Y(NDATA+2)= YUNPIN
C                    ** plotter scale mv per inch
      X(NDATA+2)= MVPERIN
      continue
      RETURN
      END
C
```

```
C
C
      SUBROUTINE LABELPOS(YBR,XPS,NSIG,
     & YUNPIN,YMIN,PVPERIN,VBEGIN,VI,VINC)
      Double precision YBR(2C1C),SECMAX(10)
      Double precision XPS(100),YPS(1CC),AMXLBL(10)
      Double precision yunpin,ymin,pvperin,vbegin,vi,vinc
      Double precision xc1(100),yo1(1CC),amovec(10C)
      Double precision xspace,yspace,nceak,nsector,aminpos
C                 need commons for calling LABCV
C
      COMMCN /LABARR/XPL,YPL,AMPVEC
      COMMCN /LABCAT/XSPACE,YSPACE
C
C     IF(nsig .ec. 0.C) goto 377
*C
C             **  LABEL PCSITIONING PCUTINE  **
C
C                    XSPACE= x-length of label(inches)
      XSPACE= .5
C                    YSPACE= y-length of label(inches)
      YSPACE= .15
C
C
C
C             NCW ASSIGN Y LCCATICN TO XPS
C
      CO 25C I= 1,NSIG
C**************************************
  25C YPS(I)= YBR(INT((XPS(I)-VI)/VINC +1))
C
C             ESTABLISH CENTER PCSITICN FCR LABEL CORRESP. TO XPS
C                NCTE: WORK IN CIRECT PLCTTER UNITS(INCHES)
C
C                    set irtial label .5 inches over peak
      CO 26C I= 1,NSIG
      YPL(I)= (YPS(I)-YMIN)/YUNPIN + .5
      XPL(I)= (XPS(I)-VBEGIN)/PVPERIN
  26C CONTINUE
C
C             ** NCW CC LABELS CVERLAP SPECTRUM **
C
C                    we can shift label up to +- 2 sectors(=.5xspace)
C
C                    figure out #of points in sector-length(s)=.25xspace)
      KSECTOR= INT(.25*XSPACE*PVPERIN/VINC)
      CO 3CC K= 2,NSIG
C                    now scan sectors(8) to det. max height
C     CO 27C J= 1,8
C                RESET SECMAX(J)
C     SECMAX(J)= -1E+6
C                    calculate peak subscrict
      KPEAK= (XPS(K)-VI)/VINC +1
      CO 27C I= KPEAK+(J-5)*NSECTOR,KPEAK+(J-4)*NSECTOR
C**************************************
  27C SECMAX(J)= MAX(SECMAX(J),YBR(I))
C
C                    now det. maximum over label region and min posib. dist.
C
      AMINPCS = 1E+6
      CO 28C J= 1,5
      AMXLBL(J)= MAX(SECMAX(J),SECMAX(J+1),SECMAX(J+2),SECMAX(J+3))
C       use NLAMIN later to decide #sectors to shift
      IF(AMINPCS .GT. AMXLBL(J)) NLAMIN= J
  28C AMINPCS= MIN(AMINPCS,AMXLBL(J))
      AMPVEC(K)= (AMXLBL(3) - YMIN)/YUNPIN
      AMINPCS= (AMINPCS-YMIN)/YUNPIN
C
C                    now check to see if initial placement ok
C
      IF(AMPVEC(K) .LT. YPL(K)-.125) GC TC 3C0
C          ** LABEL blockire plot  **
C                assign default ocsition if we can't gain by shift
      YPL(K)= AMPVEC(K)+.25
C                if label can be put less than 1.5in. above orig peak, o.k.
      IF(AMPVEC(K) .LT. YPL(K)+1.0) THEN
      YPL(K)= AMPVEC(K) + .25
C                else since we must move it up more than 1.5in., will a shift
C                    help us that much,otherwise use default shift above ok.
      ELSE IF(AMPVEC(K)-AMINPCS .GT. .25) THEN
C                yes we can by shifting
      YPL(K)= AMINPCS + .125
      XPL(K)= XPL(K) + (NLAMIN-3)*NSECTOR*VINC/PVPERIN
      AMPVEC(K)= AMINPCS
      END IF
  3CC CONTINUE
C
C             **  MUST GET RID CF LABEL OVERLAP  **
C
      CO 35C I= 2,NSIG
      CALL LABOV(I,I-1)
  35C CONTINUE
C
      RETURN
377   END
```

```
C
C
C
C
      SUBROUTINE LABCV(I,J)
C                 CHECKS FOR OVERLAP BETWEEN TWO LABEL BLOCKS J,K AND SHIFTS
      COMMON PLABARD/YPU,WPU,APPVEC
      COMMON /LABCAT/XSPACE,YSPACE
C
      Double precision xpl(100),ypl(100),appvec(100),xspace,yspace
      Double precision clearance
c
      CLEARANCE=.020d00
c
      IF(ABS(XPL(I)-XPL(J)) .GT. XSPACE+CLEARANCE) RETURN
      IF(ABS(YPL(I)-YPL(J)) .GT. YSPACE+CLEARANCE) RETURN
      YPL(I)= YPL(J) + SIGN(YSPACE+CLEARANCE,YPL(I)-YPL(J))
C                 check to see if shift moved label too close to spectrum
      IF(YPL(I) .GT. APPVEC(I) + .125) RETURN
C                       then by default label must be shifted up
      YPL(I)= YPL(J) +YSPACE+CLEARANCE
      RETURN
      END


C
C
C
C
C
      SUBROUTINE DERIVSPT(NDATA,YS,YD)
      Double precision YS(2010),YD(2C1C)
C
C           FIRST TAKE 1ST DERIV(9PT CUBIC/QUARTIC)
      DO 14C I=5,NDATA-4
      YD(I)= (8é*(YS(I-4)-YS(I+4))-142*(YS(I-3)-YS(I+3))
     & -1038*(YS(I-2)-YS(I+2))-126*(YS(I-1)-YS(I+1)) )/1188.
  14C CONTINUE
      RETURN
      END
C
c
c       find real maximum and real minimum of an array of data
c       by linear search. also returns HMAX and HMIN (?).



c
      subroutine maxmin (N,ndata,ycata,hmin,hmax)
      integer ndata, i, N
      double precision xcata(2C1C),xmax,xmin,xval
      double precision ydata(2C10),hmax,hmin,yval
C
      if( ndata .le. 1 ) go to 55OC
      hmax = ydata(N)
      hmin = ydata(N)
      xmax = N
      xmin = N
      do 5CC0 i = N+1, ndata
         yval = ydata(i)
         xval = i
         if( yval .gt. hmax ) then
           hmax = yval
           xmax = xval
         end if
         if( yval .lt. hmin ) then
           hmin = yval
           xmin = xval
         end if
 5CC0 continue
 55CC return
      end
```

```
c
c
      SUBROUTINE PEAKLOC(NDATA,YDD,X,VYPEAK,ivxpeak,NUM)
      Dimension ivxpeak(100)
      Double precision x(2010),vxpeak(100),xpeak
      Double precision ybr(2010),yc(2010)
c
c          THEN TO LOCATE PEAK POSITIONS
cc
c          FIRST TAKE 1ST DERIV(OPT CUBIC/QUARTIC)
      CALL DERIVOPT(NDATA,YDD,YC)
cc       NOW LOCATE ACCES
                  reset peak number counter
      NUM= 0
      DO 15C  I=5,NDATA-6
      IF (YD(I) .GE. 0.0) GO TO 15C
      IF (YD(I-1) .LT. 0.0) GO TO 15C
      xpeak= X(I)-YD(I)*(X(I)-X(I-1))/(YD(I)-YD(I-1))
      NUM= NUM + 1
c                              vector of all peaks!
      vxpeak(num)= xpeak
c
c       NEED APPROXIMATE INDEX POSITION OF PEAKS
c       print *,'peaks! ... one of these ....'
d       print *,ybr(i-2),ybr(i-1),ybr(i),ybr(i+1)
      If(ybr(i-1) .gt. ybr(i-2) .and. ybr(i-1) .ge. ybr(i)) then
        ivxpeak(num)=i-1
        go to 145
      endif
      If(ybr(i) .gt. ybr(i-2)) then
        ivxpeak(num)=i
        go to 145
      endif
      ivxpeak(num)=i-2
c
145   continue
d     print *,'peak=',ybr(ivxpeak(num))
  15C CONTINUE
      RETURN
      END
c
c
c
c
c
      Subroutine sortpeak(vxpeak,ivxpeak,num,xps,ixps,nsig,y,
     .  vinc,vi,Se2,hmax)
      Integer iv,nsig
      Dimension ixps(100),ivxpeak(100)
      Double precision y(2010)
      Double precision vxpeak(100),xps(100)
      Double precision vinc,vi,Se2,hmax
c
c       ASSUME BASELINE IS FLAT.  HMAX IS HEIGHT OF MAXIMUM PEAK.
c       SE2 IS SQUARE DEVIATION.
c
c     print *,'Se2=',Se2
      Do 240 i= 1,num
      iv=ivxpeak(i)
      If(y(iv) .lt. 3.0d00*Se2) go to 240
      nsig= nsig + 1
d     print *,'nsig=',nsig
      xps(nsig)= vxpeak(i)
      ixps(nsig)=ivxpeak(i)        ! approx index value of peak
  240 Continue
      Print *,'NUM  & NSIG'
      Print *,NUM,NSIG
      Return
      End
c
```

HPLOT.FOR

```
      subroutine plotdata(rdata,x,y,nsig,xcs,yscale,vf,filenm,vwcd)
      CHARACTER *(*) FILENM,plotfile*25
      Dimension ifname(1)
      Dimension xsing(2010),ysing(2010)
      Double precision xj(2010),x(2010),xps(100),xpl(100)
      Double precision yj(2010),yj(2010),ypl(100),awavec(100)
      Double precision yscale,wvcerin,vbegin,vf,vwcd,shift,fwhm
      COMMON /LABARR/XPL,YPL,AWAVEC
C
C
c       NEED SINGLE PRECISION YSING WHEN PLOTTTING
      Do 57 i=1,ndata+2
        ysing(i)=SNGL(y(i))
        xsing(i)=SNGL(x(i))
57    Continue
c
d     print *,'x and y scaling parameters...'
d     print *,xsing(ndata+1),xsing(ndata+2)
d     print *,ysing(ndata+1),ysing(ndata+2)
c
c       PLOT ON (VT132) TERMINAL?
c         possible only on vt132's and some vt100's
      Print *,'Plot on  terminal? yes = 1'
      Read *,ivtplot
      If(ivtplot .ne. 1) goto 58
      Call vtplot(ndata,xsing,ysing,N,C,0,filenm)
      Print *,'Ready?  Type anything.'
      Read *,blaagh
58    Continue

C           NEW PLOT DATA
C
      Call plots(C,0,C)
      Call plot(0.20,C.5,-3)
      Call line(xsing,ysing,ndata,1,C,C)
      Call line(xsing,ysing,ndata,1,C,C)
C       (plotted the line twice! heh heh)
c
C               ** NOW PLOT OUT LABELS **
C
      vbegin = x(ndata+1)         ! this was put here in HSCALE
      avcerin = x(ndata+2)        ! this too
      DO 575 I= 1,NSIG
C               if label if off page, shift it to default position if poss
      IF(YPL(I) .GT. YSCALE +.75 .OR. YPL(I) .LT. C.C) YPL(I)= 1.C
      CALL NUMBER(XPL(I)-.2,YPL(I)-.1C,XPS(I)*C.C654A,C.C,0)
  575 CONTINUE
d     print *,'HALT!  In plotdata;  peek labels all set! '
d     print *,'Enter any number! '
c     read *,blaagh
C
C
d     print *,'HALT!  In plotdata;  returning to henry! '
d     print *,'Enter any number! '
c     read *,blaagh
      RETURN
      END
```

B. Multi-Plot Program

'JAMES' produces a graph of up to 10 stacked plots, or up to four pages on the Versatec. The program is organized in the same way as the single spectrum program, that is, the program framework is in JAMES.FOR, the program subroutines are in JLIB.FOR, and the program plotting routines are in JPLOT.FOR. These are shown on the following pages. Figure 3 shows an example of a typical plot.

JAMES processes the data exactly as HENRY does and uses the same format for the 'Input Source Data Card'. The prompts are nearly the same as in HENRY. However, there is no VTPLOT option. Completion of each run produces the usual .PLV files but no .DAT file because no data are saved. The last prompt in the program is used to specify the vertical distance between the current plot and the next one.

JAMES.FOR

```
      CHARACTER*30 FNAME,PLCTFILE*25, title*70,None,filenm
      character*30 datfile1,datfile2,datfile3,reffilenm
      Real ud,sc,ud1,ud2,ndf,nocplots
      Integer i,j,k,m,nsig1,nsig2,nsig,sens,nsig3
      Integer ncata1,ndata2,ndata3,ncataf,iplt
      Dimension xsing(2010),ysing(2010),xit(200)
      Dimension icharfname(1),ifname(1),ip1(100),ip2(100),ip3(100)
      Dimension ixps(100),ixps1(100),ixps2(100),ixps3(100)
      Double precision xscale,yscale,vbegin,nvoerir
      Double precision x(2010),xf(2010),x1(2010),x2(2010),x3(2010)
      Double precision yps(100),vxcenk(100),xb(2010)
      Double precision xps(100),xps1(100),xps2(100),xps3(100)
      Double precision xp1(100),yp1(100),anovec(100),xspace,yspace
      Double precision c,cC,crel,vinc1,vinc2,vinc3,vincf
      Double precision a1,a2,a3,b1,b2,b3,c1,c2,c3
      Double precision yf(2010),y1(2010),y2(2010),y3(2010)
      Double precision y(2010),ys(2010),yd(2010),ybr(2010)
      Double precision hmax1,hmax2,hmaxC1,hmax02,hmax31,hmax32
      Double precision hmin,hmax,hminf,hmaxf
      COMMON /LABARR/XPL,YPL,APPVEC
      COMMON /LABDAT/XSPACE,YSPACE
c         ! program parameters follows
      YSCALE = 5.0D00
      YBEGIN=30.0d00
      nvoerir = 47.

c       MAXIMUM OF 10 PLOTS (4 PAGES)
      noplots = 0.0
      Call plots(0,0,0)
      Call plot(6.0,.4,-3)
1     Continue
      iplt = iplt + 1
      print *,'This is plot number',iplt
      Call plot(noplots,0.,-3)
C
C               **** Inquire TTY for input file ****
C
      PRINT *, 'INPUT SOURCE DATA FILE'
      READ *,FNAME
C
C
C               open file with spectra file data
      OPEN(UNIT=8,NAME=FNAME,TYPE='OLD')
C
C
C               first read in TITLE CARD
      READ (8,22) TITLE
   22 FORMAT(A70)
C               now read in ALL experimental parameters
      READ (8,*) TEMP,EXPSUR,DXTIME,CXVCL,CXCUR
      read (8,4) datfile1
      read (8,*) ndata1,vi1,vf1,vmoc1
      read (8,4,end=23) datfile2
      read (8,*) ndata2,vi2,vf2,vmoc2
      read (8,4,end=23) datfile3
      read (8,*) ndata3,vi3,vf3,vmoc3
23    read (8,*) ic1(1),ic1(2),ic1(3),ic1(4)
      read (8,*,end=24) ip2(1),ip2(2),ip2(3),ip2(4)
      read (8,*,end=24) ip3(1),ip3(2),ip3(3),ip3(4)
24    continue
C
C
C       ****************************************
C
C                 Program Main Body
C
C       ****************************************
C
C       THE FIRST FILE ENTERED MUST BE, WHEN PLOTTED,
C       TO THE LEFT OF THE SECOND FILE ENTERED;
C       THE THIRD FILE, IF ENTERED, IS THE REFERENCE.
C
C
c       GET DATA FROM FIRST FILE
      print *,'Enter UPSC (0 means stoc cur):'
      read *,uc1              ! uc= -1 if file upside down
      if(uc1.eq.0) then       ! or else uc could = sensitivity
        ncata1 = 0
        go to 9999
      end if
      Call processfile(ncata1,vi1,vf1,x1,y1,ud1,ic1,datfile1,
     .  Se21,vinc1,1,vmoc1)
      Call combcata(ndata1,x1,y1,vi1,vf1,vinc1,hmax1,Se21,
     .  xps1,ixcs1,nsig1,vbegin,nvoerir)
```

```
c
c       GET DATA FOR SECOND FILE
      print *,'Enter UFSC (0 means no second file):'
      read *,ud2
      if(ud2.eq.0) then
        ndata2 = 0
        nsig2 = 0
        go to 4000
      end if
      Call processfile(ndata2,vi2,vf2,x2,y2,ud2,ip2,datfile2,
     .  Se22,vinc2,2,vwoc2)
      Call peakdata(ndata2,x2,y2,vi2,vf2,vinc2,hmax2,Se22,
     .  xos2,ixos2,nsig2,vbegin,mvperir)

c
c       GET DATA FOR THIRD FILE
 4000 print *,'Enter UFSC (0 means no third file):'
      read *,ud3
      if(ud3.eq.0) then
        ndata3 = 0
        go to 17
      end if
      Call processfile(ndata3,vi3,vf3,x3,y3,ud3,ip3,datfile3,
     .  Se23,vinc3,3,vwoc3)
      Call peakdata(ndata3,x3,y3,vi3,vf3,vinc3,hmax3,Se23,
     .  xos3,ixos3,nsig3,vbegin,mvperir)
c
ccc     FIND MAX PEAK HEIGHT IN 1ST & 2ND
c       HALVES OF FILE 3, RESPECTIVELY.    Hope they aren't in overlap
      nd=int(ndata3/2)
      Call maxmin(1,nd,y3,hmin,hmax31)
      Call maxmin(nd+1,ndata3,y3,hmin,hmax32)
c
c       DEFAULT VALUE OF RELATIVE SCALING FOLLOWS:
      c0=hmax32/hmax31
d     Print *,'c0= ',c0
c       ASK FOR RELATIVE SCALING (C)
      If(ndata2 .eq. 0) go to 140      ! no scaling needed
17    Print *,'Relative scaling factor? (0 means default)'
      Read *,crel                ! ratio of hmax2/hmax1 desired
      If(crel .ne. 0.0) then
        c=crel*hmax1/hmax2
        go to 18
      endif
      If(c0 .eq. 0.0) then
d     Print *,'c0=0 '
        c=1.0                    ! default if no reference file is 1.0
        go to 18
      End if
      c=c0*hmax1/hmax2           ! default is reference file scaling
d     Print *,'c=c0*hmax1/hmax2=',c0,'*',hmax1,'/',hmax2,'=',c
18    Continue
d     Print *,'c= ',c
c
c       SCALE Y2 WRT Y1
      Do 140 i=1,ndata2
        y2(i)=y2(i)*c
140   Continue
c
ccc     ASSIGN YF, XF TO ENTIRE SPECTRUM
c
c       CASE WHERE NO SECOND FILE
      If(ndata2 .eq. 0) then
        do 145 i=1,ndata1
          xf(i)=x1(i)
145       yf(i)=y1(i)
        ndataf=ndata1
        vincf=vinc1
        go to 182
      End if
c
ccc     CASE WHERE FIRST TWO FILES OVERLAP
c       OVERLAP PROCEDURE FOLLOWS
                                 !will need ir ordering xcs below
      c=0.0
      ovlap=y1(ndata1)-x2(1)
      ovlp1=int(ovlap/vinc1+0.5)+1
      ovlp2=int(ovlap/vinc2+0.5)+1
c       ASK WHICH FILE TO USE FOR OVERLAP REGION
      Print *,'Which file (1 or 2) for overlap region?'
      Read *,w
      If(w .eq. 2) then
        do 150 i=1,ndata1-ovlp1
          xf(i)=x1(i)
          yf(i)=y1(i)
```

```
150     continue
        do 155 i=1,ndata2
          xf(ncatal-ovlp1+i)=x2(i)
          yf(ncatal-ovlp1+i)=y2(i)
155     continue
        rdataf=ncatal+ndata2-ovlp1
c         o=int((x1(ncatal-ovlp1)-x1(1))/vinc1+1.5)
        o=rdata1-ovlp1
      Else
        do 170 i=1,ncatal
          xf(i)=x1(i)
170       yf(i)=y1(i)
        do 180 i=1,ndata2-ovlp2
          xf(ncatal+i)=x2(ovlp2+i)
180       yf(ncatal+i)=y2(ovlp2+i)
        rdataf=ncatal+ndata2-ovlp2
c         o=int((x1(ndata1)-x1(1))/vinc1+1.5-ovlp2)
        o=rdata1-ovlp2     ! # effective points in file 1
      End if
C     Print *,'o=',o
d     Print *,'ndataf=',rdataf
        vircf=(vinc1+vinc2)/2
C     THE VALUE ABOVE FOR VINCF IS ONLY APPROXIMATE
C       BUT DOES NOT AFFECT PEAK ASSIGNMENTS
C     ALSO NOTE o ; IT WILL BE NEEDED BELOW

C       NEED TO ORDER XPS (PEAK POSITIONS)
183   Do 144 i=1,nsig1
        xps(i)=xps1(i)
        ixps(i)=ixps1(i)
144   Continue
      If(ndata2 .eq. 0) go to 245
      Do 245 j=1,nsig2
        xps(nsig1+j)=xps2(j)
        ixps(nsig1+j)=ixps2(j)+o        ! see the o!
245   Continue
      nsig=nsig1+nsig2
C
c       ENTIRE SPECTRUM IN xf(i) AND yf(i)
c
c
C       NEED TO SCALE GRAPH TO PLOTTER SIZE
      Call Maxmin(1,ndataf,yf,hminf,hmaxf)
      Call Mscale(ndataf,xf,yf,vbegin,mvperin,yunpin,0.0000,hmaxf,
     *  yscale)
!       now x(rdataf+1)=vbegin, x(rdataf+2)=mvperin, and
!       y(rdataf+1)=0.0(base val. of y), and y(rdataf+2)=yunpin(# of y
!       units per plotter inch)
c
143   Continue
c
C                         now plot out data
      Call labelcos(yf,xps,nsig,ixps,yunpin,hminf,mvperin,vbegin,
     *  v11,vircf)
      Call plotdata(ndataf,xf,yf,nsig,xps,yscale,vf2,fname,vmod1)
C
c
C                         shift origin to plot exp param
      Call plot(-1.75,8.3,-3)
      CALL SYMBOL(0.0,0.0,.1,7HEXPOS =,90.0,7)
      CALL NUMBER(0.0,0.*.1,.1,EXPSUP,90.0,2)
      CALL SYMBOL(.2,0.0,.1,7HTEMP = ,90.0,7)
      CALL NUMBER(.2,0.*.1,.1,TEMP,90.0,0)
      CALL SYMBOL(.4,0.0,.1,7HCXID = ,90.0,7)
      CALL NUMBER(.4,0.*.1,.1,CXTIME,90.0,0)
C             now plot label
      J= LEN(fname)
      DO 670 I=1,J
      Icharfname(I) = ICHAR(fname(I:I))
  670 CALL SYMBOL(.6,.1*(I-1),.1,Icharfname,90.0,0)
      call plot(1.75,-8.3,-3)
c                         reset origin
c
c       PROMPT, MORE PLOTS?
      print *,'Baseline shift of next plot (0 means quit):'
      read *,moplots
      If(moplots .eq. 0.0) go to 789
      If(ioit .gt. 10) then
        print *,'forget it, pal, you ought to go home'
        go to 789
      end if
c             now reinitialize some of the more important constants
      rsig = 0
      rsig1 = 0
      rsig2 = 0
```

```
      nsig2 = 0
      ndata1 = 0
      c = 0.0
      c0 = 0.0
      cref = 0.0
      do 787 i=1,100
        xcs(i) = 0.0
        xpl(i) = 0.0
        ypl(i) = 0.0
787     amcvec(i) = 0.0
      do 788 i=1,2010
        xf(i) = 0.0
788     yf(i) = 0.0
      go to 1
c
c                       row plot axis
789   Call plot(.5,470./nvcerin,3)
      Call plot(.5,0.,2)
      Do 667 i=1,int(470/10)
        xlt(i)=10*(i-1)/nvcerin
        call plot(.5,xlt(i),3)
667     call plot(.55,xlt(i),2)
      Do 668 i=1,int(470/10),2
      axisnv = vtegin + (i-1)*10
668   Call number(.75,xlt(i),.072,axisnv,90.0,0)
669   Continue
c
      Call plot(0.0,0.0,+999)
c
9999  END
```

JLIB.FOR

```
      SUBROUTINE PROCESSFILE(ndata,vi,vf,x,y,uc,ip,datfile,
     .  Se2,vinc,file,vmod)
c
      Dimension ip(100)
      Integer ndata,itimes,file
      Double precision vinc,a,b,c,y(2010),ys(2010)
      Double precision vi,vf,uc,Se2,x(2010)
      Character*20 datfile
c
cc      IF UD = -1.0 :  THE FILE IS UPSIDE DOWN
c       NOW READ IN DATA
7     print *,'reading data file: '//datfile
      Call Fileread(ndata,datfile,y,ud)
      If(uc .eq. -995) goto 10
      Do 10 i=1,ndata
      y(i)=ud*y(i)
10    Continue
      Call Abscissa(ndata,vi,vf,x,vinc,vmod)
c
C       SMOOTHING?
      Print *,'Smoothing desired? (0 means no.)'
      Read *, smooth
      If(smooth .eq. 0) then
        call fakesmooth(ndata,y,ys)
      else
C       call Smooth5Qtcubic(ndata,y,ys)
        call Smooth9Qtcubic(ndata,y,ys)
      endif
c
C       LEAST SQUARE FIT OF BASELINE (QUADRATIC FIT)
C           AND BASELINE SUBTRACTION
      Print *,'Number of Lsqfit iterations?'
      Read *,itimes
      If(itimes .eq. 0) then
        print *,'No baseline subtraction on this file.'
        go to 31
      End if
      Print *,'Selected Points (MV):'
      Print *,IP(1),IP(2),IP(3),IP(4)
      DO 1700 I=1,4
 1700 IP(I)=int(MAX(DBLE(1.0),DBLE((IP(I)-X(1))/VINC+1.0)))
      PRINT *,'Actual indices are:'
      PRINT *,IP(1),IP(2),IP(3),IP(4)
      PRINT *,'Baseline=apples+bears*x+coconuts*x^2'
      DO 1710 I=1,ITIMES
      CALL LSQFIT(IP,YS,A,B,C,Se2)
      PRINT *,'apples=',A,' bears=',B
      PRINT *,'coconuts=',C
1710  Call flatten(ndata,ys,a,b,c)
2000  Continue
c       RETURN Y VALUES TO Y ARRAY
      Do 2010 i=1,ndata
        y(i)=ys(i)
2010  Continue
c
31    Return
      End
c
!*********************************************************************


c
      Subroutine peakdata(ndata,x,y,vi,vf,vinc,hmax,Se2,
     . xps,ixps,nsig,vbegin,mvperir)
c
      Integer ndata,num,nsig
      Dimension ixps(100),ivxpeak(100)
      Double precision xps(100),vxpeak(100),x(2010)
      Double precision vinc,y(2010),hmax,hmin
      Double precision vi,vf,vbegin,mvperir,Se2
c
      Call Maxmin(1,ndata,y,hmin,hmax)
      Print *,'Sc. dev.= ',Se2,' hmax= ',hmax
      Print *,'Sc. dev./hmax= ',Se2/hmax
      If(Se2 .ge. .10*hmax) then
        print *,'Deviation considerable.  Baseline may be suspect.'
      Endif
      Call peakloc(ndata,y,x,vxpeak,ivxpeak,num)
      Call sortpeak(vxpeak,ivxpeak,num,xps,ixps,nsig,y,
     .  vinc,vi,Se2,hmax)

      Return
      End
!*********************************************************************
c
```

```
c       least square fit routines - lsqfit, flatten
c
      subroutine lsqfit (c, ys, a, b, c, Se2)
c       parameters are: c(*) beginning of sample points
c                       ys(*) smoothed data
c
c       returns: a, b, c - the coefficients to fitted parabolic
c                equation of form  a + bn + cn^2
      integer c(100), i, j, k, init
      double precision ys(2010)
      double precision a, b, c, parabla, queen
      double precision dev, Sdev, e2, Se2, Sys
c
c       variables used to solve for  a, b, c
c
      double precision s0, s1, s2, s3, s4, t0, t1, t2, s10, s20
      double precision s21, s31, s32, s42, t00, t11, t22, q(600)
      double precision s13,s02,s23,s12,s24,s34,t13,t02,t24
c
c       now initialize EVERYTHING
c
      j=0
      a=0
      b=0
      c=0
      s0=0.0
      s1=0.0
      s2=0.0
      s3=0.0
      s4=0.0
      t0=0.0
      t1=0.0
      t2=0.0
c
c       set constants for equations:
c                a(s0) + b(s1) + c(s2) = t0
c                a(s1) + b(s2) + c(s3) = t1
c                a(s2) + b(s3) + c(s4) = t2
c
c
      init = -1
      incr = 10
      do 800 i = 1,4
      iheo = c(i)
      if (init .eq. 0) go to 850
      init=0
      incr=50
  850 ienc = iheo+incr
      incr = 10
      do 900 k = iheo,ienc
      j = j+1
      q(j) = k
  900 continue
  800 continue
c
      s0 = j
      do 200 i = 1,j
      ic=int(q(i))
      queer=c(i)
         s1 = s1+queen
         s2 = s2+(queen**2.0)
         s3 = s3+(queer**3.0)
         s4 = s4+(queen**4.0)
         t0 = t0+ys(ic)
         t1 = t1+queen*ys(ic)
         t2 = t2+(queen**2.0)*ys(ic)
  200 continue
c
      s10 = s1/s0
      s20 = s2/s0
      s21 = s2/s1
      s31 = s3/s1
      s32 = s3/s2
      s42 = s4/s2
      s13 = s1/s3
      s02 = s0/s2
      s23 = s2/s3
      s12 = s1/s2
      s24 = s2/s4
      s34 = s3/s4
      t00 = t0/s0
      t11 = t1/s1
      t22 = t2/s2
      t13 = t1/s3
      t02 = t0/s2
      t24 = t2/s4
```

```
      a=((t13-tC2)/(s23-s12)-(t24-t13)/(s34-s23))
     . /((s13-sC2)/(s23-s12)-(s24-s13)/(s34-s23))
      b=((t11-tCC)/(s31-s2C) - (t22-t11)/(s42-s31))
     . /((s21-s1C)/(s31-s2C) - (s32-s21)/(s42-s31))
      c=((t22-t11)/(s32-s21)-(t11-tCC)/(s21-s1C))
     . /((s42-s31)/(s32-s21)-(s31-s2C)/(s21-s1C))
c
      cev=C
      Sdev=C
      Se2=C
      e2=C
      Sys=C
      do 99C i=1,j
      ic=int(a(i))
      queen=c(i)
      carablem=a+b*queen+c*(queen**2)
      dev=ys(ic)-narablem
      Sdev=Sdev+dev
      e2=dev**2
      Se2=Se2+e2
      Sys=Sys+ys(ic)
c      print *,ic,ys(ic),carablem,dev
99C   continue
      Se2=(Se2/(j-1))**.5          ! square deviation
      print *,'ave dev=',Sdev/j,' ave ys=',Sys/J
1     print *,'Tocs',tC,t1,t2
c     print *,'Squids',sC,s1,s2,s3,s4
      if(Abs(a*s0+b*s1+c*s2-t0) .ne. Abs(.CCC1*tC)) goto #300
      if(Abs(a*s1+b*s2+c*s3-t1) .ne. Abs(.CCC1*t1)) goto #300
      if(Abs(a*s2+b*s3+c*s4-t2) .ne. Abs(.CCC1*t2)) goto #30C
c
#301  return
c
c       oocs
c
#3CC  print *,'oops... lsqfit eons do not watch'
      print *,'both sides of equation:'
      print *, a*s0+b*s1+c*s2, t0
      print *, a*s1+b*s2+c*s3, t1
      print *, a*s2+b*s3+c*s4, t2
      go to #3C1
c
      end

c
c       ********************************************



c
      SUBROUTINE FLATTEN(NDATA,YS,APPLES,PEARS,CCCCNUTS)
      Double precision YS(2C10)
      double precision apples, bears, cocoruts, carablem, di
      integer i, ndata
c     Subtract least square fit of baseline from YS
      DO 13CC I=1,NDATA
      di=i
      PARABLEM=APPLES+PEARS*dI+CCCCNUTS*(dI**2.0)
      YS(I)=YS(I)-PARABLEM
13CC  CONTINUE
      RETURN
      END
c
c
c
```

```
c
c
c
      SUBROUTINE FILEREAD(NDATA,catfile,Y,uc)
      INTEGER*2 h,IH,IL
      Double precision Y(2C1C),h,i,uc
      CHARACTER*(*) catfile
      print *,catfile
c
C
      If(uc .eq. -999) ther
        open(name=catfile,type='OLD',unit=13)
        cp 47* i=1,7
        read(13,*) h
47*   Continue
        do 679 i=1,ndata
        read(13,*) I
        read(13,*) h
        y(i) = h*2**16 + I
679   Continue
      Close(unit=13)
      Goto 888
      Endif

      OPEN(ACCESS='DIRECT',NAME=catfile,TYPE='CLD',
     E UNIT=6,RECORDTYPE='FIXED')
C        READ IN FIRST FIVE PARAMETERS
      DO 50 I=1,5
      READ(6'I) M
C      WRITE(7,200) M
  200 FORMAT(I20)
   50 CONTINUE
C        THROW AWAY FIRST DATA POINT
      READ(6'6)M
      READ(6'7)M
C           NOW READ IN WORKING DATA SET
      DO 100 I=1,NDATA
      READ(6'((I*2+6)) IL
      READ(6'((I*2+7)) IH
      Y(I)= (IH*2**16+IL)
  100 CONTINUE
C
CC            NOW CLOSE OUT INPUT FILE
C
      CLOSE(UNIT=6)
C
888   Continue
      RETURN
      END



C
      SUBROUTINE ABSCISSA(NDATA,VI,VF,X,VINC,vmod)

      Double precision vinc,X(2C1C),vi,vf
      Double precision shift        ! don't really need double precision
      Integer ndata
C
CCCC
C                     ** NOW GENERATE ABSCISSA **
C                              ** VINC= mv/point
      VINC=((VF-VI)/(NDATA-1))
      DO 11C I= 1,NDATA
      X(I)= VI + (VINC*(I-1))
  110 CONTINUE
C
CC      now need to calculate the proper energy shift (in mev)
CC      to correct Pt energy dep a 4.2 K for modulation effects
CC      Kirtley & Hansma Phys Rev B 13__.2910 (1976)
CC      (In addition, FWHM value is determined for modulation:
CC         FWHM= 1.46*VMOD + 0.30)
CC                (see Kirtley's review article)
C                    ** VMOD mev rms **
C                         .5 < vmod/delta < 2.
C
      SHIFT= -1.414*VMOD*.14 + 1.13
C                         1 < vmod < 2 mev
C
      do 167 i=1,ndata
        x(i) = x(i) - shift
167   continue
C
      RETURN
      END
C
```

```
c
      SUBROUTINE FAKESMOOTH(NDATA,Y,YS)
      Double precision y(2010),ys(2010)
c
cc      A fake smooth follows (no smoothing).
c
      do 114 i = 1,ndata
114     ys(i) = y(i)
      Return
      End



c
      SUBROUTINE SMOOTH9PTCUBIC(NDATA,Y,YS)
      Double precision y(2010),ys(2010)
c
cc      The real smoothing routine is below.
cc      Also see PLIB.FOR or IETSFCUB.FOR for a 9 pt smooth.
cc-
cc         SMOOTH DATA (9PT CUBIC/QUADRATIC)
c
      DO 120 I=2,NDATA-2
      YS(I)= (-3*(Y(I-2)+Y(I+2))+12*(Y(I-1)+Y(I+1))
     & +17*Y(I))/35
  120 CONTINUE
      DO 125 I=1,2
      YS(I)= Y(I)
      YS(NDATA-I+1)= Y(NDATA-I+1)
  125 CONTINUE
      RETURN
      END



c
      SUBROUTINE SMOOTH9PTCUBIC(NDATA,Y,YS)
      Double precision Y(2010),YS(2010),YHOLD(2010)
c
cc         NEW SMOOTH DATA (9PT CUBIC/QUADRATIC)
c
      DO 120 I=5,NDATA-4
      YHOLD(I)= (-21*(Y(I-4)+Y(I+4))+14*(Y(I-3)+Y(I+3))
     & +39*(Y(I-2)+Y(I+2))+54*(Y(I-1)+Y(I+1))+59*Y(I))/231.
c     YHOLD(I)= ( -3*(Y(I-2)+Y(I+2)) + 12*(Y(I-1)+Y(I+1))
c     & +17*Y(I) )/35.
  120 CONTINUE
      DO 125 I=1,4
      YHOLD(I)= Y(I)
      YHOLD(NDATA-I+1)= Y(NDATA-I+1)
  125 CONTINUE
c           now transfer from YHOLD to YS
      DO 130 I= 1,NDATA
  130 YS(I)= YHOLD(I)
      RETURN
      END

c



c
      SUBROUTINE MSCALE(NDATA,X,Y,VBEGIN,MVPERIN,YUNPIN,YMIN,
     & YMAX,yscale)

      Double precision y(2010),x(2010)
      Double precision vbegin,mvperin,yunpin,ymin,ymax,yscale
c
ccc       We want to slightly reduce to scale so everything fits
cc        plotter y-scale: y-units per inch
c
      YUNPIN= 1.2*(YMAX-YMIN)/YSCALE
c
c         ADD SCALE PARAMETERS INTO ARRAYS
      Y(NDATA+1)= YMIN
      X(NDATA+1)= VBEGIN
      Y(NDATA+2)= YUNPIN
c                 ** plotter scale mv per inch
      X(NDATA+2)= MVPERIN
      continue
      RETURN
      END
c
```

```
c
c
      SUBROUTINE PEAKLOC(NDATA,YPP,X,VXPEAK,ivxpeak,NUM)
      Dimension ivxpeak(100)
      Double precision x(2010),vxpeak(100),xpeak
      Double precision ybr(2010),yc(2010)
c
ccc
c           TRY TO LOCATE PEAK POSITIONS
c
c           FIRST TAKE 1ST DERIV(OPT CUBIC/QUARTIC)
      CALL DERIVOPT(NDATA,YPP,YC)
c        NOW LOCATE NODES
c                 reset peak number counter
      NUM= 0
      DO 150  I=5,NDATA-6
      IF (YC(I) .GE. 0.0) GO TO 150
      IF (YC(I-1) .LT. 0.0) GO TO 150
      XPEAK= X(I)-YC(I)*(X(I)-X(I-1))/(YC(I)-YC(I-1))
      NUM= NUM + 1
c                          vector of all peaks!
      vxpeak(num)= xpeak
c
cc      NEED APPROXIMATE INDEX POSITION OF PEAKS
cd      print *,'peaks! ... one of these ....'
cd      print *,ybr(i-2),ybr(i-1),ybr(i),ybr(i+1)
      If(ybr(i-1) .gt. ybr(i-2) .and. ybr(i-1) .ge. ybr(i)) then
        ivxpeak(num)=i-1
        go to 145
      endif
      If(ybr(i) .gt. ybr(i-2)) then
        ivxpeak(num)=i
        go to 145
      endif
      ivxpeak(num)=i-2
c
145   continue
d     print *,'peak=',ybr(ivxpeak(num))
  150 CONTINUE
      RETURN
      END
c
c
c
c
c
      Subroutine sortpeak(vxpeak,ivxpeak,num,xps,ixps,nsig,y,
     .  vinc,vi,Se2,hmax)
      Integer iv,nsig
      Dimension ixps(100),ivxpeak(100)
      Double precision y(2010)
      Double precision vxpeak(100),xps(100)
      Double precision vinc,vi,Se2,hmax
c
cc      ASSUME BASELINE IS FLAT.  HMAX IS HEIGHT OF MAXIMUM PEAK.
cc      SE2 IS SQUARE DEVIATION.
ccc
c     print *,'Se2=',Se2
      Do 240 i= 1,num
      iv=ivxpeak(i)
      If(y(iv) .lt. 3.0d00*Se2) go to 240
      nsig= nsig + 1
d     print *,'nsig=',nsig
      xps(nsig)= vxpeak(i)
      ixps(nsig)=ivxpeak(i)        ! approx index value of peak
  240 Continue
      Print *,'NUM  & NSIG'
      Print *,NUM,NSIG
      Return
      End
c
```

```
c
c
      SUBROUTINE LABELPOS(YRR,XPS,NSIG,ixps,
     & YUNITN,YMIN,MYPERIN,VBEGIN,VI,VINC)
      integer ixps(100)
      Double precision YRR(2010),SECMAX(10)
      Double precision XPS(100),YPS(100),APXLBL(10)
      Double precision yunitn,ymin,myperin,vbegin,vi,vinc
      Double precision xcl(100),ypl(100),ampvec(100)
      Double precision xspace,yspace,nceak,nsector,awinpcs
c                need commons for calling LABCV
c
      COMMON /LABARR/XPL,YPL,AMPVEC
      COMMON /LABDAT/XSPACE,YSPACE
c
c
      If(nsig .eq. 0.0) goto 377
*
c             **  LABEL POSITIONING ROUTINE  **
      DO 250 I= 1,NSIG
  250 YPS(I)= YRR(ixps(i))
c
c             ESTABLISH CENTER POSITION FOR LABEL CORRESP. TO XPS
c                NOTE: WORK IN DIRECT PLOTTER UNITS(INCHES)
c
      DO 260 I= 1,NSIG
      YPL(I)= YPS(I)/YUNPIN + .05
      XPL(I)= (XPS(I)-VBEGIN)/MYPERIN
  260 CONTINUE
      do 266 i=2,nsig
      if(ypl(i) .gt. ypl(i-1)-.05 .and. ypl(i) .lt. ypl(i-1)+.05) then
        ypl(i) = ypl(i) + .1
      if(ypl(i) .gt. ypl(i-2)-.05 .and. ypl(i) .lt. ypl(i-2)+.05) then
        ypl(i) = ypl(i) - .2
      endif
      endif
266   CONTINUE
      RETURN
377   END
c          -


c
c
      SUBROUTINE DERIVSPT(NDATA,YS,YD)
      Double precision YS(2010),YD(2010)
c
c           FIRST TAKE 1ST DERIV(SPT CUBIC/QUARTIC)
      DO 14C I=5,NDATA-4
      YD(I)= (84*(YS(I-4)-YS(I+4))-142*(YS(I-3)-YS(I+3))
     & -193*(YS(I-2)-YS(I+2))-126*(YS(I-1)-YS(I+1)) )/1188.
  14C CONTINUE
      RETURN
      END
c
c
c       find real maximum and real minimum of an array of data
c       by linear search. also returns HMAX and HMIN (?).


c
      subroutine maxmin (N,ndata,ydata,hmin,hmax)
      integer ndata, i, N
      double precision xdata(2010),xmax,xmin,xval
      double precision ydata(2010),hmax,hmin,yval
c
      if( ndata .le. 1 ) go to 5500
      hmax = ydata(N)
      hmin = ydata(N)
      xmax = N
      xmin = N
      do 5000 i = N+1, ndata
         yval = ydata(i)
         xval = i
         if( yval .gt. hmax ) then
           hmax = yval
           xmax = xval
         end if
         if( yval .lt. hmin ) then
           hmin = yval
           xmin = xval
         end if
 5000 continue
 5500 return
      end
```

JPLOT.FOR

```
      Subroutine plotdata(ndata,x,y,nsig,xps,yscale,vf,filenm,vrod)
      CHARACTER* 4(*) FILENM,plotfile*35
      Dimension ifname(1)
      Dimension xsing(2010),ysing(2010)
      Double precision xj(2010),x(2010),xds(100),xd!(100)
      Double precision y(2010),yj(2010),yd!(100),arpvec(100)
      Double precision yscale,pvcerin,vbegin,vf,vrod,shift,fwhm
      COMMON /LABARR/XPL,YPL,ARPVEC
C
C
c       NEED SINGLE PRECISION YSING WHEN PLOTTTING
      Do 57 I=1,ndata+2
        ysing(i)=SNGL(y(i))
        xsing(i)=SNGL(x(i))
57    Continue
      Do 59 I=1,ndata
59    ysing(i) = -ysing(i)
C
d     print *,'x and y scaling parameters...'
d     print *,xsing(ndata+1),xsing(ndata+2)
d     print *,ysing(ndata+1),ysing(ndata+2)
C
C          NOW PLOT DATA
C
      Call line(ysing,xsing,ndata,1,0,0)
C
C               ** NOW PLOT OUT LABELS **
C
      vbegin = x(ndata+1)          ! this was put here in HSCALE
      pvcerin = x(ndata+2)         ! this too
      DO 575 I= 1,NSIG
C               If label if off page, shift it to default position if ost!
      IF(YPL(I) .GT. YSCALE .OR. YPL(I) .LT. 0.0) YPL(I)= 1.0
      CALL NUMBER(-1*YPL(I),XPL(I)-.12,.045,XPS(I)*0.06548,90.0,0)
  575 CONTINUE
d     print *,'HALT!  In plotdata;  peak labels all set! '
d     print *,'Enter any number! '
d     read *,blaagh
C
C
c     print *,'HALT!  In plotdata;  returning to James! '
d     print *,'Enter any number! '
d     read *,blaagh
      RETURN
      END
```

C. Quick Plot

QKPLT.FOR produces a one-page plot which does not assign peak positions adjacent to the peaks. Instead, each peak is marked by an asterick and the position and y-value of the peaks are printed in a separate file. QKPLT.FOR saves a great deal of time by not printing out all the peak positions.

QKPLT.FOR processes the data much the same as HENRY.FOR but is not broken down into program blocks. No *.DAT files are created, only *.PLT files. An example of the output from QKPLT.FOR is shown in Fig. 4.

QKPLOT.FOR

```
      CHARACTER*30 FNAME,PLOTFILE*35, title*70,None
      character*30 datfile
      Real ud,sd
      Integer i,j,k,w,nsig,sens
      Integer ndata
      Dimension ifname(1),ic(100),ixps(100)
      Double precision xscale,yscale,vbegin,avperin
      Double precision x(2010),xps(100)
      Double precision xpl(100),yypeak(100),xb(2010)
      Double precision yps(100),ypl(100),awpvec(100),xspace,yspace
      Double precision a,b,c,vinc
      Double precision y(2010),ys(2010),yd(2010),ybr(2010)
      Double precision ymin,ymax,hmin,hmax
      COMMON /LARAPP/XPL,YPL,AMPVEC
      COMMON /LABDAT/XSPACE,YSPACE
c           ! program parameters follows
      XSCALE=20.0d00
      YSCALE=0.50d00
      VBEGIN=20.0d00
      AVPERIN=55.80d00

c
c                ****  Inquire TTY for input file  ****
c
      PRINT *, 'INPUT SOURCE DATA FILE'
      READ *,FNAME
c
c
c               create name for plot file
      DO 30 I=1,30
   30 IF(ICHAR(FNAME(I:I)) .EQ. 46 .AND.
     & ICHAR(FNAME(I+1:I+1)) .EQ. 32) GO TO 40
   40 PLOTFILE= FNAME
      PLOTFILE(I:I+3)= '.PLT'
c               and open plot file
      OPEN(NAME=PLOTFILE,UNIT=10,TYPE='NEW')
c               now open file with spectra file data
      OPEN(UNIT=8,NAME=FNAME,TYPE='OLD')
      print *,'Parameter file is: '//fname
      print *,'Plot file is: '//plotfile
c
c               first read in TITLE CARD
      READ (8,22) TITLE
   22 FORMAT(A70)
c               now read in ALL experimental parameters
      READ (8,*) TEMP,EXPOSR,DXTIME,CYYCL,CXCUR
      read (8,*) datfile
      read (8,*) ndata,vi,vf,vmod
      read (8,*) ic(1),ic(2),ic(3),ic(4)
      print *,'Parameters read in. Proceeding...'
c
c
c       ****************************************
c
c                 Program Main Body
c
c       ****************************************
c
c
      GET DATA FROM FIRST FILE
      print *,'Enter UPSD (0 means stop run):'
      read *,ud             ! ud= -1 if file upside down
      if(ud .eq. 0) then       ! or else ud could = sensitivity
        ndata = 0
        go to 9999
      end if
      Call processfile(ndata,vi,vf,x,y,ud,ic,datfile,
     .  a,b,c,Se2,vinc,1)
      Call peakdata(ndata,x,y,vi,vf,vinc,a,b,c,hmax,Se2,
     .  xps,ixps,nsig,vbegin,yscale,avperin)

c
100   Call SmoothSetcubic(ndata,y,ys)
      Call SmoothSetcubic(ndata,ys,y)

c
142   Continue
c
c       (SC, MAYBIN BELOW: a, b, c, hmin, and hmax are not important.)
      Call Maxmin(1,ndata,y,a,b,c,ymin,ymax,hmin,hmax)
      Call Scale(ndata,x,y,vbegin,avperin,yunpin,ymin,ymax)
      print *,' just called maxmin and scale'
c
```

```
      Call Labelpos(y,xps,nsig,yuncin,ymin,mvperin,
     .  vbegin,vi,vinc)
      print *,'just called labelpos'

                        now plot cut data
      CALL PLOTS(53,C,10)
      CALL PLOTDATA(NDATA,X,Y,NSIG,XPS,YSCALE,MVPERIN,
     & VBEGIN,VF,fname,VMOD)
      print *,'just called plots and plotdata'


                     first plot axes
      mvp=sngl(mvperin)
      vb=sngl(vbegin)
      CALL AXIS(0.0,0.0,3HMSV,-1,47C./mvp,0.0,999.,
     & 10./mvp)
      DO 630 I= 0,INT(470/100)
      Do 620 i=1,5
      XLOC= 100*(i-1)/mvp
      YLOC= -0.4
      AXISMV= (i-1)*100+vb
  630 CALL NUMBER(XLOC,YLOC,.1E,AXISMV,C.0,C)

  898 CONTINUE
      CALL PLOT(8.5,-.5,999)
      CLOSE(UNIT=10)
      print *,'axes, etc, set up. about to write peakfile'
C
C*****************************************************************
C
C       PRINTOUT OF PEAK POSITIONS AND PEAK HEIGHTS
C2C5  CONTINUE
      None='None'
      Print *,'Did you use sensitivities for UPSDs? 0 means no.'
      Read *,sens
      Call peakfile(fname,temp,expsur,cxtime,vmod,nsig,
     .  ixcs,y,hmax,xps,ud,0,sens,catfile,rone,none,1)
      print *,'File of peak positions and heights in '//fname
9999  END


      SUBROUTINE PROCESSFILE(ndata,vi,vf,x,y,ud,ip,datfile,
     .  a,b,c,Se2,vinc,file)
C
      Dimension ip(100)
      Integer ndata,itimes,file
      Double precision vinc,a,b,c,y(2010),ys(2010)
      Double precision vi,vf,uc,Se2,x(2010)
      Character*30 datfile
C
C       IF UD = -1.0 :  THE FILE IS UPSIDE DOWN
C       NOW READ IN DATA
7     print *,'reading data file: '//datfile
      Call fileread(ndata,catfile,y)
      Do 10 i=1,ndata
      y(i)=uc*y(i)
10    Continue
      Call Abscisse(ndata,vi,vf,x,vinc)
      Call Smooth9ptcubic(ndata,y,ys)
C
C       LEAST SQUARE FIT OF BASELINE (QUADRATIC FIT)
C           AND BASELINE SUBTRACTION
      Print *,'Number of Lsofit iterations?'
      Read *,itimes
      If(itimes .eq. 0) then
        print *,'No baseline subtraction on this file.'
        go to 31
      End if
C     READ (5,5) IP(1),IP(2),IP(3),IP(4)
      Print *,'Selected Points (mV):'
      Print *,IP(1),IP(2),IP(3),IP(4)
      DO 1700 I=1,4
 1700 IP(I)=int(MAX(DBLE(1.0),DBLE((IP(I)-X(1))/VINC+1.0)))
      PRINT *,'Actual indices are:'
      PRINT *,IP(1),IP(2),IP(3),IP(4)
      PRINT *,'Baseline=apples+bears*x+coconuts*x^2'
      DO 1710 I=1,ITIMES
      CALL LSOFIT(IP,YS,A,B,C,Se2)
      PRINT *,'apples=',A,' bears=',B
      PRINT *,'coconuts=',C
1710  CALL FLATTEN(NDATA,YS,A,B,C)
2000  CONTINUE
      CALL SMOOTH9PTCUBIC(NDATA,YS,Y)
C
31    Return
      End
C
C*****************************************************************
```

```
c
      Subroutine peakdata(ndata,x,y,vi,vf,vinc,a,b,c,hmax,Se2,
     . xos0,ixos0,nsig0,vbegin,yscale,myderiv)
c
      Integer ndata,num,nsig0
      Dimension ixos0(100),ivxpeak(100)
      Double precision vxpeak(100),x(2010),xos0(100)
      Double precision vinc,y(2010),a,b,c,hmax,hmin,ymax,ymin
      Double precision vi,vf,vbegin,yscale,myderiv,Se2
      Double precision bsimm,ymax1
c
      Call Maxmin(1,ndata,y,a,b,c,ymin,ymax,hmin,hmax)
      Print *,'Std. dev.= ',Se2,' hmax= ',hmax
      Print *,'Std. dev./hmax= ',Se2/hmax
      If(Se2 .ge. .10*hmax) then
        print *,'Deviation considerable.  Baseline may be suspect.'
      Endif
      Call peakloc(ndata,y,x,vxpeak,ivxpeak,num)
      Call baseline(vi,vf,vinc,y,ymin,bsimm,ymax1)
      Call sortpeak(vxpeak,ivxpeak,num,xos0,ixos0,nsig0,y,
     .  vinc,vi,bsimm,ymax1)
      Return
      End
!**********************************************************************

c
c       SUBROUTINE FOR WRITING PEAK HEIGHTS INTO A FILE
      Subroutine peakfile(yahoo,temp,exposur,oxtime,vmod,nsig,ixos,
     .  y,hmax1,xos,ud1,ud2,sens,datfile1,datfile2,datfile3,c)
c
      Dimension ixos(100)
      Real temp,exposur,oxtime,vmod,ud1,ud2
      Integer nsig,ncata2,sens
      Character*30 yahoo,datfile1,datfile2,datfile3
      Double precision c,y(2010),hmax01,xos(100),shift
c
      Open(name='yahoo',unit=17,type='new')
      Write (17,9210) yahoo
9210  Format(12x,a10)


      Write (17,9220) temp,exposur,oxtime
9220  Format(12x,'Temp=',f10.2,'  Expos=',f10.2,'  Oxid. time=',f10.2)
      Write (17,9230)
9230  Format(15x,'xos          y              y/ymax1')
C       NEED SHIFT FOR CORRECTION OF PEAK POSITIONS
      Call Correct(vmod,shift,fwhm)
      Do 8888 k=1,nsig
      ix=ixos(k)              ! This gives index value of xos(k)
      Write (17,9240) (xos(k)-shift)*8.0454P,y(ix),y(ix)/hmax01
9240  Format(12x,f10.2,'    ',f10.2,'    ',f10.6)
8888  CONTINUE
      Write (17,9250)
9250  Format(' ')
d     print *,'about to write ud1'
d     print *,'ud1=',ud1
      Write (17,9270) ud1
9270  Format(12x,'File 1 was multiplied by a factor of',f10.2)
      If(ud2 .eq. 0) then
        write (17,9275)
9275    format(12x,'There was no second file.')
      Else
        write (17,9280) ud2
9280    format(12x,'File 2 by a factor of                ',f10.2)
      Endif
      If(sens .ne. 0) then
        write (17,9285) Abs(ud1*10C)
9285    format(12x,'Sensitivity of file 1 (mV) =',f10.2)
      If(ud2 .ne. 0) then
        write (17,9290) Abs(ud2*10C)
9290    format(12x,'Sensitivity of file 2 (mV) =',f10.2)
      endif
      Endif
      Write (17,9293) datfile1
9293  Format(12x,'First file was      ',a30)
      Write (17,9296) datfile2
9296  Format(12x,'Second file was     ',a30)
      Write (17,9300) datfile3
9300  Format(12x,'Reference file was ',a30)
      Write (17,9303) c
9303  Format(12x,'Scaling factor y2 = c*y2:  c = ',f10.4)
9260  Close(unit=17)
      Return
      End
c
!**********************************************************************
c
c       least square fit routines - lscfit, flatter
```

```
c
      subroutine isofit (p, ys, a, b, c, Se2)
c       parameters are: p(*) beginning of sample points
c                       ys(*) smoothed data
c
c       returns: a, b, c - the coefficients to fitted parabolic
c                equation of form  a + bp + cp^2
      integer p(100), i, j, k, init
      double precision ys(2010)
      double precision a, b, c, parabem, queen
      double precision dev, Sdev, e2, Se2, Sys
c
c       variables used to solve for  a, b, c
c
      double precision s0, s1, s2, s3, s4, t0, t1, t2, s10, s20
      double precision s21, s31, s32, s42, t00, t11, t22, c(600)
      double precision s13,s02,s23,s12,s24,s34,t13,t02,t24
c
c       now initialize EVERYTHING
c
      j=0
      a=0
      b=0
      c=0
      s0=0.0
      s1=0.0
      s2=0.0
      s3=0.0
      s4=0.0
      t0=0.0
      t1=0.0
      t2=0.0
c
c       set constants for equations:
c               a(s0) + b(s1) + c(s2) = t0
c               a(s1) + b(s2) + c(s3) = t1
c               a(s2) + b(s3) + c(s4) = t2
c


c
      init = -1
      incr = 19
      do 8200 i = 1,4
      ibeg = p(i)
      if (init .eq. 0) go to 8050
      init=0
      incr=59
 8050 iend = ibeg+incr
      incr = 19
      do 8100 k = ibeg,iend
      j = j+1
      c(j) = k
 8100 continue
 8200 continue
c
      s0 = j
      do 8200 i = 1,j
      io=int(c(i))
      queen=c(i)
         s1 = s1+queen
         s2 = s2+(queen**2.0)
         s3 = s3+(queen**3.0)
         s4 = s4+(queen**4.0)
         t0 = t0+ys(io)
         t1 = t1+queen*ys(io)
         t2 = t2+(queen**2.0)*ys(io)
 8200 continue
c
      s10 = s1/s0
      s20 = s2/s0
      s21 = s2/s1
      s31 = s3/s1
      s32 = s3/s2
      s42 = s4/s2
      s13 = s1/s3
      s02 = s0/s2
      s23 = s2/s3
      s12 = s1/s2
      s24 = s2/s4
      s34 = s3/s4
      t00 = t0/s0
      t11 = t1/s1
      t22 = t2/s2
      t13 = t1/s3
      t02 = t0/s2
      t24 = t2/s4
```

```
      a=((t12-t02)/(s22-s12)-(t24-t13)/(s24-s23))
     . /((s12-s02)/(s22-s12)-(s24-s13)/(s24-s23))
      b=((t11-t00)/(s21-s20) - (t22-t11)/(s42-s21))
     . /((s21-s10)/(s21-s20) - (s32-s21)/(s42-s21))
      c=((t22-t11)/(s32-s21)-(t11-t00)/(s21-s10))
     . /((s42-s11)/(s32-s21)-(s31-s20)/(s21-s10))
c
      dev=0
      sdev=0
      se2=0
      e2=0
      sys=0
      do 400 i=1,j
      ic=int(q(i))
      queen=q(i)
      parablem=a+b*queen+c*(queen**2)
      dev=ys(ic)-parablem
      sdev=sdev+dev
      e2=dev**2
      se2=se2+e2
      sys=sys+ys(ic)
c      print *,ic,ys(ic),parablem,dev
400   continue
      se2=(se2/(j-1))**.5          ! square deviation
      print *,' ava dev=',sdev/j,' ava ys=',sys/j
4     print *,'equids',s0,s1,s2,s3,s4
      if(Abs(a*s0+b*s1+c*s2-t0) .ge. Abs(.0001*t0)) goto 9300
      if(Abs(a*s1+b*s2+c*s3-t1) .ge. Abs(.0001*t1)) goto 9300
      if(Abs(a*s2+b*s3+c*s4-t2) .ge. Abs(.0001*t2)) goto 9300
c
9301  return
c
c       eqns
c
9300  print *,'eqns... lsqfit eqns do not match'
      print *,'both sides of equation:'


      print *, a*s0+b*s1+c*s2, t0
      print *, a*s1+b*s2+c*s3, t1
      print *, a*s2+b*s3+c*s4, t2
      go to 9301
c
      end

c
c       ***********************************************




c
      SUBROUTINE FLATTEN(NDATA,YS,APPLES,BEARS,COCONUTS)
      Double precision YS(2010)
      double precision apples, bears, coconuts, parablem, di
      integer i, ndata
c     Subtract least square fit of baseline from YS
      DO 1300 I=1,NDATA
      di=i
      PARAPLEM=APPLES+BEARS*dI+COCONUTS*(dI**2.0)
      YS(I)=YS(I)-PARAPLEM
1300  CONTINUE
      RETURN
      END
```

```
c
      SUBROUTINE PLOTDATA(NDATA,X,Y,NSIG,XPS,YSCALE,PVPERIN,
     & VBEGIN,VF,FILENM,VMOD)
      CHARACTER *(*) FILENM
      Dimension ifname(1)
      Dimension xsing(2010),ysing(2010)
      Double precision xj(2010),x(2010),xos(100),xol(100)
      Double precision y(2010),yj(2010),yol(100)
      Double precision yscale,pvperin,vbegin,vf,vmod,shift,amovec(100)
      COMMON /LABADD/XPL,YPL,AMPVEC
c
d     print *,'in plotdata, about to find xsing, ysing'
c       NEED SINGLE PRECISION YSING WHEN PLOTTING
      Do 57 i=1,ndata+2
        ysing(i)=SNGL(y(i))
        xsing(i)=SNGL(x(i))
d       print *,xsing(i),ysing(i)
57    Continue
c
c           NOW PLOT DATA
c
      CALL ORIGIN(0.0,0.5,0)
      CALL SPEED(3)
      CALL LINE(Xsing,Ysing,NDATA,1,0,2)
d     print *,'in sub plotdata: already called LINE'
c
c               ** NOW PLOT OUT LABELS **
c
  580 CALL ASPECT(.6)
      DO 57* I= 1,NSIG
c                 if label off page, shift it to default position if ossi
      IF(YPL(I) .GT. YSCALE +.75 .OR. YPL(I) .LT. 0.0) YPL(I)= 1.0
      CALL SYMBOL(XPL(I),YPL(I),.15,IN*,0.0,1)
  57* CONTINUE
c
c
c             now plot FWHM, and label
c
c
      J= LEN(filenm)
      PRINT *,filenm
      DO 670 I=1,J
      IFNAME(I)= ICHAR(filenm(I:I))
  670 CALL SYMBOL((VF-VBEGIN)/PVPERIN-5.+(I-1)*.15*.6,.3,.15,
     & IFNAME,0.0,0)
      CALL SYMBOL((VF-VBEGIN)/PVPERIN-5,.1,.15,16HINST ENG FWHM =
     & ,0.0,16)
      DO 55 I= 1,2
      CALL PLOT((VF-VBEGIN)/PVPERIN-5+.6*.15*16,.1,3)
      CALL PLOT((VF-VBEGIN)/PVPERIN-5+.6*.15*16 + FWHM/PVPERIN,.1,2)
      CALL PLOT((VF-VBEGIN)/PVPERIN-5+.6*.15*16 + FWHM/PVPERIN,.25,2)
      CALL PLOT((VF-VBEGIN)/PVPERIN-5+.6*.15*16,.25,2)
      CALL PLOT((VF-VBEGIN)/PVPERIN-5+.6*.15*16,.1,2)
   55 CONTINUE
      RETURN
      END
c
c
c
c
      SUBROUTINE CORRECT(VMOD,SHIFT,FWHM)
c               this subroutine calculates the proper energy shift (in mev)
c                 to correct sh energy cen ; 4.2 K for modulation effects
c                   Kirtley & Hansma Phys Rev B 13 ,2910 (1976)
C                     In addition, FWHM value is determined for modulation
c
c
C                       (see Kirtley's review article)
c                     ** VMOD meV rms **
c                          .5 < vmod/delta < 2.
      Double precision shift        ! don't really need double precision
c
      SHIFT= -1.414*VMOD*.14 + 1.12
C                    1 < vmod < 2 mev
      FWHM= 1.48*VMOD + 0.20
      print *,'FWHM=',FWHM,'SHIFT=',SHIFT,'VMOD=',VMOD
      RETURN
      END
c
c
```

```
C
C
      SUBROUTINE FILEREAD(NDATA,datfile,Y,file)
      INTEGER*2 M,IH,IL
      Double precision Y(2010)
      CHARACTER*(*) datfile
      print *,datfile
      OPEN(ACCESS='DIRECT',NAME=datfile,TYPE='OLD',
     & UNIT=6,RECORDTYPE='FIXED')
C
C
C        READ IN FIRST FIVE PARAMETERS
      DO 50 I=1,5
      READ(6'I) M
C     WRITE(7,200) M
  200 FORMAT(I20)
   50 CONTINUE
C        THROW AWAY FIRST DATA POINT
      READ(6'6)M
      READ(6'7)M
C           NOW READ IN WORKING DATA SET
      DO 100 I=1,NDATA
      READ(6'(I*2+6)) IL
      READ(6'(I*2+7)) IH
      Y(I)= (IH*2**16+IL)
  100 CONTINUE
C
C           NOW CLOSE OUT INPUT FILE
C
      CLOSE(UNIT=6)
C
      RETURN
      END



C
      SUBROUTINE ABSCISSA(NDATA,VI,VF,X,VINC)

      Double precision vinc,Y(2010),vi,vf
      Integer ndata
C
C
C           ** NOW GENERATE ABSCISSA **
C
C                        ** VINC= pv/point
      VINC=((VF-VI)/(NDATA-1))
      DO 110 I= 1,NDATA
      X(I)= VI + (VINC*(I-1))
  110 CONTINUE
      RETURN
      END
C
C
C
C



      SUBROUTINE SMOOTHOPTCUBIC(NDATA,Y,YS)
      Double precision Y(2010),YS(2010),YHOLD(2010)
C
C           NOW SMOOTH DATA (OPT CUBIC/QUADRATIC)
C
      DO 120 I=5,NDATA-4
      YHOLD(I)= (-21*(Y(I-4)+Y(I+4))+14*(Y(I-3)+Y(I+3))
     & +39*(Y(I-2)+Y(I+2))+54*(Y(I-1)+Y(I+1))+59*Y(I))/231.
C      YHOLD(I)= ( -3*(Y(I-2)+Y(I+2)) + 12*(Y(I-1)+Y(I+1))
C     & +17*Y(I) )/35.
  120 CONTINUE
      DO 125 I=1,4
      YHOLD(I)= Y(I)
      YHOLD(NDATA-I+1)= Y(NDATA-I+1)
  125 CONTINUE
C              now transfer from YHOLD to YS
      DO 130 I= 1,NDATA
  130 YS(I)= YHOLD(I)
      RETURN


      END
C
C
```

```
c
c
      SUBROUTINE SCALE(NDATA,X,Y,VBEGIN,#VPERIN,YUNPIN,YMIN,
     & YMAX)

      Double precision y(2010),x(2010)
      Double precision vbegin,#vperin,yunpin,ymin,ymax,vscale
      YSCALE= 9.50d00              ! made it double precision
c
c
c         we went to slightly reduce to scale so everything fits
c         plotter y-scale: y-units per inch
c
      YUNPIN= 1.2*(YMAX-YMIN)/YSCALE
      YMIN= .92*YMIN
      IF(YMIN .LT. 0.0) YMIN= 1.1*YMIN/.92
  140 CONTINUE
c
C           ADD SCALE PARAMETERS INTO ARRAYS
      Y(NDATA+1)= YMIN
      X(NDATA+1)= VBEGIN
      Y(NDATA+2)= YUNPIN
c                   ** plotter scale mv per inch
      X(NDATA+2)= #VPERIN
      continue
      RETURN
      END
c
c
```

```
c
      SUBROUTINE PEAKLOC(NDATA,YBP,X,VYPEAK,ivxpeak,NUM)
      Dimension ivxpeak(100)
      Double precision x(2010),vxpeak(100),xpeak
      Double precision ybr(2010),yd(2010)
c
c          TRY TO LOCATE PEAK POSITIONS
c
C          FIRST TAKE 1ST DERIV(TRY CUBIC/QUARTIC)
      CALL DERIVSPT(NDATA,YBP,YD)
c        NOW LOCATE NODES
c                reset peak number counter
      NUM= 0
      DO 150  I=5,NDATA-6
      IF (YD(I) .GE. 0.0) GO TO 150
      IF (YD(I-1) .LT. 0.0) GO TO 150
      YPEAK= X(I)-YD(I)*(X(I)-X(I-1))/(YD(I)-YD(I-1))
      NUM= NUM + 1
c                           vector of all peaks!
      vxpeak(num)= xpeak
c
c       NEED APPROXIMATE INDEX POSITION OF PEAKS
      If(ybr(i-1) .gt. ybr(i-2) .and. ybr(i-1) .ge. ybr(i)) then
        ivxpeak(num)=i-1
        go to 150
      endif
      If(ybr(i) .gt. ybr(i-2)) then
        ivxpeak(num)=i
        go to 150
      endif
      ivxpeak(num)=i-2
c
  150 CONTINUE
      RETURN
      END
c
```

```
C
      SUBROUTINE BASELINE(VI,VF,VINC,YPP,YMIN,BSINMN,YMAX1)
      Double precision vi,vf,vinc,ymin,bsinmn,ymax1
      Double precision YPP(2010)
      Double precision baseint,np20mv
C
C           LOCATE THE SIGNIFICANT PEAK POSITIONS: XPS
C
C                     first must estatlish baseline
C
C                      YMAX1= max height of spect. w. bkgrnd removed
      YMAX1= -1E+6
C           zero min baseline integral(integrate over 20 mv)/(20 mv).
C   Initialization  to -YMIN will essentially shift-correct & invt.-spec.
C                   to the proper place for correct beline determination
C     BASEINT= -YMIN
C                   * of points IN 20 mv region
C
      NP20MV= 20./VINC
      DO 205 I=INT((MAX(VI,50.0000)-VI)/VINC + 1),
     *  INT((MAX(VI,50.0000)-VI)/VINC + 1) + NP20MV - 1
  205 BASEINT= BASEINT + YPP(I)/NP20MV
      PRINT *,'BASELINE INTEGRAL & NP20MV'
      PRINT *,BASEINT,NP20MV
C
C                  now serch for the min baseline integral over spectrum
C
C                      first initialize baseline integral minimum
      BSINMN= 1.E+6
      DO 210 I=INT((MAX(VI,50.0000)-VI)/VINC + 1),
     *  INT((MIN(VF-25.0000,4000.0000)-VI)/VINC + 1)
     *BASEINT= BASEINT + (YPP(I+NP20MV)-YPP(I))/NP20MV
      IF(BASEINT .GT. BSINMN) GO TO 1100
      BSINMN= BASEINT
 1100 IF(YPP(I) .GT. YMAX1) YMAX1= YPP(I)
  210 CONTINUE
C                  now reshift BSINMN  to original positions
      BSINMN= BSINMN + YMIN
      PRINT *,'GET BASELINE INTEG MIN  & MAX PEAK HEIGHT '
      PRINT 501,BSINMN,YMAX1
  501 FORMAT(4E16.6)
      RETURN
      END
C
C
C
C
C
C
      SUBROUTINE SORTPEAK(VXPEAK,IVXPEAK,NUM,XPS,IXPS,NSIG,YPP,
     & VINC,VI,BSINMN,YMAX1)
      Dimension IXPS(100),IVXPEAK(100)
      Double precision YPP(2010)
      Double precision VXPEAK(100),XPS(100)
      Double precision vinc,vi,bsinmn,ymax1
C         now that baseline is established(BSINMN),sort through VXPEAK
C
      DO 240 I= 1,NUM
      IF(YPP((VXPEAK(I)-VI)/VINC+1) .LT. .1*(YMAX1-BSINMN) + BSINMN)
     &  GO TO 240
      NSIG= NSIG + 1
      XPS(NSIG)= VXPEAK(I)
      IXPS(NSIG)=IVXPEAK(I)        ! approx index value of peak
  240 CONTINUE
      PRINT *,'NUM  & NSIG'
      PRINT *,NUM,NSIG
      RETURN
      END
C
C
```

```
      SUBROUTINE LABELPOS(YPP,YPS,NSIG,
     & YUNPIN,YMIN,MVPERIN,VBEGIN,VI,VINC)
      Double precision YPP(2010),SECMAX(10)
      Double precision XPS(100),YPS(100),AMXLPL(10)
      Double precision yunpin,ymin,mvperin,vbegin,vi,vinc
      Double precision xpl(100),ypl(100),ampvec(100)
      Double precision xspace,yspace,npeak,nsector,aminpos
c               need commons for calling LABCV
C
      COMMON /LABAPP/YPL,YPL,AMPVEC
      COMMON /LABDAT/XSPACE,YSPACE
c
C
C*
c             **  LABEL POSITIONING ROUTINE  **
c
c                     XSPACE= x-length of label(inches)
      XSPACE= .5
c                     YSPACE= y-length of label(inches)
      YSPACE= .15
c
c
c
c             NOW ASSIGN Y LOCATION TO YPS
c
      DO 250 I= 1,NSIG
c**************************************
  250 YPS(I)= YPP(INT((XPS(I)-VI)/VINC +1))
c
c           ESTABLISH CENTER POSITION FOR LABEL CORRESP. TO XPS
c              NOTE: WORK IN DIRECT PLOTTER UNITS(INCHES)
c
c                   set intial label .5 inches over peak
      DO 260 I= 1,NSIG
      YPL(I)= (YPS(I)-YMIN)/YUNPIN + .5


      YPL(I)= (YPS(I)-VBEGIN)/MVPERIN
  260 CONTINUE
c
C             ** NOW DO LABELS OVERLAP SPECTRUM **
C
C                   we can shift label up to +- 2 sectors(=.5xspace)
C
c                   figure out # of points in sector-length(s)=.25xspace)
      NSECTOR= INT(.25*XSPACE*MVPERIN/VINC)
      DO 300 K= 2,NSIG
C                   now scan sectors(8) to det. max height
      DO 270 J= 1,8
C             RESET SECMAX(J)
      SECMAX(J)= -1E+6
C                   calculate peak subscript
      NPEAK= (YPS(K)-VI)/VINC +1
      DO 270 I= NPEAK+(J-5)*NSECTOR,NPEAK+(J-4)*NSECTOR
c**************************************
  270 SECMAX(J)= MAX(SECMAX(J),YPP(I))
C
c                   now det. maximum over label region and min posit. dist.
C
      AMINPOS = 1E+6
      DO 290 J= 1,5
      AMXLPL(J)= MAX(SECMAX(J),SECMAX(J+1),SECMAX(J+2),SECMAX(J+3))
c                             use NLMIN later to decide #sectors to shift
      IF(AMINPOS .GT. AMXLPL(J)) NLMIN= J
  290 AMINPOS= MIN(AMINPOS,AMXLPL(J))
      AMPVEC(K)= (AMXLPL(?) - YMIN)/YUNPIN
      AMINPOS= (AMINPOS-YMIN)/YUNPIN
C
c                   now check to see if initial placement ok
c
      IF(AMPVEC(K) .LT. YPL(K)-.125) GO TO 300
c         ** LABEL blocking plot  **
c               assign default position if we can't gain by shift
      YPL(K)= AMPVEC(K)+.25
c                   if label can be put less than 1.5in. above orig peak, o.k.
      IF(AMPVEC(K) .LT. YPL(K)+1.0) THEN
      YPL(K)= AMPVEC(K) + .25
c                 else since we must move it up more than 1.5in., will a shift
c                       help us that much,otherwise use default shift above pk.
      ELSE IF(AMPVEC(K)-AMINPOS .GT. .25) THEN
C                   yes we gain by shifting
      YPL(K)= AMINPOS + .125
      YPL(K)= YPL(K) + (NLMIN-3)*NSECTOR*VINC/MVPERIN
      AMPVEC(K)= AMINPOS
      END IF
  300 CONTINUE
c
  250 CONTINUE
c
      RETURN
      END
```

```
c
c
c
      SUBROUTINE DERIVSPT(NDATA,YS,YD)
      Double precision YS(2010),YD(2010)
c
c          FIRST TAKE 1ST DERIV(SPT CUBIC/QUARTIC)
      DO 140 I=5,NDATA-4
      YD(I)= (84*(YS(I-4)-YS(I+4))-142*(YS(I-3)-YS(I+3))
     & -193*(YS(I-2)-YS(I+2))-126*(YS(I-1)-YS(I+1)) )/1100.
  140 CONTINUE
      RETURN
      END
c
c
c       find real maximum and real minimum of an array of data
c       by linear search. also returns HMAX and HMIN (?).
c
      double precision xdata(2010),xmax,xmin,xval
      double precision ydata(2010),hmax,hmin,ymax,ymin,yval,a,b,c
c
      if(ndata .le. 1 ) go to 5500
      ymax = ydata(N)
      ymin = ydata(N)
      xmax = N


      xmin = N
      do 5000 i = N+1, ndata
         yval = ydata(i)
         xval = i
         if( yval .gt. ymax ) then
           ymax = yval
           xmax = xval
         end if
         if( yval .lt. ymin ) then
           ymin = yval
           xmin = xval
         end if
 5000 continue
      hmax=ymax-a-b*xmax-c*(xmax**2.0)
      hmin=ymin-a-b*xmin-c*(xmin**2.0)
 5500 return
      end
```

D. Add5

Add5.FOR is a program used to add together and average the data points for up to five files. It was used often to add together files recorded for the same junction before being processed by the single spectrum program.

When ADD5.FOR is used, it first asks for the 'Input Source Data Card' which, in this case, can consist of up to five files. The input source data card is the same format as that used for the single spectrum program. ADD5.FOR next prompts for the UPSD. -1 is entered if the program is upside down, and sensitivities may also be entered. 0 is entered if no more files are to be added together. Next, the subroutine Fileread is called to read in the data points from the files and to inform the user which file is being read. The above process is repeated for each file.

After the files are read, the data points are averaged and the subroutine Writefile is called, which writes a file with the new data points and notifies the user of its completion by printing "All done data in". The new file will have a .CMP extension.

By using negative UPSD entries, ADD5 can be made to subtract files from each other. This is useful in comparing the growth and disappearance of spectral features when studying a range of exposures of an adsorbate.

ADD5.FOR

```
      CHARACTER*30 FNAME,title*70,hcrm,filern
      character*30 datfile1,datfile2,datfile3
      character*30 datfile4,datfile5
      Real ud,sd,ud1,ud2,uc3,uc4,uc5,ncf
      Integer ndata1,ndata2,ndata3,ncataf
      Integer ndata4,ndata5
      Double precision yf(2010),y1(2010),y2(2010),y3(2010)
      Double precision y4(2010),y5(2010),what
      Double precision y(2010),ysave(2010),yc(2010),ybr(2010)
C
C
C              ****  inquire TTY for input file  ****
C
      PRINT *, 'INPUT SOURCE DATA FILE'
      READ *,FNAME
C
C
C            create name for new (CMP) file
      DO 31 I=1,30
   31 IF(ICHAR(FNAME(I:I)) .EQ. 46 .AND.
     & ICHAR(FNAME(I+1:I+1)) .EQ. 32) GO TO 41
   41 filern= FNAME
      filern(I:I+3)= '.CMP'
C
C            now open file with spectra file data
      OPEN(UNIT=8,NAME=FNAME,TYPE='OLD')
C
C
C            first read in TITLE CARD
      READ (8,22) TITLE
   22 FORMAT(A70)
      read (8,*) datfile1
      read (8,*) ndata1,vi1,vf1,vmcd1
      read (8,*,end=23) datfile2
      read (8,*) ndata2,vi2,vf2,vmcd2
      read (8,*,end=23) datfile3
      read (8,*) ndata3,vi3,vf3,vmcd3
      read (8,*,end=23) datfile4
      read (8,*) ndata4,vi4,vf4,vmcd4
      read (8,*,end=23) datfile5
      read (8,*) ndata5,vi5,vf5,vmcd5
23    continue
C
C
C       ****************************************
c
c                Program Main Body
c
C       ****************************************
c
c
c       GET DATA to be made added together
      print *,'Enter UPSD (0 means no more files):'
      read *,ud1              ! ud= -1 if file upside down
      if(ud1.eq.0) then         ! or else ud could = sensitivity
        ndata1 = 0
        go to 140
      end if
      Call Fileread(ndata1,datfile1,y1)
      Do 10 i=1,ndata1
      y1(i)=ud1*y1(i)
10    Continue
c
      print *,'Enter UPSD (0 means no more files):'
      read *,ud2              ! ud= -1 if file upside down
      if(ud2.eq.0) then         ! or else ud could = sensitivity
        ndata2 = 0
        go to 140
      end if
      Call Fileread(ndata2,datfile2,y2)
      Do 20 i=1,ndata2
      y2(i)=ud2*y2(i)
20    Continue
c
      print *,'Enter UPSD (0 means no more files):'
      read *,uc3              ! ud= -1 if file upside down
      if(uc3.eq.0) then         ! or else ud could = sensitivity
        ndata3 = 0
        go to 140
      end if
      Call Fileread(ndata3,datfile3,y3)
      Do 30 i=1,ndata3
      y3(i)=uc3*y3(i)
30    Continue
c
       print *,'Enter UPSD (0 means no more files):'
       read *,uc4              ! ud= -1 if file upside down
       if(uc4.eq.0) then         ! or else ud could = sensitivity
         ndata4 = 0
         go to 140
       end if
       Call Fileread(ndata4,datfile4,y4)
       Do 40 i=1,ndata4
       y4(i)=uc4*y4(i)
 40    Continue
 c
```

```
      print *,'Enter UPSC (0 means no more files):'
      read *,uc5              ! uc= -1 if file upside down
      if(uc5.ne.0) then       ! or else ud could = sensitivity
        ndata5 = 0
        go to 140
      end if
      call filereac(rdata5,catfile5,y5)
      do 50 i=1,ndata5
      y5(i)=uc5*y5(i)
50    continue
c
140    Continue

      rdataf = max(ndata1,rdata2)
      ndataf = max(ndata3,ndataf)
      rdataf = max(ndata4,rdataf)
      ndataf = max(ndata5,rdataf)
c
      if(uc1 .ne. 0.0) ncf = 1
      if(uc2 .ne. 0.0) ncf = ncf + 1
      if(uc3 .ne. 0.0) ncf = ncf + 1
      if(uc4 .ne. 0.0) ncf = ncf + 1
      if(uc5 .ne. 0.0) ncf = ncf + 1
c
c     print *,'# data points, & # data files ',ndataf,ncf
c
      do 150 i=1,ndataf
        what = (y1(i)+y2(i)+y3(i)+y4(i)+y5(i))/ncf
        yf(i) = what
150   continue
c
c
      Call writefile(ndataf,yf,filenm)

c
9999  END
!**********************************************************************


      SUBROUTINE FILEREAD(NDATA,datfile,Y)
      INTEGER*2 M,IH,IL
      Double precision Y(2010)
      CHARACTER*8(*) datfile
      print *,'File being read: ',datfile
      OPEN(ACCESS='DIRECT',NAME=datfile,TYPE='OLD',
     & UNIT=4,RECORDTYPE='FIXED')
C
C
C        READ IN FIRST FIVE PARAMETERS
      DO 50 I=1,5
      READ(4'I) M
   50 CONTINUE
C        THROW AWAY FIRST DATA POINT
      READ(4'4)M
      READ(4'7)M
C           NOW READ IN WORKING DATA SET
      DO 100 I=1,NDATA
      READ(4'(I*2+6)) IL
      READ(4'(I*2+7)) IH
C      Y(I)= (IH*2**16+IL)
      Y(I)= IH*2**16+IL
  100 CONTINUE
C
C            NOW CLOSE OUT INPUT FILE
C
      CLOSE(UNIT=6)
C
      RETURN
      END
c
      SUBROUTINE WRITEFILE(NDATA,Y,datfile)
      INTEGER*2 M,IH,IL
      Double precision y(2010),ysave(2010)
      integer ndata
      CHARACTER*8(*) datfile
C
C        READ IN FIRST FIVE PARAMETERS
      DO 50 I=1,7
      YSAVE(I)=0
   50 CONTINUE
C           NOW READ IN WORKING DATA SET
      DO 100 I=1,NDATA
      IH = INT(Y(I)/(2**16) + 0.5)
      IL = Y(I) - IH*2**16
      YSAVE(I*2+6)=IL
      YSAVE(I*2+7)=IH
  100 CONTINUE
C
      open(name=datfile, err=999, type='new', unit=13)
      do 300 i=1,2*ndata+7
      write(13,*) ysave(i)
300   continue
999   close(unit=13,err=1300)
1300  continue
      print *,'All done.  Data in  ',datfile
      return
      END
```

IV. Suggested Improvements

There are several improvements which would be useful for analyzing IETS data. One is to specify the relative scaling of the peak heights to a reference peak in the spectra or to arbitrarily set a particular peak or feature to be a certain height with all other features scaled accordingly. The spectra presented in this thesis are of such complexity and undergo such variation in peak position and intensity that a reference peak would be really useful. Of all the features present, the likely candidate is the bulk Al-O stretch appearing near 945 cm^{-1}. Unfortunately, this feature is not often well-resolved, at least not in the work presented here, because of the Zr-O stretch at approximately 910 cm^{-1}. Nonetheless, and despite the fact that some variation in the intensity of the Al-O stretch would be expected as oxidation times and conditions are varied, it is probably the best choice for a reference feature.

Another improvement which might prove useful is to subtract one spectrum from another to produce a difference spectrum. One of the main problems is, of course, that the baselines must be similar. But even if there was some offset, it would provide useful visual information on exactly which spectral features are varying and to what degree. ADD5 may be used to subtract spectra from each other and, if this could be combined with scaling the two spectra to a set reference peak, an informative if not publishable difference spectrum might result. This would be useful when comparing spectra of the same chemical system obtained using different exposures and/or temperatures.

A further improvement is to do away with the "Input Source Data Card" and replace it with a series of prompts to the user. This could potentially save a great deal of time because the editing required to change the card for each spectrum would no longer be required.

V. Acknowledgments

I would like to acknowledge Dave Hsu, whose hard work and long hours at the Chem Vax made these programs what they are.

References

1. M. K. Templeton, PhD Thesis, California Institute of Technology (1984).

2. G. Gajda, PhD Thesis, California Institute of Technology (1986).

3. J. D. Langan and P. K. Hansma, Surface Sci. **52**, 211 (1975).

Figure Captions

Figure 1: Example of a single spectrum Versatec plot produced by HENRY.FOR.

Figure 2: Printout of a file containing the peak locations and heights produced by HENRY.FOR.

Figure 3: Example of multiple spectra plotted by JAMES.FOR.

Figure 4: A spectrum produced by QKPLT.FOR.

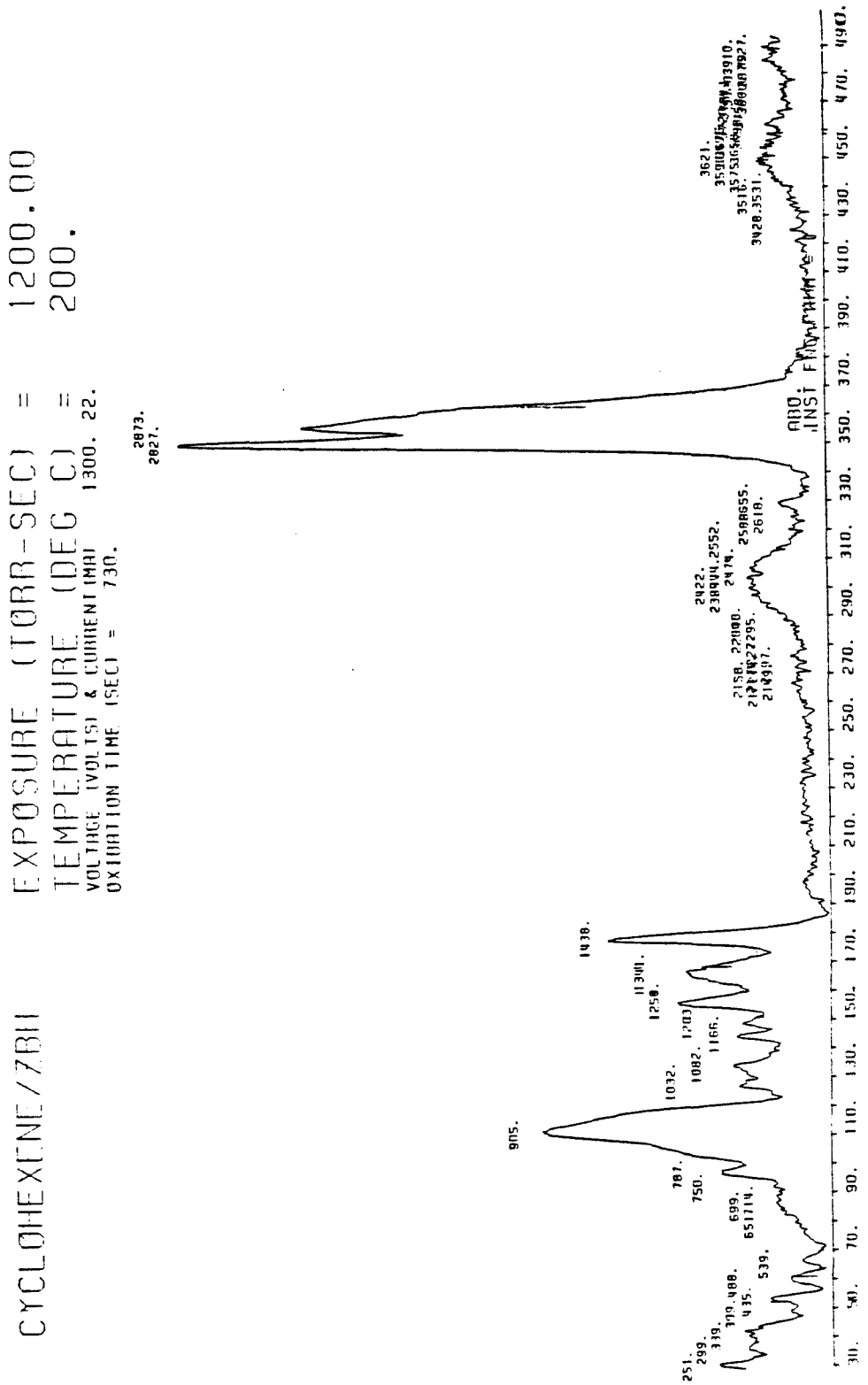
CYCLOHEXENE/ZBII
EXPOSURE (TORR-SEC) = 1200.00
TEMPERATURE (DEG C) = 200.
VOLTAGE (VOLTS) & CURRENT(MA) 1300. 22.
OXIDATION TIME (SEC) = 730.
2873.
2827.
905.
1438.
1258.
1166.
1082.
1032.
781.
750.
699.
539.
435.
339.
299.
251.
2422.
2618.
3621.
3518.
3428.3531.
ANO.
INST
30.
70.
90.
110.
130.
150.
170.
190.
210.
230.
250.
270.
290.
310.
330.
350.
370.
390.
410.
430.
450.
470.

Figure 1

```
APU.CAT
Temp=      25.00  Expos=    1200.00  Oxid. time=     680.00
    xps            y          y/ymaxl
    256.26      10952.11      0.229611
    295.50      10486.15      0.219842
    494.63       2981.77      0.062513
    548.73       2175.38      0.045607
    597.60       3339.95      0.070022
    670.19       6830.98      0.143212
    691.00       7303.87      0.153126
    697.49       7303.87      0.153126
    915.14      47698.53      1.000000
   1041.28       8105.90      0.169940
   1075.33      10822.42      0.226892
   1109.61      12882.42      0.270080
   1178.61       7604.02      0.159418
   1224.19       5328.17      0.111705
   1270.32       9374.99      0.196547
   1324.65       2277.87      0.047755
   1363.82       4561.58      0.095634
   1394.60       5092.73      0.106769
   1463.24       8476.39      0.177707
   1874.04       1605.81      0.033750
   1879.12       1832.66      0.038422
   1907.19       2044.78      0.042869
   2172.15       6462.92      0.135495
   2187.40       7689.61      0.161213
   2213.91       6907.73      0.144821
   2241.29       8122.99      0.170319
   2295.44       5628.92      0.118010
   2318.68       4984.22      0.104494
   2440.89      19809.44      0.415305
   2465.41      20270.14      0.424964
   2508.43      20551.63      0.430865
   2526.11      21172.08      0.443894
   2626.55       2924.23      0.061309
   2656.58       1266.89      0.026560
   2872.00      21665.07      0.454208
   2950.14      24812.78      0.520200
   3049.81       3888.02      0.081512
   3566.60       1712.10      0.035894
   3591.31       1627.13      0.034113
   3619.10       2648.86      0.055533
   3640.81       2816.84      0.059055
   3686.00       4164.24      0.087303
   3723.92       2737.99      0.057402
   3757.53       2614.96      0.054823

File 1 was multiplied by a factor of       5.00
File 2 by a factor of                      5.00
Sensitivity of file 1 (nV) =     500.00
Sensitivity of file 2 (nV) =     500.00
First file was      [LF.CH]APU078.LDA;1
Second file was     [LF.CH]APU079.LDA;1
Reference file was None
Scaling factor y2 = c*y2;  c =    1.000000
```

Figure 2

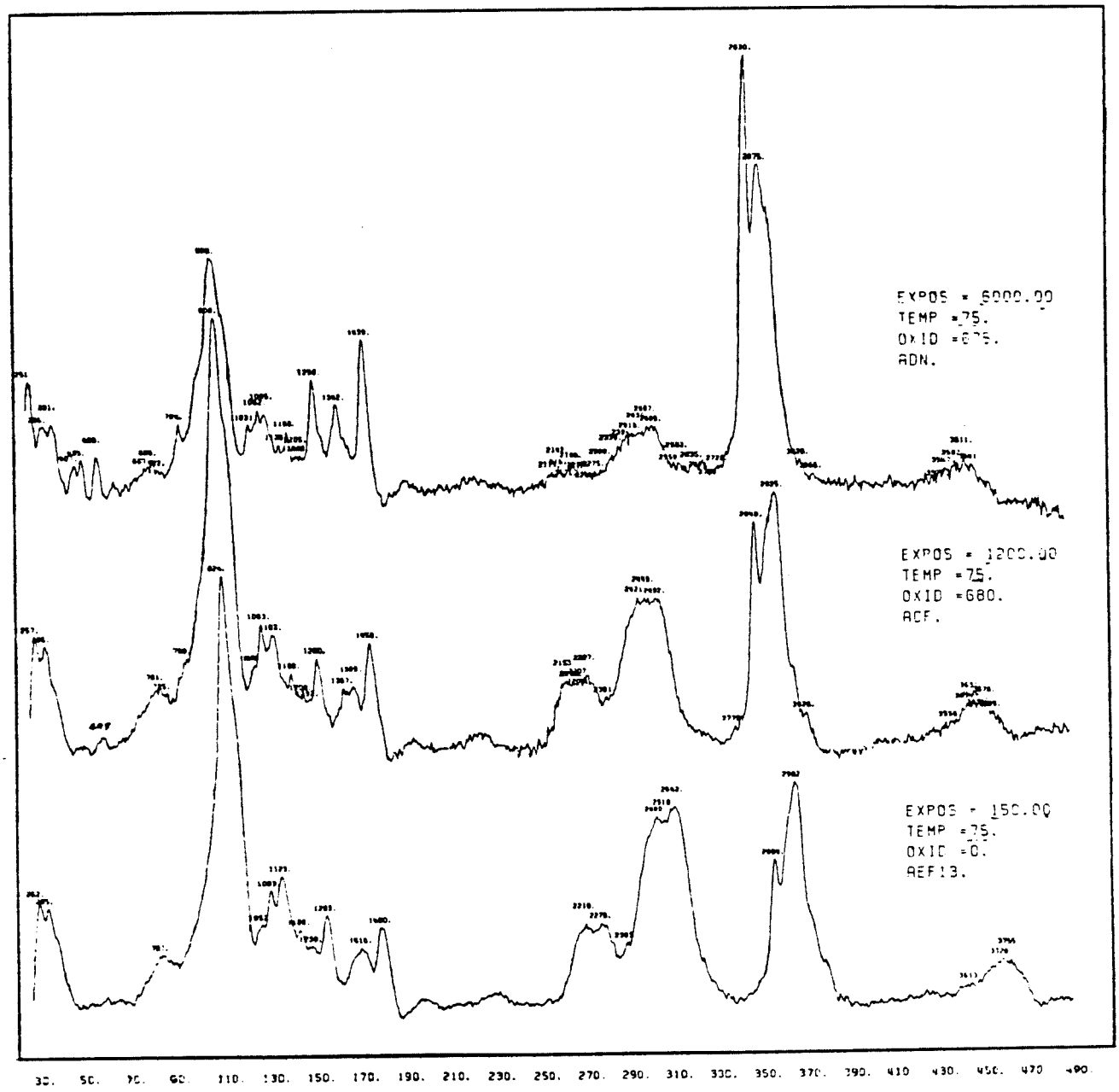
EXPOS = 6000.00
TEMP =75.
OXID =675.
ADN.
EXPOS = 1200.00
TEMP =75.
OXID =680.
ACF.
EXPOS = 150.00
TEMP =75.
OXID =0.
AEF13.
30. 50. 70. 90. 110. 130. 150. 170. 190. 210. 230. 250. 270. 290. 310. 330. 350. 370. 390. 410 430. 450. 470 490.

Figure 3

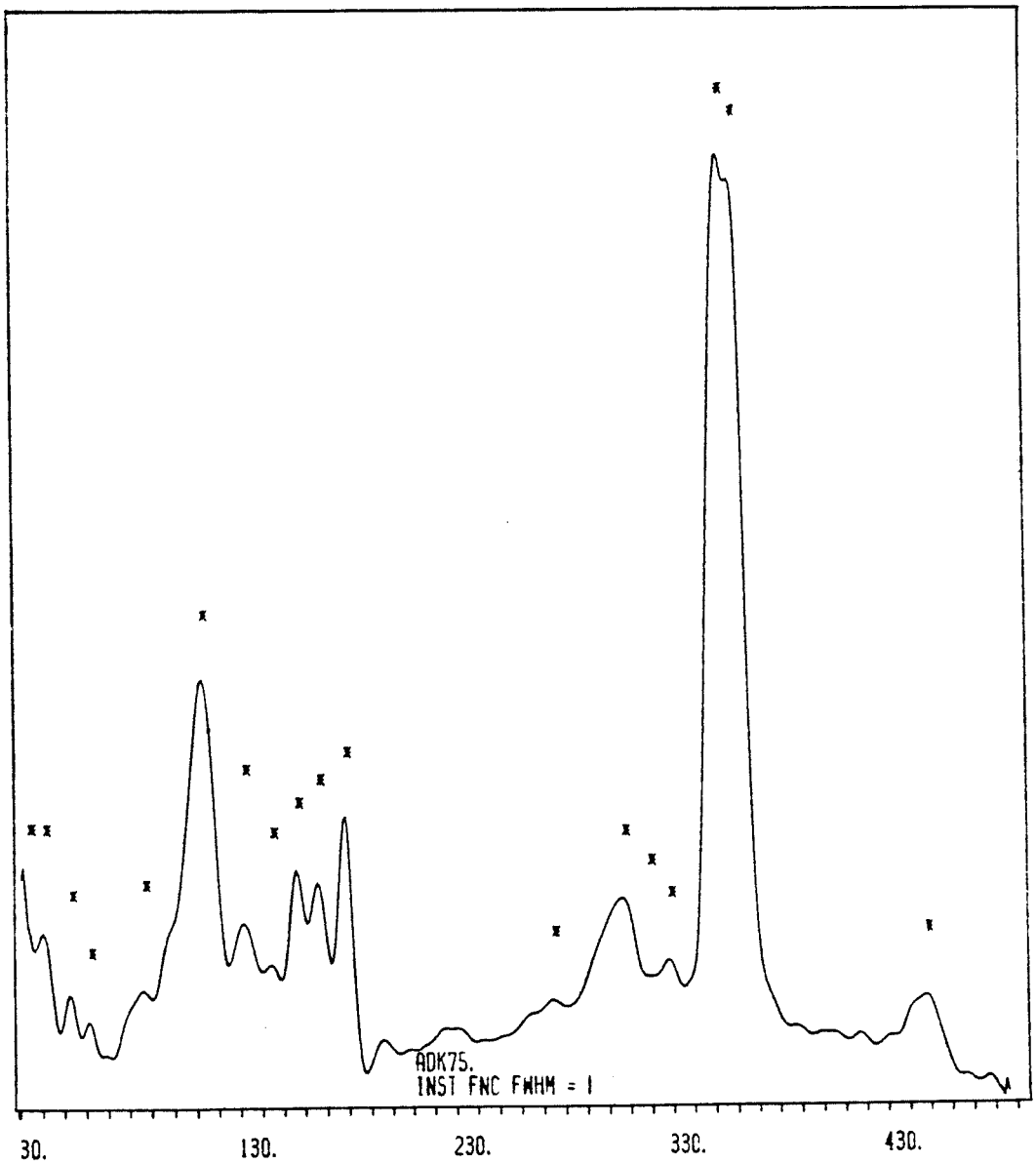

Figure 4